Not for Publication
Presented Before the Division of Gas and Fuel Chemistry
American Chemical Society
Atlantic City, New Jersey, Meeting, September 13-18,1959

PROCESS FOR THE ECONOMICAL UTILIZATION OF IDLE STANDBY OILGAS PLANTS TO PRODUCE LOW-COST PETROCHEMICALS

Virgil Stark and Emery Parker

North American Utility & Construction Corp.
405 Lexington Avenue
New York 17, N.Y.

Natural gas covering over 97% of the requirements of the U.S. gas industry(1) has almost completely replaced manufactured gas produced from coal, coke or oil, which still represents over 99% of the gas distributed in Europe (9).

In most cases, in the U.S.A., gas plants have been converted to produce oilgas and are being maintained as standby facilities to cover peakloads, sometimes so required by State Utility Commissions. However, in general, such plants (appr. 150 gas generators), are operated for less than 15 days per year.

This situation is economically unsound, when considering the important capital investment in such plants, the required maintenance, and the necessity of having skilled labor available all year round for only a few days' operation per year.

On the other hand, natural gas contracts generally limit the quantity of natural gas available for peakloads, which may be as high as 4 times the lowest sendout volume. Price for extra peakload gas may be up to 6 times the average cost of natural gas. With the increase in space heating load, the dynamic competition of other fuels and the upward trend in the cost of natural gas, the peakload problem is becoming increasingly acute.

A solution is proposed which is believed to solve the peakload problem of the gas industry. Its application will permit continuous year round operation of presently idle gas plants.

This solution provides to produce oilgas with a higher than conventional heat value and which may contain up to 50% higher hydrocarbons (C_2 to C_8). Recovery, fractionation and further processing of such hydrocarbons would then make available basic petrochemicals. Due to the high value of petrochemicals recovered from the oilgas, the residual gas can be made available at a lower cost than that of natural gas. The residual gas is more readily interchangeable with natural gas than oilgas. During most of the year, residual gas may be used to cover heat and power requirements; during peakload periods, it can be made available for gas distribution and liquid fuels are used for the plant.

The process can make available to the chemical industry basic petrochemicals such as ethylene, propylene, butylene-butadiene, cyclopentadiene, benzene, toluene, cumene and styrene. Production would be nearer to large consumption

areas, as for instance on the East Coast of the U.S.A., and possibly at lower cost than that prevailing on the Gulf Coast.

Taking ethylene as an example: 62.6% of the total U.S.production originates from the Gulf Coast at a price of appr. 5cents/lb. and only 15.4% from the East Coast at appr. 6 cents/lb. such prices being based on plants of 200 to 300 million pounds per year capacity (8).

With this solution, it would be possible to produce ethylene at a price of appr. 2.5 cents/lb., in New England in a plant having a capacity of only 43 million pounds per year (oilgas plant of 10,000 MCFD). In this case, the residual gas is valued at 30% below the average cost of natural gas, and the other products at their market value in this area.

A plant with an annual capacity of 26 million pounds of ethylene (6,000 MCFD gas plant) would still be economically feasible with this solution, whereas such relatively small plants are not competitive when using other processes. By application of the proposed solution at a single converted gas plant in the N.Y. metropolitan area, 150 million pounds of ethylene could be obtained and this right near major markets for the products.

The growth of the petrochemical industry has been dynamic and continues at an unprecedented rate. During the last two decades, production in the U.S.A. had doubled about every five years. In 1958, it amounted to appr. 5 billion dollars annually, and is expected to grow to 20 billion dollars by 1967(6).

In papers presented at the World Petroleum Congress held recently in New York, as well as in several publications (6, 7) production of petrochmicals over a decade has been forecast as per following Table.

Anticipated Increase in Production of some Basic Petrochemicals in the United States in a Decade in Billion Pounds

	1955	1965
Ethylene	3.05	6.50
Propylene	1.60	2.70
Butylene-Butadiene	2.15	3.60
Aromatics	3.00	8.00
Styrene	1.01	1.75
All Petrochemicals	31.50	85.00

Natural gas is the principal source (50%) from which ethylene is produced in the U.S. (8). Natural gas contains relatively small percentages of ethane from which ethylene is produced by thermocracking, after recovery of ethane from natural gas. In our case, the ethylene is already present as such in the oilgas (over 20% by volume) in addition to other hydrocarbons the total content of which may be as high as 50% by volume. This allows lower capital investment and permits the economical recovery of hydrocarbons in smaller plants.

The Stark Process (U.S.Patent No. 2,714,060) proposed in this paper has been described previously in several publications (2, 3, 4, 5,11)This process offers a great deal of flexibility regarding the degree of hydrocarbon recovery, purity and type of products which can be obtained.

A number of schemes, A to E, mostly new, have been worked out to show various possibilities in recovery and production of petrochemicals and their economics are outlined hereafter.

In all of the following schemes, oilgas is the basic charge stock for the proposed recovery and petrochemical plants. The oilgas is produced in existing converted, reactivated or new gasplant facilities.

The conventional oilgas generator permits vapor phase cracking with steam but without catalyst. A variety of fuels such as Bunker C oil, residuum crude oils, and crude oil may be used for oilgas making. The oilgas generator can be heated by heavy oil, tar or gas. By suitable adjustment of the operating conditions, particularly of the cracking temperature, an oilgas of desired analysis and heat value (700 Btu/cf to 1600 Btu/cf) can be produced. As the hydrocarbon content of the gas (C_2 to C_8) increases, the heating value of the oilgas increases accordingly. It may range between 5 mol percent for a 700 Btu/cf gas to 50 mol percent for a 1600 Btu/cf gas(10).

The present study is based on a typical oilgas of 1250 Btu/cf having the following analysis expressed in mol percent, based on operating data available from various plants.

CH_4	33.0%	
C_2	24.0%	
C_3	6.6%	
C_4	3.8%	
C_5	1.2%	
C_6-C_8	3.4%	
H_2	16.0%	
CO, CO_2, O_2, N_2	12.0%	Heat value 1250 Btu/cf
	100.0%	Gravity 0.86

The combined percentage of unsaturated hydrocarbons and aromatics in above analysis represents appr. 33%. The residual gas after recovery of higher hydrocarbons will have a heat value and gravity nearer to the natural gas and may be used as a substitute thereof, with better interchangeability and characteristics than the conventional oilgas of 1000 Btu/cf. The residual gas may, however, also be used within the plant itself to provide for heat and power requirements. Depending on local market conditions, by crediting the market value of the recovered petrochemicals, this may result in a lower cost for residual gas than for the price of natural gas in the specific area.

The H_2S is removed from the oil and the tar is separated and dehydrated at the gas plant by conventional procedures. The oilgas accumulated in the holder is compressed and sent to the recovery plant.

As the organic sulphur compounds generally contained in the oilgas (appr. 30 grains/100 cf) are removed from the gas during the recovery processing, the residual gas will be practically free of organic sulphur and can, if so desired, be used in a catalytic generator for the production of hydrogen, which cannot be obtained from the oil directly because of this sulphur (12). This allows also to build ammonia plants starting from heavy oil as the only charge stock. In such case, hydrogen could be produced from the residual gas and any balance of the residual gas could be used to cover the important heat and power requirements of the ammonia plant. This possibility is not covered in this paper.

Schemes A to E are outlined below:

Scheme A (Fig. 1)

This plant proposes the recovery of appr. 70% of C_3, and more than 98% of C_4 to C_8 cuts (2). The residual gas will have the following appr. analysis in mol percent:

CH_4	38.0%
C_2	27.0%
C_3^+	2.6%
H_2	18.4%
CO, O_2, CO_2, N_2	14.0%
	100.0%
Heat value	970 Btu/cf
Gravity	0.68

Scheme B (Fig.2)

Recovery of 88% of the C_2 fraction and appr. 98% of the higher hydrocarbons(C_3-C_8) is proposed. The residual gas will have the followinf appr. analysis in mol percent:

CH_4	49.2%
C_2^+	9.1%
H_2	24.7%
CO, CO_2, O_2, N_2	17.0%
	100.0%
Heat value	750 Btu/cf
Gravity	0.58

The residual gas can be enriched to a gas of 1000 Btu/cf and appr. 0.70 gravity using appr. 4% of the annual output of the recovered C_3 cut.

Scheme C (Fig.3)

Provides for the addition to the recovery plant as per Scheme A of another Plant (P1) to handle 50% of the residual gas.

Part of the residual gas, with addition of benzene, is sent to Plant P1, where all of the propylene in the gas with the benzene is catalytically converted to cumene (C_9H_{12}), and the ethylene with the benzene is converted to ethylbenzene (C_8H_{10}) an aromatic solvent remaining as byproduct. The ethylbenzene can then be dehydrogenated into styrene (C_8H_8) in an additional plant P2.

The quantity of cumene and styrene produced may be varied by changing the percentage of volume of residual gas processed in plants P1 and P2.

Scheme D (Fig. 3)

Shows conditions when all of the residual gas is processed in plants P1 and P2, otherwise at the same conditions as Scheme C.

Scheme E (Fig. 4)

Refers to an alternate in which the first plant is limited to the extraction of 95% of C_4 and heavier fractions. Plants similar to D are provided, however, all of the C_3 will be used in Plant P1 resulting in greater cumene production than provided for in the preceding scheme, but no propylene cut is recovered.

A typical example is given for a plant with a daily capacity of 6,000 MCFD of oilgas corresponding to the operation of only one large size conventional oilgas generator unit.

An oilgas of 1250 Btu/cf, typical analysis as above, based on 345 days of operation per year, has been assumed; this amounts to an input in the extraction plant of 7,500 MM Btu/day or 2,587,700 MM Btu/year. Consumption of heavy oil for gas making and heating of the oilgas generator based on 13.5 gal/MCF is 764,000 bbl/year.

The following tables illustrate the economics of such typical plant for each of above schemes, based on present market conditions prevailing in the New England area.

Table I, indicates quantities produced, as well as charge stocks, on an annual basis.

Table II, shows the upgrading, i.e. market value of the product obtained less the cost of charge stocks (heavy oil and benzene) with corresponding unit prices for each product.

Residual gas has been estimated at the cost of heavy fuel in equivalent Btu, i.e. 35¢/MMBtu, plus 10% for difference in efficiency and cost of preheating of the heavy oil making a total of 38.5¢/MMBtu. This is 30% lower than the average cost of natural gas in the New England region (appr. 55¢/MMBtu). It makes possible to use residual gas as fuel, either partially or totally, for petrochemical or power plants or gas distribution. Above calculations do not reflect credit for the much higher value of residual gas when used for peakload requirements (other substitutes being up to 6 times higher)

An economic evaluation for each scheme is summarized in Table III.

The required capital investments should be established separately for each project, however, an indication has been given in Tabulation III.

Equity has been assumed at 50% of the capital requirements, interest rate at 6 percent per annum on balance of required capital with amortization over 10 years resulting in an average annuity of 3.59%

Cost of utilities and labor on which these studies are based:

Steam	70¢/1000 lbs.
Electricty	1.1¢/KWH
Fuel oil	$2.20/Bbl
Fuel gas	38.5¢/MCF
Water	0.5¢/1000 gals
Skilled labor	$2.40/hour

A conservative figure of 20¢ per MCF has been used for the cost of oil-gas at holder including tar dehydration.

The return on total capital is defined as income plus interest dividedby the total capital.

The payout is defined as number of years resulting from the capital investment divided by net income ater taxes plus depreciation.

Tabulation III shows that the net return on capital equity after taxes is 21% to 72% and payout 4.7% to 2.1 years based on above conditions.

Figs. 5 and 6 illustrate payout and percentage of net income after taxes on the equity(**50% of capital**) for Schemes A thru E above, for plants of capacities from 3,000 MCFD to 10,000 MCFD based on present market conditions in the New England area.

A specific study should be made for each case as the economics will depend on the local and market conditions.

If payout of 5 years is taken as a basis for Scheme B and for a plant of 10,000 MCFD capacity, the cost of ethylene for a production of 43 million pounds per year (instead of 26 million pounds/year in a 6,000 MCFD plant) may be as low as 2.5¢/lb in the New England area.

The cost of styrene under above conditions for a plant of 10,000 MCFD, using this process will be only appr. 8¢/lb. and of cumene 5.3¢/lb. i.e. appr. 30% lower than market prices in the New England area.

It is to be emphasized that, depending on market conditions, plants of smaller capacity become economically feasible by application of this process. This may be of special importance for plants outside the United States where smaller quantities of petrochemicals are marketable and can be produced at much lower cost than they can be imported.

The application of this process will result in the following advantages:

1) Utilization of idle investment in gas plants by operating them all year round, instead on only less than two weeks a year.

2) Possibility of making available to the gas industry a better substitute gas at much lower cost than other substitutes for peakloads and appr. 30% lower than the average yearly cost of natural gas in the area.

3) Possibility of making available to the chemical industry basic petrochemicals closer to the consuming markets (for instance the East of the U.S.) at a price possibly lower than prevailing on the Gulf Coast of U.S.A.

4) To obtain a high net income on equity capital after taxes (21% to 72%) and payout of the investment in 2 - 5 years.

5) Possibility to install plants of small capacity which is, in general, not economically possible with other processes.

6) Economic utilization of heavy oils, either Bunker C oil or crude oil, which may be either in oversupply or too far from market areas.

This process may show even better economics when applied in other countries even if installation of gas plant equipment may be required, because chemicals are generally imported and their cost is higher than in U.S.A whereas labor is less expensive.

Application of this process may benefit both the gas and chemical industries and may contribute to better standards of living in many countries.

REFERENCES

1. Gas Facts AGA 1957
2. Typical Application for the Production of a Low Cost Gas as a Substitute for Natural Gas - Virgil Stark AGA Production Conference May 1957
3. Gas Plant to Cut Ethylene - Chemical Week June 22, 1957.
4. Process Union Begets Low Cost Ethylene - Chemical Week - August 1957
5. Process for Economic Solution of Peak & Standby Problems - Virgil Stark - Gas Journal July 1955
6. Petro Chemicals - A Myriad of New Products by T.C. Ponder NYT - May 31, 1959
7. Problem Time for Petro Chemical Previews - Chemical Week June 20, 1959
8. Ethylene Chemical Outlook - Chemical Week May 9, 1959
9. International Gas Conference, Rome 1958
10. Selection of Oil for High BTU Oil Gas - H. R. Linden & E. Pettyjohn - Institute of GasTechnology - Bulletin 12 - 1952
11. The Utilization of Gaseous Fuels by Modern Industry - Virgil Stark - World Power Conference - Rio de Janiero 1954
12. Developments in the Concentric Catalytic Generator - Virgil Stark - AGA CEP-56.1

TABLE I

PRODUCTS AND REQUIRED CHARGE STOCKS

FOR DIFFERENT SCHEMES FOR A TYPICAL 6000 MCF/D PLANT

		A	B	C	D	E
PRODUCTS						
Residual Gas	MM BTU /yr	1,675,000	1,020,000	1,280,000	950,000	970,000
Tar	MM gals/yr	14.10	14.10	14.10	14.10	14.10
Ethylene	MM lbs /yr		26.30			
Propylene Cut	MM gals/yr	2.83	3.85	2.83	2.83	
Butadiene-Butylenes Cut	MM gals/yr	2.23	2.23	2.23	2.23	2.23
Cyclopentadiene-Pentene Cut	MM gals/yr	.67	.67	.67	.67	.67
BTX (Benzene-Toluene-Xylene)	MM gals/yr	2.16	2.16	2.16	2.16	2.16
Styrene	MM lbs /yr			41.90	83.80	84.50
Cumene	MM lbs /yr			5.04	10.04	38.20
Aromatic Solvent	MM gals/yr			.82		
CHARGE STOCKS						
Heavy oil for oil-gas making and heating oil-gas generator	MM bbl /yr	.764	.764	.764	.764	.764
Benzene	MM gals/yr			5.750	11.500	14.100
Alternate Benzene required, if Benzene from BTX is used	MM gals/yr			4.320	10.070	12.670

TABLE II

UPGRADING VALUES IN MILLION DOLLARS/YEAR FOR DIFFERENT SCHEMES FOR A TYPICAL 6000 MCF/D PLANT WITH UNIT PRICES OF PRODUCTS

	Unit Prices	A	B	C	D	E
VALUE OF PRODUCTS						
Residual Gas	$.385/MMBTU	.645	.392	.492	.366	.373
Tar	$.10 /gal	1.410	1.410	1.410	1.410	1.410
Ethylene	$.05 /lb		1.313			
Propylene	$.14 /gal	.396	.539	.396	.396	
Butadiene-Butylenes	$.09 /gal	.200	.200	.200	.200	.200
Cyclopentadiene-Pentenes	$.09 /gal	.060	.060	.060	.060	.060
BTX	$.18 /gal	.389	.389	.389	.389	.389
Styrene	$.12 /lb			5.020	10.040	10.120
Cumene	$.08 /lb			.403	.806	3.060
Aromatic Solvent	$.15 /gal			.123	.246	.308
TOTAL		3.100	4.303	8.493	13.913	15.920
COST OF CHARGE STOCKS						
Heavy oil for oil-gas making and heating oil-gas generator	$2.20 /bbl	1.680	1.680	1.680	1.680	1.680
Benzene	$.31 /gal			1.780	3.560	4.360
TOTAL		1.680	1.680	3.460	5.240	6.040
UPGRADING VALUES (Equal to Value of Products less Cost of Charge Stocks)		1.420	2.623	5.033	8.673	9.880

TABLE III

ECONOMIC EVALUATION OF DIFFERENT SCHEMES

IN MILLION DOLLARS/YEAR FOR A TYPICAL 6000 MCF/D PLANT

	A	B	C	D	E
Estimated Capital Investment	2.10	3.90	6.10	8.20	7.90
Financing, Equity (50%)	1.05	1.95	3.05	4.10	3.85
Loan	1.05	1.95	3.05	4.10	3.85
COSTS, MM $/yr					
Gas Manufacturing Plant incl. tar processing, but excl. charge stock	.416	.416	.416	.416	.416
Petrochemical Plant					
Utilities and Chemicals	.097	.234	.878	1.659	1.720
Labor	.080	.193	.216	.216	.193
Miscellaneous incl. maint., insur., gen. man., sales, royalties etc.	.135	.263	.568	.870	.914
Depreciation (10 yrs)	.193	.375	.571	.764	.727
Interest, 6% amort. 10 yrs. (average 3.59% per year)	.038	.070	.110	.147	.138
TOTAL.	.959	1.551	2.759	4.072	4.108
Upgrading (Value of Products, less Costs of Charge Stock)	1.420	2.623	5.033	8.673	9.880
Income	.461	1.072	2.274	4.601	5.772
Income Taxes (52%)	.240	.556	1.182	2.395	3.000
Net Income	.221	.516	1.092	2.206	2.772
% Return on Equity after Taxes	21.0	26.5	35.8	53.8	72.0
% Return on Capital Investment after Taxes	12.3	15.0	19.7	28.7	36.9
Payout after Taxes	4.7	4.2	3.4	2.6	2.1

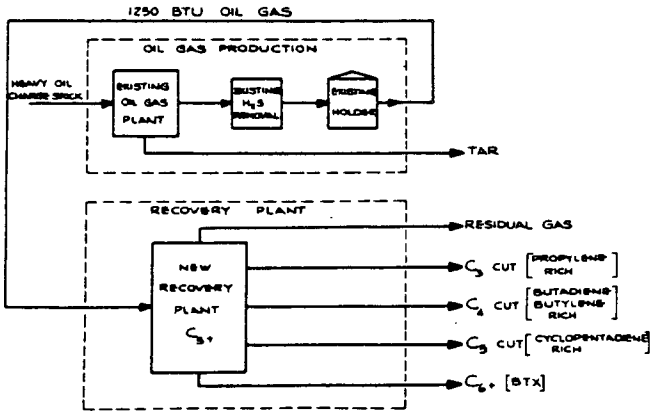

SCHEME A

FIG. I

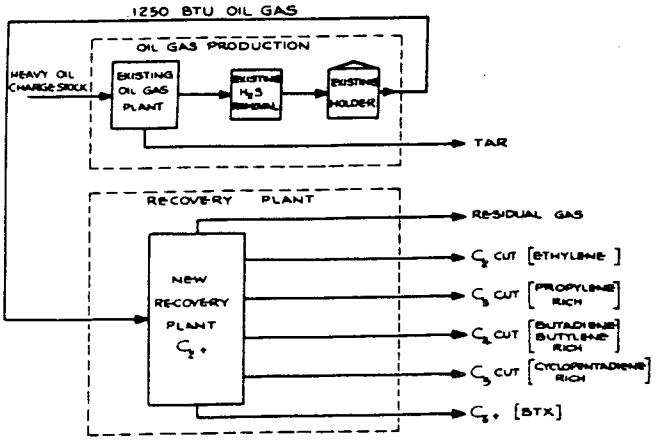

SCHEME B

FIG. II

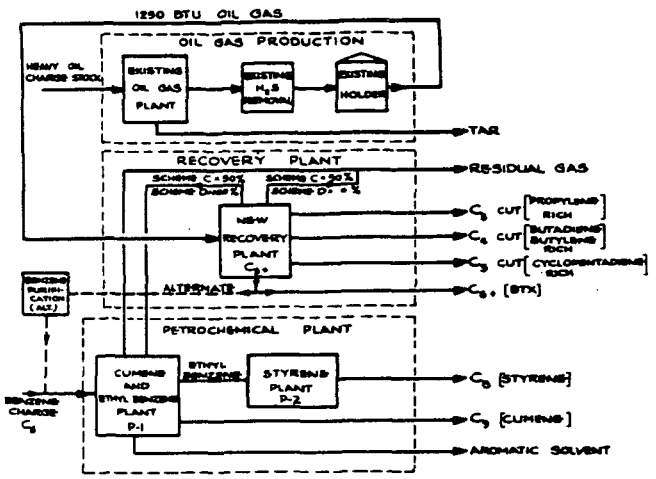

SCHEMES C AND D

FIG III

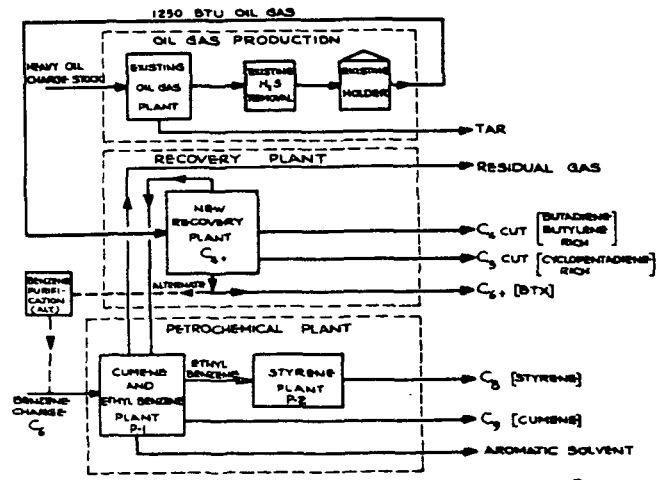

SCHEME E

FIG IV

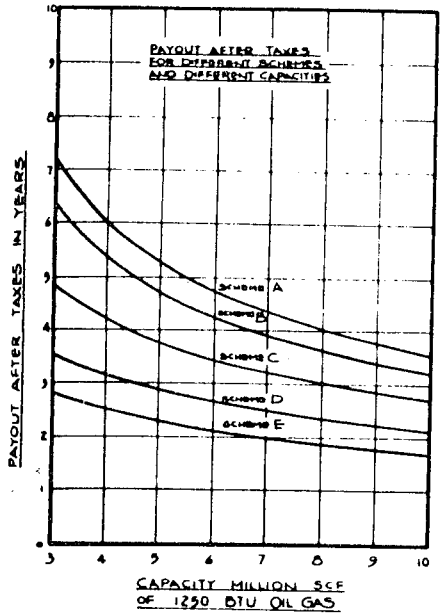
PAYOUT AFTER TAXES FOR DIFFERENT SCHEMES AND DIFFERENT CAPACITIES
PAYOUT AFTER TAXES IN YEARS
SCHEME A
SCHEME B
SCHEME C
SCHEME D
SCHEME E
CAPACITY MILLION SCF OF 1250 BTU OIL GAS

FIG V

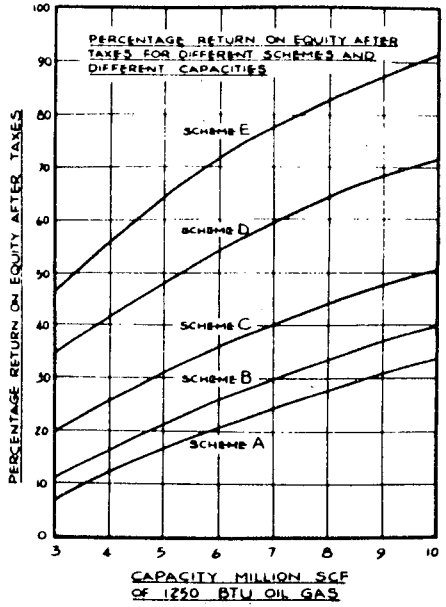
PERCENTAGE RETURN ON EQUITY AFTER TAXES FOR DIFFERENT SCHEMES AND DIFFERENT CAPACITIES
PERCENTAGE RETURN ON EQUITY AFTER TAXES
SCHEME E
SCHEME D
SCHEME C
SCHEME B
SCHEME A
CAPACITY MILLION SCF OF 1250 BTU OIL GAS

FIG VI

Not for Publication

Presented before the Division of Gas and Fuel Chemistry
American Chemical Society

Atlantic City, New Jersey, Meeting, September 13-18, 1959

Hydrogenation of Coals and Chars to Gaseous Hydrocarbons

Raymond W. Hiteshue, Robert B. Anderson, and Sam Friedman
U.S. Department of the Interior, Bureau of Mines, Pittsburgh, Pa.

INTRODUCTION

The hydrogenation of coal is being considered in this country and abroad for production of high B.t.u. gas for meeting peak-load demands of the gas industry and as a method for augmenting future supplies of natural gas. Experiments on the hydrogenation of coal and chars to gaseous products have been investigated by Dent,[3] Channabasappa,[1] and the Bureau of Mines[2] at 500 to 3000 pounds per square inch gauge, 500 to 750°C., with very long residence times. Recently the Bureau of Mines extended these studies[4] to 6000 pounds per square inch gauge and 800°C. with a coal from Rock Springs, Wyoming, using very short residence times. This paper discusses the amenability of other coals and chars to conversion to gaseous hydrocarbons at 6000 pounds per square inch gauge and 800°C.

EXPERIMENTAL PROCEDURE

A flow sheet of the apparatus is shown in figure 1. Hydrogen flowed from a storage vessel into the bottom of the reactor through a preheat zone and into the bed of coal or char. After a constant flow of hydrogen was established, the reactants were heated to 800°C. in 1-1/2 minutes by passing a high current through the tube at points E and E_1. Hydrocarbon vapors and gases and excess hydrogen passed at pressure into a small condenser-receiver where the bulk of the oils were collected in a small glass vial. Noncondensible gases were reduced to atmospheric pressure, passed into a small gasholder, and after an appropriate storage period they were sampled, metered, and finally vented. At the end of an experiment, the reactor and its charge were cooled to room temperature by spraying with cold water. After the bulk of the unreacted solids were removed, the reactor was washed with benzene to remove the remainder of solids and high molecular weight oils. The unreacted solids and benzene washings were filtered and the solids were extracted with benzene in a Soxhlet apparatus. The percentage of coal reacted was then calculated by subtracting the weight percent of unreacted organic solids (organic benzene insolubles) from 100. The filtrate and extract were not analyzed.

Oils which were collected in the condenser-receiver were analyzed semi-quantitatively in a mass spectrometer using a low ionizing voltage technique. Gaseous hydrocarbons in the effluent gas stream were also analyzed by the mass spectrometer.

Yields of oils and hydrocarbon gases were expressed as weight percentages based on moisture- and ash-free coal or char. Total yields on this basis would be larger than 100 by an amount equal to the percentage of hydrogen absorbed based on moisture- and ash-free coal or char.

Studies were made with high-volatile bituminous coals from Pittsburgh, Pennsylvania and Rock Springs, Wyoming, a lignite from Rockdale, Texas, a medium-volatile anthracite from Luzerne County, Pennsylvania, and a char from Rock Springs, Wyoming coal. The char was prepared by heating the coal in helium for 2 hours at 600° C.; it represents the type of material which could be produced commercially by carbonization at low temperatures. Ultimate analyses of the substrates are shown in table 1. The coals and char were all pulverized and screened to 30 x 60 mesh. Ammonium molybdate was added[5/] to a weight of water 1.3 times the weight of coal or char to provide 1 percent molybdenum on the substrate. After standing for 5 minutes, the solution was added to the substrate and concentrated by evaporating on a hot plate with constant stirring at 100°C. The mixture was finally dried on a tray in air at 70° C. for 20 hours.

Experiments were conducted at 6000 pounds per square inch gauge and 800° C. and residence times of zero to 15 minutes. Zero residence time is defined as the time at which the coal attains reaction temperature. Flow of hydrogen was 100 standard cubic feet per hour, corresponding to a nominal linear velocity at pressure and temperature of 0.5 foot per second. In all cases, this rate of flow was sufficient to absorb the heat of reaction and thus maintain adequate control of temperatures.

RESULTS

Conversions of coal and char to gases and liquids are shown in figure 2. Bituminous coal and lignite were more readily hydrogenated than the char and anthracite. This observation is reasonable because of the less condensed structures of lower rank coals. Increase in residence time from "0" to 15 minutes resulted in an increase in conversion for Texas lignite from 90 to 97 percent, based on moisture- and ash-free feed, and an increase in conversion with the bituminous coals from 75 to about 90 percent. Although conversions for char and anthracite were low at "0" time, they increased to 67 and 53 percent, respectively, during the first three minutes and at the end of 15 minutes the conversion of char and anthracite amounted to 84 and 65 percent, respectively.

The carbonaceous residues remaining in the reactor from bituminous coals and lignite were agglomerated, whereas, residues from char and anthracite were free-flowing. Agglomeration was less severe with Texas lignite than with bituminous coals.

Yields of oil from bituminous coals and lignite were independent of residence time. Virtually no oils were produced from char or anthracite. As shown in figure 3, yields from Texas lignite, Rock Springs, Wyoming and Pittsburgh coals were 32, 26, and 20 percent, based on moisture- and ash-free coal, respectively. As yields of oil

did not increase with increase in retention time, it appears that the bulk of the oils were formed during heating to 800° C. Past experiments have shown that the formation of oil begins at about 400° C., increases rapidly as the coal is heated to 525° C., and from there on decreases because of cracking reactions.

About 90 percent of the oil was collected as overhead material in the condenser-receiver, the remainder condensed in the connecting piping between the reactor and the receiver. Overhead oils produced from bituminous coals and lignite boiled below 300° C. and contained less than 4 percent asphaltenes. Table 2 shows the various compounds in the overhead product which were identified by mass spectrometer. It is believed that oils produced from Pittsburgh coal contained the highest quantity of alkyl benzenes and naphthalene.

Yields of gaseous products as a function of residence time are shown in figure 4. The highest yields of gases were obtained with char, followed by anthracite, Pittsburgh-seam coal, Rock Springs, Wyoming, coal, and Texas lignite. The yield of gaseous hydrocarbons at the end of 15 minutes from char was about 94 percent and the yield from Texas lignite or Rock Springs coal was about 67 to 70 percent, based on moisture- and ash-free feed. In all cases, the formation of gaseous hydrocarbons increased very rapidly during the first three minutes, and from there on the rate was smaller and approximately constant.

Methane in the gaseous products increased and C_2 and C_3 hydrocarbons decreased with increasing rank or carbon content of the substrates. Composition of gaseous products did not vary with residence time. Average compositions of the gases are shown below:

	Composition, volume-percent			Heating value, B.t.u.'s per standard cubic foot of hydrocarbons
	C_1	C_2	C_3	
Texas lignite	82	15	3	1170
Wyoming coal	88	10	2	1110
Pittsburgh coal	90	9	1	1085
Anthracite	92	7	1	1090
Char	92	8	-	1045

As the flow of hydrogen was high in these experiments, the concentration of hydrocarbon gases in the effluent stream was only 2 to 4 percent. If coal was hydrogenated in a continuous unit at high partial pressures of hydrogen, the effluent gases would be recycled and the gaseous products could be removed by scrubbing with an appropriate solvent. As some hydrogen would also be removed by scrubbing, it would probably be necessary to use a low-temperature fractionation system to enrich the product sufficiently to meet specifications for commercial fuels. In this apparatus, product distribution is affected by retention time of the volatile products as well as pressure, temperature, and residence time of the coal. The effect of increasing retention time of volatiles from 6 to 30 seconds by reducing flow of hydrogen from 100 standard cubic foot per hour to 20 standard cubic foot per hour is shown in figure 5

for Rock Springs, Wyoming coal. Increase in retention time of volatiles resulted in a significant increase in yield of gaseous products and a very substantial decrease in yields of liquid hydrocarbons. For example, an increase in retention time of the volatiles from 6 to 30 seconds resulted in increasing the yield of gaseous products from 70 to 82 percent and in decreasing the yield of oil from 26 to 4-1/2 percent, based on moisture- and ash-free coal. In addition, the oil was transformed from a relatively high molecular weight product to a low-boiling material very high in benzene and naphthalene. Similar results would probably be obtained with other ranks of coal. Further increase in retention time of volatiles would probably result in production of only gaseous hydrocarbons from coal.

It was not possible to hydrogenate char or anthracite at 800° C. and 6000 pounds per square inch gauge at the lower (20 standard cubic feet per hour) flow rates of hydrogen because of uncontrolled temperatures. Under these conditions, temperatures increased to over 1000° C. and as a result, the reactor ruptured. Uncontrolled temperatures did not occur with bituminous coals and lignite under identical conditions. This overheating may be related to the type of reactions which took place. It is believed that coal, when heated rapidly to 800° C., first undergoes thermal decomposition with simultaneous hydrogenation of reactive fragments to produce oil, gaseous hydrocarbons, and a carbonaceous residue. As temperatures increase, thermal cracking of oils takes place with production of additional hydrocarbon gases and residue. Residues remaining at 800° C. are then slowly hydrogenated to gaseous hydrocarbons. Reactions are much different with char or anthracite, as only hydrogenation to gaseous hydrocarbons occurs. Thus, reactions with bituminous coals or lignite are partly endothermic and exothermic, whereas, all of the reactions with char or anthracite are exothermic. With char or anthracite, the rate of heat release is sufficiently high to cause overheating. When char was mixed with equal weights of asphaltenes or heavy oil, overheating did not occur. In this case, endothermic reactions associated with thermal decomposition of these high molecular weight materials probably absorbed sufficient heat from the exothermic reactions to prevent overheating. Overheating with char or anthracite at the lower flow rates (20 standard cubic feet per hour) of hydrogen could also be prevented by dispersing the materials in a bed of sand. No overheating occured with char or anthracite at high flow rates (100 standard cubic feet per hour) of hydrogen. It is of interest to point out that a natural graphite from Madagascar did not react at 800° C. and 6000 pounds per square inch gauge.

Literature Cited

1/ Channabasappa, K.C., and Linden, H.R., Ind. Eng. Chem., 48, 900-5 (1956).

2/ Clark, E.L., Pelipetz, M.G., Storch, H.H., Weller, S., and Schreiber, S., Ind. Eng. Chem., 42, 861-5 (1950).

3/ Dent, F.J., "Production of Gaseous Hydrocarbons by the Hydrogenation of Coal," Gas Research Board, Communication GRB 13, London, England, 1944.

4/ Hiteshue, R.W., Anderson, R.B., and Schlesinger, M.D., Ind. Eng. Chem., 49, 2008-10 (1957).

5/ Weller, S., and Pelipetz, M.G., Ind. Eng. Chem., 43, 1243 (1951).

Table 1. Ultimate analyses of substrates

	Moisture	Ash	Carbon	Hydrogen	Nitrogen	Sulfur	Oxygen*
	As received, percent						
Texas lignite	2.3	17.4	54.8	4.4	1.2	1.9	18.0
Wyoming coal	0.6	1.9	75.1	5.4	1.8	0.7	14.5
Pittsburgh coal	0.6	8.6	73.9	5.0	1.7	1.5	8.7
Anthracite	0.1	9.3	83.6	2.4	0.3	0.9	3.4
Wyoming char	0.6	2.9	87.9	2.2	1.9	0.6	3.9
			Moisture- and ash-free, percent				
Texas lignite			68.2	5.5	1.5	2.4	22.4
Wyoming coal			77.0	5.5	1.8	0.8	14.9
Pittsburgh coal			81.4	5.5	1.9	1.6	9.6
Anthracite			92.3	2.6	0.3	1.0	3.8
Wyoming char			91.1	2.3	2.0	0.6	4.0

* By difference.

Table 2. Analyses of Overhead Oils

Compound type	Molecular weight
Alkyl benzenes	78-190
Phenylnaphthalenes	204-288
Phenols	94-164
Phenanthrenes-Anthracenes	178-290
Fluorenes	166-278
Acenaphthenes-Biphenyls	154-238
Benzopyrenes-Perylenes	252-294
Naphthalenes	128-240
Binaphthyls	254-296
Indenes	116-130
Naphthols	144-214
Chrysenes	228-298
Indans	118-188
Pyrenes	202-300

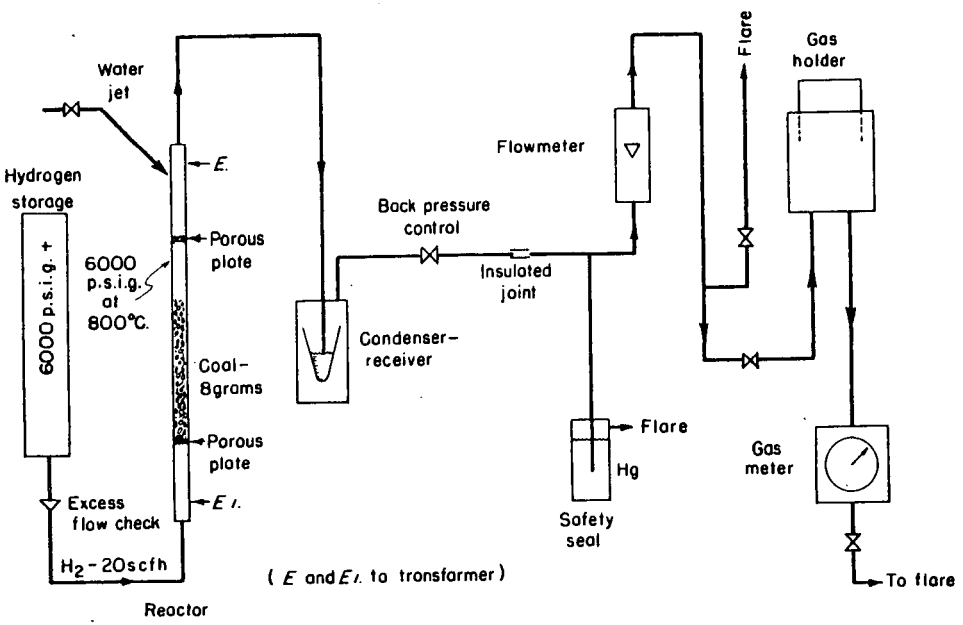

Figure 1.-Semi-continuous unit for the hydrogenation of dry coal.

L-4752

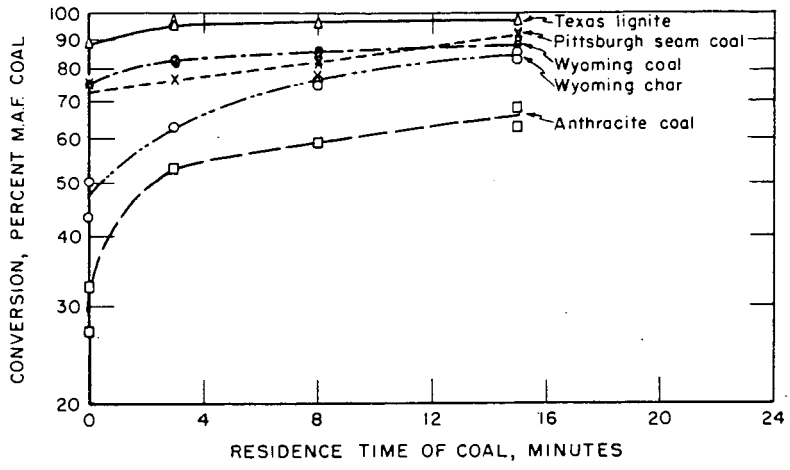

Figure 2. - Effect of residence time on conversion.

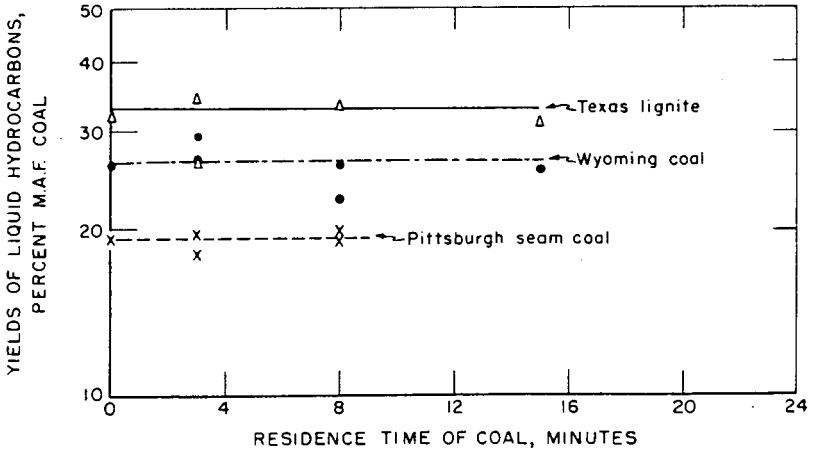

Figure 3.- Effect of residence time on yield of liquid hydrocarbons.

L-5812
5-20-59

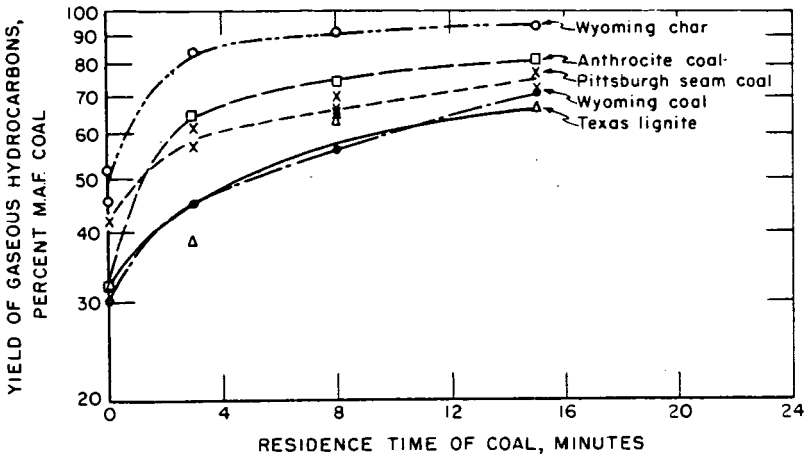

Figure 4. - Effect of residence time on yield of gaseous hydrocarbons.

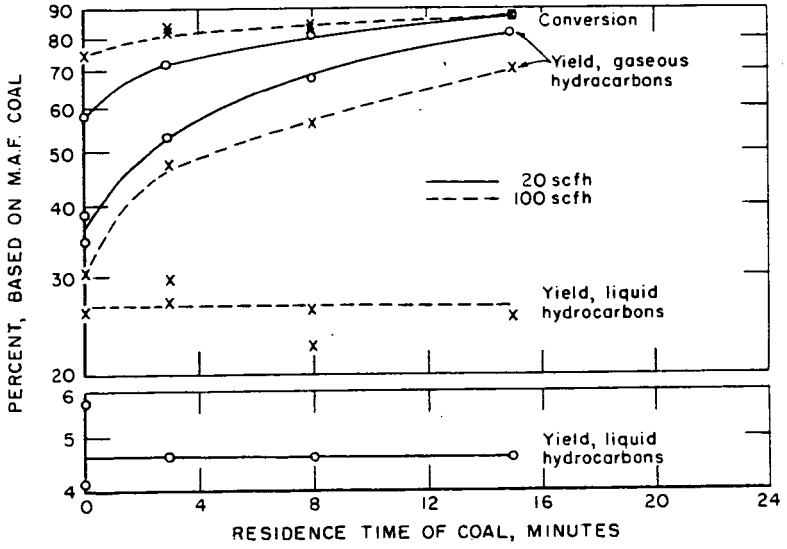

Figure 5. - Effect of residence time on product distribution for Wyoming coal at two gas rates.

L-5813
5-20-59

NOT FOR PUBLICATION
Presented Before the Division of Gas and Fuel Chemistry
American Chemical Society

Atlantic City, New Jersey, Meeting, September 13-18, 1959

PRODUCTION OF NATURAL GAS SUBSTITUTES BY CONTINUOUS PRESSURE HYDROGENOLYSIS OF PETROLEUM OILS

E. B. Shultz, Jr., N. Mechales and H. R. Linden
Institute of Gas Technology
Chicago, Illinois

High-pressure hydrogasification is a vapor-phase, thermal hydrogenolysis process for nearly complete conversion of distillate, crude and residual petroleum oils to fuel gases of high methane content. The required hydrogen supply may be generated by catalytic steam reforming of a portion of the product gas,[5,10] or by partial oxidation of fresh or byproduct oil streams.[4]

Studies by Dent and others[1,3,6] of the effects of operating variables and feedstock properties on the yield and composition of products of high-pressure hydrogasification have been directed primarily to the development of a process for producing gases of 500-600 B.t.u./SCF (SCF refers to standard cubic feet measured at 60°F., 30 inches of mercury absolute pressure, and saturated with water vapor). Work done at the Institute of Gas Technology[11,13] has been in the range of operating conditions suitable for production of high-heating-value natural gas substitutes.

Gases of about 900 B.t.u./SCF are best produced at hydrogen to oil feed ratios corresponding approximately to the stoichiometric requirements for methane formation. Lower feed ratios result in excessive liquid products formation and carbon deposition, and higher feed ratios result in excessive hydrogen dilution. High-heating-value gas production is also favored by high pressures and long residence times. Typical operating conditions for a flow reactor are 1400°F. maximum temperature, 1500 p.s.i.g., and residence times ranging from about 100 seconds for paraffinic oils to several hundred seconds for the less reactive, higher C/H weight ratio oils; under these conditions, only about 10 wt. % of the feedstock is converted to liquid products consisting of low-boiling aromatic hydrocarbons. In low-heating-value gas production, substantially lower pressures and residence times, and higher temperatures and hydrogen feed ratios, can be employed.[3]

The major problem in operation of high-pressure hydrogasification processes is control of carbon deposition. The two continuous processes currently being developed for fluid feedstocks use different methods of overcoming the normal carbon-forming tendencies of crude and residual oils during hydrogenolysis. The British Gas Council[1,3,6] has used a fluidized coke bed reactor to handle carbon laydown of somewhat less than one-half of the Conradson carbon residue of the feedstock. In the work described here, crude or residual oils were first subjected to a pretreatment step essentially equivalent to many of the hydrocracking processes now under development.[2,8,15] Pretreatment over commercial cobalt molybdate hydrogenation catalyst at 850°F. and 1500 p.s.i.g., converted these feeds to products with either negligible or greatly reduced Conradson carbon residue, and with substantially lower C/H weight ratio. When complete conversion into a distillate product was not possible, the higher-boiling fractions containing the carbon-forming constituents were separated before charging to the hydrogasification reactor.

APPARATUS AND PROCEDURE

The apparatus comprised hydrogen and oil feed systems, prehydrogenation and hydrogasification reactors, product liquid recovery sections and a product gas metering system. A flow sheet has been presented in a preliminary study.[13]

Hydrogen was fed from storage cylinders, replenished at intervals by compression of commercial-grade cylinder hydrogen. Oil was fed from a weigh vessel through a reciprocating proportioning pump. In all runs, oil and hydrogen were mixed and introduced at room temperature.

The downflow prehydrogenator for crude and residual oil pretreatment was constructed of Type 316 stainless steel. It was 5-3/4 inches in outside diameter, 3 inches in inside diameter, and 40 inches in inside length, and was equipped at both ends with Autoclave Engineers self-sealing closures. A thermowell, 3/8 inch in outside diameter, extended concentrically into the reactor. In some runs, the prehydrogenator inside diameter was reduced to 2 inches by insertion of a stainless steel sleeve, 35 inches in length.

When the full volume of the prehydrogenator was employed, the reactants were passed through a 19-inch preheat zone of 3/8-inch diameter periclase spheres before entering the 16-inch catalyst bed, composed of equal volumes of 1/8-inch tablets of a commercial cobalt molybdate on alumina catalyst and 1/8-inch fused alumina pellets, randomly mixed. When the sleeve was used, a 20-inch catalyst bed composed of undiluted 1/8-inch cobalt molybdate tablets was located in the center of the reactor above a 9-inch zone filled with 3/8-inch diameter periclase spheres. The reported feed oil space velocity for diluted catalyst was based on the sum of the volumes of catalyst and fused alumina charged (0.0353 cu.ft. each); for undiluted catalyst, it was based on a catalyst charge volume of 0.0353 cu.ft.

The downflow hydrogasifier was constructed of 19-9DL alloy. It was 6 inches in outside diameter, 3 inches in inside diameter, and 35 inches in inside length. A 3/8-inch diameter thermowell extended into the reaction zone. The vessel was equipped at the top with an Autoclave Engineers self-sealing closure; the bottom consisted of an integral water-cooled tailpiece, which was sealed with a simple gasketed closure. In some of the tests, a sleeve similar to the one used in the prehydrogenator was inserted to reduce the inside diameter to 2 inches. For both the prehydrogenator and hydrogasifier, high-pressure condenser-separators were provided, from which gases were continuously recovered and liquids intermittently removed.

A 100 cu.ft./hr. wet-test meter was used to measure product gas flow rates. A proportional sample of product gas was collected in a water-sealed holder for analysis.

Reactor temperatures were sensed by Chromel-Alumel thermocouples, and pressures by Bourdon tube gages. Temperatures were measured and recorded by means of a potentiometer strip-chart; reactor and orifice pressures were also recorded.

In initial tests, the prehydrogenator and hydrogasifier were operated simultaneously, with the entire effluent from the prehydrogenation step passing to the hydrogasifier. However, the periods of adequate catalyst performance at the high temperatures required for complete removal of carbon-forming materials from residual and low-grade crude oils were limited by catalyst carbon deposition. Consequently, it appeared more practical to operate the prehydrogenator at less severe conditions, and to separate any high-boiling, asphaltene-containing materials from the hydrogasifier feed. This was simulated by pre-

hydrogenation, distillation of the liquid products, and hydrogasification of the 0°-360°C. fraction. The hydrogen to oil feed ratio to the hydrogasifier was adjusted to account for the hydrogen consumed in prehydrogenation.

Product gases, and 0°-160°C. fractions of product liquids, were analyzed with a Consolidated Engineering Co. Model 21-103 mass spectrometer. Other analyses were conducted in accordance with standard ASTM methods, with the following exceptions: prehydrogenator product liquid 500-gram distillations were carried out at atmospheric pressure using a procedure similar to ASTM Method D1160-56T;[14] carbon and hydrogen ultimate analyses were made by combustion train, with the Grace and Gauger modification[7] of ASTM Method D271-44.

Specific gravities and ideal gas heating values were calculated from gas analyses. Feed and product gas volumes and heating values were calculated at conditions of 60°F., 30 inches of 32°F. mercury absolute pressure, saturated with water vapor. Specific gravities were computed from the average molecular weight of the dry gas, and were based on air of molecular weight 28.97.

PROCESS CHARACTERISTICS

Selected prehydrogenation and hydrogasification results for typical feedstocks are shown in Tables 1-3 to illustrate the characteristics of the process under the preferred operating conditions. The premium feedstocks, kerosine and diesel oil, required no pretreatment before hydrogasification. The properties of Aruba reduced crude were sufficiently improved by prehydrogenation to permit use of the total product oil as hydrogasification charge stock. The relatively low-grade Taparito crude oil still had a substantial Conradson carbon residue after prehydrogenation, so that only the 0°-360°C. distillate fraction was used as hydrogasification charge stock. Recycle of the residue fraction to effect further conversion to distillate was found to be practical. Prehydrogenation results for Boscan crude oil are also shown to illustrate that, after fractionation, an acceptable hydrogasification charging stock could be obtained from a crude oil feedstock typical of the lowest grade suitable for the process. The prehydrogenation conditions used in obtaining the data of Table 2 were determined to give practical on-stream periods of the commercial catalyst used.

Table 3 shows the hydrogasification results of the distillate and prehydrogenated oils at about 1400°F. maximum reaction temperature and hydrogen to oil feed ratios corresponding to the stoichiometric requirements for methane formation. The distillate oils, and the 0°-360°C. fraction of the prehydrogenated Taparito crude oil, did not give carbon deposition in the hydrogasifier; the prehydrogenated Aruba reduced crude charge, which had a Conradson carbon residue of 0.41 wt. %, did give a small carbon deposit. This suggests that even small amounts of objectionable high-boiling fractions in the prehydrogenated oil should be removed to ensure carbon-free hydrogasifier operation.

Because of the high reactivity associated with its low C/H weight ratio, kerosine gave results comparable to those of the other feedstocks at considerably less severe conditions; kerosine produced approximately 900 B.t.u./SCF gas of high methane-plus-ethane content at 500 p.s.i.g. and approximately 50 seconds residence time, whereas the other feedstocks required a pressure of 1500 p.s.i.g. at a residence time of approximately 300 seconds. The relatively high ethane content of the product gas from kerosine is typical of operation at comparatively short residence times with paraffinic (low C/H weight ratio) charging

Table 1.-PROPERTIES OF DISTILLATE OIL FEEDSTOCKS

Feed oil designation	Kerosine	Diesel Oil
Specific gravity		
60°F./60°F.	0.805	0.838
°API	44.2	37.3
Viscosity, centistokes at 100°F.	n.d.	2.862
Ultimate analysis, wt. %		
Carbon	85.88	86.27
Hydrogen	14.05	13.50
Sulfur	0.04	0.30
Ash	n.d.	0.000
Carbon/hydrogen wt. ratio	6.11	6.39
Distillation (ASTM D158-41), °F.		
Initial boiling point	349	382
10%	384	452
20%	396	470
30%	406	486
40%	413	497
50%	421	507
60%	429	520
70%	439	536
80%	450	554
90%	470	580
End point	518	639
Distillation residue and loss, %	2	2
Heat of combustion, B.t.u./lb.[a]	19960	19730

[a]Estimated from Reference 9.

Table 2.-PREHYDROGENATION OF CRUDE AND RESIDUAL OILS

Feed oil designation	Aruba Reduced Crude		Taparito Crude			Boscan Crude	
Run No.	71		80			100	
Prehydrogenation conditions							
Maximum temp., °F.	850		850			845	
Average catalyst bed temp., °F.	835		825			810	
Pressure, p.s.i.g.	1500		1500			1500	
Feed ratio, SCF H_2/lb.	31.59		32.96			31.98	
Feed oil space velocity, cu.ft. oil/cu.ft. catalyst bed-hr.	0.87[a]		0.42[b]			0.42[b]	
Prehydrogenator off-gas							
Wt. % of carbon in feed	5.8		4.6			5.0	
Composition, mole %							
N_2 + CO + CO_2	0.5		0.4			0.3	
H_2	97.2		97.7			97.7	
CH_4	1.1		0.7			0.9	
Higher paraffins	1.0		1.0			1.0	
Olefins	0.2		0.2			0.1	
Total	100.0		100.0			100.0	
Catalyst carbon, wt. % of carbon in feed	n.d.		0.86			0.94	
Oil properties	Feed	Total Product[c]	Feed	Total Product	0°-360°C. Fraction[d]	Feed	Total Product
Specific gravity 60°F./60°F.	0.925	0.851	0.948	0.888	0.842	1.003	0.894
°API	21.5	34.8	17.8	27.8	36.5	9.6	26.7
Viscosity, S.S.U. at 122°F.	203	34.8	66.0[e]	106.0	32.6	3084[e]	95.5
Ultimate analysis, wt. %							
Carbon	84.88	86.17	84.90	85.55	86.22	81.64	86.39
Hydrogen	11.73	12.55	11.38	12.02	13.00	10.52	12.57
Sulfur	1.62	0.20	1.56	1.01	0.19	5.40	1.58
Ash	0.05	n.d.	0.07	0.03	trace	0.24	0.08
Carbon/hydrogen wt. ratio	7.24	6.87[f]	7.46	7.12[f]	6.63	7.76	6.98
Conradson carbon residue, wt. %	7.4	0.41[f]	9.1	4.3[f]	0.0	14.9	5.0
Distillation, wt. %							
0°-160°C.	1.1	8.4	2.7	6.7	16.5	1.7	7.9
160°-200°C.	1.1	8.4	2.4	6.5	12.8	2.1	6.7
200°-300°C.	25.5	40.4	12.9	25.0	43.0	16.1	22.0
300°C.-end point	12.3	20.6	7.2	15.0	21.4	--	11.8
Residue and loss	60.0	22.2	74.8	46.8	6.3	80.1	51.6
End point, °C.	355	332[g]	320	341[g]	363	300	333[g]
Heat of combustion, B.t.u./lb.[h]	19120	19370	18980	19200	19540	18810	19290

[a] Catalyst bed consisted of 0.0353 cu.ft. undiluted cobalt molybdate catalyst.

[b] Catalyst bed consisted of 0.0353 cu.ft. cobalt molybdate and 0.0353 cu.ft. fused alumina pellets, randomly mixed.

[c] Feedstock for hydrogasification Run No. 72.

[d] Feedstock for hydrogasification Run No. 89 - composite of 0°-360°C. fractions of product oils from four prehydrogenation tests at 850°F.

[e] S.S.F. at 122°F.

[f] Calculated from value for residue fraction.

[g] Obtained at 400°C. pot temperature.

[h] Estimated from Reference 9.

Table 3.-HYDROGASIFICATION OF DISTILLATE OILS AND PREHYDROGENATED CRUDE AND RESIDUAL OILS

Feed oil designation	Kerosine	Diesel Oil	Total Prehydrogenated Aruba Reduced Crude	0°-360°C. Fraction of Prehydrogenated Taparito Crude
Run No.	62A	33-C	72	89
Oil rate, lb. C/hr.	3.06	1.50	1.51	1.50
Hydrogen feed ratio				
% of stoichiometric[a]	98.0	99.9	99.5	100.3
SCF/lb.	27.67	29.51	31.13	30.54
Pressure, p.s.i.g.	500	1500	1500	1500
Temperature, °F.				
Average[b]	1325	1335	1355	1305[c]
Maximum	1400	1395	1405	1395
Residence time, sec.[d]	51.0	301	304	319
Hydrogen consumption, SCF/lb.	16.2	22.3	23.9	22.6
Product recovery, wt. % of oil + hydrogen fed	103.5	101.7	99.0	97.2
Product distribution, %				
Gas	88.9	93.2	91.1	91.0
Liquid	11.1	6.8	8.7	9.0
Carbon	nil	nil	0.2	nil
Product gas yield,				
SCF/lb.	29.58	30.19	29.20	29.28
SCF/cu.ft. reactor-hr.	726.9	362.8	353.1	354.2
Net thermal recovery, %[e]	90.4	88.9	80.1	80.1
Product gas properties				
Composition, mole %				
$N_2 + CO + CO_2$	0.8	0.4	1.2	0.4
H_2	38.8	23.8	24.7	27.2
CH_4	40.5	69.7	69.7	66.2
C_2H_6	17.1	5.3	3.4	5.4
C_3H_8	0.4	--	--	0.1
1-Butane	0.1	--	--	--
Olefins	1.0	0.1	--	--
Benzene	1.2	0.7	1.0	0.7
Toluene	0.1	--	--	--
Total	100.0	100.0	100.0	100.0
Heating value, B.t.u./SCF	909	893	872	868
Specific gravity (air = 1)	0.495	0.482	0.478	0.466

[a] Stoichiometric for complete conversion of C + H in feed oil to methane.

[b] Based on average of temperatures measured at centers of three equal zones.

[c] Interpolated value.

[d] Based on dry product gas volume at reactor pressure and average temperature.

[e] $\frac{\text{Heat of combustion of product gas - heat of combustion of feed hydrogen}}{\text{heat of combustion of feed oil}} \times 100.$

stocks. The conditions employed for diesel oil, also a highly reactive material, are somewhat more severe than required for production of a natural gas substitute; satisfactory results have been obtained at approximately twice the feed rate (one-half the residence time) than that employed in the test reported in Table 3.

Liquid product formation was on the order of 10 wt. % of the feedstock, and tended to increase with the C/H weight ratio of the feedstock at comparable operating conditions. The conversion efficiency of the process is indicated by net thermal recoveries of approximately 80 to 90% under the typical process conditions of Table 3; this parameter is a measure of the fraction of the heat of combustion in the feedstock which is recovered in the product gas.

EFFECTS OF PROCESS VARIABLES

The most effective control over hydrogasification product distribution can be exerted with the hydrogen to oil feed ratio. Table 4 shows that an increase in hydrogen feed ratio from 50 to 100% of stoichiometric reduced carbon formation from diesel oil from about 12% of the total weight of oil and hydrogen fed, to essentially zero; this was accompanied by a significant decrease in liquid products formation. Conversion to gas increased correspondingly. The gaseous product distribution (Figure 1) also changed considerably as 100% of stoichiometric feed ratio was approached, showing an abrupt increase in hydrogen breakthrough and a more gradual increase in ethane yield.

At 50% of stoichiometric feed ratio, there was little change in gaseous product distribution with increases in reactor pressure since the equimolar methane-ethane-hydrogen system was close to equilibrium at the long residence times employed. At 75 and 100% of stoichiometric feed ratio, the high ethane yields characteristic of aliphatic and alicyclic hydrocarbon hydrogenolysis systems were obtained,[12] and the hydrogen utilized for methane formation increased considerably with increases in pressure and corresponding increases in residence time.

The above results reflect the transition from control by pyrolysis reactions at the lowest feed ratio, to control by hydrogenolysis reactions at the highest feed ratio. The liquid products also reflect this transition. The proportion of benzene in the liquid products increased greatly with feed ratio, while the proportion of higher-boiling aromatics was greatly reduced.

Figure 2 correlates gaseous product yields from diesel oil with residence time, at approximately 100% of stoichiometric feed ratio. It can be seen that at residence times sufficient for completion of the primary gasification reactions as indicated by nearly constant net gasification (weight of product gas less weight of feed hydrogen, both per unit weight of feed oil), the gaseous product distribution was not affected by pressure over the 500-1500 p.s.i.g. range. This is characteristic of operating conditions where gas composition is primarily determined by the secondary, low molecular weight paraffin hydrogenolysis reactions: $C_n H_{2n+2} + H_2 \longrightarrow CH_4 + C_{n-1} H_{2n}$, which appear to be pressure insensitive.

Further insight into the nature of the hydrogenolysis reactions can be gained from the data of Table 5 on the effect of temperature on conversion of the 0°-300°C. fraction of prehydrogenated Taparito crude oil. Stoichiometric hydrogen feed ratio and 1500 p.s.i.g. were employed, and the diameter of the hydrogasifier was reduced to 2 inches to permit better temperature control over a 1100°-1400°F. range at four-fold variations in oil feed rate. Feedstock conversion to gas increased greatly with increases in temperature, and increased only slightly with increases in residence time. Low conversions to gas were accompanied by corresponding increases in liquid products and substantially lower

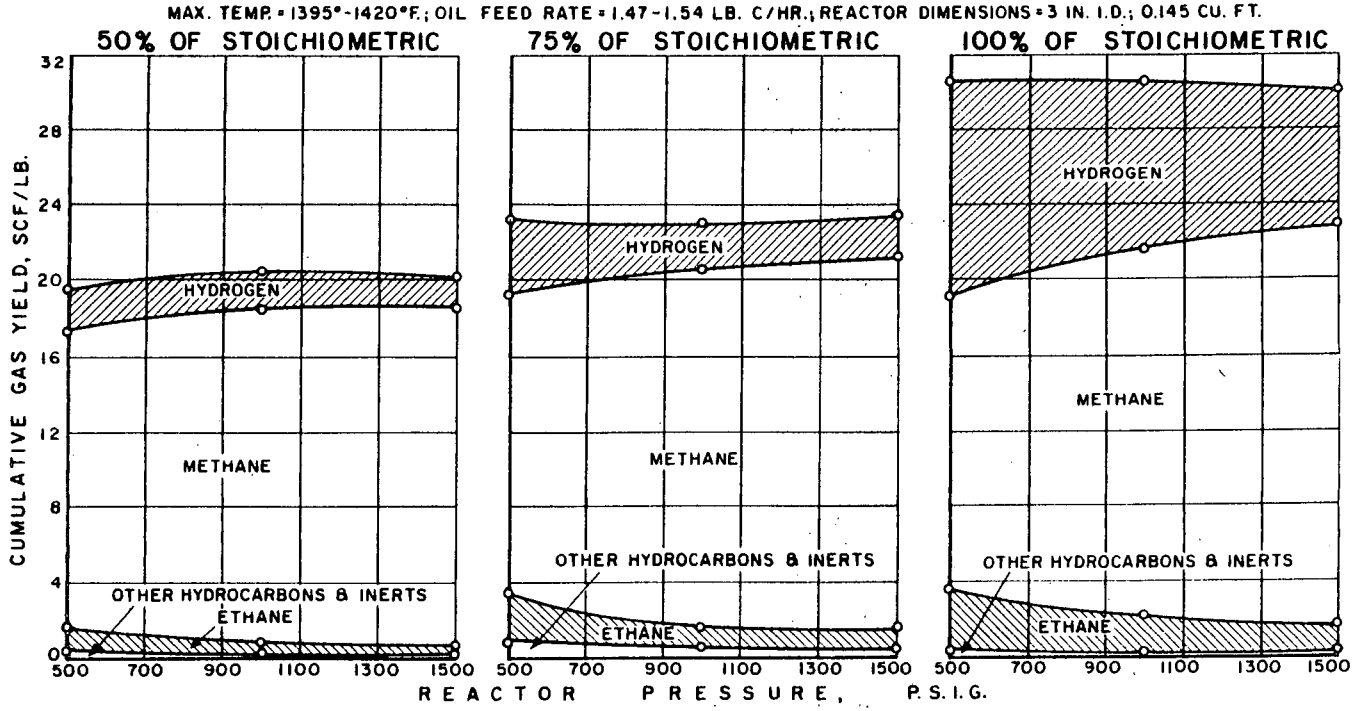

Figure 1.-EFFECTS OF HYDROGEN FEED RATIO AND PRESSURE ON GASEOUS PRODUCT YIELDS FROM DIESEL OIL

Table 4.-EFFECTS OF HYDROGEN FEED RATIO AND PRESSURE ON HYDROGASIFICATION OF DIESEL OIL

Max. Temp.: 1395°-1420°F. Oil Feed Rate: 1.47-1.54 lb. C/hr.
Reactor Dimensions: 3 in. Inside Diameter, 0.145 cu.ft.

Pressure, p.s.i.g.	500			1000			1500		
Hydrogen feed ratio, % of stoichiometric	50.0	75.0	100.1	51.6	73.2	100.4	49.7	73.7	99.9
Residence time, sec.	153	131	99.5	298	254	196	443	375	301
Product distribution, %									
Gas	72.3	86.7	90.4	76.2	86.5	90.8	76.6	88.5	93.2
Liquid	15.9	12.1	9.6	11.5	12.2	9.2	11.2	9.7	6.8
Carbon	11.8	1.2	nil	12.3	1.3	nil	12.2	1.8	nil
Product liquid properties									
0°-160°C. fraction									
Wt. % of total	45.6	54.9	62.4	52.8	54.2	75.4	49.1	58.5	82.4
Benzene content, mole %	81.8	83.2	89.8	84.2	83.1	92.4	85.6	84.2	94.8
160°C.-plus fraction									
Wt. % of total	53.1	44.4	36.6	46.1	45.1	23.4	49.9	40.4	16.5
C/H wt. ratio	16.19	15.05	14.49	16.16	16.10	14.98	16.01	16.11	14.87

Table 5.-EFFECTS OF REACTOR TEMPERATURE AND OIL FEED RATE ON HYDROGASIFICATION OF 0°-360°C. FRACTION OF PREHYDROGENATED TAPARITO CRUDE

Feed Ratio: 98.0-102.5% of stoichiometric. Pressure: 1500 p.s.i.g.
Reactor Dimensions: 2 in. Inside Diameter, 0.0644 cu.ft.

Feed rate, lb. C/hr.	1.33			0.67			0.34		
Residence time, sec.	150-180			290-350			620-750		
Maximum temperature, °F.	1100	1300	1400	1100	1300	1400	1100	1300	1400
Product distribution, %									
Gas	75.2	86.2	89.9	75.1	87.1	91.9	79.1	89.2	92.3
Liquid	24.8	13.8	10.1	24.9	12.9	8.1	20.9	10.8	7.7
Carbon	nil	nil	nil	nil	nil	nil	nil	nil	nil
Gaseous product yields, SCF/lb.									
H_2	21.8	14.3	9.7	20.9	14.3	9.1	17.3	10.6	6.2
CH_4	4.1	10.9	18.7	5.2	12.7	20.3	5.9	15.0	21.6
C_2H_6	2.7	5.1	1.8	3.3	4.5	1.1	3.7	3.3	0.5
C_3H_8	1.5	0.1	--	1.3	--	--	1.1	--	--
Other	0.7	0.2	0.3	0.4	0.1	0.2	0.2	0.1	0.2
Product liquid properties									
0°-160°C. fraction									
Wt. % of total	41.7	70.1	72.3	49.3	66.4	71.1	59.6	68.6	81.0
Benzene content, mole %	31.7	92.7	94.9	52.2	91.0	94.4	71.5	95.4	94.9
160°C.-plus fraction									
Wt. % of total	56.8	29.2	26.3	49.1	32.3	27.8	37.8	30.4	17.6
C/H wt. ratio	10.66	13.90	15.53	11.96	13.94	15.74	14.58	15.83	15.60

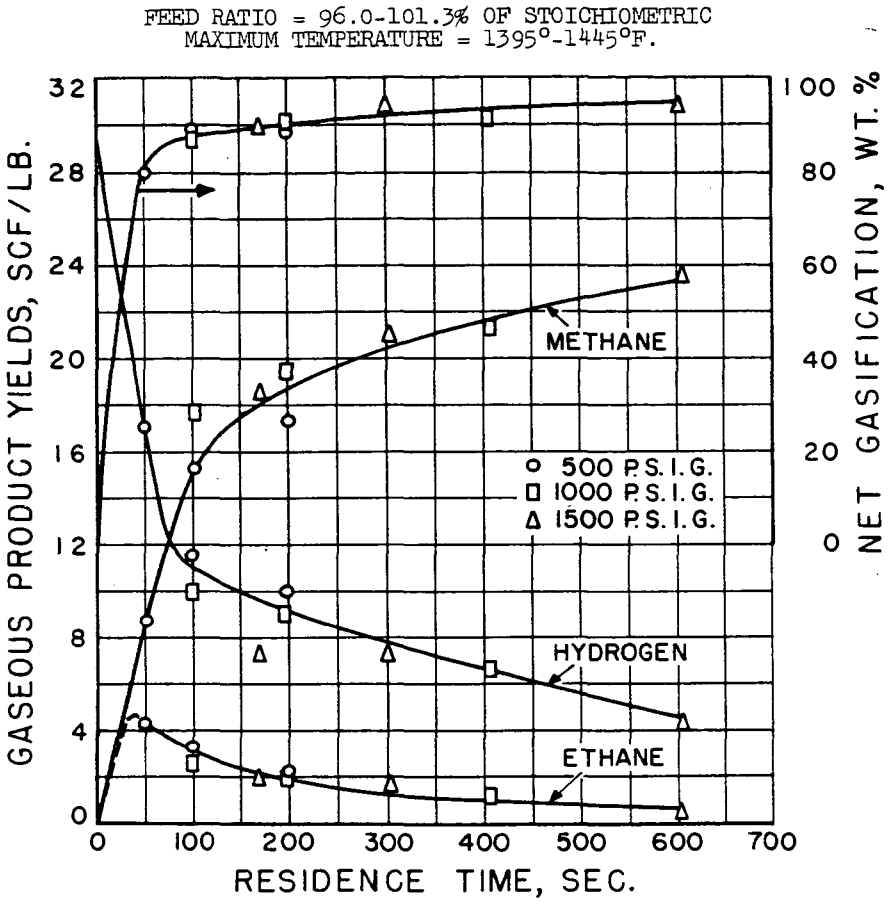

Figure 2.-EFFECTS OF RESIDENCE TIME
ON GASEOUS PRODUCT YIELDS FROM DIESEL OIL

aromaticity of these liquid products. This was particularly evident in the highest feed rate run (shortest residence time) at 1100°F., where a substantial breakthrough of unreacted or partially converted feedstock was indicated by the low C/H weight ratio of the higher-boiling fraction of the liquid products, and the low benzene content of the lower-boiling fraction.

The gaseous product distributions in Table 5 clearly show the sequence of paraffin hydrogenolysis reactions leading to the formation of methane as the ultimate product. At 1100°F., ethane formation was still increasing toward its optimum value with increases in residence time, whereas at 1300° and 1400°F., ethane formation had passed its optimum. At 1100°F., propane formation had also passed its optimum within the range of residence times investigated. These trends are comparable with the results of previous batch reactor tests with low molecular weight paraffin hydrocarbons which indicated that, as temperature is increased, maxima in propane and ethane yields are obtained at approximately 1075° and 1200°F., respectively.[12]

INTEGRAL PROCESS CONCEPTS

Two hydrogen production schemes appear to be feasible for application in an integrated hydrogen production-prehydrogenation-hydrogasification process for conversion of crude and residual oils:

1) Catalytic steam reforming of a portion of the product gas, with reformer fuel requirements supplied by prehydrogenator recycle oil.
2) Partial oxidation (Texaco process[4]) of prehydrogenator recycle oil.

The flow diagrams of Figures 3 and 4, showing material requirements for all streams, are based on the production of 1 million SCF/hr. net pipeline gas from Taparito crude oil. A third integral process concept, not presented, would be autothermic catalytic reforming of product gas with steam and oxygen.

In Figure 3, the process gas feed supply for conventional catalytic steam reforming is provided by an increase in hydrogasification capacity of about 47% above that required for the net product gas yield. Fuel requirements for reforming are supplied with a portion of the prehydrogenator recycle oil.

When partial oxidation of prehydrogenator recycle oil is used for hydrogen production (Figure 4), somewhat less feed oil is required and byproduct aromatics production and prehydrogenation and hydrogasification duties are substantially reduced. Further, compression costs are considerably lower, since less make-up hydrogen and recycle hydrogen are used, and the pressure level of the hydrogen supply is higher (about 400 p.s.i.g. compared to about 100 p.s.i.g. for the reforming scheme). However, 276,000 SCF/hr. of oxygen must be supplied from an external source.

In the computations for Figures 3 and 4, actual data from Runs 80 and 89 (Tables 2 and 3) were employed for the prehydrogenation and hydrogasification steps. Published data for the Texaco partial oxidation step were used.[4] Practical operating feed ratios of 3 moles of steam per mole of carbon to the reforming and shift steps in Figure 3, and 2 moles of steam per mole of CO to the shift step in Figure 4, were employed.[5,10] For simplicity, complete conversion in the reforming and shift steps, and complete removal of CO_2 were assumed. Other assumptions made in these calculations are: saturated steam is available at 200 p.s.i.a. through waste heat recovery; fresh crude oil enters at 77°F.; reforming and preheat furnaces are 75% efficient.

Assuming costs of $2.50/barrel of feed crude oil and $6.00/ton of oxygen, and a crude aromatics byproduct credit of 10 cents/gallon, net

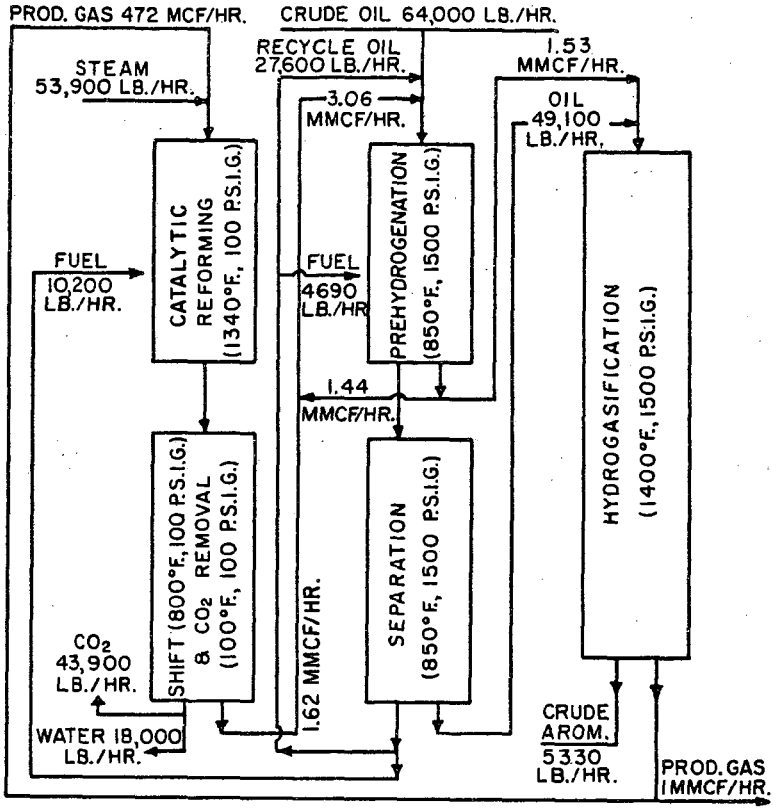

MCF=10^3SCF, MMCF=10^6SCF

In, lb./hr.		Out, lb./hr.	
Oil	64,000	Product Gas	35,000
Steam	53,900	CO_2	43,900
	117,900	Crude Aromatics	5,330
		Oil for Ref. Fuel	10,200
		Oil for Prehydrog. Preheat	4,700
		Water	18,000
		Loss	770
			117,900

Figure 3.-HYDROGEN PRODUCTION BY CATALYTIC STEAM REFORMING OF PRODUCT GAS

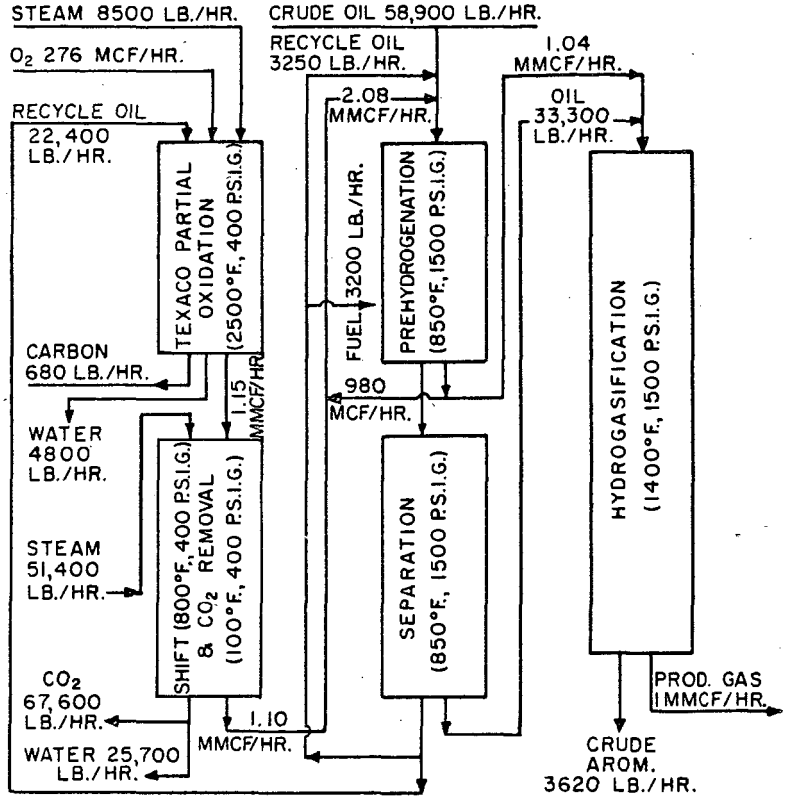

MCF=10^3SCF, MMCF=10^6SCF

In, lb./hr.		Out, lb./hr.	
Oil	58,900	Product Gas	35,000
O_2	22,900	CO_2	67,600
Steam to Texaco	8,500	Crude Aromatics	3,620
Steam to Shift	51,400	Carbon from Texaco	680
	141,700	Water from Texaco	4,800
		Water from Shift	25,700
		Oil for Prehydrog. Preheat	3,200
		Loss	1,100
			141,700

Figure 4.-HYDROGEN PRODUCTION BY PARTIAL OXIDATION OF RECYCLE OIL

material costs of 55 and 60 cents/million B.t.u. net product gas were computed for the schemes of Figures 3 and 4, respectively. No estimate of other operating costs, or of investment costs, can be offered at this time.

ACKNOWLEDGMENT

This study was conducted under sponsorship of the Gas Operations Research Committee of the American Gas Association with the financial support of the Promotion-Advertising-Research Plan of the Association. The guidance and counsel of the Project Supervising Committee under the chairmanship of B. J. Clarke, and of T. L. Robey, N. K. Chaney and Wm. F. Morse, Jr., of the American Gas Association, are gratefully acknowledged. H. L. Feldkirchner, A. E. Richter and R. F. Johnson assisted in the collection of operating data. Analytical work was supervised by D. M. Mason and J. E. Neuzil.

LITERATURE CITED

(1) Chem. Eng. 65, 64, 66, 68 (August 25, 1958).
(2) Cottingham, P. L., White, E. R., Frost, C. M., Ind. Eng. Chem. 49, 679-84 (1957).
(3) Dent, F. J., Edge, R. F., Hebden, D., Wood, F. C., Yarwood, T. A., Gas Council (London) Research Commun. GC 37 (November 1956).
(4) Eastman, DuB., Ind. Eng. Chem. 48, 1118-22 (1956).
(5) Eickmeyer, A. G., Marshall, W. H., Jr., Chem. Eng. Progr. 51, 418-21 (1955).
(6) Gas J. 293, 484 (1958).
(7) Grace, R. J., Gauger, A. W., Ind. Eng. Chem., Anal. Ed. 18, 563-5 (1946).
(8) Gwin, G. T., Heinrich, R. L., Hoffmann, E. J., Manne, R. S., Meyer, H. W. H., Miller, J. R., Thorpe, C. L., Ind. Eng. Chem. 49, 668-72 (1957).
(9) Linden, H. R., in Kirk, R. E., Othmer, D. F., "Encyclopedia of Chemical Technology," vol. 6, pp. 913-35, Interscience Encyclopedia, New York, 1951.
(10) Linden, H. R., Reid, J. M., Petrol. Refiner 35, 189-95 (June 1956).
(11) Shultz, E. B., Jr., Channabasappa, K. C., Linden, H. R., Ind. Eng. Chem. 48, 894-905 (1956).
(12) Shultz, E. B., Jr., Linden, H. R., Ind. Eng. Chem. 49, 2011-6 (1957).
(13) Shultz, E. B., Jr., Linden, H. R., Petrol. Refiner 36, 205-10 (September 1957).
(14) Smith, P. E., master of gas technology thesis, Illinois Institute of Technology, June 1952.
(15) Stevenson, D. H., Heinemann, H., Ind. Eng. Chem. 49, 664-7 (1957).

NOT FOR PUBLICATION
Presented Before the Division of Gas and Fuel Chemistry
American Chemical Society
Atlantic City, New Jersey, Meeting, September 13-18, 1959

PRODUCTION OF PIPELINE GAS BY METHANATION OF SYNTHESIS GAS OVER RANEY NICKEL CATALYSTS

H. A. Dirksen and H. R. Linden
Institute of Gas Technology
Chicago, Illinois

The technically most advanced method for the production of a high-heating-value (pipeline) gas from coal comprises gasification of the coal with steam and oxygen to a low-heating-value synthesis gas, followed by catalytic conversion of the hydrogen and carbon monoxide content of the purified synthesis gas to methane.[1,23] The major effort has been expended on the gasification step because of its wide applicability. Fixed-bed and suspension gasification processes have been developed to a pilot plant scale, [7,11,33,34] and some have been operated successfully on a commercial scale.[15,17,21,36]

The methanation step has also been studied extensively, but much of the work has been concerned with catalyst development and, therefore, has involved small-scale experiments. In studies by the British Fuel Research and Gas Research Boards[3,8-10] the development of fixed- and moving-bed reactors has been stressed. Initially, studies by the U.S. Bureau of Mines [7,35] and the Institute of Gas Technology[23] were also conducted in relatively small fixed-bed reactors. In these investigations, supported nickel catalysts were employed nearly without exception.

The largest-scale fixed-bed methanation data for the production of high-heating-value fuel gas were reported by Dent and Hebden,[8] who achieved near-equilibrium conversion of 3.6:1 H_2/CO ratio synthesis gas for 3500 hours in a 9.5-inch diameter by 10-inch deep catalyst bed at 20 atmospheres, 2000 std. cu. ft./cu.ft. catalyst-hr. fresh feed gas space velocity, and 6:1 recycle ratio. A coimpregnated nickel-alumina-china clay catalyst was employed.

The design of large-scale fixed-bed reactors for essentially complete conversion of hydrogen and carbon monoxide to methane at high throughputs presents difficult engineering problems. Large quantities of exothermic heat of reaction must be removed without causing excessive temperature gradients to occur in the catalyst bed. This requires either complex heat exchange equipment in the catalyst bed when a fluid coolant is used, or the use of high product gas recycle rates. In both instances, the investment and operating costs are high.

Fluid-bed reactors appeared to be better suited for the menthanation process because of the high rates of heat transfer obtainable with relatively simple heat exchange equipment. The ease of addition and withdrawal of catalyst also seemed to be a significant advantage. However, restriction of the possible range of operating conditions by the fluidization characteristics of the solids-gas system employed, and catalyst attrition, were recognized as major problems. Further, scale-up of fluid-bed reactors for synthesis operations was known to be difficult[16] and was not fully demonstrated on a commercial scale until recently.[17,21]

In 1954, the U.S. Bureau of Mines achieved satisfactory fluid-bed operation in a 1-inch diameter reactor with a partially extracted Raney nickel catalyst;[31] attempts to utilize fluid-bed iron catalysts

were not successful, and the performance of supported nickel catalysts was found to be difficult to reproduce.[14] Russian investigators have also reported high conversion capacities of partially extracted Raney nickel catalysts in fluid-bed operation.[4,5] A systematic study of this methanation technique was, therefore, initiated by the Institute of Gas Technology as part of its pipeline-gas-from-coal research program.

EXPERIMENTAL

In all of the work reported here, the catalysts were prepared by caustic leaching of 40-200 mesh Raney alloy with a nominal composition of 42 wt. % nickel and 58 wt. % aluminum.[24,25] Synthesis gas was produced by catalytic steam reforming of natural gas in a tube furnace,[20] or by suspension gasification of coal with steam and oxygen in a slagging downflow pressure reactor.[34] Facilities were also available to increase the H_2/CO ratio of synthesis gas produced from coal from the usual 1:1-1.5:1 range to 3:1 by catalytic conversion of CO with steam to form H_2 and CO_2. In some instances, CO_2 from bottle storage was added to the 3:1 H_2/CO ratio reformed natural gas to simulate the composition of synthesis gas from coal after CO shift and before CO_2 removal.

Except for a limited number of tests of sulfur tolerance, synthesis gas was purified, by passage through fixed beds of iron oxide and activated carbon, to a sulfur content of less than 0.01 grain per 100 SCF (standard cubic foot at 60°F., 30 inches of mercury and saturated with water vapor), and generally to about 0.001 grain per 100 SCF. Details of the analytical procedures for determination and identification of sulfur compounds in synthesis gas have been presented elsewhere.[22,28,32]

Three major methods of operation were employed in the study of fluid-bed methanation of synthesis gas over Raney nickel catalysts:

1. Catalyst evaluation tests and process variable studies in a battery of approximately 1-inch inside diameter Dowtherm-jacketed reactors (Figure 1). The effect of catalyst preparation on initial activity and total methane production capacity was determined with purified synthesis gases of approximately 3:1 H_2/CO ratio, and either negligible or 30 mole % average CO_2 content. Nominal test conditions were: 10,000 SCF/cu.ft. catalyst-hr. space velocity, 75, 150 and 300 p.s.i.g. reactor pressure, and 100 cc. initial alloy volume. (Space velocities are based on the initial dry alloy volume). A systematic study was also made of the variables of synthesis gas H_2/CO ratio, synthesis gas CO_2 and organic sulfur content, space velocity and operating pressure. Catalyst bed temperature was controlled by adjustment of pressure in the Dowtherm-jacket and reflux condenser, with the Dowtherm maintained at the boiling point by an electric heater surrounding the jacket. Temperatures, although difficult to maintain constant throughout the bed because of the high exothermicity of the reaction, were normally within 700°-800°F.

2. Capacity tests of a 6-inch inside diameter pilot plant reactor (Figure 2). Dowtherm "A" circulating through an external jacket and through six internal bayonets was used to heat the catalyst to reaction temperature at the start of operation, and then, as increasing quantities of exothermic heat of reaction were released, to remove heat from the catalyst bed. This was accomplished by controlling the Dowtherm temperature between the limits of 750°F. (corresponding to a vapor pressure of 144 p.s.i.g.) and 496°F. (the atmospheric boiling point) with a gas-fired heater upstream from the reactor, and a flash chamber and reflux condenser downstream from the reactor. The flash temperature was controlled with a nitrogen back-pressure system. The high circulation rate (30 gal./min.) allowed most of the Dowtherm to remain in liquid form. Purified synthesis gas produced by catalytic steam

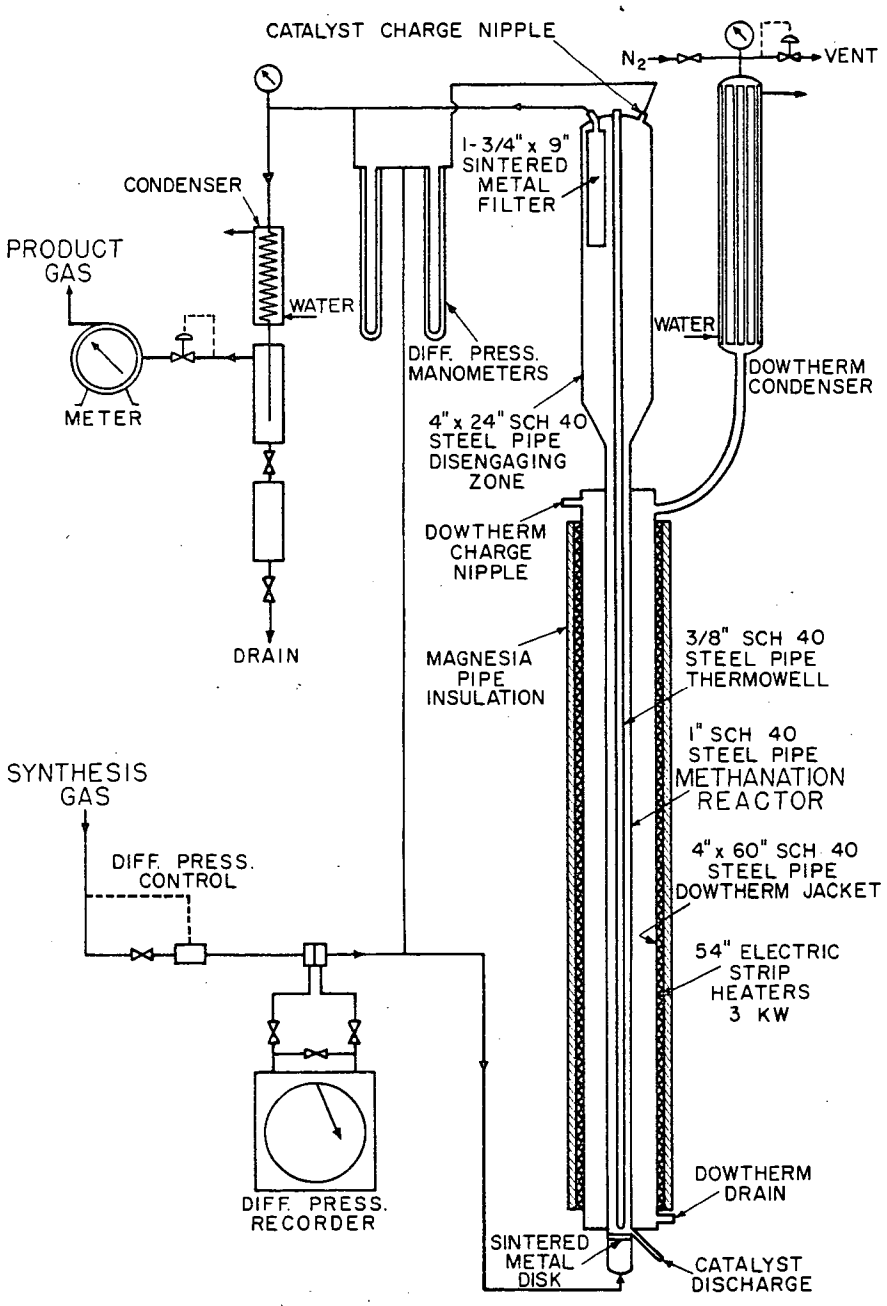

Fig. 1.-LABORATORY FLUID-BED METHANATION UNIT

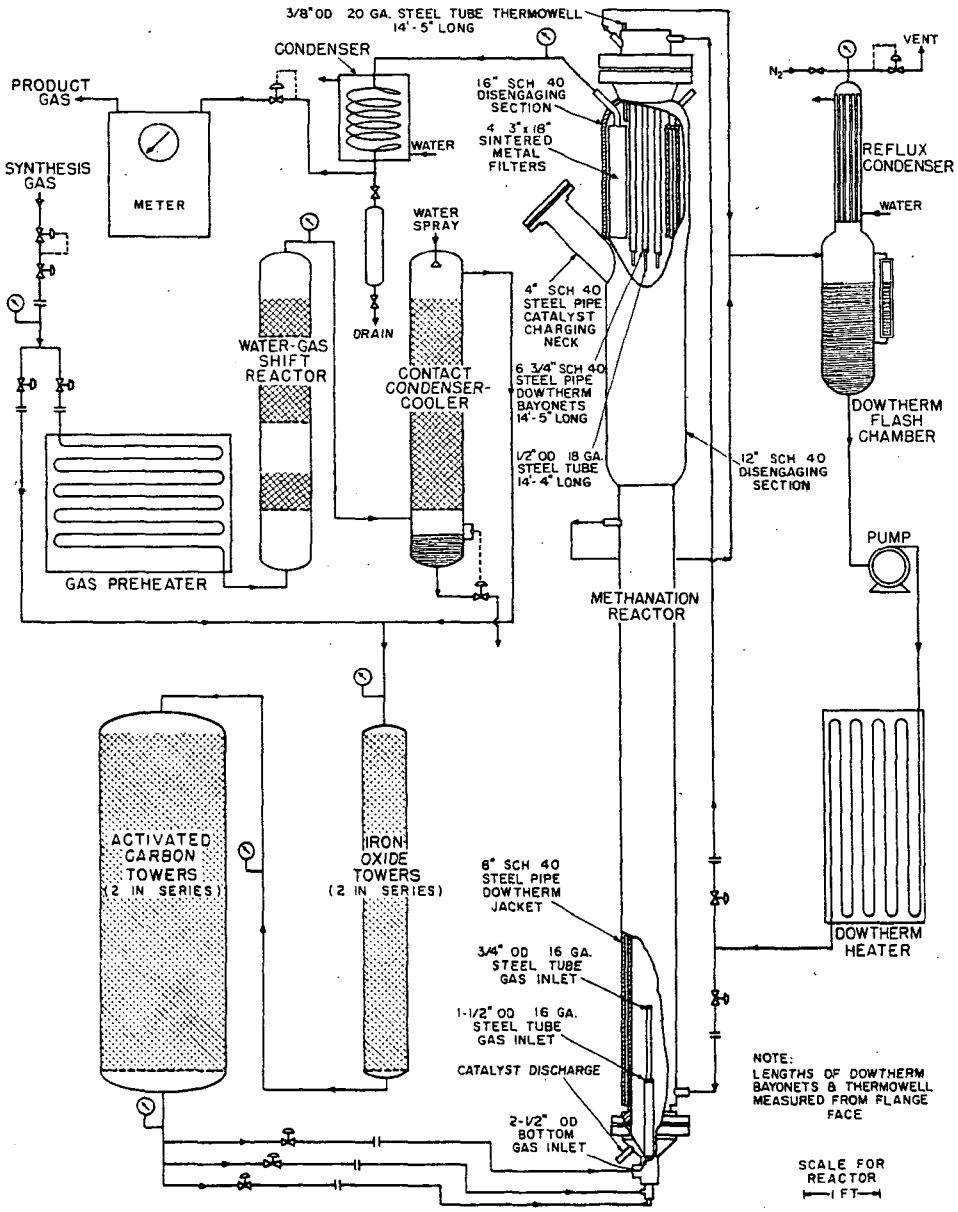

Fig. 2.-FLUID-BED METHANATION PILOT UNIT

reforming of natural gas was used as feed at pressures up to 190 p.s.i.g. After a series of short tests, comprising 177 hours of steady-state operation with a batch of catalyst prepared from 0.343 cu.ft. of alloy, the reactor was slightly modified to the design depicted in Figure 2 to permit attainment of a synthesis gas capacity of 3000 SCF/hr. with a 0.5 cu. ft. catalyst charge; initially, the cooling bayonets were constructed of 1/2-inch Schedule 40 pipe, the disengaging section was smaller, and the porous stainless steel gas filters were also smaller and located in a side offtake.

3. Exploratory pilot plant tests of simulated integrated pipeline-gas-from-coal operation involving the process steps of a) suspension gasification of coal with steam and oxygen to produce synthesis gas at a nominal rate of 20,000 SCF/hr., b) preliminary purification with iron oxide for bulk removal of hydrogen sulfide, c) temporary pressure storage and withdrawal at 3000 SCF/hr., d) adjustment of synthesis gas composition by partial carbon monoxide shift of a portion of the synthesis gas, e) final purification with iron oxide and activated charcoal to less than 0.01 grain of sulfur per 100 SCF, and f) methanation over fluidized Raney nickel catalyst in the reactor depicted in Figure 2.

CATALYST PREPARATION AND HANDLING

The 42 wt. % nickel-58 wt. % aluminum alloy was supplied by the Raney Catalyst Company. The structure of the crushed alloy is shown in Figure 3. The highly fractured condition of the catalyst particle is typical of the material used in the test program. The dark homogeneous regions are Ni_2Al_3 (gamma) phase, the light homogeneous regions are $NiAl_3$ (beta) phase, and the elongated mottled regions are a fine-grained eutectic mixture consisting of alpha phase (less than 0.05 wt. % nickel) and beta phase. Metallographic studies of caustic-etched particles showed that the gamma phase is more resistant to attack than are the other two phases, although x-ray analyses of caustic-treated alloy indicated the presence of all of the three original phases even when the aluminum content had been reduced to 5 wt. % or less. The major product of caustic leaching recovered in the catalyst was identified by x-ray as beta-alumina-trihydrate, and the presence of small crystallites of metallic nickel was also indicated when the aluminum conversion by caustic leaching was substantial.

Orginally, the activation procedure reported by the U. S. Bureau of Mines was employed.[31] This procedure was based on the assumption that an active catalyst could be prepared by extraction, with dilute caustic, of only 3-5 % of the aluminum content, and that the amount of aluminum removed was determined by a stoichiometric relationship such as:[25]

$$2Al + 2NaOH + 2H_2O \longrightarrow 2NaAlO_2 + 3H_2 \qquad (1)$$

It was further assumed that this procedure could be repeated a number of times to restore the activity of the catalyst.

After development of the necessary analytical techniques, it was shown in this study that at least 20% of the aluminum had to be converted before significant activity for the methanation reaction was obtained, and that considerably higher conversions were required to produce a long-lived catalyst. Further, the presence of large amounts of $Al_2O_3 \cdot 3H_2O$ in the extracted alloy confirmed that in addition to Reaction (1), sodium aluminate or direct aluminum hydrolysis reactions occur:[25]

$$2NaAlO_2 + 4H_2O \longrightarrow Al_2O_3 \cdot 3H_2O + 2NaOH \qquad (2)$$

$$2Al + 6H_2O \longrightarrow Al_2O_3 \cdot 3H_2O + 3H_2 \qquad (3)$$

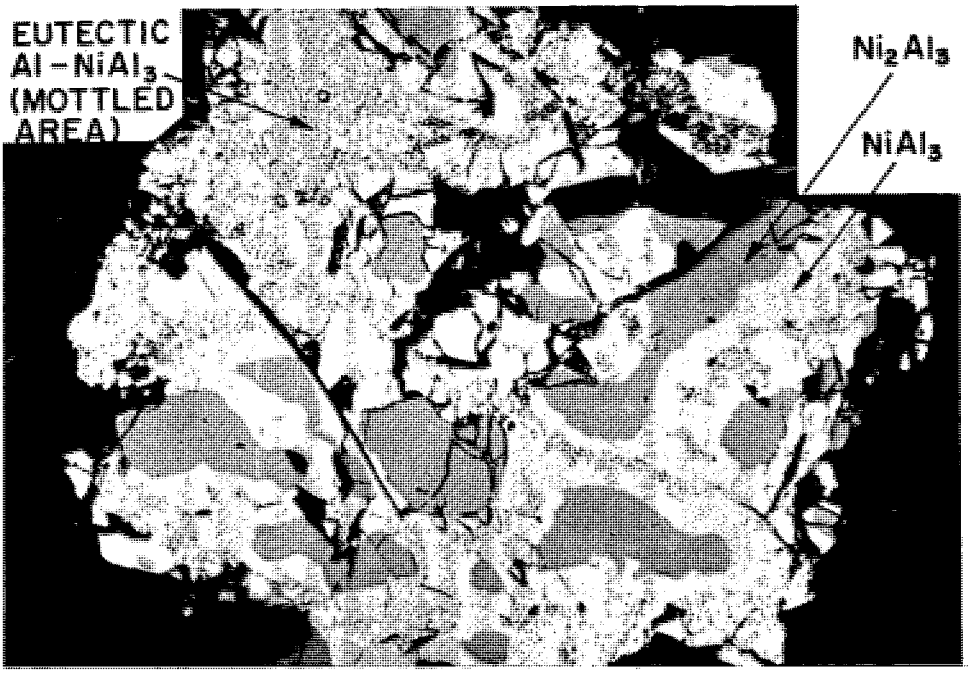

Fig. 3.-MICROSTRUCTURE OF 42 WT.% NICKEL - 58 WT.% ALUMINUM ALLOY (X 500)

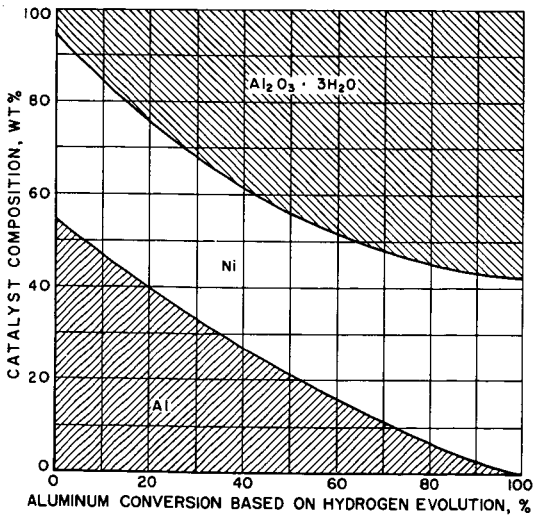

Fig. 4.-COMPOSITION OF RANEY NICKEL CATALYSTS PREPARED BY CAUSTIC LEACHING AT CONTROLLED RATE AND AMOUNT OF HYDROGEN EVOLUTION

Efforts to reduce aluminum oxide formation under conditions allowing only partial aluminum conversion were not successful. (In commercial Raney nickel catalyst preparation,[25] the alloy is added to an excess of concentrated caustic which apparently favors aluminum removal as aluminate.)

Since 3 moles of hydrogen are evolved per 2 moles of aluminum converted to either aluminate or alumina, it was possible to follow the progress of catalyst activation by measurement of hydrogen evolution. In the standard procedure for preparing laboratory batches of catalyst, 100 cc. (162 g.) of 42 wt. % nickel-58 wt. % aluminum alloy and 280 cc. of water were placed in a 2-liter three-neck flask. One neck of the flask held a mercury thermometer, the center neck held a reflux condenser, and the third neck held a buret for caustic or quench water addition. A wet-test meter was connected to the reflux condenser to measure the evolved hydrogen. A magnetic stirrer was used to slightly agitate the alloy. Fifteen cc. of a 26 wt. % sodium hydroxide solution was added, causing hydrogen evolution to begin, accompanied by a large heat release. When the temperature reached the boiling point after about 8 to 12 minutes, enough water was added to prevent flash vaporization, but not enough to reduce the temperature below the boiling point. The reaction was permitted to proceed at the boiling point until either an apparent 30, 65 or 85% of aluminum conversion had occurred. For example, the 2.88 SCF of hydrogen corresponding to 65% of apparent aluminum conversion of 162 g. of alloy was evolved in 34 to 42 minutes. At the desired point, the reaction was quenched by the addition of large amounts of cold water and the caustic liquid decanted from the wet catalyst. The catalyst was washed neutral to litmus and stored in methanol.

Figure 4 shows the relationship between chemical analysis of the catalysts prepared in accordance with the standard procedure, and the percent of aluminum conversion indicated by hydrogen evolution. It was necessary to further develop conventional procedures[8,18] to make these analyses. The most reliable technique consisted of drying the sample by heating in a stream of dry hydrogen, and passing dry hydrogen chloride over it to volatilize the aluminum metal as aluminum chloride. The aluminum chloride was recovered, precipitated with ammonia, and ignited to the oxide. The residue from the hydrogen chloride treatment was boiled with nitric acid, and filtered. The residue from the filtration was ignited to obtain the quantity of alumina not dissolved by this treatment. The filtrate was diluted to volume; on one aliquot, alumina was determined by double precipitation with benzoate and ignition to the oxide; on another aliquot, nickel was determined by dimethylglyoxime.

Batches of pilot plant catalysts were prepared only by the original activation method, which consisted of leaching a suspension of the alloy in water at a maximum temperature of 120°-130°F. by slow addition of sufficient dilute sodium hydroxide solution to convert 5% of the aluminum content in accordance with Reaction (1). After 4 to 6 hours, vigorous hydrogen evolution stopped, and the catalyst was washed neutral to litmus and stored in water. No reliable analyses of pilot plant catalysts are available, since the analytical technique had not been fully developed at that time.

The particle size distribution of the alloy used in the preparation of laboratory batches was standardized by combining individual screen fractions in the fixed proportions shown below; the screen analysis of the 0.343 cu. ft. of alloy for the original pilot plant batch is also given:

U.S.S. Sieve	Alloy Size Distribution, Wt.% Standard Laboratory Charge	Pilot Plant Charge
+40	0	1.2
-40 + 60	15	15.8
-60 + 80	15	10.1
-80 + 100	10	9.7
-100 + 140	35	34.7
-140 + 200	25	28.3
-200	0	0.2

In the pilot plant study, the prepared catalyst was charged as a water slurry and, in the majority of the laboratory tests, as a methanol slurry. Charging was done under a nitrogen blanket. Transfer as a slurry was used to avoid the possibility of catalyst oxidation, which could result in catalyst deactivation. After the slurry had been charged into the reactor, it was dried in a stream of nitrogen before introduction of synthesis gas. The catalyst temperature was raised to a level not exceeding 650°F., which was sufficient to initiate reaction of the synthesis gas, causing further temperature rise which had to be controlled by adjustment of the Dowtherm temperature level. Since the reactors were shut down repeatedly without change of the catalyst charge, it was necessary to store the catalyst in the reactor under nitrogen. In case of extended tests which were interrupted only temporarily, such as by scheduled weekend shutdowns, the catalyst temperature was maintained at 400°-500°F.

In catalyst life tests, the above charging and startup procedures gave exceedingly poor reproducibility of results. Rapid loss of catalyst through the porous stainless steel filters occurred in many attempts to make an extended run; the particles escaping from the reactor were very small and only a minor portion could be recovered. A common occurrence which preceded an abrupt reduction in conversion capacity was lifting of the bed into the disengaging zone and deposit on the filters, requiring blow-back to reduce pressure; this frequently took place after a weekend shutdown. No specific cause for this type of failure could be established, but it was found that by making the following revisions in these procedures it was possible to greatly improve the consistency of the catalyst performance data:

1. Store in methanol for not longer than 24 hours.

2. Predry in nitrogen at 250°F. for 2 hours to obtain free-flowing material.

3. Charge to unit under nitrogen blanket.

4. Start up slowly with hydrogen as fluidizing medium at approximately 1 ft./sec. superficial velocity, and gradually replace hydrogen with synthesis gas after attainment of the desired temperature and pressure.

5. During interruption of an extended test, shut down in nitrogen at 450°F. and atmospheric pressure and start up with hydrogen as above.

PROCESS VARIABLES

A number of thermodynamic analyses of the methanation reaction system have been made[3,9,14,23] in an effort to evaluate the influence of the major operating variables: pressure, temperature and H_2/CO ratio,

on the equilibrium conversion of the feed gas to methane, water vapor, carbon dioxide and carbon. In these analyses the chemical reactions:

$$CO + 3H_2 \longrightarrow CH_4 + H_2O \quad (4)$$

$$2CO + 2H_2 \longrightarrow CH_4 + CO_2 \quad (5)$$

$$CO + H_2O \longrightarrow CO_2 + H_2 \quad (6)$$

$$2CO \longrightarrow C + CO_2 \quad (7)$$

$$CO + H_2 \longrightarrow H_2O + C \quad (8)$$

$$CH_4 \longrightarrow 2H_2 + C \quad (9)$$

were employed as the basis of the equilibrium product distribution calculations. Under conditions of chemical equilibrium in the absence of carbon formation, any two of the first three reactions will define the system. When equilibrium carbon formation is to be included, one of the three carbon-forming Reactions (7), (8) and (9) must also be considered. The results of the various thermodynamic studies show that in the absence of carbon formation, nearly stoichiometric conversion of 1:1 to 3:1 H_2/CO ratio synthesis gases to methane can be attained at 650°F. and 25 atmospheres (353 p.s.i.g.); equilibrium methane yields decrease with increases in temperature and decreases in pressure, but remain reasonably high below 900F. at pressures from 1 to 25 atmospheres.

The calculation of equilibrium carbon yields is complicated by lack of information on the nature of the carbon deposited on methanation catalysts. Standard thermodynamic data are normally based on carbon in the form of beta-graphite[27], whereas under actual experimental conditions the deposited carbon may be in different forms, and, therefore, have different thermodynamic properties. For example, removal of excessive carbon from the system may involve carbide formation with the metallic catalyst component.

Carbon deposition boundary data based on equilibrium constants obtained from actual methanation reaction systems catalyzed by precipitated nickel[9] show substantially lower limiting feed gas H_2/CO ratios than data based on beta-graphite.[14] For example, at 900°F., the minimum H_2/CO ratios calculated from the experimental equilibrium data are 1.75:1 at one atmosphere, and 1.5:1 at 25 atmospheres. In comparison, when beta-graphite is used as the form of carbon, the minimum H_2/CO ratios at 900°F. are 3.25:1 at one atmosphere, and 2.6:1 at 25 atmospheres. For the calculations based on experimental results, the limiting H_2/CO ratio drops to 1:1 at 600°F., whereas for the beta-graphite data, freedom from carbon formation is not indicated anywhere in the low-temperature range below H_2/CO ratios of 2.6:1. Addition of steam or CO_2 to the feed gas lowers the limiting H_2/CO ratios.

The presence of CO_2 in the feed also has the desirable tendency to suppress hydrogen breakthrough. For example, if only the stoichiometric relationships are considered, a 3:1 H_2/CO ratio feed gas could give methane yields ranging from 0.125 moles to 0.25 moles/mole $H_2 + CO$, while complete CO conversion is maintained. Thus, unless CO conversion via the CO_2-forming Reactions (5) or (6) is limited by equilibrium hindrance, the actual methane yield may be substantially below the theoretically attainable level.

To establish the range of suitable fluid-bed operating conditions with Raney nickel catalysts, a series of exploratory tests was made in the laboratory reactors. Synthesis gases of about 1.5:1 and 3:1 H_2/CO ratio and various CO_2 contents were methanated over catalyst charges prepared by leaching of 100 cc. of alloy with dilute caustic for more than 4 hours. Pressure levels of 27, 75 and 150 p.s.i.g. were investigated, which permitted up to fourfold variations in space velocity at constant superficial feed gas velocity. With purified synthesis gas produced by steam-oxygen gasification of coal (42-47 mole % H_2, 31-32 mole % CO, 15-19 mole % CO_2, 1-2 mole % CH_4, 4-5 mole % N_2) complete CO and nearly complete

H_2 conversions were obtained at superficial feed gas velocities up to approximately 0.7 ft./sec. This corresponds to a space velocity of 8000 SCF/cu. ft. catalyst-hr. at 150 p.s.i.g. At superficial velocities below 0.3 ft./sec., carbon recoveries in the product gas tended to be low, possibly as a result of carbon deposition on overheated, incompletely fluidized catalyst.

In a series of parallel tests with 2.8-3.4:1 H_2/CO ratio synthesis gases containing only small amounts of CO_2, CH_4 and N_2, no significant CO breakthrough was observed at space velocities as high as 9000 SCF/cu. ft. catalyst-hr. at 27 p.s.i.g., and 15,000 SCF/cu. ft. catalyst-hr. at 75 and 150 p.s.i.g. Satisfactory operation in all other respects was also obtained over a superficial feed gas velocity range of 0.1-3.3 ft./sec., except for one instance of apparent low carbon recovery in the product gas at 0.1 ft./sec. and 150 p.s.i.g.

In an additional series of tests, the effect of 20-30 mole % CO_2 dilution of 3.2-3.8:1 H_2/CO synthesis gas was investigated at pressures of 75, 150 and 300 p.s.i.g. At gas feed rates corresponding to space velocities of 7000-23,000 SCF/cu. ft. catalyst-hr. and superficial velocities of 0.2-2.4 ft./sec., no significant CO breakthrough was observed, and carbon recoveries in the product gas were approximately 100%.

The 1.049-inch inside diameter reactors used in the last series and in subsequent tests had approximately 60% more annular space than the reactors used initially, since the diameter of the thermowell had been decreased from 0.840 inches to 0.675 inches. As a result, catalyst bed depths and superficial gas velocities at equivalent operating conditions were about 60% of the values with the original reactor design. This was probably responsible for an increase in the maximum temperature level of the catalyst bed from 650°-750°F. to 690°-790°F. under conditions giving essentially complete CO conversion.

A summary of the average yield data for these three series of tests is presented in Table 1. The data show the expected trend of increase in methane content, and decrease in hydrogen content, of the product gas as pressure is increased. At 75 p.s.i.g., there was little suppression of hydrogen breakthrough due to the effects of feed gas CO_2 content. However, at 150 p.s.i.g., substantial reduction in hydrogen breakthrough was observed at the lower space velocities. At 300 p.s.i.g., the combined effect of high pressure and presence of CO_2 in the feed gas resulted in nearly complete suppression of hydrogen breakthrough except at the very high space velocities. The tendency toward increases in hydrogen breakthrough with increases in space velocity for the high H_2/CO ratio synthesis gases was not clearly defined at all pressure levels, possibly due to variations in feed gas composition. In the tests with the high CO_2-content 3:1 H_2/CO ratio gases there was a slight reduction in the quantity of CO_2 leaving the reactor compared to the quantity entering.

Although only some of the product gases had CO concentrations readily detectable by the analytical procedures employed (mass spectrometer supplemented by infrared analysis), it appears that the carbon monoxide shift reaction $CO + H_2O \longrightarrow CO_2 + H_2$ closely approached equilibrium in all tests, since CO concentrations of less than 1 mole %, and normally as low as 0.1-0.5 mole %, would give experimental equilibrium constants consistent with the theoretical values.

CATALYST PERFORMANCE

The important catalyst performance variables are activity and total conversion capacity. In this study, activity is defined in terms of the percentage of the synthesis gas $H_2 + CO$ content that is converted to methane

Table 1.-EFFECT OF OPERATING CONDITIONS ON FLUID-BED METHANATION YIELDS WITH RANEY NICKEL CATALYST

CO_2-Containing 1.5:1 H_2/CO Ratio Feed Gas

Pressure, p.s.i.g.		27		75	150
Space velocity, SCF/cu. ft. cat.-hr.[a]		1200-2200		2300-4400	3000-8000
Moles product gas/mole feed		0.56		0.56	0.55
Moles water formed/mole feed		0.07		0.07	0.07
Gas composition, mole %	Feed		Feed		
CO_2	16	51	16	52	53
CO	31	--	32	--	--
H_2	47	4	46	2	1
CH_4	1	35	1	36	36
N_2[b]	5	10	5	10	10

Essentially CO_2-Free 3:1 H_2/CO Ratio Feed Gas

Pressure, p.s.i.g.		27	75	150
Space velocity, SCF/cu. ft. cat.-hr		1000-9000	1000-15,000	1000-15,000
Moles product gas/mole feed		0.30	0.30	0.27
Moles water formed/mole feed		0.23	0.23	0.24
Gas composition, mole %	Feed			
CO_2	1	6	6	5
CO	24	--	--	--
H_2	74	11-14	11	8
CH_4	0	78-75	78	82
N_2[b]	1	5	5	5

CO_2-Containing 3:1 H_2/CO Ratio Feed Gas

Pressure, p.s.i.g.		75	150		300
Space velocity, SCF/cu. ft. cat.-hr		8000-23,000	7000-21,000		7000-17,000
Moles product gas/mole feed		0.45	0.45		0.43
Moles water formed/mole feed		0.20	0.20		0.21
Gas composition, mole %	Feed			Feed	
CO_2	27	56	59-56	25	54-52
CO	16	--	--	17	--
H_2	56	5	2-5	57	1-3
CH_4	0	36	36	0	42
N_2[b]	1	3	3	1	3

[a]Space velocities outside this range gave either less than 90% carbon recovery in the product gas or substantial CO breakthrough.
[b]Reported N_2 content of product gases may include small percentage of CO.

or methane equivalent: % H_2-CO Conversion =

$$100 \frac{4\left[\left(\frac{\text{Moles Dry Prod. Gas}}{\text{Moles Dry Feed Gas}}\right)\left(\text{Mole \% } CH_4\text{-Equiv. in Dry Prod. Gas}\right) - \left(\text{Mole \% } CH_4\text{-Equiv in Dry Feed Gas}\right)\right]}{\text{Mole \% } H_2 + CO \text{ in Dry Feed Gas}},$$

where the methane-equivalent is the sum of: mole percentage multiplied by carbon number for each gaseous hydrocarbon. At complete conversion to methane of any synthesis gas in the 1:1-3:1 H_2/CO ratio range by the necessary combination of Reactions (4) and (5), or (4) and (6), a value of 100% would be obtained. If ethane is also produced, the H_2-CO conversion based on the above definition could slightly exceed 100%; however, the maximum value at complete conversion of 0.75:1-2.5:1 H_2/CO ratio synthesis gases to ethane would be only 114%. The total conversion capacity of the catalyst is defined as the weight of net methane equivalent per unit weight of original alloy nickel content, or the volume of net methane equivalent per unit weight of original alloy, produced by the catalyst during the period in which it maintains 70% H_2-CO conversion or more.

Sulfur tolerance limits of standard fluid-bed Raney nickel catalysts prepared by 65 and 85% aluminum conversion were determined to establish synthesis gas purification requirements. In these tests, CO_2-containing, 3:1 H_2/CO ratio synthesis gases having organic sulfur contents (mainly in the form of COS) of 0.5 to 4 grains per 100 SCF were methanated at space velocities of 5000 to 13,000 SCF/cu.ft. catalyst-hr. and 75 p.s.i.g. Each test was made with a fresh batch of catalyst, and continued until most of the catalyst activity had been lost. It was observed that the catalyst activity dropped rapidly to less than 70 to 80% H_2-CO conversion when the total sulfur exposure attained a level of approximately 0.5 lb./100 lb. of nickel. This agrees quite well with similar sulfur poisoning test results obtained in studies with supported nickel catalysts.[35] It was determined by measurement of H_2S and organic sulfur liberated from a poisoned catalyst by acid treatment that essentially all of the organic sulfur introduced in the course of a test was removed by the catalyst. From a linear extrapolation of these results, adequate catalyst activity could be expected for about 1500 hours when a gas containing 0.01 grain of sulfur per 100 SCF is fed at a rate of 10,000 SCF/cu.ft. catalyst-hr.

Typical results of a catalyst life test with purified synthesis gas are given in Table 2. In this test, H_2-CO conversion dropped to approximately 80% in 1010 hours of operation at 75 p.s.i.g.; at that time, the pressure level was increased to 150 p.s.i.g., which resulted in an increase in H_2-CO conversion to a level of about 90%. However, after 1300 hours of operation, the H_2-CO conversion dropped to 70% and the run was terminated. Only 45% of the original catalyst volume (measured under methanol) was recovered, so the decrease of conversion capacity cannot be ascribed solely to activity loss.

The CO_2-free heating values shown in Table 2 are lower than would be desirable for use of the process as a source of a natural gas supplement. This is typical of operation at relatively low pressure and high space velocity with a high H_2/CO ratio synthesis gas. However, gas of approximately 900 B.t.u./SCF CO_2-free heating value was produced for about 500 hours in a similar run in which the pressure was maintained at 150 p.s.i.g. through the entire operating period. By adjustment of the H_2/CO ratio to minimize hydrogen breakthrough, and reduction of the nitrogen content of the synthesis gas, it is also possible to produce 900 B.t.u./SCF CO_2-free gas at 75 p.s.i.g. and 10,000 SCF/cu.ft. catalyst-hr. space velocity for limited periods.

Table 2.-TYPICAL PERFORMANCE DATA FOR STANDARD FLUID-BED RANEY NICKEL CATALYST[a]

Duration of test, hr.		300		500		720		970		1070		1300
Feed gas												
H_2/CO ratio		2.98		3.12		3.22		3.28		3.05		3.65
Sulfur, grains/100 SCF		0.0010		0.0004		0.0005		0.0007		0.0005		0.0008
Pressure, p.s.i.g.		75		75		75		75		150		150
Temperature, °F.												
Bottom of reactor		790		725		735		710		750		685
9 inches from bottom		795		770		780		775		800		755
18 inches from bottom		785		780		780		795		795		800
27 inches from bottom		785		780		780		795		790		790
Feed gas												
Space velocity, SCF/cu.ft. cat.-hr		11,578		11,556		12,248		11,981		10,210		10,584
Superficial inlet velocity, ft./sec.		1.27		1.20		1.29		1.20		0.59		0.58
Product gas[b]												
SCF/SCF feed		0.495		0.506		0.499		0.522		0.488		0.573
Carbon recovery, %		100		98		100		98		100		100
Hydrogen recovery, %		66		68		71		68		69		69
Oxygen recovery, %		80		79		76		79		77		82
Composition, mole %	Feed		Feed		Feed		Feed		Feed		Feed	
CO_2	28.1	59.6	26.9	54.5	22.5	47.0	25.3	49.5	26.8	55.7	25.5	44.7
CO	17.7	0.1	16.3	0.6	17.3	1.1	16.9	2.7	17.6	0.6	15.6	5.4
H_2	52.7	4.5	50.9	7.1	55.7	11.8	55.5	16.3	53.7	5.9	56.9	24.4
CH_4	0.3	33.2	3.6	35.6	2.3	37.0	0.9	28.9	0.6	35.9	0.4	22.2
C_2H_6	--	--	0.1	0.2	0.3	0.3	0.2	0.3	0.2	0.2	0.2	0.4
N_2	1.2	2.6	2.2	2.1	1.9	2.8	1.2	2.3	1.1	1.7	1.4	2.9
Total	100.0	100.0	100.0	100.0	100.0	100.0	100.0	100.0	100.0	100.0	100.0	100.0
CO_2-free specific gravity, air = 1.000		0.528		0.505		0.484		0.442		0.514		0.407
CO_2-free heating value, B.t.u./SCF		856		840		784		701		863		584
Water formation, moles/mole feed gas												
By hydrogen balance		0.1821		0.1852		0.1796		0.1875		0.1736		0.1820
By oxygen balance		0.1486		0.1470		0.1487		0.1441		0.1651		0.1230
H_2-CO conversion, %		92		86		87		78		94		68

[a] Run No. 498, Catalyst No. 59B prepared by 65% aluminum conversion of 100 cc. (162g.) of 40-200 mesh 42 wt. % nickel-58 wt. % aluminum alloy.

[b] Excluding water formed by methanation reactions.

Table 3 summarizes the test results for five extended runs in which more than 1000 lb. net CH_4-equivalent/lb. Ni was produced. Included are results of an early test with a catalyst which was activated by three successive caustic extractions (No. 25C). It can be seen that the conversion capacities obtained after the first two extractions were very small. Extended operation was possible only after most of the aluminum had been extracted. This run was discontinued voluntarily before the H_2-CO conversion had decreased to the minimum acceptable level. In a test with another early catalyst preparation (No. 33A) it was possible to obtain a total conversion capacity of 2770 lb. net CH_4-equivalent/lb. Ni by successive pressure increases from 75 to about 300 p.s.i.g. The attrition rate in this test was the lowest of any completed so far; unfortunately, the analytical data for Catalyst 33A are not reliable, since they were obtained at a time when the procedures were still under development. For example, the significant difference in the composition of fresh and recovered catalyst was not observed in the three most recent tests (Catalysts 66B, 59B and 59A2). It has also not been possible to reproduce the composition of fresh Catalyst 33A, which shows an unusually high nickel and low alumina content.

On the basis of the data of Table 3, at the currently quoted cost of 90 cents per lb. for pulverized 42 wt. % nickel-58 wt. % aluminum Raney alloy in 25,000 lb. lots,[2e] alloy costs per 1000 SCF of methane-equivalent would be in the range of 3 to 6 cents, assuming no nickel credit for the spent catalyst. If these results could be duplicated on a commercial scale, catalyst costs should not be a major factor in determining the final cost of producing pipeline gas from coal via the methanation process.[1a]

PILOT PLANT TESTS

The fluid-bed pilot unit was operated intermittently over a period of ten months with the original 0.343 cu. ft. charge of caustic-extracted 42 wt. % nickel-58 wt. % aluminum Raney catalyst. Nine runs with steady-state periods ranging from 7 to 47-1/2 hours were made with a cumulative steady-state operating period of 177 hours. During this time, approximately 47,000 SCF of net methane-equivalent, corresponding to 125 lb./lb. Ni, were produced. Typical operating data from this series of runs are given in Table 4.

The alloy used in the preparation of the pilot plant catalyst had a bulk density of approximately 110 lb./cu. ft. Assuming no volume change during extraction, the static bed height in the reactor would have been approximately 2 feet. It appears from the temperature patterns observed in the reactor at the higher feed rates that the actual bed height during operation was approximately 3 feet.

The feed gas was introduced through the two lower inlets, with 2/3 or more fed at the bottom of the reactor, and the remainder at the 18-inch level. Pressure levels in the reactor were generally increased with increases in feed rate, so that the superficial bottom feed gas velocity was maintained in the 0.2-0.6 ft./sec. range (calculated on the basis of inlet temperature, reactor pressure and cross-sectional area of the empty reactor). To maintain product gas quality as throughput rate and pressure were increased, it was necessary to increase the catalyst bed temperature from approximately 700°F. at space velocities of less than 1000 SCF/cu. ft. catalyst-hr. to 900°F. at space velocities of 5000 to 6000 SCF/cu. ft. catalyst-hr.

Table 3.-SUMMARY OF CATALYST LIFE TEST RESULTS

Catalyst No.	25C					66B	59B		59A2	33A			
Run No.	407	409	411			516	498		511	444			
Catalyst preparation													
Maximum temperature, °F	160	174	180			205	204		206	208			
Activation duration, min	25	32	48			32	74[a]		74[a]	More than 4 hr.			
Aluminum conversion, %[b]	24	24	23			65	65		65	85			
Predrying in N_2	No	No	No			2 hr. at 250°F.	No		2 hr. at 250°F.	No			
Catalyst composition, wt. %[c]													
Aluminum	29.8	18.7	5.4			16.2 (16.8)	14.9 (11.4)		15.8 (15.4)	11.4 (0)			
Nickel	32.5	30.3	31.7			32.6 (32.3)	29.6 (31.9)		32.6 (31.4)	49.1 (20.1)			
$Al_2O_3 \cdot 3H_2O$	37.7	51.0	62.9			51.2 (51.0)	55.5 (52.5)		51.6 (53.2)	39.5 (79.9)			
Operating conditions													
Run duration, hr	48	40	300	310	25	1180	1010	280	1500	850[d]	610[d]	270[d]	
Number of shut downs	11					10	16		19	44			
Pressure, p.s.i.g.	75	75	75-81	150-161	298-300	150	75	150	75	75-86	122-160	300-310	
Maximum temperature, °F.	760-835	770-785	775-805	800-885	855-880	690-805	750-815	750-805	720-830	755-875	765-875	785-885	
Feed gas													
H_2/CO ratio	3.7-4.2	3.6-3.8	3.2-4.2	3.0-3.5	3.0-3.2	2.5-3.7	2.2-4.6	2.8-3.7	2.5-3.8	2.6-3.9	2.0-3.4	2.4-3.7	
CO_2 content, mole %	1	1	0-2	0-1	1	0-32	11-37	25-27	0-32	21-31	23-31	34-43	
Superficial velocity, ft./sec.	1.0-1.2	1.1-1.2	1.0-1.2	0.5-0.6	0.3	0.5-1.0	1.0-1.5	0.6	0.9-1.7	1.0-1.4	0.5-0.7	0.2-0.4	
Space velocity, SCF/cu.ft. cat.-hr	9,400-10,800	9,700-10,600	9,200-11,900	8,500-10,400	9,400-9,700	9,200-16,500	9,500-13,700	10,100-10,600	8,000-14,800	10,100-12,300	7,400-10,700	6,400-12,000	
Net equivalent methane yield	1440					1970	2100		2270		2770[d]		
lb./lb. nickel	14.5					19.9	21.3		22.9		27.9[d]		
1000 SCF/lb. alloy						25	45		40		70		
Catalyst recovery, vol.%	--												

[a] Double preparation (200 cc. of alloy)

[b] Based on nominal 58 wt. % aluminum content of alloy.

[c] Recovered catalyst analyses are given in parenthesis.

[d] Includes a number of short tests at a variety of operating conditions.

Table 4.-TYPICAL FLUID-BED PILOT UNIT METHANATION TEST RESULTS WITH RANEY NICKEL CATALYST AND PURIFIED 3:1 H_2/CO RATIO SYNTHESIS GAS

	0.343 cu.ft. of original alloy							0.5 cu.ft. of catalyst	
Run No.	P-7	P-11		P-15		P-19		P-20	P-21
Total steady state duration, hr	6	75	84	126.5	131.5	166		19.75	37.75
Pressure, p.s.i.g.	11	143	162	190	190	167		110	103
Temperature, °F									
Bottom of Reactor	705	730	810	870	800	890		750	860
9 inches from bottom	--	--	--	--	--	--		805	925
18 inches from bottom	695	745	815	870	805	900		820	935
27 inches from bottom	--	--	--	--	--	--		800	830
36 inches from bottom	690	675	735	775	665	745		785	730
54 inches from bottom	710	575	630	680	565	650		--	--
72 inches from bottom	710	590	640	670	545	650		--	--
90 inches from bottom	700	585	640	670	535	640		--	--
Dowtherm inlet temperature, °F.									
Jacket	700	580	635	665	515	595		720	605
Bayonets	700	575	640	660	510	600		720	605
Feed gas									
Space velocity, SCF/cu.ft. cat.-hr.	712	3491	3751	5709	5588	5923		4410	5761
Total gas rate, SCF/hr.	244	1198	1287	1958	1917	2031		2205	2881
Gas rate, bottom reactor, %	68	82	79	80	81	82		78	89
Gas rate, 12 inches from bottom, %	--	--	--	--	--	--		22	11
Gas rate, 18 inches from bottom, %	32	18	21	20	19	18		--	--
Superficial bottom inlet velocity, ft./sec.	0.35	0.34	0.34	0.47	0.44	0.57		0.87	1.49
Product gas[a]									
SCF/SCF feed	0.302	0.339	0.312	0.304	0.347	0.293		0.282	0.297
Carbon recovery, %	100	99	98	102	100	98		100	105
Hydrogen recovery, %	64	74	72	70	73	64		67	67
Oxygen recovery, %	6	18	13	7	12	15		12	19
Composition, mole %	Feed	Feed		Feed		Feed		Feed	Feed
CO_2	1.2	2.4	1.4	7.4	5.8	1.0	2.9	4.3	1.5	6.5	1.9	5.6	2.7	8.8
CO	20.3	--	24.6	--	--	23.3	--	--	22.3	--	23.1	--	22.0	--
H_2	77.3	24.8	72.6	20.1	14.0	74.8	13.9	26.1	75.1	16.4	73.2	6.1	73.7	5.4
CH_4	0.2	69.5	0.3	69.4[b]	77.1	0.4	79.8	66.6	0.2	73.8	0.4	84.4	0.6[b]	82.1
N_2[c]	1.0	3.3	1.1	3.1	3.1	0.5	3.4	3.0	0.9	3.3	1.4	3.9	1.0	3.7
Total	100.0	100.0	100.0	100.0	100.0	100.0	100.0	100.0	100.0	100.0	100.0	100.0	100.0	100.0
CO_2-free specific gravity, air = 1.000		0.445		0.463	0.496		0.500	0.435		0.484		0.540		0.543
CO_2-free heating value, B.t.u./SCF		791		818	863		865	781		843		912		916
Water Formation, moles/mole feed gas														
By hydrogen balance		0.2818		0.1931	0.2057		0.2287	0.2026		0.2742		0.2461		0.2481
By oxygen balance		0.2125		0.2238	0.2378		0.2354	0.2231		0.2149		0.2374		0.2217
By condensate measurement		0.2158		0.2315	0.2146		0.2288	0.2127		0.2013		0.2335		0.2489
H_2-CO conversion, %		85		96	98		97	93		88		97		98

[a]Excluding water formed by methanation reactions.

[b]Includes small amount of C_2H_6.

[c]May include some CO not distinguishable from N_2 by mass spectrometer analysis when present in small concentrations.

Complete CO conversion was obtained over the entire range of space velocities investigated, and H_2-CO conversions were normally above 90%. Some of the variation in the H_2-CO conversions was the result of small changes in feed gas H_2/CO ratio. The product distribution was very close to equilibrium values[9,14] calculated on the basis of Reactions (4) and (6), except when catalyst activity limited H_2-CO conversion at high space velocities and relatively low temperatures. Reduction in temperature of approximately 70°F. below the level necessary to maintain equilibrium conversions resulted in a significant increase in H_2 breakthrough, CO_2 formation, and total dry product gas volume, accompanied by a decrease in CH_4 concentration (compare the two test periods reported for Runs P-11 and P-15). The increased amounts of combined oxygen (CO_2) and free hydrogen in the product gas were balanced by decreased water formation. At temperatures high enough to maintain adequate catalyst activity there was little net carbon dioxide formation.

The catalyst bed temperature increase with increases in throughput rate was accompanied by a decrease in Dowtherm inlet temperature from approximately 700°F. to 600°F. This indicates that it was possible to remove the exothermic heat of reaction at the lower space velocities under essentially isothermal conditions, whereas at the high throughput rates a temperature difference of approximately 300°F. between the catalyst bed and the Dowtherm was required. For a heat of reaction of approximately 100,000 B.t.u./pound-mole of methane (equivalent to approximately 65 B.t.u./SCF of H_2 + CO converted), and assuming an actual catalyst bed height of 3 feet equivalent to a heat transfer area of 8.7 sq. ft., the overall heat transfer coefficient between the catalyst bed and the circulating Dowtherm was on the order of 50 B.t.u./hr.-sq. ft.-°F. It is estimated that the overall coefficient for the cooling bayonets was actually on the order of 100 B.t.u./hr.-sq.ft.-°F. because of the lower Dowtherm film resistance at the high flow rates in the bayonets as compared to the jacket.

The test program with the original charge of catalyst was discontinued because of excessive pressure drops through the reactor. Inspection of the reactor offtake section showed that the four 1-1/2 x 9-inch porous stainless steel gas filters were clogged with a considerable quantity of catalyst fines. Since this condition was probably aggravated by the offtake design and inadequate filter area, these equipment components were modified by the addition of a 16-inch diameter x 2-foot section to the disengaging zone. This section housed four 3 x 18-inch porous stainless steel filters with a combined area three times as large as that of the original installation.

In addition, the 1/2-inch Schedule 40 cooling bayonets were enlarged to 3/4-inch Schedule 40 pipe to give an increase of approximately 25% in the cooling surface to catalyst volume ratio (17.0 sq. ft./cu. ft. to 21.4 sq. ft./cu. ft.). The gas inlet system was also enlarged to reduce the high pressure drop encountered at the higher gas rates. It was hoped that these changes would permit attainment of the nominal 3000 SCF/hr. synthesis gas capacity desired for integrated pilot plant operation.

The modified reactor was operated at approximately 100 p.s.i.g. with a catalyst charge consisting of approximately 1/3 recovered catalyst from the preceding test period, and 2/3 of catalyst prepared by the original procedure, which had been stored under water for nearly one year. The total catalyst volume, measured under water, was approximately 0.5 cu. ft. In two runs totalling 44 hours of steady-state operation with H_2/CO ratio synthesis gas produced by reforming of natural gas, feed gas rates ranging from 1400 to 3300 SCF/hr. were investigated. Gases of

about 900 B.t.u./SCF and 84 mole % CH_4 content were produced up to the highest feed rate, confirming that the desired capacity of the reactor could be attained. Typical run data for the modified reactor are given in the last two columns of Table 4. They indicate substantially lower hydrogen breakthrough, and somewhat higher H_2-CO conversion, than were obtained with the original catalyst charge and reactor design.

On the basis of these pilot plant test results, it appears that a practical full-scale, dense-phase fluid-bed methanation reactor can be designed for high-capacity, one-pass operation, although such a reactor will have a relatively shallow catalyst bed. For example, at typical operating conditions of 1 ft./sec. superficial feed gas velocity, 5000 SCF/cu.ft. catalyst-hr. feed gas space velocity, 300 p.s.i.g., 750°F. catalyst bed temperature, 550°F. coolant temperature and at a heat transfer coefficient of 100 Btu/hr.-sq.ft.-°F, a 10-foot diameter methanation reactor would require about 2500 1-inch tubes for heat removal, and would contain an unexpanded catalyst bed about 6.6 ft. deep, equivalent to an unexpanded catalyst volume of 360 cu.ft. Such a reactor would handle a synthesis gas rate of about 1.8 million SCF/hr. corresponding to a methane production rate of about 450,000 SCF/hr., or over 10 million SCF/day. Lean-phase fluidization may give more flexibility of operation; each of the two reactors constructed by the M. W. Kellogg Company for SASOL in South Africa reportedly handles 9.5 million SCF/hr. of synthesis gas at 5000 tons/hr. catalyst circulation.[17]

INTEGRATED PIPELINE-GAS-FROM-COAL OPERATION

The process steps shown in Figure 5 were investigated in a number of exploratory runs. Although only short on-stream periods were possible because of rapid catalyst failure, the indicated operating conditions and results should be representative of those attainable in steady-state operation. The catalysts used in these runs were prepared before the activation, handling and startup procedures described in the preceding sections had been developed. Catalyst failure appeared to be the result of attrition or disintegration, which caused lifting of the bed into the disengaging and filter zone of the reactor, where severe overheating occurred.

The design and operation of the suspension coal gasifier have been fully described elsewhere.[34] However, the use of CO_2 instead of air to pressurize the coal feed tank was a departure from the previous procedure, necessitated by the requirement for a low N_2 content of the synthesis gas when a high-heating-value product gas is desired. Intermediate partially purified synthesis gas storage was provided, since the generating capacity under the preferred operating conditions is 20,000 SCF/hr. for limited on-stream periods, whereas the nominal capacity of the remainder of the plant is 3000 SCF/hr.

One of the major problems of integrated operation investigated in the exploratory pilot plant tests was synthesis gas purification. The use of fixed-bed iron oxide purification (9 lb. Fe_2O_3/bushel) for bulk H_2S removal, and of separate CO_2 removal from the methanated gas, is probably uneconomical in comparison to hot carbonate, ethanolamine or Rectisol scrubbing of the raw synthesis gas for combined H_2S, CO_2 and partial organic sulfur removal.[2,12,17,21,29,37] However, the scheme employed here has the advantage of allowing CO_2 to remain in the purified synthesis gas, which is beneficial for two reasons: first, it inhibits hydrogen breakthrough and carbon formation, and second, it provides a diluent as a heat sink for some of the exothermic heat of reaction with-

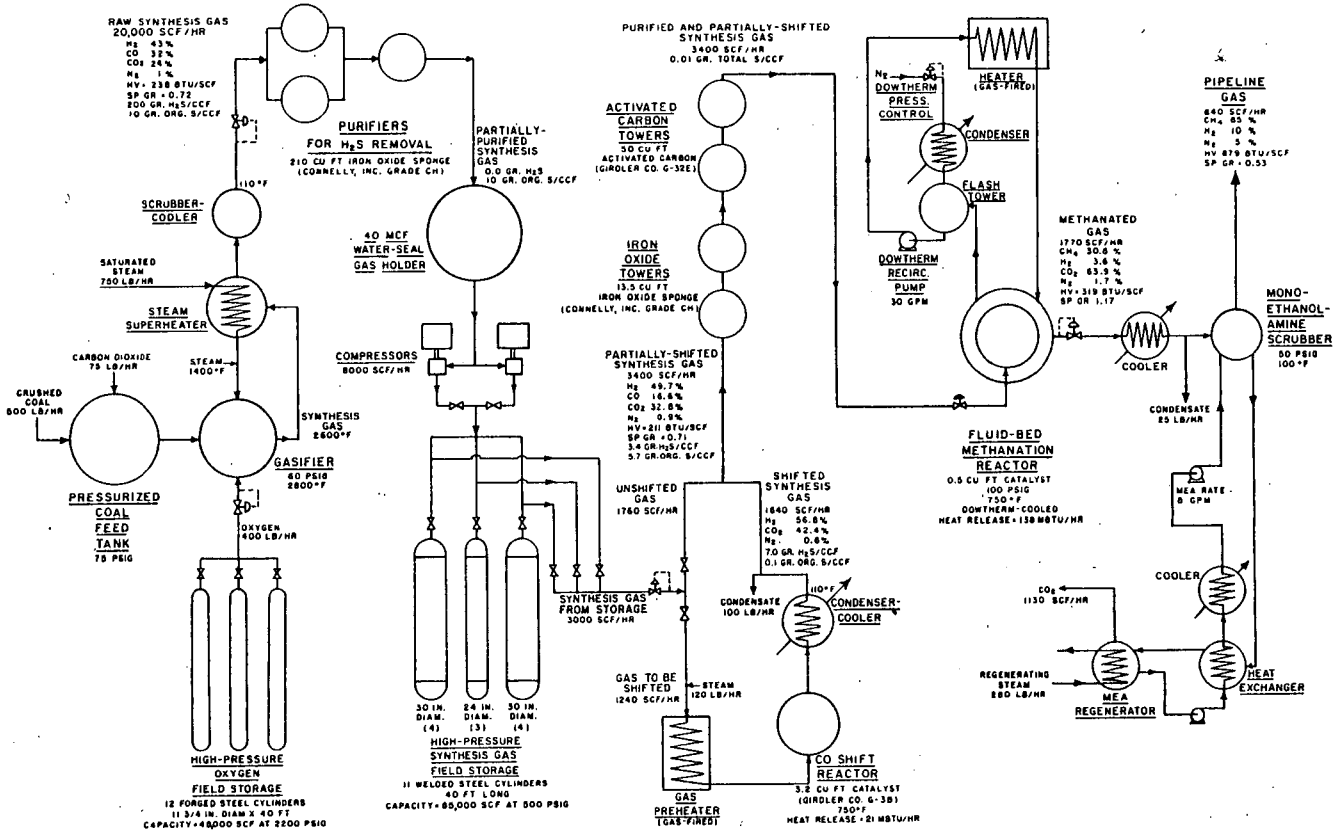

Fig. 5.-SCHEMATIC DIAGRAM OF INTEGRATED PIPELINE-GAS-FROM-COAL PILOT PLANT OPERATION

out the use of gas recycle. Further, in relatively small-scale operation, the highly effective trouble-free and well known iron oxide purification technique appeared preferable from practical considerations.

The organic sulfur (COS and CS_2) concentration of 10 grains/100 SCF used in Figure 5 is only nominal, since it varied considerably with the sulfur content of the coal. In one test with a 4 wt. % sulfur content bituminous coal, the raw gas after bulk H_2S removal contained 26 grains of organic sulfur per 100 SCF; satisfactory operation of the purification system at 3200 SCF/hr. feed rate was still obtained. However, in view of the limited capacity of activated carbon for organic sulfur removal at high partial pressures of CO_2,[30] it would have been desirable to reduce the load on the carbon towers by the addition of another conventional purification step for selective catalytic conversion of COS and CS_2 to H_2S by hydrolysis and hydrogenation.[13] With the scheme shown in Figure 5, the synthesis gas bypassing the CO shift reactor had the original organic sulfur content, although the remainder contained only a small amount, since COS and CS_2 conversion proceeds simultaneously with catalytic CO shift. The resulting reappearance of H_2S was easily handled by a second set of small iron oxide towers.

The final CO_2 removal step shown in Figure 5 had not yet been put into operation when the pilot plant program was interrupted to overcome catalyst problems. In practice, it is unlikely that monoethanolamine scrubbing would be competitive with other processes, such as hot carbonate, at the high CO_2 concentrations and pressures involved.[2,12]

CONCLUSIONS

The technical feasibility of a pipeline-gas-from-coal process utilizing a fluid-bed, partially extracted Raney nickel alloy catalyst for the synthesis gas methanation step was demonstrated. However, rapid mechanical deterioration of this catalyst occurred frequently without a clear indication of the exact causes. This problem was overcome on a laboratory reactor scale by careful control of the caustic leaching step employed for activation of the alloy, by predrying of the catalyst to insure a free-flowing, readily fluidizable charge, and by slow startup in hydrogen. However, successful use of these techniques in the operation of a pilot-plant-scale reactor has yet to be demonstrated. In process variables studies, the use of CO_2-containing, 3:1 H_2/CO synthesis gases was shown to have a beneficial effect on H_2-CO conversion to methane under operating conditions where the catalyst activity was sufficient to permit close approach to equilibrium of the CH_4-CO_2-H_2O-CO-H_2 system. Organic sulfur tolerance of the catalyst at high contamination levels was approximately 0.5 lb./100 lb. of nickel, indicating the need for purifying synthesis gas to a sulfur content of less than 0.01 grain/100 SCF if active catalyst life is not to be limited below a practical economic level. The total catalyst conversion capacity with purified synthesis gas at 10,000 SCF/cu. ft. catalyst-hr. synthesis gas space velocity, and operating pressures of 75-150 p.s.i.g., was approximately 20,000 SCF of methane/lb. of original Raney alloy, or 2000 lb. of methane/lb. of nickel. This corresponded to an active catalyst life of 1000-1500 hours and an original alloy cost on the order of 5 cents/1000 SCF of methane. Since generally less than half of the catalyst was recovered at the end of a test of this duration, it appears that catalyst life was limited by attrition rather than by deactivation.

ACKNOWLEDGMENT

This study was supported by the Promotion-Advertising-Research Plan of the American Gas Association under sponsorship of its Gas Operations Research Committee. The counsel and technical assistance of E. H. Smoker, W. D. McElroy, B. J. Clarke, D. A. Vorum and O. B. J. Fraser, and the other members of the Project Supervising Committee, are gratefully acknowledged. T. L. Robey, N. K. Chaney and Wm. F. Morse, Jr. of the American Gas Association gave valuable support in the planning and guidance of the program. D. McA. Mason was responsible for the development of catalyst and synthesis gas sulfur analysis procedures. J. R. Dvorak of the Armour Research Foundation carried out the metallographic work.

LITERATURE CITED

(1) Alberts, L. W., Bardin, J. S., Beery, D. W., Jones, H. R., Vidt, E. J., Chem. Eng. Progr. 48, 486-93 (1952).
(2) Benson, H. E., Field, J. H., Haynes, W. P., Chem. Eng. Progr. 52, 433-8 (1956).
(3) Booth, N., Wilkins, E. T., Jolley, L. J., Tebboth, J. A., Gas Research Board (Brit.) GRB 21/11 (August 1948).
(4) Chernyshev, A. B., Gudkov, S. F., "The Mechanism of Methane Synthesis on a Fused Nickel Catalyst," in Chernyshev, A. B., "Izbrannye Trudy," 307-10, Akad. Nauk SSSR, 1956.
(5) Chernyshev, A. B., Gudkov, S. F., "A Study of the Methane Synthesis Process in Equipment Having A Fluidized Catalyst Bed," in Chernyshev, A. B., "Izbrannye Trudy," 311-8, Akad. Nauk SSSR, 1956.
(6) Churchill, H. V. and Associates, "Chemical Analysis of Aluminum," 2nd Ed., 110-1, Aluminum Research Laboratories, New Kensington, Pa., 1941.
(7) Cooperman, J., Davis, J. D., Seymour, W., Ruckes, W. L., U. S. Bur. Mines Bull. 498 (1951).
(8) Dent, F. J., Hebden, D., Gas Research Board (Brit.) GRB 51 (November 1949).
(9) Dent, F. J., Moignard, L. A., Eastwood, A. H., Blackburn, W. H. Hebden, D., Gas Research Board (Brit.) GRB 20/10 (February 1948).
(10) Department of Scientific and Industrial Research (Brit.), Fuel Research Tech. Paper No. 57 (1953).
(11) Dressler, R. G., Batchelder, H. R., Tenney, R. F., Wenzell, L. P. Jr., Hirst, L. L., U. S. Bur. Mines, Rept. Invest. 5038 (1954).
(12) Eickmeyer, A. G., Chem. Eng. 65, 113-6 (August 25, 1958).
(13) Girdler Co., The, Louisville, Ky., Catalyst Bull. GC-1256 (December 27, 1956).
(14) Greyson, M., Demeter, J. J., Schlesinger, M. D., Johnson, G. E., Jonakin, J., Myers, J. W., U. S. Bur. Mines, Rept. Invest. 5137 (1955).
(15) Grossman, P. R., Curtis, R. W., ASME Trans. 76, 689-95 (1954).
(16) Hall, C. C., Taylor, A. H., Chem. and Process Eng. 36, 92-4 (1955).
(17) Hoogendoorn, J. C. and Salomon, J. M., Brit. Chem. Eng. 2, 238-44, 308-12 (1957).
(18) Katell, S., Coal Age 63, 116-8 (September 1958).
(19) Kolthoff, I. M., Sandell, E. B., "Textbook of Quantitative Inorganic Analysis," 3rd Ed., 318-20, 689-90, The Macmillan Co., New York, 1952.
(20) Linden, H. R., Reid, J. M., Petroleum Refiner 35, 189-95 (June 1956).
(21) Linton, J. A., Tisdall, G. C., Coke and Gas 19, 402-7, 442-7 (1957); ibid. 20, 148-53 (1958).

(22) Mason, D.McA., Hakewill, H., Jr., Inst. of Gas Technol. Research Bull. No. 5 (January 1959).
(23) Pyrcioch, E. J., Dirksen, H. A., von Fredersdorff, C. G., Pettyjohn, E. S., Am. Gas Assoc. Proc. 1954, 813-36.
(24) Raney, M., U. S. Patent 1,628,190 (May 10, 1927).
(25) Raney, M., U. S. Patent 1,915,473 (June 27, 1933).
(26) Raney, M., Private Communication, April 7, 1959.
(27) Rossini, F. D., Pitzer, K. S., Arnett, R. L., Braun, R. M., Pimentel, G. C., "Selected Values of Physical and Thermodynamic Properties of Hydrocarbons and Related Compounds," Carnegie Press, Pittsburgh, 1953.
(28) Sands, A. E., Grafius, M. A., Wainwright, H. W., Wilson, M. W. U. S. Bur. Mines, Rept. Invest. 4547 (1949).
(29) Sands, A. E., Schmidt, L. D., Ind. Eng. Chem. 42, 2277-87 (1950).
(30) Sands, A. E., Wainwright, H. W., Egleson, G. C., U. S. Bur. Mines, Rept. Invest. 4699 (1950); Amer. Gas Assoc. Proc. 1950, 564-602.
(31) Schlesinger, M. D., Demeter, J. J., Greyson, M., Ind. Eng. Chem. 48, 68-70 (1956).
(32) Shaw, J. A., Ind. Eng. Chem. Anal. Ed. 12, 668-71 (1940).
(33) Strimbeck, G. R., Cordiner, J. B., Jr., Taylor, H. G., Plants, K. D., Schmidt, L. D., U. S. Bur. Mines, Rept. Invest. 4971 (1953); Am. Gas Assoc. Proc. 1952, 778-817.
(34) von Fredersdorff, C. G., Pyrcioch, E. J., Pettyjohn, E. S. Inst. of Gas Technol. Research Bull. No. 7 (January 1957).
(35) Wainwright, H. W., Egleson, G. C., Brock, C. M., U. S. Bur. Mines, Rept. Invest. 5046 (1954).
(36) Weir, H. M., Ind. Eng. Chem. 39, 48-54 (1947).
(37) Wenzell, L. P., Jr., Dressler, R. G., Batchelder, H. R., Ind. Eng. Chem. 46, 858-62 (1954).

NOT FOR PUBLICATION

Presented Before the Division of Gas and Fuel Chemistry
American Chemical Society
Atlantic City, New Jersey, Meeting, September 13-18, 1959

PRODUCTION OF PIPELINE GAS BY HIGH-PRESSURE, FLUID-BED HYDROGASIFICATION OF CHAR

E. J. Pyrcioch and H. R. Linden
Institute of Gas Technology
Chicago, Illinois

Production of high-methane-content (pipeline) gas by direct hydrogenation of coal or low-temperature char[2-9,14,15] has three major advantages over the two-step partial coal oxidation-synthesis gas methanation process:[1,13] large reduction, or potential elimination, of oxygen requirements; elimination of the extreme synthesis gas purification requirements prior to catalytic methanation; and greater thermal efficiency through reduction of exothermic heats of reaction. Complete feed utilization will result if less than half of the more reactive coal or char constituents is hydrogasified and the residue is used as a source of hydrogen. However, essentially complete hydrogasification of lignites and some subbituminous coals may be feasible; hydrogen could then be produced by the reforming of a portion of the product gas or the primary natural gas supply.

In earlier phases of this investigation,[5,14] it was demonstrated in batch reactor tests that gases containing 60-80 volume % methane could be produced by hydrogasification of the lower-rank coals at 1350°F. and 2500-4000 p.s.i.g. By adjustment of hydrogen-coal ratios, gasifications on a moisture-, ash-free (MAF) basis up to 80 wt. % were obtained with bituminous coal, and over 90 wt. % with lignite. However, the residues from bituminous coal hydrogasification were severely agglomerated. As this would hinder smooth operation of a continuous hydrogasification reactor, a pretreatment step yielding nonagglomerating, reactive chars was needed. Optimum reactivity and substantial reduction of agglomeration tendencies of bituminous coal were obtained by fluidized pretreatment in air and nitrogen for about one hour at a maximum temperature of about 600°F; pretreatment with steam as the fluidizing medium did not reduce agglomeration tendencies to the same extent, and pretreatment with carbon dioxide produced chars with the highest agglomeration tendency and also lower reactivity.[5] Lignite, although essentially nonagglomerating during hydrogasification, was benefited by elimination of CO_2; reactivity was only slightly increased by fluidized pretreatment at about 500°F.[5]

REACTOR DESIGN

After the feasibility of preparing sufficiently reactive, nonagglomerating feeds had been established, a design for a fluid-bed hydrogasification unit was developed. To obtain reliable information on the effects of the process variables, it was deemed necessary to have positive control over bed depth. This required parallel upward flow of pulverized coal or char, and of hydrogen, with discharge through a standpipe. It was felt that if a single-stage cocurrent-flow reactor could not produce gas of the desired heating value, or give hydrogasification yields required for a balanced process, multistage operation could be simulated by a series of operations in a single reactor.

The main design problem was selection of the bed depth, hydrogen superficial velocity and coal feed rate which, at nominal design operating conditions of 1400°F., 1000 p.s.i.g. and 60-325 mesh particle size range, would give a) sufficient agitation for free movement of the bed, b) sufficient gas residence time for utilization of most of the hydrogen feed, and c) hydrogen/coal ratios sufficient for gasification of a substantial portion of the coal feed. Tests were made in glass models of upflow reactors with carbon dioxide at a atmospheric pressure and temperature to simulate the mass velocity of hydrogen at reaction conditions. In a 2-inch diameter reactor with a 1-inch standpipe, adequate fluidization of a 5-foot char bed was obtained at a superficial gas velocity of about 0.06 ft./sec. This corresponded to a gas residence time of 1.3-1.4 seconds and, at a char feed rate of about 4 lb./hr., to a char residence time of 30 minutes and an equivalent hydrogen/char ratio of 20 SCF/lb. It appeared from the batch reactor test results that these conditions should give acceptable gasification results; however, the reactor was designed to accommodate an approximately 9-foot bed for greater operational flexibility.

APPARATUS

The high-pressure semicontinuous coal hydrogasification pilot unit consists of an interconnected pressure vessel assembly that includes a reactor, a char feed hopper, a screw feeder and an ungasified-char-residue receiver (Figure 1). The reactor is designed for a working pressure of 3500 p.s.i.g. at 1500°F. and is fabricated of 19-9 DL alloy. It has an inside effective length of 113 inches, an outside diameter of 5 inches, and an inside diameter of 2 inches. A 1-inch diameter standpipe, of a selected height, provides the reaction annulus, controls the height of the char bed, and serves for the removal of the residual char and product gases from the top of the reactor. Self-sealing closures at the top and bottom of the reactor are of the modified Bridgman type with a stainless steel seal ring.

The char feed hopper is fabricated of Type 316 stainless steel and has an inside diameter of 5 inches, an outside diameter of 6-3/4 inches, and has recently been extended to an inside height of 120 inches. It is fitted with confined gasket-type closures at the top and the bottom. Capacity of the hopper is about 40 pounds of char. In most of the tests reported here, the original hopper with an inside height of 60 inches and half of the present char capacity was used. The hopper is parallel to the reactor and is joined to it by a horizontal feed-screw-housing 24 inches in length (see Figure 2 for details).

The ungasified-char receiver has the same dimensions as the original hopper, and is also fabricated of Type 316 stainless steel. The top of the residue receiver is joined to the bottom of the reactor by a short tube with a self-sealing closure, (modified and full Bridgman, respectively). The residue receiver also acts as a separator for the product gas and the ungasified char. The product gas is passed through a porous stainless steel filter, a water-cooled condenser, and a bank of gas filters for final cleanup. Pressure on the hydrogasification unit is maintained by an externally loaded back-pressure regulator.

Char is transferred through the housing connecting the feed hopper and the reactor by means of a rotating spiral screw with an outside diameter of 5/8 inch, a root diameter of 1/4 inch, and a pitch of 0.40 inch. Delivery of char to the screw within the feed hopper is by gravity. A variable-speed electric motor drive, with belt coupling, rotates the screw. Normal operation is at 25-85 r.p.m. for char rates of 1.5 to 6 lb./hr. Commercial electrolytic hydrogen, recom-

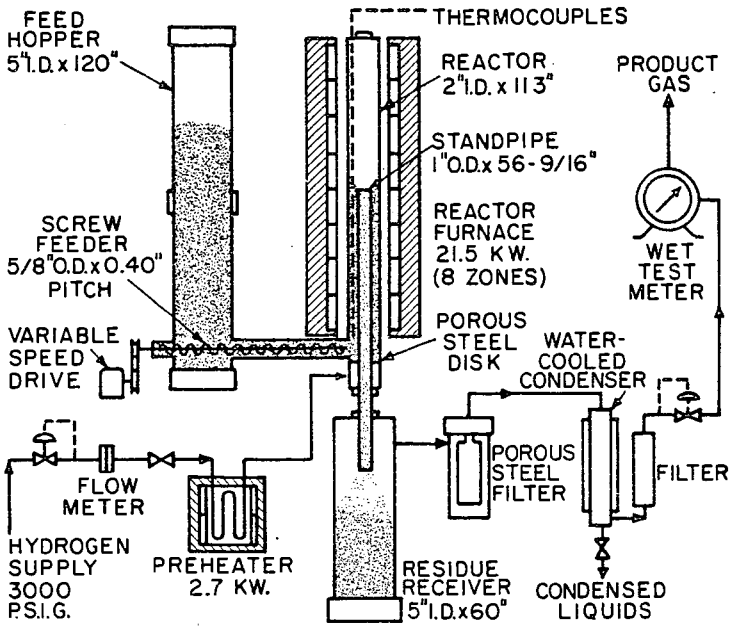

Fig. 1.-COAL HYDROGASIFICATION PILOT UNIT

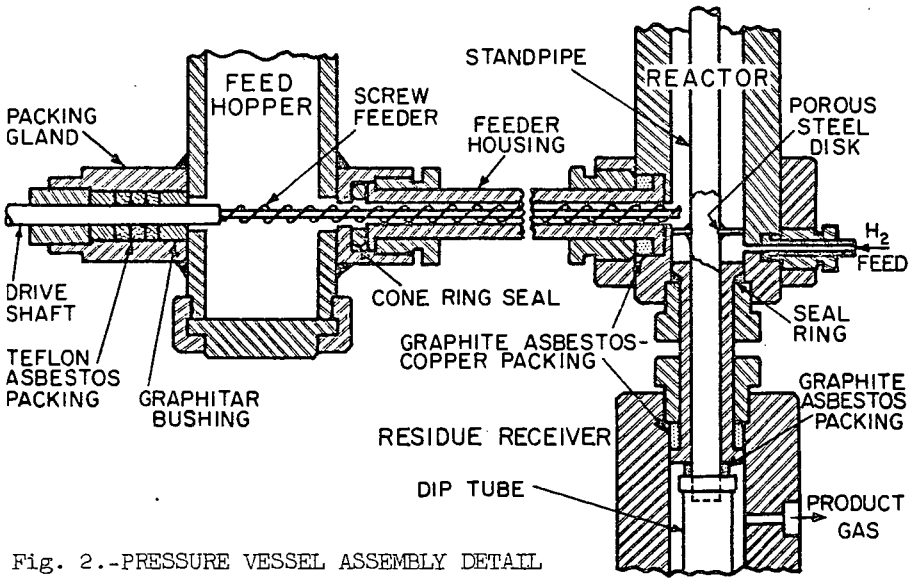

Fig. 2.-PRESSURE VESSEL ASSEMBLY DETAIL

pressed to 3000 p.s.i.g., is fed from a manifolded cylinder bank. A regulator reduces the pressure to a level depending on the desired reactor pressure and hydrogen flow rate. Flow is controlled by a manually operated needle valve, and is metered by a plate orifice with flange pressure taps. Hydrogen enters the reactor preheated to 150°F.

The char bed (reaction) volume is 0.07391 cu.ft. when a nominal 5-foot standpipe (4.714-foot true height) of 1-inch diameter is used. The reactor cross-sectional area, based on a 2-inch by 1-inch annulus, and corrected for two 1/4-inch diameter thermowells that extend the length of the reactor, is 0.01568 sq.ft. A sintered steel disk, of 0.0025-inch mean pore size, which is fastened to the standpipe just below the point where char from the screw feeder enters the reactor, serves as a base for the char bed and as a distributor for the feed hydrogen as it enters the reactor below the disk.

The reactor is heated externally by a 21.5 kw. electric furnace having eight individually controlled heating zones. Char bed temperatures are sensed in ten locations with chromel-alumel thermocouples. Feed hydrogen and gas stream temperatures are also sensed with chromel-alumel thermocouples.

Reactor pressure, differential pressure across the reactor and differential pressure across the hydrogen orifice are continuously recorded. Product gas volume is measured with a wet test meter, and product gas specific gravity is indicated and recorded by a continuous gravitometer.

EXPERIMENTAL PROCEDURE

Feed batches were prepared by crushing and screening the char to a 60-325 mesh size, and drying in air at 110°C. in a forced-convection oven. After the char had been charged to the hopper, the preheated unit was purged with nitrogen and pressurized with hydrogen. The hydrogen orifice meter was then calibrated against the wet test gas meter, the desired hydrogen feed rate established, and the char screw feeder started at a preset rate.

When the char bed reached the top of the standpipe, the differential pressure across the reactor became constant. This differential was normally 20-25 inches of water column, which agreed closely with the value predicted from the bulk density of the expanded char bed; severe fluctuations of differential pressure were an indication of mechanical operating difficulties, such as bypassing of feed hydrogen around the porous steel distributing disk, or plugging of the reactor at the char feed inlet.

The steady-state operating period began when the product gas specific gravity reached a constant value. A composite gas sample was continuously bled into a 10 cu.ft. water-sealed gas holder during the steady-state period; spot gas samples were also taken periodically to confirm other observations relating to attainment of steady operating conditions.

Upon termination of the test, which normally lasted from 4-1/2 to 5-1/2 hours, the unit was depressurized, purged and allowed to cool. Char remaining in the feed hopper, solid residues and condensed liquids were then removed and weighed. Samples of char feed and solid residues were subjected to proximate, ultimate and sieve analyses, and their heating values were determined. Product gases were analyzed with a Consolidated Engineering Co. Model 21-103 mass spectrometer. Carbon monoxide content was determined by infrared

analysis with a Perkin-Elmer Model 12-C infrared spectrometer.

The properties of the composite gas samples, and the char and residue weights corrected to a dry basis, were used in the computation of hydrogasification test results. The char feed rate was computed from the difference between the charged and recovered weights, and from the total feed time. Hydrogen and product gas volumes for the steady-state period were corrected to 60°F. and 30 inches of mercury pressure, and are reported as standard cubic feet (SCF) on a dry basis. Gas heating values and specific gravities were computed from the gas analysis; heating values are reported at 60°F., 30 inches of mercury pressure and saturated with water vapor, whereas specific gravities are for dry gas referred to dry air.

RESULTS

A low-temperature bituminous coal char (Montour No. 10 Mine) supplied by the Research and Development Division of the Consolidation Coal Co. was used in this study. This material was produced in a fluidized carbonization process at much more severe conditions than those employed in the earlier pretreatment study; in batch hydrogasification tests it produced a free-flowing residue, but had significantly less reactivity than chars produced at optimum pretreatment conditions.[5] It was selected for a study of process variables because of its ready availability and uniform properties, and the prospect of minimum handling difficulties. Unlike the feed material employed in the laboratory semiflow study reported by Hiteshue and others,[12] the char was not impregnated with a catalyst. Typical properties of the feed char and the hydrogasification residues are given in Table 1, and selected results for operation at 500, 1000 1500 and 2000 p.s.i.g., 1400° and 1500°F. nominal temperature and nominal char feed rates of 2, 4.5 and 6 lb./hr., are given in Table 2. Precise control of char feed rate was not practical; actual values for each feed rate level varied considerably, and the overall range was 1.6-6.3 lb./hr. Normally, hydrogen feed rates corresponded to a superficial velocity of about 0.06 ft./sec., the level required to maintain free flow of char through the reactor; this was equivalent to rates ranging from 34-35 SCF (dry)/hr. at 500 p.s.i.g., to 130-133 SCF (dry)/hr. at 2000 p.s.i.g. Consequently, with the exception of a few tests at a higher hydrogen rate than the minimum, the hydrogen residence time based on the free reaction volume with the 5-foot standpipe was nearly constant at 1.2-1.5 minutes.

The average reactor temperatures reported in Table 2 are based on measurements taken 1, 8, 18, 28, 42, and 54 inches above the bottom of the char bed. The closer spacing at the bottom, where temperatures are lowest, is partially responsible for the substantial difference between the average and maximum temperatures; the latter closely approach the nominal temperature levels of 1400° and 1500°F.

The effects of char feed rate and pressure on hydrogasification results at 1400°F. are shown graphically in Figure 3. The char feed rate expressed as space velocity or reciprocal space velocity is used as the independent variable. Char residence times can be computed by assuming a typical bulk density of the expanded bed of 25 lb./cu.ft. The available data for the low-temperature bituminous coal char exhibit the expected trends: increase in the percent of char hydrogasified (on a moisture-, ash-free basis) with increases in pressure and decreases in char space velocity; increase in gaseous hydrocarbon

Table 1.-PROXIMATE, ULTIMATE AND SCREEN ANALYSES OF CHAR FEEDS AND RESIDUES

Run No.	19		17		45		13		43	
Operating conditions										
Reactor pressure, p.s.i.g.	521		516		1007		1031		1015	
Maximum reactor temperature, °F.	1415		1405		1405		1410		1510	
Char feed rate, lb./hr.[a]	2.07		5.95		1.92		6.26		1.57	
Sample	Feed	Residue	Feed	Residue	Feed	Residue	Feed	Residue	Feed	Residue
Proximate analysis, wt. %										
Moisture	0.1	7.1	0.4	4.3	0.0	6.2	0.1	7.0	0.0	6.4
Volatile matter	17.2	3.2	17.1	3.6	17.4	3.8	17.6	4.2	17.1	3.2
Fixed carbon	74.7	79.9	74.4	82.7	75.1	78.7	74.2	79.9	75.3	79.1
Ash	8.0	9.8	8.1	9.4	7.5	11.3	8.1	8.9	7.6	12.3
Total	100.0	100.0	100.0	100.0	100.0	100.0	100.0	100.0	100.0	100.0
Ultimate analysis, wt. % (dry basis)										
Carbon	77.6	83.6	77.4	84.7	78.7	83.9	77.6	84.4	78.1	83.0
Hydrogen	3.15	1.55	3.32	1.82	3.19	1.57	3.38	1.82	3.18	1.28
Sulfur	0.93	0.95	0.93	0.89	0.93	0.76	1.05	0.97	0.93	0.67
Ash	8.0	10.6	8.1	9.8	7.5	12.0	8.1	9.6	7.6	13.2
Nitrogen + oxygen (by difference)	10.32	3.30	10.25	2.79	9.68	1.77	9.87	3.21	10.19	1.85
Total	100.0	100.0	100.0	100.0	100.0	100.0	100.0	100.0	100.0	100.0
Heating value, B.t.u./lb. (dry basis)	12,877	13,035	12,765	13,214	12,889	12,859	12,133	13,256	12,743	12,584
Screen analysis, wt. %[b]										
+ 40 mesh	0.0	0.0	0.0	0.0	0.1	0.4	0.0	0.0	0.2	0.2
+ 60 mesh	0.0	0.4	0.0	0.2	0.4	0.2	0.2	0.0	0.2	0.4
+ 80 mesh	5.2	1.2	7.2	2.4	10.1	2.2	2.8	1.2	9.4	1.0
+100 mesh	22.0	17.8	21.6	13.6	10.6	7.6	14.2	10.2	12.6	5.6
+140 mesh	10.0	11.2	8.4	8.2	18.4	15.4	9.2	8.6	18.6	14.6
+200 mesh	33.0	33.0	34.6	28.8	23.8	20.0	31.6	32.0	22.2	20.0
+325 mesh	20.6	26.0	19.2	27.6	27.2	29.6	24.4	35.0	25.7	31.8
-325 mesh	9.2	10.4	9.0	14.2	9.4	24.6	17.6	12.0	11.1	26.4
Total	100.0	100.0	100.0	100.0	100.0	100.0	100.0	100.0	100.0	100.0

Run No.	44		28		31		40		32	
Operating conditions										
Reactor pressure, p.s.i.g.	1001		1518		1512		2012		2004	
Maximum reactor temperature, °F.	1505		1405		1435		1425		1415	
Char feed rate, lb./hr.[a]	6.08		1.76		5.27		2.03		5.75	
Sample	Feed	Residue	Feed	Residue	Feed	Residue	Feed	Residue	Feed	Residue
Proximate analysis, wt. %										
Moisture	0.0	5.5	0.1	11.0	0.1	6.9	0.0	10.0	0.1	5.6
Volatile matter	17.9	2.0	16.8	2.9	17.6	2.8	19.7	4.4	19.7	4.1
Fixed carbon	74.1	82.3	76.4	76.0	75.7	81.7	73.1	74.2	73.0	79.1
Ash	8.0	10.2	6.7	10.1	6.6	8.6	7.2	11.4	7.2	11.2
Total	100.0	100.0	100.0	100.0	100.0	100.0	100.0	100.0	100.0	100.0
Ultimate analysis, wt. % (dry basis)										
Carbon	78.4	85.5	78.8	83.1	78.8	85.6	78.5	82.7	78.5	83.4
Hydrogen	3.19	1.25	3.16	1.60	3.16	1.68	3.22	1.73	3.22	2.20
Sulfur	0.85	0.67	1.06	1.27	0.98	1.13	0.93	0.78	0.93	0.93
Ash	8.0	10.8	6.7	11.3	6.6	9.2	7.2	12.7	7.2	11.9
Nitrogen + oxygen (by difference)	9.56	1.78	10.28	2.73	10.46	2.39	10.15	2.09	10.15	1.57
Total	100.0	100.0	100.0	100.0	100.0	100.0	100.0	100.0	100.0	100.0
Heating value, B.t.u./lb. (dry basis)	12,760	12,966	13,015	12,892	13,032	13,432	13,011	12,832	13,011	13,142
Screen analysis, wt. %[b]										
+ 40 mesh	0.0	0.2	0.0	0.0	0.0	0.9	0.0	0.2	0.2	0.2
+ 60 mesh	0.4	0.2	0.0	0.0	2.0	1.0	1.4	0.2	1.8	1.0
+ 80 mesh	9.2	2.8	24.8	5.2	18.4	7.5	9.0	3.0	13.2	6.3
+100 mesh	11.4	10.4	18.1	11.2	15.0	15.0	12.8	5.8	12.7	12.0
+140 mesh	19.2	20.8	21.0	23.9	20.9	24.9	11.6	13.8	20.0	19.1
+200 mesh	22.0	23.4	20.7	23.7	18.4	22.1	25.2	18.4	21.7	20.9
+325 mesh	26.8	27.3	11.7	19.0	16.2	17.5	32.4	27.8	19.7	21.0
-325 mesh	11.0	14.4	3.7	17.0	9.1	11.1	7.6	30.8	10.7	19.5
Total	100.0	100.0	100.0	100.0	100.0	100.0	100.0	100.0	100.0	100.0

a. Based on weight of dry char.
b. U. S. standard sieve series.

Table 2.-OPERATING DATA FOR FLUID-BED HYDROGASIFICATION OF LOW-TEMPERATURE CHAR AT HIGH PRESSURES

Feed Char: Low-Temperature Bituminous Coal Char, Consolidation Coal Co. Montour No. 10 Mine.[a]
Particle Size: 60-325 Mesh, U. S. Standard Sieve Series. Char Bed Height: 4.714 ft. Char Bed Volume: 0.07391 cu.ft.

Run No.	19	17	45	11	13	43	22	44	28	25	31	40	41	32
Operating conditions														
Reactor pressure, p.s.i.g.	521	516	1007	1046	1031	1015	1015	1001	1518	1527	1512	2012	2012	2004
Reactor temperatures, °F.														
Maximum	1415	1405	1405	1410	1410	1510	1500	1505	1405	1390	1435	1425	1410	1415
Average	1340	1315	1350	1375	1385	1445	1465	1465	1265	1260	1320	1340	1305	1325
Char rate, lb./hr.	2.07	5.95	1.92	3.59	6.26	1.57	3.68	6.08	1.76	3.93	5.27	2.03	4.40	5.75
Hydrogen rate, SCF/hr.	34.48	34.87	66.50	65.54	66.37	65.50	68.02	69.81	93.15	94.61	102.34	131.45	130.26	132.90
Hydrogen/char ratio, SCF/lb.	16.68	5.86	34.65	18.25	10.60	41.85	18.47	11.49	52.88	24.10	19.43	64.69	29.59	23.12
Char space velocity, lb./cu.ft.-hr.[b]	28.0	80.8	26.0	48.6	84.7	21.2	49.9	82.2	23.8	53.1	71.3	27.5	59.6	77.8
Hydrogen residence time, min.	1.35	1.34	1.33	1.38	1.34	1.29	1.23	1.18	1.49	1.47	1.31	1.34	1.38	1.33
Operating results														
Product gas rate, SCF (dry)/hr.	30.38	37.97	52.82	51.61	54.79	49.50	54.50	51.57	81.28	76.34	77.57	100.36	89.63	92.41
Product gas yield, SCF (dry)/lb.	14.70	6.38	27.52	14.38	8.75	31.63	14.80	8.49	46.14	19.45	14.73	49.39	20.36	16.08
Product gas net B.t.u. recovery, M B.t.u./lb	2.99	1.79	4.53	3.16	2.11	5.19	3.63	2.20	5.46	3.65	3.37	5.62	4.08	3.58
Gaseous hydrocarbon space-time yield, SCF (dry) cu.ft.-hr.	148	199	252	293	335	267	359	380	261	394	505	407	601	669
Net moisture-, ash-free char hydrogasified, wt. %[c]	26.4	16.3	42.7	29.3	21.1	52.9	32.4	21.3	48.2	32.5	30.3	58.0	40.6	35.5
Carbon gasified, wt. %	23.7	12.1	42.7	28.4	17.7	53.5	30.6	20.9	47.2	32.1	30.5	63.9	43.4	36.2
Feed hydrogen reacted, SCF(dry)/lb.	7.96	2.62	17.62	10.51	6.28	23.89	11.66	8.16	18.57	12.61	12.34	30.74	19.91	16.26
Char residue, lb./lb.	0.687	0.706	0.483	0.650	0.727	0.414	0.699	0.700	0.455	0.609	0.612	0.260	0.501	0.605
Condensed liquid products,[d] lb./lb.	0.0170	0.0031	0.0551	0.0201	0.0174	0.0681	0.0294	0.0395	0.0549	0.0759	0.0381	0.0685	0.0578	0.0445
Residue moisture, lb./lb.	0.0364	0.0284	0.0207	0.0531	0.0500	0.0259	0.0511	0.0364	0.0297	0.0410	0.0378	0.0282	0.0201	0.0326
Material balance, %	98.6	88.8	97.0	98.5	98.8	100.0	107.4	97.5	99.6	102.4	97.5	93.7	96.4	101.1
Product gas properties														
Gas composition, mole %														
N_2	2.7	4.0	1.5	2.4	2.5	1.6	2.9	0.7	1.2	2.1	1.7	0.7	1.3	2.5
CO	1.9	3.9	1.3	1.5	2.5	1.5	2.1	5.2	0.6	0.6	2.0	0.4	1.4	1.2
CO_2	0.2	2.5	0.1	0.3	0.4	0.2	0.2	0.5	0.1	0.2	0.1	0.1	0.1	0.2
H_2	59.2	50.8	61.9	53.9	49.4	56.8	46.1	39.2	74.4	59.0	48.1	68.8	47.6	42.6
CH_4	35.4	38.4	34.5	39.9	44.7	39.9	48.7	54.2	23.1	37.5	47.7	29.2	48.8	53.1
C_2H_6	0.4	0.2	0.4	1.4	0.3	--	--	0.1	0.5	0.3	0.2	0.6	0.6	0.3
Benzene	0.2	0.2	0.3	0.6	0.2	--	--	0.1	0.1	0.3	0.2	0.2	0.2	0.1
Total	100.0	100.0	100.0	100.0	100.0	100.0	100.0	100.0	100.0	100.0	100.0	100.0	100.0	100.0
Heating value, B.t.u./SCF (sat.)	562	568	564	621	624	584	639	687	482	580	646	530	661	678
Specific gravity, air = 1	0.295	0.370	0.275	0.332	0.374	0.294	0.354	0.396	0.207	0.289	0.343	0.234	0.343	0.369

a. Operating conditions and results based on weight of dry char

b. $\frac{\text{char bed volume}}{\text{cu.ft./min. hydrogen at reactor pressure and temperature}}$

c. $100 \left[\frac{\text{wt. of product gas - wt. of hydrogen in}}{\text{wt. of moisture-, ash-free char}}\right]$

d. Hydrocarbons + water

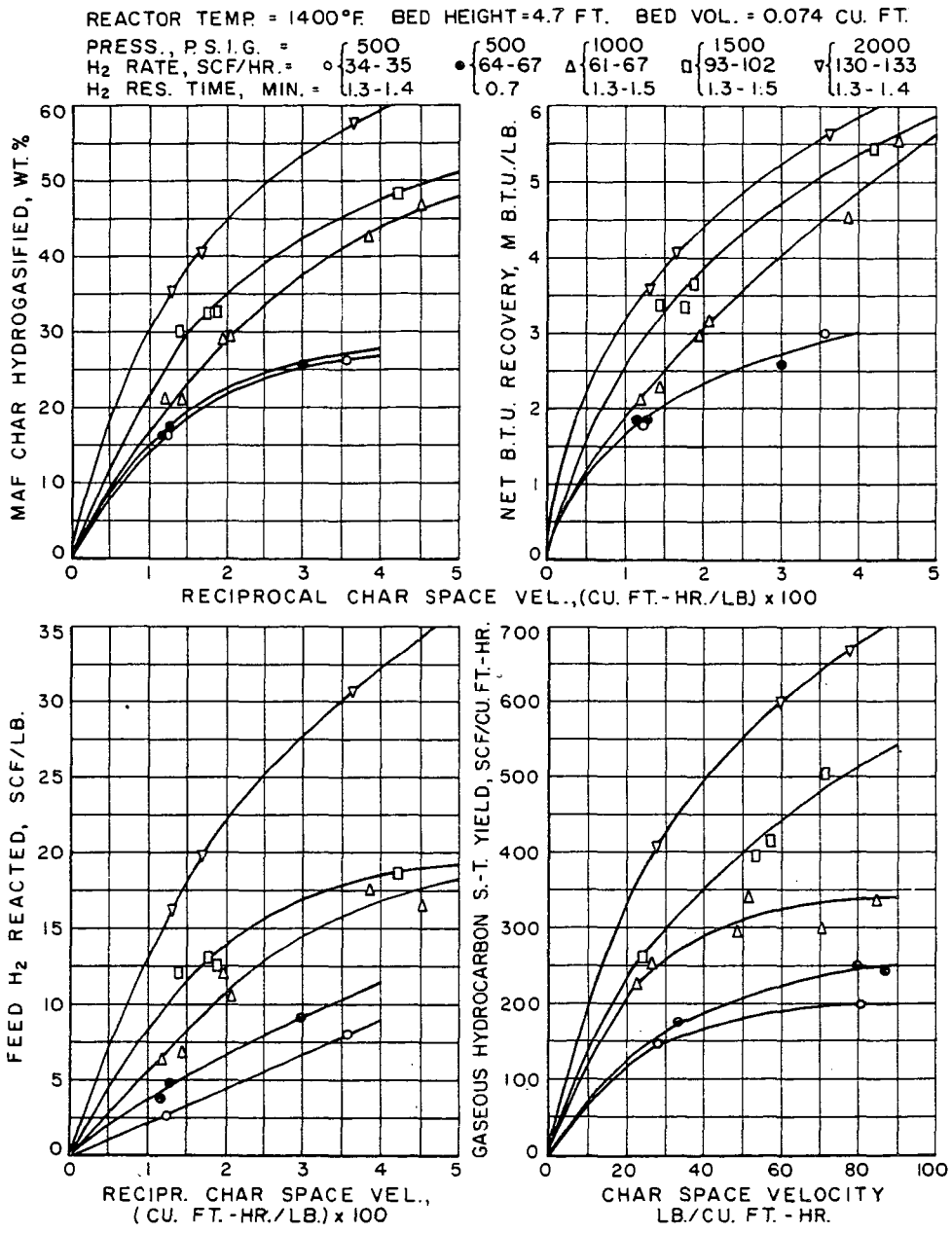

Fig. 3.-FLUID-BED HYDROGASIFICATION RESULTS WITH LOW-TEMPERATURE CHAR

(primarily methane) space-time yield with increases in pressure and increases in char space velocity. The increases in char conversion are accompanied by equivalent increases in the quantity of feed hydrogen reacted – the difference between the amount of hydrogen fed and the amount of unreacted hydrogen contained in the product gas, both per pound of dry char. The net B.t.u. recovery – the difference between the heat of combustion of the product gas and the heat of combustion of the feed hydrogen, both per pound of dry char – also exhibits the same trends as the conversion of char to gas. The data at 500 p.s.i.g. further show that an increase in hydrogen rate to double the level required to maintain a minimum superficial velocity results in a measurable increase in char conversion, gaseous hydrocarbon space-time yield, and quantity of feed hydrogen reacted. Similar results were obtained at higher pressures when the hydrogen feed rate was increased.

The effect of an increase in temperature from 1400° to 1500°F. is indicated in Table 2 in a series of runs at 1000 p.s.i.g. at each of the three feed rate levels. Except for the somewhat erratic behavior of the net B.t.u. recovery, which is an exceedingly sensitive parameter since it is obtained from a relatively small difference of two experimentally determined quantities, this increase in temperature resulted in a small but significant improvement in hydrogasification results.

The char feed and residue analysis data of Table 1 show that, in the course of hydrogasification, the volatile matter and oxygen-plus-nitrogen contents of the char were reduced to a small fraction of the original values, hydrogen content was reduced to about one-half of the original value, and sulfur content remained about the same. The increase in moisture content was caused by water formation through evolution of bound water or reactions of oxygen-containing coal constituents and gasification products with hydrogen; most of this water condensed in the residue receiver and moistened the char residue. Systematic variations of residual char properties with hydrogasification conditions appeared to exist, such as more severe reduction in hydrogen and volatile matter contents at the higher reaction temperature. The screen analyses of the feed and residual chars indicate some size reduction; however, analyses of the residues remaining in the reactor after shutdown showed this was not due to accumulation of larger particles in the reactor.

In the product distributions reported in Table 2, the condensed liquid products consisted primarily of water. Material balances can be seen to be near 100%, and the two parameters of net moisture-, ash-free char hydrogasified and carbon hydrogasified follow similar trends and are of approximately the same magnitude. In conjunction with the consistent behavior of the operating results over the range of test conditions employed, this indicates reliability of the reported data, in spite of the uncertainties introduced by fluid-bed operation at extremely low superficial gas velocities.

DISCUSSION OF RESULTS

The data obtained with low-temperature bituminous coal char and a 5-foot bed height show that a more reactive feed material, a deeper bed, or a number of countercurrent stages will be necessary to achieve both high conversions and high product gas heating values in a single-pass fluid-bed operation. However, an alternate technique for the production of a high-methane-content gas, comprising a hydrogen separation and recycle step, may be more attractive in spite of the

additional process steps required; the gasification rate would be increased by the resulting increase in hydrogen partial pressure, and problems of exothermic heat removal and control of gas-solids contacting greatly simplified. After completion of the present fluid-bed study, moving-bed operation allowing truly countercurrent single-pass contacting may also have to be considered.

Of considerable practical significance are the unexpectedly high gaseous hydrocarbon space-time yields obtained with the bituminous char at 1400°F. A series of studies by Gorin and others[10,11,16,17] of the kinetics of Disco char gasification with H_2-steam mixtures and pure H_2 in a fluid-bed batch reactor at pressures up to 30 atmospheres (426 p.s.i.g.) and temperatures of 1500°-1700°F. are of interest in this connection. Direct comparison is not possible, since results are reported as differential gasification rates, i.e., rates corresponding to zero bed weight, which is equivalent to conditions where no equilibrium hindrance or other inhibiting effects of reaction products exist. The integral gasification rates obtained in this study would, therefore, be expected to be lower than equivalent differential rates, although this difference should be relatively small at low conversions. It appears that, due to the lower reactivity of Disco char, differential rates of methane formation extrapolated to the conditions of the present study are substantially lower than the integral rates reported in Table 2. For example, in terms of the units employed by Gorin and others, integral rates of methane formation in the 5-foot fluid bed at 1500°F. and 1000 p.s.i.g. ranged from about 70-100 x 10^{-4} lb. moles CH_4/lb. atom C per minute over a range of about 50-20% carbon gasification; this is approximately equivalent to extrapolated differential rates for Disco char and pure hydrogen at 1600°F.

At the relatively low pressures and high temperatures employed in the Disco char gasification study, steam was found to greatly accelerate methane formation, in addition to increasing char gasification by reactions leading to the formation of CO, CO_2 and H_2. However, the effect of steam on methane formation decreased rapidly with increases in pressure. This was confirmed in an exploratory fluid-bed test at 1000 p.s.i.g., 1500°F. and 1.1:1 H_2/steam mole ratio, in which the gaseous hydrocarbon space-time yield was 12% lower than in a test at the same conditions with H_2 feed only; a small increase in the rate of gaseous hydrocarbon formation was indicated by comparison with extrapolated data at the same inlet H_2 partial pressure.

The large increase in gaseous hydrocarbon space-time yield with increases in char feed rate, while the hydrogen rate was held nearly constant at each pressure level (Figure 3), occurred in spite of increased equilibrium hindrance from product methane. Since there was no clearly defined tendency for a shift in the source of the hydrogen contained in the gaseous hydrocarbons, this must have been caused primarily by an increase in average reactivity of the char bed. The quantity of feed hydrogen reacted increased nearly in proportion to the gaseous hydrocarbon formation, and corresponded to 80-100% of the hydrogen contained in the gaseous hydrocarbons over the whole range of operating conditions, except for some tests at 500 p.s.i.g. Conversely, the relatively small change in residual char properties with increases in char feed rate and pressure (Table 1) is consistent with the assumption that the increase in the amount of hydrogen supplied by the char was also roughly proportional to the increase in gaseous hydrocarbon formation.

CONCLUSIONS

The feasibility of producing high-methane-content fuel gas by continuous fluid-bed hydrogenolysis of a low-temperature bituminous coal char was demonstrated. In spite of the relatively low reactivity

of the feed material, it was possible to achieve about 40% conversion in a 5-foot bed at 2000 p.s.i.g. and 1400°F. when producing an approximately 50 mole % methane content gas. At these conditions, the gaseous hydrocarbon (mostly methane) production rate was about 600 SCF (dry)/hr.-cu.ft. bed volume, which is sufficiently high to be of commercial interest. Larger conversions were obtained at pressures as low as 1000 p.s.i.g., but at greatly reduced char space velocities, resulting in lower methane production. No major difficulties were encountered in operation of the fluid-bed reactor at an inlet hydrogen superficial velocity of only 0.06 ft./sec. at 500-2000 p.s.i.g. and 1400°-1500°F. Significant improvements in results are expected with deeper beds and more reactive feed materials.

ACKNOWLEDGMENT

This study was supported by the Gas Operations Research Committee of the American Gas Association with funds provided by the Promotion-Advertising-Research Plan of the Association. The guidance and counsel of the Project Supervising Committee under the chairmanship of B. J. Clarke, of T. L. Robey and N. K. Chaney of the American Gas Association, and of M. A. Elliott, director of the Institute of Gas Technology, were very helpful. S. Volchko was primarily responsible for the operation of the pilot unit. Analytical work was done under the supervision of D. M. Mason and J. E. Neuzil.

LITERATURE CITED

(1) Alberts, L. W., Bardin, J. S., Beery, D. W., Jones, H. R., Vidt, E. J., Chem. Eng. Progr. 48, 486-93 (1952).
(2) Austin, G. T., "High Temperature Hydrogenation of Coal," Ph.D. thesis, Purdue University, 1943.
(3) Bray, J. L., Howard, R. E., "Hydrogenation of Coal at High Temperatures," Rept. 1, Purdue Univ. Eng. Expt. Station, Lafayette, Ind., Research Ser. 90 (September 1943).
(4) Bray, J. L., Morgal, P. W., Ibid., Rept. 2, Research Ser. 93 (July 1944).
(5) Channabasappa, K. C., Linden, H. R., Ind. Eng. Chem. 50, 637-44 (1958).
(6) Dent, F. J., Gas J. 244, 502-7 (1944) [Gas World 121, 378-88 (1944)].
(7) Dent, F. J., Gas Research Board (Brit.), Publ. GRB 13/3 (January 1950).
(8) Dent, F. J., Blackburn, W. H., Millett, H. C., Inst. Gas. Engrs. (London), Publ. 167/56 (November 1937) [Gas J. 220, 470, 473-5 (1937)].
(9) Ibid., Publ. 190/73 (December 1938) [Gas J. 224, 442-5 (1938)].
(10) Goring, G. E., Curran, G. P., Tarbox, R. P., Gorin, E., Ind. Eng. Chem. 44, 1051-65 (1952).
(11) Goring, G. E., Curran, G. P., Zielke, C. W., Gorin, E., Ind. Eng. Chem. 45, 2586-91 (1953).
(12) Hiteshue, R. W., Anderson, R. B., Schlesinger, M.D., Ind. Eng. Chem. 49, 2008-10 (1957).
(13) Pyrcioch, E. J., Dirksen, H. A., von Fredersdorff, C. G., Pettyjohn, E. S., Am. Gas Assoc. Proc. 1954, pp.813-36.
(14) Shultz, E. B., Jr. Channabasappa, K. C., Linden, H. R., Ind. Eng. Chem. 48, 894-905 (1956).
(15) Stockman, C. H., Bray, J. L., Purdue Univ. Eng. Expt. Station, Lafayette, Ind., "Hydrogenation of Coal at High Temperatures," Rept. 3, Research Ser. 111 (November 1950).
(16) Zielke, C. W., Gorin, E., Ind. Eng. Chem. 47, 820-5 (1955).
(17) Ibid., 49, 396-403 (1957).

NOT FOR PUBLICATION

Presented Before the Division of Gas and Fuel Chemistry
American Chemical Society

Atlantic City, New Jersey, Meeting, September 13-18, 1959

PROCESS ANALYSIS OF COAL HYDROGASIFICATION WITH STEAM AND RECYCLED HYDROGEN

C. G. von Fredersdorff
Institute of Gas Technology
Chicago, Illinois

Processes currently under investigation for the production of pipeline gas when needed comprise 1) direct pressure hydrogenation or hydrogasification of hydrocarbonaceous materials as coal and oil shale and 2) catalytic conversion to methane of synthesis gas from coal gasification. Although the latter is the technically more advanced method for synthesis of high heating value gases, coal hydrogasification is considered the more acceptable process for adoption for three principal reasons 1) achievable large reduction to potential elimination of oxygen requirements 2) elimination of sulfur purification necessity except in product gas, and 3) improvement in thermal efficiency through reduction of exothermic heats of reaction.

The hydrogasification process requires external hydrogen, which, as with the synthesis gas methanation process, is obtained, of course, through steam decomposition. The requisite steam decomposition proceeds either by 1) catalytic or partial-combustion reforming of a portion of the product gas or of the primary natural gas supply preferably in those instances where nearly complete conversion of solid fuels to high Btu gas may be realized, i.e. hydrogasification of lignite, reactive non-caking subbituminous coals and chars, oil shale and tar sands or 2) oxygen-steam gasification of solid fuel residues from incomplete hydrogasification of less reactive coals and coal chars. Generally, pressure hydrogasification will not readily convert much over 50% of the carbonaceous matter of most bituminous coals, and due to thermodynamic and kinetic limitations, product gases contain moderate quantities of unreacted hydrogen.

Since costs chargeable to hydrogen production represent a major portion of the total cost of pipeline gas, a potentially advantageous modification of the coal hydrogasification process comprises 1) methane separation by liquefaction or other suitable means to insure maximum heating value of the product gas 2) recycling of the recovered hydrogen to insure full utilization of the gasifying medium and 3) admission of steam in the reactor hydrogasification zone to promote additional hydrogen formation via steam decomposition from the exothermic heat of the coal hydrogenation reactions, thereby improving the heat balance and further decreasing fuel requirements. To be economically attractive the advantages gained must, of course, outweigh the cost increment of product gas separation.

The key concept of the hydrogen recycle process is gasification of coal by simultaneous reaction with steam and recycled hydrogen at elevated pressure and temperature to achieve as near as possible a thermal balance between exothermic and endothermic reactions and to substantially eliminate external hydrogen requirements. The hydrogen produced internally by this scheme would be supplemented by water-gas shift of the hot product gas with additional steam to convert available carbon monoxide. An evaluation of process feasibility requires a thermodynamic

analysis of the $C-H_2-H_2O$ and $C-H_2-H_2O-O_2$ systems supplemented with interpretation of available kinetic data.

THERMODYNAMIC ANALYSIS OF COAL GASIFICATION WITH STEAM AND HYDROGEN

I. Definition of the Process

Fig. 1 shows a schematic diagram of the proposed coal gasification process. Recycled hydrogen is assumed at 800°F. through heat exchange with the product gas. Process steam is assumed superheated to 1000°F. from an external source. For fixed-bed operation the solid fuel may be fed at the top of the reactor, and for fluid-bed operation the coal charge may be injected with the hydrogen feed stream. After preliminary cleaning of dust, the raw gas, comprising essentially CH_4, H_2, CO, CO_2 and unreacted steam is passed to catalytic water-gas-shift. The gas, then at approximately 1000°F., is cooled in the hydrogen recycle heat exchanger, scrubbed with water to condense unreacted steam, and purified of CO_2, H_2S and other sulfur bearing gases prior to methane separation by liquefaction. Some arrangement of heat exchangers as shown would be necessary to preserve refrigeration economy in liquefaction. The liquid methane could be vaporized and the cold H_2 reheated by the incoming warm gases. The warm H_2 is recompressed by a booster to complete the recycle circuit.

This process may not necessarily require a water-gas shift step, in which event the recycled gas comprises a mixture of hydrogen with moderate amounts of carbon monoxide. Some CO shift would presumably occur in the gasification reactor itself, since moderate excess steam would always be present at the recycle gas introduction point. However, the presence of CO may interfere with the efficient separation of CH_4 by liquefaction. If a water-gas shift reactor is used, then the methane could be separated from the CH_4-H_2 mixture by molecular effusion in "diffusion" cascades, as an alternative to liquefaction.

In the process analysis, which will be directed to operating conditions of the reactor it is assumed that recycled gas consists of hydrogen only. The important variables to be established are temperatures and pressures to make the process thermodynamically feasible. The criteria of feasibility are 1) heat requirements of the reactor per MCF of methane produced, and 2) ratio of hydrogen produced to hydrogen consumed in the process. An analysis of the equilibria and heat effects of the $C-H_2-H_2O$ system is first necessary to establish whether the process can be operated without oxygen as a source of heat through partial combustion.

II. Thermodynamic Analysis of $C-H_2-H_2O$ System

A. Defining Equations

The system is completely defined by the reactions:

$C + 2H_2 \longrightarrow CH_4$	Reaction 1
$C + H_2O \longrightarrow CO + H_2$	Reaction 2
$CO + H_2O \longrightarrow CO_2 + H_2$	Reaction 3

The concentrations of the five gaseous components are solved by a procedure of Parent and Katz.[8] The material balance (Table 1) and relationships are:

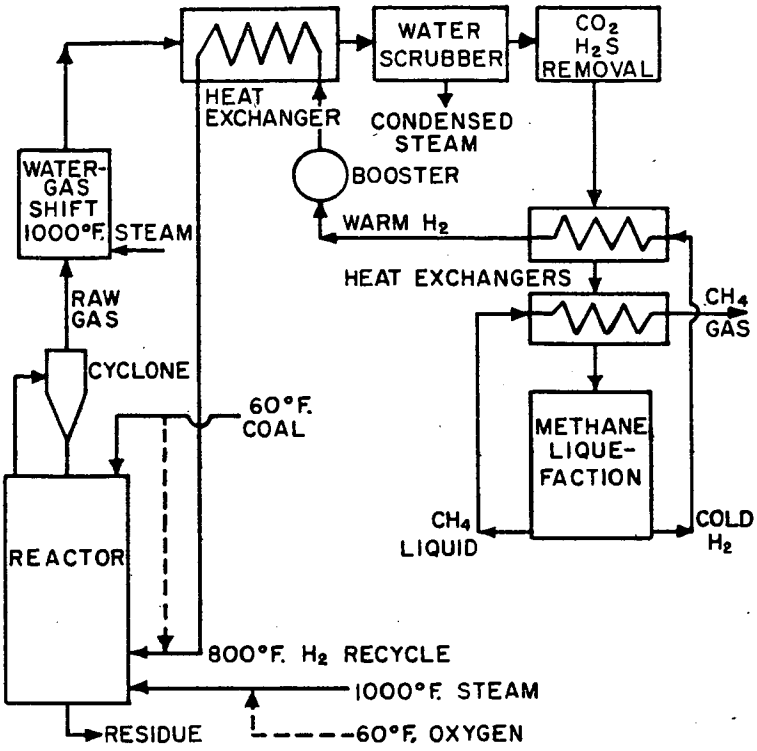

Fig. 1.-SCHEMATIC FLOW DIAGRAM OF HYDROGEN RECYCLE GASIFICATION PROCESS

Table 1.-MATERIAL BALANCE OF THE C-H_2-H_2O SYSTEM

Component	Initial Amount Moles/Mole Inlet Steam	Equilibrium Partial Pressure, Atm.	Equilibrium Molar Quantities, Moles/ Mole Inlet Steam
C	excess	--	--
H_2	a	X	x
H_2O	1.0	Y	y
CO	0	Z	z
CO_2	0	M	m
CH_4	0	W	w
Total		P	N

a) Reaction 1. Equilibrium, for ideal gases

$$K_1 = W/\gamma_c X^2 \tag{1}$$

where γ_c = activity of carbon to hydrogenation

b) Reaction 2. Equilibrium, for ideal gases

$$K_2 = ZX/\gamma_c' Y \tag{2}$$

where γ_c' = activity of carbon to steam

c) Reaction 3. Equilibrium, for ideal gases

$$K_3 = XM/ZY \tag{3}$$

d) Hydrogen balance

$$a = x + y + 2w - 1 \tag{4}$$

e) Oxygen balance

$$y + z + 2m = 1 \tag{5}$$

f) Carbon balance

$$c_g = z + m + w = \text{moles carbon gasified per mole inlet steam} \tag{6}$$

g) Total pressure

$$P = X + Y + Z + M + W \tag{7}$$

h) Total moles at equilibrium

$$N = x + y + z + m + w \tag{8}$$

The following solution from Equations 1, 2, 3 and 7 obtains:

a) CH_4 partial pressure, Atm

$$W = K_1 \gamma_c X^2 \tag{9}$$

b) H_2O partial pressure, Atm

$$Y = \frac{X(X+K_2\gamma_c')}{2K_2K_3\gamma_c'}\left[-1 + \sqrt{1 + \frac{4K_2K_3\gamma_c'(P-X-W)}{(X+K_2\gamma_c')^2}}\right] \tag{10}$$

c) CO partial pressure, Atm

$$Z = K_2 Y \gamma_c'/X \tag{11}$$

d) CO_2 partial pressure, Atm

$$M = P - X - Y - Z - W = K_3YZ/X \qquad (12)$$

For selected temperature, total pressure and assumed carbon activity, equilibrium partial pressures are computed successively by assigning arbitrary X values, or hydrogen partial pressure. Molar quantities are found from:

a) multiplication of the oxygen balance (Equation 5) by P/N, yielding:

$$N = P/\left[Y + Z + 2M\right] \qquad (13)$$

b) law of additive pressures:

$$x = NX/P,\ y = NY/P,\ z = NZ/P,\ m = NM/P,\ w = NW/P \qquad (14)$$

The required H_2/H_2O inlet molar ratio for the system, from Equation 4, must be zero or positive for a valid solution. Equation 6 yields the quantity of carbon gasified, and the gas composition is defined by the molar quantities. The fraction of steam decomposed, SD, is given by:

$$SD = 1-y \qquad (15)$$

One criterion of process feasibility is the ratio, R, of hydrogen produced to hydrogen consumed, taking into account the CO as equivalent to hydrogen,

$$R = \frac{1-y+z}{2w}\ ,\ \frac{\text{moles } H_2 \text{ available}}{\text{moles } H_2 \text{ consumed}} \qquad (16)$$

As a basis for correction of R for actual fuels, experimental data of Channabassappa and Linden on bituminous coal containing about 75 weight % carbon, and 5 weight % hydrogen, (dry basis) indicate that approximately 80% of the coal feed hydrogen content appears as CH_4 and higher hydrocarbons in the product gas.[2] An approximation of the quantity of hydrogen available from coal for hydrogasification, expressed as moles/mole inlet steam, is therefore taken to be $0.8\ r_H\ C_g/f$, where R_H = hydrogen/carbon molar ratio in coal, and f = fraction carbon gasified. With a coal feed containing 75 weight % C and 5 weight % H, and 95% carbon gasification, this becomes $(0.8)(0.4)c_g/0.95 = 0.336\ c_g$. The corrected ratio, R', hydrogen available to hydrogen consumed, may be written for this case:

$$R' = \frac{1-y+z+0.336c_g}{2w} \quad \text{(corrected for coal)} \qquad (17)$$

The recycle gasification process will be independent of an external source of hydrogen if $R' \geq 1.0$.

The second test of process feasibility is the net heat effect of the system, ΔH_R, in Btu/lb. mole CH_4 produced. This is given by:

$$\Delta H_R = \Delta H_1 + \frac{1}{w}\left[(1-m-y)\,\Delta H_2 + m\,\Delta H_3 + C_g\,\Delta H_c + a\,\Delta H_{H_2} + \Delta H_{H_2O}\right] \qquad (18)$$

where ΔH_1, ΔH_2, ΔH_3 = heat of reaction, in Btu/lb. mole, of Reactions 1, 2 and 3, respectively, with reactants and products at the temperature of the system, and ΔH = enthalpy of reactant, Btu/lb. mole, between inlet and system outlet temperature.

Thermodynamic equilibrium constants and enthalpy data of the Bureau of Standards[12] were used in all calculations.

B. Equilibrium Computations

The range of variables considered for the C-H_2-H_2O system are 50,100 and 200 atmospheres, and 1000, 1100, 1200 and 1300°K. with 60°F. inlet carbon, 1000°F. inlet steam, and 800°F. recycled hydrogen. The activity of carbon, γ_c', with respect to the carbon-steam Reaction 2 is taken at unity in all cases. Since experimental results on coal hydrogenation have demonstrated that methane concentrations based on β-graphite-hydrogen equilibrium can be exceeded by as much as 10-20%,[2] it is necessary to consider at least two activities of the carbon, i.e., γ_c = 1.0 and 1.5, with respect to the carbon-hydrogen Reaction 1. The choice of γ_c = 1.5 results in CH_4 concentrations approximately 20% in excess of β-graphite-hydrogen equilibrium.

Results of the computations, the majority of which were performed on an ALWAC III digital computer, are listed in Table 2; although many more results were obtained than are tabulated there, those presented are selected as representative of conditions for which the ratios: H_2 available/H_2 consumed, are within the range 0.5-1.4. These data can be plotted against H_2/H_2O inlet molar ratio to determine conditions for which R is exactly 1.0, the point at which the process, at equilibrium, would be independent of external hydrogen.

Typical plots over a wide range of H_2/H_2O inlet molar ratios are given in Fig. 2 for 200 atmospheres, γ_c = 1.0, 1200°K. (1700°F.) and 1300°K. (1880°F.). In these plots the equilibrium gas compositions and heat effects are shown, and two curves for H_2 available/H_2 consumed are included: one for pure carbon and one for coal containing 75 weight % C and 5 weight % H. It can be seen for the conditions 200 atmospheres, = 1200°K. (1700°F.), and γ_c = 1.0 (Fig. 2A), that at a 1.0 ratio of H_2 available/H_2 consumed, with coal as fuel, the process is endothermic by 35,000 Btu/lb. mole CH_4, and that the equilibrium CH_4 content is nearly 30% (wet basis). The endothermicity decreases with increasing H_2/H_2O inlet molar ratio; however, the ratio of H_2 available/H_2 produced also decreases. Thus at extremely high H_2/H_2O inlet molar ratios the process approaches thermal balance, but requires external hydrogen. At low H_2/H_2O inlet molar ratios the process has sufficient hydrogen, but lacks heat. This is as anticipated, since at low H_2/H_2O inlet molar ratios the endothermic steam decomposition reactions predominate because steam is present in large excess, whereas at high H_2/H_2O inlet molar ratios, the exothermic hydrogenation reactions predominate, since hydrogen is present in large excess.

Therefore, the process cannot attain a self-balanced condition from the standpoint of both hydrogen and heat requirements at 200 atmospheres, 1200°K. (1700°F.), with 1000°F. preheated steam and 800°F. preheated hydrogen. The same results are observed at 200 atmospheres, 1300°K. (1800°F.), and γ_c = 1.0 (Fig. 2B), where, with a 1.0 ratio of H_2 available/H_2 consumed for coal as fuel, the heat requirement is nearly 50,000 Btu/lb. mole CH_4. An examination of all other conditions given in Table 2 shows that process heat requirements are in the range 25,000-100,000 Btu/lb. mole CH_4 at the operating point determined by a 1.0 ratio of H_2 available/H_2 produced. This heat deficiency will always prevail at all possible gasification temperatures.

Alternate methods for supplying the heat requirements are 1) high preheat of reactants, 2) indirect internal heat exchange with a high-temperature heat transfer fluid, or 3) partial combustion of coal with oxygen within the reactor. In view of the large heat deficiency and the need for rapid heat transfer, the third alternative appears most attractive. This automatically provides a high-temperature zone where a portion of the inlet steam is rapidly decomposed, desirable because

Table 2, Part 1.-EQUILIBRIUM CONCENTRATIONS AND HEAT EFFECTS OF THE C-H_2-H_2O SYSTEM

C as β-Graphite, 60°F.; Inlet H_2 at 800°F.; Inlet Steam at 1000°F.; $\gamma_c' = 1.0$

Pressure, Atm. Abs.	50	50	50	50	50	50	50	50	50	50	50	50
Temp., °K.	1000	1000	1000	1100	1100	1100	1200	1200	1200	1300	1300	1300
Inlet H_2/H_2O Molar Ratio	0.157	0.465	0.877	0.537	0.831	1.21	1.63	2.11	2.73	2.52	3.14	3.98
Carbon Activity, γ_c	1.0	1.0	1.0	1.0	1.0	1.0	1.0	1.0	1.0	1.0	1.0	1.0
Mole %												
H_2	20.00	22.00	24.00	32.00	34.00	36.00	48.00	50.00	52.00	60.00	62.00	64.00
H_2O	32.68	31.75	29.99	22.35	21.45	20.24	11.41	10.58	9.62	5.18	4.72	4.22
CO	8.52	7.53	6.51	16.16	14.60	13.02	18.93	16.83	14.73	19.62	17.31	14.97
CO_2	19.14	14.93	11.19	10.66	8.70	6.91	3.13	2.48	1.90	0.92	0.72	0.53
CH_4	19.66	23.79	28.31	18.83	21.25	23.83	18.53	20.11	21.75	14.28	15.25	16.28
Wet Products/Inlet H_2O, Molar Ratio	1.258	1.446	1.698	1.671	1.870	2.123	2.731	3.087	3.550	3.752	4.258	4.940
C Gasified/Inlet H_2O, Molar Ratio	0.595	0.669	0.781	0.763	0.833	0.929	1.11	1.22	1.36	1.31	1.42	1.57
Steam Decomp., %	58.9	54.1	49.1	62.7	59.9	57.0	68.8	67.3	65.8	80.5	79.9	79.1
H_2 Available/H_2 Consumed, for pure C	1.41	0.945	0.626	1.43	1.10	0.837	1.19	0.961	0.765	1.44	1.18	0.953
ΔH_R, MBtu/lb. Mole CH_4	57.1	31.8	14.2	75.6	55.4	39.1	77.9	62.1	48.4	116.3	97.7	80.7

Pressure, Atm. Abs.	50	50	50	50	50	50	50	50	50	50	50	50
Temp., °K.	1000	1000	1000	1100	1100	1100	1200	1200	1200	1300	1300	1300
Inlet H_2/H_2O Molar Ratio	0.228	0.650	1.28	0.472	0.814	1.27	1.35	1.83	2.45	1.69	2.15	2.74
Carbon Activity, γ_c	1.5	1.5	1.5	1.5	1.5	1.5	1.5	1.5	1.5	1.5	1.5	1.5
Mole %												
H_2	18.00	20.00	22.00	28.00	30.00	32.00	42.00	44.00	46.00	52.00	54.00	56.00
H_2O	29.81	28.51	26.07	20.90	20.01	18.72	11.30	10.50	9.56	5.67	5.27	4.83
CO	8.64	7.43	6.18	17.28	15.44	13.55	21.41	18.99	16.53	24.77	22.19	19.59
CO_2	19.66	14.57	10.07	12.19	9.73	7.49	4.01	3.16	2.39	1.47	1.19	0.92
CH_4	23.89	29.49	35.68	21.63	24.82	28.24	21.28	23.35	25.52	16.09	17.35	18.66
Wet Products/Inlet H_2O, Molar Ratio	1.285	1.536	1.908	1.598	1.821	2.116	2.454	2.792	3.238	2.995	3.350	3.806
C Gasified/Inlet H_2O, Molar Ratio	0.671	0.791	0.991	0.817	0.910	1.04	1.15	1.27	1.44	1.27	1.36	1.49
Steam Decomp., %	61.7	56.2	50.3	66.6	63.6	60.4	72.3	70.7	69.1	83.0	82.3	81.6
H_2 Available/H_2 Consumed, for pure C	1.19	0.747	0.456	1.36	1.01	0.745	1.19	0.949	0.742	1.63	1.35	1.10
ΔH_R, MBtu/lb. Mole CH_4	43.1	19.3	3.3	68.5	47.3	30.7	73.4	56.7	42.6	121.3	101.1	83.3

Table 2, Part 2.-EQUILIBRIUM CONCENTRATIONS AND HEAT EFFECTS OF THE C-H_2-H_2O SYSTEM

C as β-Graphite, 60°F.; Inlet H_2 at 800°F.; Inlet Steam at 1000°F.; $\gamma_c' = 1.0$

Pressure, Atm. Abs.	100	100	100	100	100	100	100	100	100	100	100	100
Temp., °K.	1000	1000	1000	1100	1100	1100	1200	1200	1200	1300	1300	1300
Inlet H_2/H_2O Molar Ratio	0.139	0.331	0.560	0.512	0.689	0.896	1.092	1.29	1.52	2.07	2.35	2.67
Carbon Activity, γ_c	1.0	1.0	1.0	1.0	1.0	1.0	1.0	1.0	1.0	1.0	1.0	1.0
Mole %												
H_2	15.00	16.00	17.00	25.00	26.00	27.00	37.00	38.00	39.00	50.00	51.00	52.00
H_2O	35.99	35.46	34.52	26.90	26.28	25.51	16.95	16.42	15.83	8.66	8.28	7.89
CO	6.25	5.78	5.29	12.45	11.70	10.93	18.22	17.19	16.15	19.65	18.45	17.24
CO_2	20.64	17.60	14.78	12.66	11.17	9.75	5.81	5.17	4.56	1.85	1.63	1.42
CH_4	22.12	25.16	28.41	22.99	24.85	26.81	22.02	23.22	24.46	19.84	20.64	21.45
Wet Products/Inlet H_2O, Molar Ratio	1.197	1.308	1.441	1.546	1.657	1.787	2.136	2.275	2.432	3.122	3.333	3.574
C Gasified/Inlet H_2O, Molar Ratio	0.587	0.635	0.699	0.744	0.791	0.849	0.934	1.04	1.10	1.29	1.36	1.43
Steam Decomp., %	56.9	53.6	50.3	58.4	56.5	54.4	63.8	62.6	61.5	72.9	72.4	71.8
H_2 Available/H_2 Consumed, for pure C	1.22	0.930	0.707	1.09	0.921	0.772	1.09	0.963	0.847	1.08	0.973	0.870
ΔH_R, MBtu/lb. Mole CH_4	44.3	28.9	16.9	51.2	40.8	31.8	65.3	56.6	48.8	79.6	71.6	64.1

Pressure, Atm. Abs.	100	100	100	100	100	100	100	100	100	100	100	100
Temp., °K.	1000	1000	1000	1100	1100	1100	1200	1200	1200	1300	1300	1300
Inlet H_2/H_2O Molar Ratio	0.125	0.367	0.672	0.346	0.538	0.763	0.936	1.15	1.41	1.79	2.08	2.40
Carbon Activity, γ_c	1.5	1.5	1.5	1.5	1.5	1.5	1.5	1.5	1.5	1.5	1.5	1.5
Mole %												
H_2	13.00	14.00	15.00	21.00	22.00	23.00	32.00	33.00	34.00	44.00	45.00	46.00
H_2O	32.76	32.18	31.05	25.14	24.63	23.94	16.15	15.64	15.06	8.55	8.19	7.80
CO	6.57	5.99	5.40	13.86	12.96	12.04	20.09	18.86	17.62	22.08	20.66	19.25
CO_2	22.75	18.93	15.37	15.67	13.71	11.84	7.06	6.23	5.43	2.33	2.05	1.77
CH_4	24.92	28.90	33.18	24.33	26.70	29.18	24.70	26.27	27.89	23.04	24.10	25.18
Wet Products/Inlet H_2O, Molar Ratio	1.178	1.315	1.488	1.421	1.538	1.675	1.985	2.129	2.295	2.832	3.034	3.268
C Gasified/Inlet H_2O, Molar Ratio	0.639	0.708	0.803	0.765	0.821	0.888	1.03	1.09	1.17	1.34	1.42	1.51
Steam Decomp., %	61.4	57.7	53.8	64.3	62.1	59.9	67.9	66.7	65.4	75.8	75.1	74.5
H_2 Available/H_2 Consumed, for pure C	1.18	0.863	0.626	1.21	0.999	0.819	1.10	0.955	0.827	1.06	0.943	0.835
ΔH_R, MBtu/lb. Mole CH_4	40.6	23.9	11.2	55.9	43.1	32.4	62.2	52.7	44.2	72.5	64.2	56.5

Table 2, Part 3.-EQUILIBRIUM CONCENTRATIONS AND HEAT EFFECTS OF THE C-H_2-H_2O SYSTEM

C as β-Graphite, 60°F.; Inlet H_2 at 800°F.; Inlet Steam at 1000°F.; $\gamma_C' = 1.0$

Pressure, Atm. Abs.	200	200	200	200	200	200	200	200	200	200	200	200
Temp., °K.	1000	1000	1000	1100	1100	1100	1200	1200	1200	1300	1300	1300
Inlet H_2/H_2O Molar Ratio	0.112	0.234	0.372	0.214	0.725	3.12	0.025	1.281	2.367	1.158	1.739	2.578
Carbon Activity, γ_C	1.0	1.0	1.0	1.0	1.0	1.0	1.0	1.0	1.0	1.0	1.0	1.0
Mole %												
H_2	11.00	11.50	12.00	17.50	20.00	25.00	22.50	30.00	33.00	37.50	40.00	42.50
H_2O	38.59	38.29	37.80	31.75	29.73	20.64	23.98	20.73	17.60	14.23	12.97	11.40
CO	4.57	4.34	4.10	10.50	8.61	4.77	21.18	13.69	10.60	21.53	18.40	15.22
CO_2	22.05	19.87	17.79	17.75	12.27	3.73	16.04	6.64	3.80	4.43	3.24	2.22
CH_4	23.79	26.00	28.31	22.50	29.39	45.86	16.30	28.94	35.00	22.31	25.39	28.66
Wet Products/Inlet H_2O, Molar Ratio	1.145	1.213	1.290	1.287	1.590	3.00	1.296	2.100	2.792	2.240	2.641	3.218
C Gasified/Inlet H_2O, Molar Ratio	0.577	0.609	0.648	0.654	0.799	1.63	0.694	1.035	1.379	1.08	1.24	1.48
Steam Decomp., %	55.8	53.6	51.2	59.1	52.7	38.2	69.9	56.5	50.9	68.1	65.7	63.3
H_2 Available/H_2 Consumed, for pure C	1.12	0.933	0.774	1.25	0.711	0.191	2.30	0.701	0.411	1.16	0.853	0.609
ΔH_R, MBtu/lb. Mole CH_4	37.5	27.6	19.2	57.5	25.5	-13.5	136.8	34.4	16.0	78.9	56.8	39.4

Pressure, Atm. Abs.	200	200	200	200	200	200	200	200	200	200	200	200
Temp., °K.	1000	1000	1000	1100	1100	1100	1200	1200	1200	1300	1300	1300
Inlet H_2/H_2O Molar Ratio	1.108	0.263	0.444	0.266	0.382	0.510	0.604	0.712	0.830	1.128	1.375	1.662
Carbon Activity, γ_C	1.5	1.5	1.5	1.5	1.5	1.5	1.5	1.5	1.5	1.5	1.5	1.5
Mole %												
H_2	9.50	10.00	10.50	15.50	16.00	16.50	23.50	24.00	24.50	33.00	34.00	35.00
H_2O	34.91	34.58	33.99	28.64	28.35	27.95	21.01	20.73	20.40	13.27	12.78	12.23
CO	4.79	4.51	4.22	10.69	10.25	9.81	17.77	17.16	16.55	22.82	21.35	19.84
CO_2	24.19	21.42	18.78	18.66	17.16	15.70	11.07	10.32	9.59	4.99	4.36	3.77
CH_4	26.61	29.49	32.51	26.51	28.24	30.04	26.65	27.79	28.96	25.92	27.51	29.16
Wet Products/Inlet H_2O, Molar Ratio	1.135	1.220	1.319	1.304	1.371	1.445	1.641	1.708	1.781	2.170	2.333	2.523
C Gasified/Inlet H_2O, Molar Ratio	0.631	0.676	0.732	0.728	0.763	0.803	0.911	0.944	0.981	1.17	1.24	1.33
Steam Decomp., %	60.4	57.8	55.2	62.6	61.1	59.6	65.5	64.6	63.7	71.2	70.2	69.1
H_2 Available/H_2 Consumed, for pure C	1.09	0.880	0.708	1.11	0.971	0.850	1.08	0.990	0.903	1.07	0.935	0.810
ΔH_R, MBtu/lb. Mole CH_4	34.4	23.5	14.5	46.9	39.0	32.0	57.6	51.6	46.1	68.5	58.9	50.2

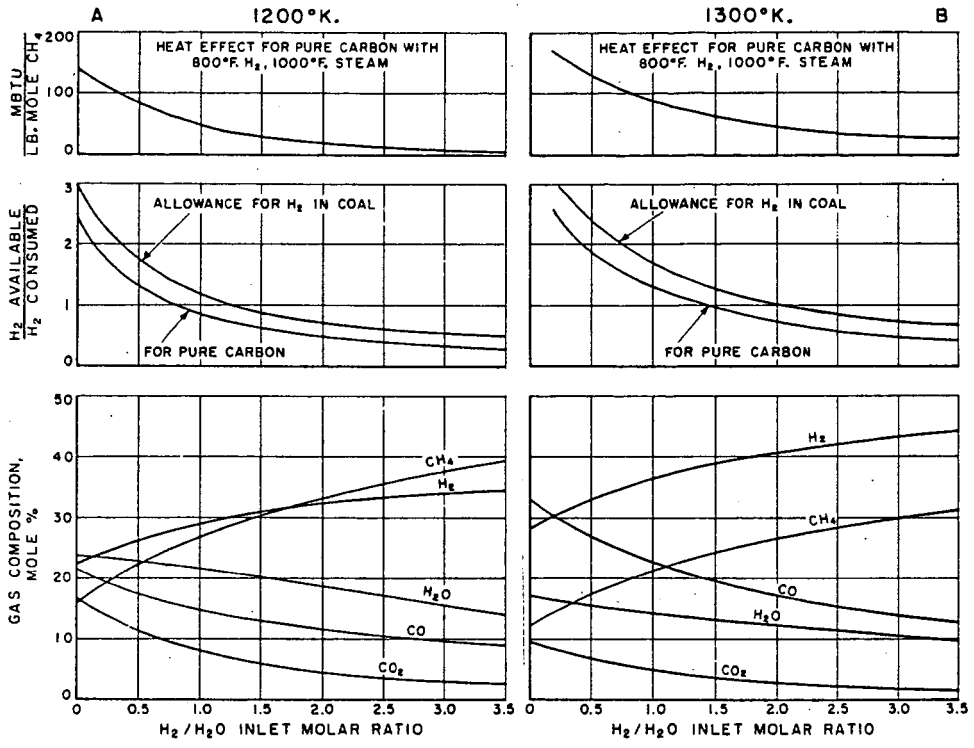

Fig. 2.-EFFECT OF H_2/H_2O RATIO ON EQUILIBRIUM GAS COMPOSITION, H_2 PRODUCTION/CONSUMPTION RATIO, AND NET HEAT EFFECT, FOR THE C-H_2-H_2O SYSTEM AT 200 ATMOSPHERES AND 1200° AND 1300°K.

steam decomposition rates are relatively slow at the temperatures most favorable to high methane production rates. Since equilibrium steam decompositions cannot be achieved in practice, the C-H_2-H_2O system with oxygen admission is analyzed below on the more realistic basis of equilibrium attained only in the carbon-hydrogen and water-gas-shift reactions, with arbitrary assignment of steam decomposition values.

III. Thermodynamic Analysis of C-H_2-H_2O-O_2 System with Arbitrary Inlet Steam Decomposition

A. Defining Equations

The system is completely defined by Reactions 1 and 3 in equilibrium, Reaction 2 nonequilibrium, and Reaction 4 to completion:

$$C + O_2 \longrightarrow CO_2 \qquad \text{Reaction 4}$$

The method of solution is similar to that given for the C-H_2-H_2O system. The material balance is given in Table 3.

Table 3.-MATERIAL BALANCE OF THE C-H_2-H_2O SYSTEM WITH OXYGEN

Component	Initial Amount Moles/Mole Inlet Steam	Equilibrium Partial Pressure, Atm.	Equilibrium Molar Quantities, Moles/ Mole Inlet Steam
C	excess	--	--
O_2	b	0	0
H_2	a	X	x
H_2O	1.0	Y	y
CO	0	Z	z
CO_2	0	M	m
CH_4	0	W	w
Total		P	N

All previous material balance and equilibrium relationships apply except that Equation 2 is not used, and the new oxygen balance becomes:

$$y + z + 2m = 1 + 2b \qquad (19)$$

By manipulation of Equations 1, 3, 7, 15 and 19, the solution for partial pressures and total moles at equilibrium may be written in iterative form:

a) CH_4 partial pressure, Atm.

$$W = K_1 \gamma_c X^2 \qquad (9)$$

b) CO partial pressure, Atm.

$$Z = \frac{1}{2}\left[\frac{X(1+d)}{K_3} + 2e\right]\left[1 - \sqrt{1 - \frac{4Xde}{K_3\,[X(1+d)/K_3+2e]^2}}\right] \qquad (20)$$

where $d = \dfrac{SD + 2b}{1-SD}$

$e = P - X - W$

SD = fraction steam decomposed

c) CO_2 partial pressure, Atm.

$$M = Z \Big/ \left[\frac{Xd}{K_3 Z} - 2\right] \qquad (21)$$

d) H_2O partial pressure, Atm.

$$Y = P-X-M-Z-W = XM/K_3Z \qquad (22)$$

e) Total moles at equilibrium/mole inlet steam

$$N = P(1+2b)/(Y + Z + 2M) \quad (23)$$

By assigning arbitrary X (H_2 partial pressure) values, equilibrium concentrations of all other components are computed for a given temperature, pressure, oxygen/steam inlet molar ratio, assumed steam decomposition and assumed activity of the carbon. Gas compositions are computed from Equation 14, and the amount of carbon gasified from Equation 6. The inlet H_2/H_2O molar ratio is determined by Equation 4, for the case of pure carbon as gasification fuel. The ratio may be corrected for hydrogen available from coal as gasification fuel. Under the conditions assumed in the derivation of the previous correction term, the actual H_2/H_2O inlet molar ratio, a', to the reactor, with coal as fuel, would be:

$$a' = x + y + 2w - 1 - 0.336\ c_g \quad (24)$$

One feasibility criterion of the recycle gasification process with oxygen admission is again the ratio H_2 available/H_2 consumed, Equations 16 and 17. If this ratio is equal to or greater than unity, the process will be independent of an external hydrogen source. By selection of the proper O_2/H_2O inlet molar ratio, the process may be made thermally balanced or slightly exothermic to compensate for heat losses. The net heat effect, Btu/lb mole CH_4 produced, is written in the form:

$$\Delta H_R = \Delta H_1 + \frac{1}{w}\left[(1 - m - y)\ \Delta H_2 + m\Delta H_3 + b\Delta H_4 + c_g \Delta H_c + a\Delta H_{H_2} + b\Delta H_{O_2} + \Delta H_{H_2O} \right] \quad (25)$$

where ΔH_1, ΔH_2, ΔH_3 and ΔH_4 = heat of the respective reactions, in Btu/lb mole, with reactants and products at the temperature of the system, and ΔH = enthalpy of reactant, Btu/lb. mole, between inlet and system outlet temperatures.

An additional calculation for judging the potential efficiency of the gasification process comprises estimation of reactant requirements per MCF CH_4 produced:

a) Lb. steam (reactor only) = $47.5/w$ (26)

b) Lb. carbon = $31.7\ c_g/w$ (27)

c) Lb. coal (75% C, 5% H, at 95% carbon gasification) = $44.5\ c_g/w$ (28)

d) SCF Oxygen = $1000\ b/w$ (29)

e) Fraction carbon gasified to CH_4 = w/c_g (30)

B. Equilibrium Computations

A limited number of calculations were made at conditions believed favorable for the practical operation of the proposed process. The choice of conditions is based on:

a) Inlet steam decompositions in the range 30-50%, comparable to those achieved in oxygen-steam gasification of pulverized coal,[9,11] or in oxygen-steam fired fixed-bed gasification processes.[1,13]

b) Experimental data on the hydrogenation of coal char in the presence of steam indicate that methane formation rates are too slow to be of commercial interest at pressures below 30 atmospheres and temperatures much below 1200°K. (1700°F.).[15] Hydrogenation rates increase moderately with pressure and rapidly with temperature. However, temperatures above 1200°K. are thermodynamically unfavorable for high methane content of the product gases, despite the increased

hydrogenation rates. Favorable operating conditions appear to be 1200°K. (1700°F.) and 30-50 atmospheres. An increase to 200 atmospheres would permit lower operating temperatures of the hydrogenation zone, perhaps 1000-1100°K. (1340-1520°F.), to take advantage of the more favorable thermodynamic conditions without significantly affecting the hydrogenation reaction rates.

Results of the equilibrium computations and heat effects at 50 and 200 atmospheres, 1200°K. (1700°F.) and 1.0 activity of carbon, are given in Figs. 3 and 4 for 30-40% steam decomposition and 0.1-0.15 O_2/H_2O inlet molar ratio. All data are plotted against H_2/H_2O inlet molar ratio based on pure carbon as fuel. If desired, a correction may be applied for H_2/H_2O inlet molar ratios based on coal as fuel (Equation 24). The plots show general trends:

a) The ratio H_2 available/H_2 consumed decreases from values greater than 1.0 at low H_2/H_2O inlet molar ratios to values less than 1.0 at high H_2/H_2O inlet molar ratio.

b) Equilibrium CH_4 contents increase with H_2/H_2O inlet molar ratios.

c) At the chosen O_2/H_2O inlet molar ratios, the net heat effect, ΔH_R Btu per lb. mole CH_4, is highly negative (exothermic) at low H_2/H_2O inlet molar ratios, and becomes less negative at high H_2/H_2O inlet molar ratios.

The explanation of the trend of the ΔH_R curve lies in the fact that both the O_2/H_2O inlet molar ratio and total inlet steam decomposition were fixed at arbitrary values in these calculations. Under the conditions assumed, the heat available from oxidation is always somewhat greater than that required to decompose the given amount of steam. At a low H_2/H_2O inlet molar ratio to the gasifier, the quantity of methane formed is small. As a consequence the net heat effect per mole CH_4 produced is highly negative (exothermic). At higher H_2/H_2O inlet molar ratios, the quantity of methane increases and more sensible heat is required to bring the reactants to the operating temperature, resulting in a less exothermic heat effect per mole CH_4 produced.

In Fig. 3A for 30% steam decomposition, 0.1 O_2/H_2O inlet molar ratio, 50 atmospheres and 1200°K. (1700°F.), the gasification process becomes independent of external hydrogen if the H_2/H_2O inlet molar ratio is no greater than 1.8, the point at which the ratio H_2 available/H_2 consumed (corrected for coal) approaches unity. At this point, 1) the net heat effect is practically zero with 800°F. preheated recycled hydrogen, 1000°F. steam and 60°F. coal and oxygen, and 2) equilibrium methane content of the wet gas is approximately 15% (21% dry basis). The process would require H_2 recycle in the ratio 3.5 moles/mole CH_4.

In Fig. 3B, for 40% steam decomposition, 0.15 O_2/H_2O inlet molar ratio, 50 atmospheres and 1200°K. (1700°F.), the process would be independent of external hydrogen if the H_2/H_2O inlet molar ratio were no greater than 2.5, the point at which the corrected ratio, for coal, of H_2 available/H_2 consumed approaches unity. In this case the net heat effect is again practically zero for the same reactant preheats, and the equilibrium methane content of the wet gas is approximately 18% (22% dry basis). Under these conditions, the required H_2 recycle is 3.4 moles/mole CH_4 produced.

In Fig. 4A, 30% steam decomposition, 0.1 O_2/H_2O inlet molar ratio, 200 atmospheres and 1200°K. (1700°F.), the process would be hydrogen self-sufficient at H_2/H_2O inlet molar ratios no greater than 0.75, the point at which the corrected ratio, for coal, of H_2 available/H_2 consumed approaches unity. Here the net heat effect is approximately 20,000 Btu/lb. mole CH_4 exothermic, which would be sufficient to compensate for radiation and convection heat losses. The equilibrium

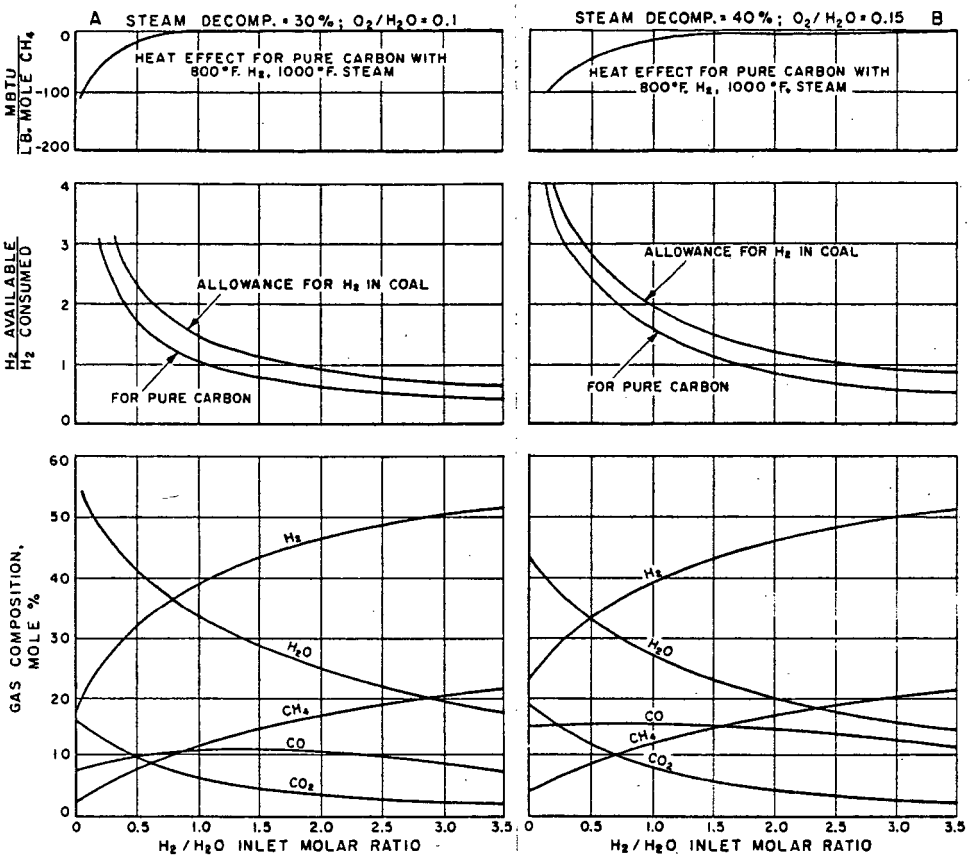

Fig. 3.-EFFECT OF H_2/H_2O RATIO ON EQUILIBRIUM GAS COMPOSITION, H_2 PRODUCTION/CONSUMPTION RATIO, AND NET HEAT EFFECT, FOR THE C-H_2-H_2O SYSTEM AT 1200°K. AND 50 ATMOSPHERES, WITH 30 AND 40% STEAM DECOMPOSITION, AND 0.1 AND 0.15 O_2/H_2O INLET MOLAR RATIO, RESPECTIVELY

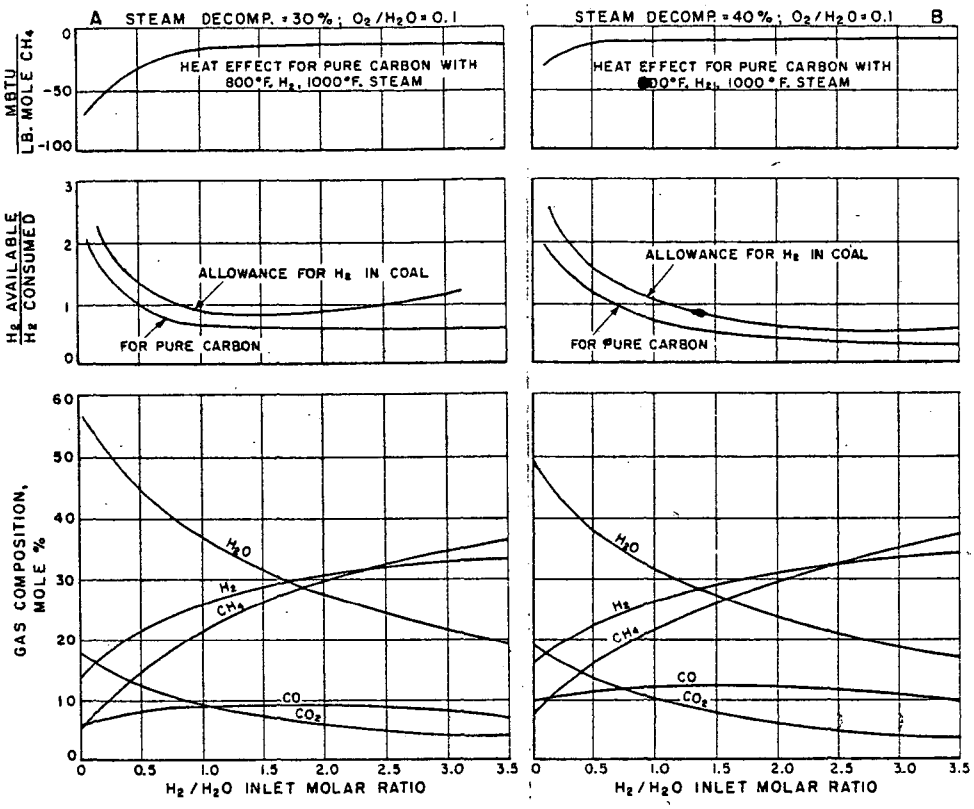

Fig. 4.-EFFECT OF H_2/H_2O RATIO ON EQUILIBRIUM GAS COMPOSITION, H_2 PRODUCTION/CONSUMPTION RATIO, AND NET HEAT EFFECT, FOR THE C-H_2-H_2O SYSTEM AT 1200°K. AND 200 ATMOSPHERES, WITH 0.1 O_2/H_2O INLET MOLAR RATIO 30 AND 40% STEAM DECOMPOSITION

methane content is approximately 18% on the wet basis, (30% dry basis), and the process would require H_2 recycle of 1.8 moles/mole CH_4 produced.

In Fig. 4B, 40% steam decomposition, 0.1 O_2/H_2 inlet molar ratio, 200 atmospheres and 1200°K. (1700°F.), the process would again be self-sufficient with respect to hydrogen if the H_2/H_2O inlet molar ratio were no greater than 1.0. The net heat effect is less exothermic than in the previous case, approximately 10,000 Btu/lb. mole CH_4 at the same reactant preheats. The equilibrium methane content is approximately 21% on the wet basis, or 31% dry basis, with a required H_2 recycle of 1.7 moles/mole CH_4 produced.

These results demonstrate that operating conditions can be found where the proposed process, with O_2 admission and H_2 recycle, appears thermodynamically feasible. It should be noted, since oxygen is required, that the process reduces to an adaptation of the Lurgi pressure gasifier with provision for H_2 recycle in the upper portions of the fixed fuel bed, or to an adaptation of present fluid-bed coal hydrogenation reactors with provision for addition of steam and oxygen either in the same reactor or in a separate vessel to gasify the coal residue. Since this method of methane production by H_2 recycle takes advantage of the exothermic heat of coal hydrogenation to compensate in part for the endothermic heats of the steam decomposition reactions which continue to occur to a small extent at hydrogenation temperatures, it appears that by virtue of the potentially greater thermal efficiency, both oxygen and coal requirements per MCF CH_4 can be reduced from those of other gasification processes. The potential magnitude of this reduction can be seen from a comparison of the theoretical material requirements in Table 4, based on Figs. 3 and 4, with actual requirements for several gasification processes operated on pilot plant and large scale (Table 5). In Table 4, the oxygen and coal requirements based on Figs. 3A and 3B were increased by 20% to compensate for radiation and convection heat losses, since the theoretical heat effects were not sufficiently exothermic for these two cases.

Table 4.-THEORETICAL MATERIAL REQUIREMENTS (REACTOR ONLY) FOR METHANE PRODUCTION BY HYDROGEN RECYCLE AND OXYGEN-STEAM ADMISSION

Reference Figure	Fig. 3A	Fig. 3B	Fig. 4A	Fig. 4B
Conditions:				
Pressure, Atm.	50	50	200	200
Outlet Temp., °F.	1700	1700	1700	1700
O_2/H_2O Inlet Molar Ratio	0.1	0.15	0.1	0.1
H_2/H_2O Inlet Molar Ratio	1.8	2.4	0.75	1.0
Inlet Steam, °F.	1000	1000	1000	1000
Recycled Hydrogen, °F.	800	800	800	800
Inlet Oxygen, °F.	60	60	60	60
Inlet Steam Decomp., %	30	40	30	40
Requirements/MCF CH_4:				
Pure Carbon, lb.	73.5*	74.5*	64.5	63
Coal, at 95% Gasification, lb.	103*	104*	90.5	88
Steam, lb.	111	79	151	110
Oxygen, 100%, SCF	280*	298*	318	230
Oxygen, 95%, SCF	295*	314*	335	242
Theoretical Percent Carbon Appearing as CH_4	43	43	49	51

* Increased by 20% over theoretical values.

Table 5.-TYPICAL MATERIAL REQUIREMENTS FOR METHANE PRODUCTION FROM SYNTHESIS GAS (COAL GASIFIER ONLY)

Process*	USBM[9]	PAN[4]	K-T[10]	IGT[11]	L[3]	WGS[1]	PROD.[13]
Nominal Conditions:							
Coal Type	Bit.	Bit.	Bit.	Bit.	Char	Coke	Barley Anth.
Pressure, Atm.	21	1	1	7.5	21	1	1
Outlet Temp., °F.	2500	2350	2300	2500	1100	1200	880
O_2/H_2O Inlet Molar Ratio	1.5	0.65	0.81	0.45	0.77	0.38	0.29
Inlet Steam, °F.	625	930	250	1500	500	210	285
Inlet Oxygen, °F.	625	930	100	100	500	210	285
Inlet Steam Decomp., %	25	25	25	31	34	54	52
Carbon Gasified, %	90	84	85	92	97	99.5	99.4
Requirements/MCF CH_4:							
Carbon, lb.	96.5	119	112	93.5	84	100	87
Coal (or coke), lb.	137	185	168	125	112	111	110
Steam, lb.	42	77	85	131	360	152	154
Oxygen, 100%, SCF	1332	1060	1444	1248	584	1144	951
Oxygen, 95%, SCF	1408	1118	1520	1312	615	1204	1000
Percent Carbon Appearing as CH_4 by Methanation	33	26.7	28	34	38	32	36.6

*PAN = Panindco Process; K-T = Koppers-Totzek Gasifier; L = Lurgi Unit; WGS = Water Gas Set; PROD. = Producer

The data in Table 5 were computed on the basis of 4 SCF CO-plus-H_2 in synthesis gas from coal to yield 1 SCF CH_4 by catalytic methanation. The material requirements pertain only to the coal gasification reactor. Data for Lurgi pressure gasification were adjusted to take into account the methane content of the raw gas.

ESTIMATION OF REACTOR SIZE FROM AVAILABLE DATA ON REACTION RATES

I. Reaction Rate Data

Comprehensive experimental data on reaction rates of hydrogen-steam mixtures with carbon in the form of low temperature (Disco) char have been reported by Gorin, Goring, Zielke and coworkers.[3,6,14,15] The data were obtained from a 1.5-inch I.D. fluidized bed of 65/100 mesh fuel particles, operated at 1-30 atmospheres and 1500-1700°F. Methane production rates and total carbon gasification rates, expressed as moles C gasified/mole C-min., were determined for pure H_2 and for H_2/H_2O inlet molar ratios in the range 0.1-2.0 at carbon burnoffs or percent gasifications of 0-100%. The total carbon gasification rate is the sum of the rate of CH_4 production and the rate of the steam reactions with carbon. Under the conditions of the investigations, the percent utilization of H_2 and decomposition of steam were small, so the exit gases contained only a few percent CH_4, CO and CO_2. As a consequence, the data do not take into account the retarding effects on the rates as appreciable concentrations of methane and other components appear in the gas in a practical gasification system.

The data reported by Zielke and Gorin[15] indicate that steam has a marked effect in increasing the methane-formation rate; the increase, which is pressure dependent, ranges from 2 to 100 times the rate in a pure H_2 atmosphere, at 1700°F. and 1-30 atmospheres total pressure. The CH_4 rate increases with total pressure raised to a power between 0.1 and 1.5, depending upon H_2/H_2O inlet molar ratio and percent carbon burnoff, and decreases rapidly with decreasing temperature. The total carbon gasification rate follows approximately the same trends, except that at high H_2/H_2O inlet molar ratios this rate becomes equal to the CH_4 rate by virtue of less steam being available for carbon gasification under these conditions. The CH_4 formation rates for Disco char do not appear to be sufficiently high at pressures below 30 atmospheres and temperatures less than 1700°F. to be of particular interest commercially.

To facilitate reactor calculations, plots of data are required showing CH_4 formation and total carbon gasification rates at 50 atmospheres as affected by H_2/H_2O inlet molar ratio and percent carbon burnoff. These graphs were obtained by first plotting the reported rates against pressure (1-30 atmospheres) on logarithmic scales, for each H_2/H_2O inlet molar ratio investigated (0.32, 1.0 and 2.0) at 0-100% carbon burnoff. The resulting nearly straight lines were extrapolated to 50 atmospheres. The extrapolated points were then replotted in the desired form, Fig. 5. The linear CH_4 rate plot, Fig. 5A, was extended (dotted lines) beyond the range of H_2/H_2O inlet molar ratios investigated. The total carbon gasification rate plot, Fig. 5B, was also extended by continuing the trend of the curves (dotted lines) to a 4.0 H_2/H_2O inlet molar ratio. In effect, Figs. 5A and 5B are based entirely upon moderate extrapolations; however, they are believed to be justified.

II. Reactor Design Estimate

A. Procedure

Evaluation, from the standpoint of kinetics, of the hydrogen recycle gasification process with oxygen-steam admission, requires an estimate of the hydrogenation zone fuel bed depth. To avoid unnecessary complications it is assumed that 1) the temperature gradient in the hydrogenation zone of an actual reactor may be approximated with an effective average temperature (1700°F.), and 2) the velocity distribution of gases at a given cross-section of the reactor may be approximated by piston-type flow at an average velocity (constant velocity distribution).

The basic design relationship is given by a material balance[7] over a differential bed height, dh, in which an incremental quantity of CH_4, dn_m, is formed:

$$dn_m = r_m\, dh = -q\, F_o\, dB \qquad (31)$$

where dB = incremental fractional burnup of carbon in the element of fuel bed

dn_m = incremental CH_4 formed, lb. mole hr.-sq. ft. reactor cross section

r_m = CH_4 formation rate, lb. mole/hr.-cu. ft. reactor

$q = r_m/r_t$ = ratio, CH_4 formation rate/total gasification rate

F_o = carbon input rate to reactor, lb. mole/hr.-sq. ft.

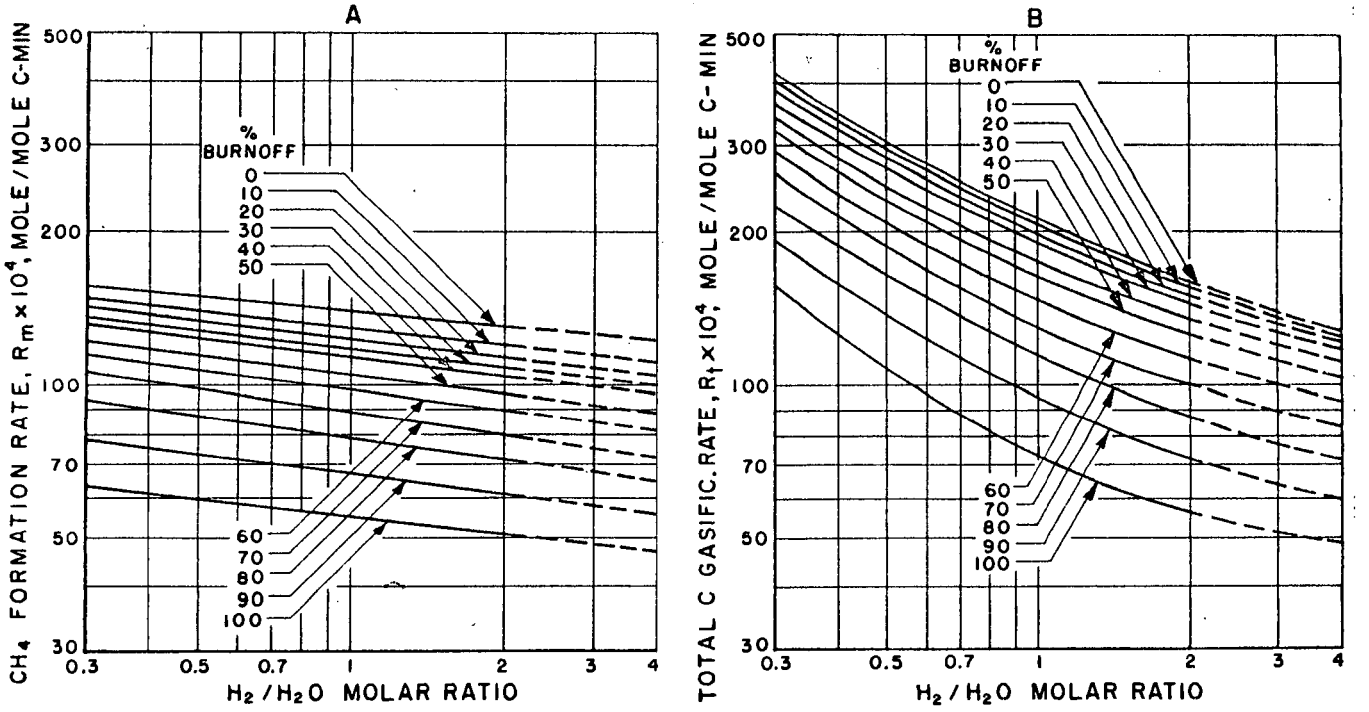

Fig. 5.-METHANE FORMATION AND TOTAL CARBON GASIFICATION RATES FOR DISCO CHAR IN H_2-H_2O ATMOSPHERE AT 1700°F., 50 ATMOSPHERES, AND VARIOUS BURNOFFS OF CARBON

For a fixed fuel bed, with countercurrent flow of gases with respect to the coal feed, this relationship may be integrated graphically over the limits from the start of the hydrogenation zone, h = 0, where the burnup is B_o, to the top of the bed, h = H, where the burnup B = 0 (fresh coal feed):

$$\int_0^H \frac{dh}{F_o} = \frac{H}{F_o} = -\int_{B_o}^0 \frac{q\,dB}{r_m} = -\int_{B_o}^0 \frac{dB}{r_t} \qquad (32)$$

At a fixed temperature and pressure the quantities r_m, r_t and q are dependent upon carbon burnoff and the composition of the reacting gases. An acceptable relationship to take into account the effect of gas composition in retarding the reaction rates is given by the ratio of the actual partial-pressure product of the reacting components to the equilibrium constant of the particular reaction. By use of this concept, the recommended forms of the rate equations are:

$$R_t' = R_m \left[1 - \frac{p_{CH_4}}{K_1 p_{H_2}^{\,2} \gamma_c}\right] + \left[R_t - R_m\right] \left[1 - \frac{p_{CO}\, p_{H_2}}{K_2 p_{H_2O}\, \gamma_c'}\right] \qquad (33)$$

$$R_m' = R_m \left[1 - \frac{p_{CH_4}}{K_1 p_{H_2}^{\,2} \gamma_c}\right] \qquad (34)$$

where R_m = CH_4 formation rate given in Fig. 5A, uncorrected for retarding effects, lb. mole/lb. mole C-min.

R_t = total carbon gasification rate given in Fig. 5B, uncorrected for retarding effects, lb. mole/lb. mole C-min.

R_m' = CH_4 formation rate, corrected for retarding effects, lb. mole/lb. mole C-min.

R_t' = total carbon gasification rate, corrected for retarding effects, lb. mole/lb. mole C-min.

p = actual partial pressure of gaseous components at point of reaction, atm.

γ_c = activity of carbon with respect to hydrogenation reaction

γ_c' = activity of carbon with respect to carbon - steam reaction

These rate equations are considered to give conservative results.[15]

The conversion factors between Equations 32-34 are:

$$r_m = 60 \rho_c y_c R_m'/12 \qquad (35)$$

$$r_t = 60 \rho_c y_c R_t'/12 \qquad (36)$$

where ρ_c = bulk density of fuel, lb./cu. ft.

y_c = weight fraction carbon in fuel

For practical purposes the product $\rho_c y_c$ can be considered constant throughout the hydrogenation zone, for fuels of normal ash content. By use of Equation 36, the design Equation 32 may be put in the form:

$$(5\rho_c y_c)\left[\frac{H}{F_o}\right] = \int_0^{B_o} \frac{dB}{R_t'} \qquad (37)$$

B. Fixed-Bed Reactor

1. Design Conditions. The integral in Equation 37 is the area under a curve of reciprocal total carbon gasification rate, $1/R_t'$, plotted against fractional burnoff, B, in the hydrogenation zone. Since R_t' (Equation 33) depends upon the partial pressures of gaseous constituents and upon the burnoff at a given position in the fuel bed, a material balance is required to relate the variation of gas composition with burnoff throughout the fuel bed. The outlet gas composition of the reactor is based on the equilibrium values given in Fig. 3B at the point where the ratio H_2 available/H_2 consumed (for coal) is unity, for 1200°K. (1700°F.), 50 atmospheres, 40% steam decomposition, 0.15 O_2/H_2O inlet molar ratio, and 2.4 H_2/H_2O inlet molar ratio. This outlet composition is 47.2% H_2, 17.9% H_2O, 13.5% CO, 3.5% CO_2 and 17.9% CH_4.

The calculation of gas composition variation with burnoff through the fuel bed is based on, 1) hydrogen, oxygen and carbon balances, 2) 80% of the hydrogen content of the coal released to appear in CH_4 in the hydrogenation zone, weighted linearly according to percent carbon burnoff, and 3) maintenance of water-gas-shift equilibrium. The third assumption is not strictly correct, since experimental evidence indicates that the water-gas shift reaction may be far removed from equilibrium under the operating conditions in coal gasification with H_2-H_2O mixtures.[6] However, since the principal discrepancy would lie in the actual CO_2/CO ratio over that theoretically calculated, the assumption of water-gas shift equilibrium will be sufficiently accurate. Final results of the material balances are given in the following.

2. Material Balance for Oxidation Zone. Expressions for the molar quantities of hydrogen (x'), steam (y'), carbon monoxide (z'), carbon dioxide (m'), methane (w'), total moles (N'), and carbon gasified (c_g'), as moles/mole inlet steam are:

$$w' = 0 \text{ (no } CH_4) \qquad (38)$$

$$m' = \frac{K_3\,(1\text{-}SD')\,(SD' + 2b)}{2K_3\,(1\text{-}SD') + a' + SD' - 2w'} \qquad (39)$$

$$z' = SD' + 2b - 2m' \qquad (40)$$

$$y' = 1 - SD' \qquad (41)$$

$$x' = K_3 y' z'/m' \qquad (42)$$

$$N' = x' + y' + z' + m' + w' \qquad (43)$$

$$c_g' = z' + m' + w' \qquad (44)$$

Fractional burnoff in oxidation zone:

$$B' = c_g'/c_g \qquad (45)$$

where SD' = steam decomposition in oxidation zone:

a' = H_2/H_2O inlet molar ratio corrected for coal. Note a' = 0 prior to H_2 recycle point

b = O_2/H_2O inlet molar ratio

c_g = carbon gasified at equilibrium outlet conditions of the hydrogenation zone.

These relationships are readily solved for a given temperature (which determines K_3), known values of a' and b, assumed value of steam decomposition, SD', and known value of equilibrium carbon gasification, c_g.

3. Material Balance for Hydrogenation Zone. Expressions for the molar quantities of hydrogen (x"), steam (y"), carbon monoxide (z"), carbon dioxide (m"), methane (w"), total moles (N") and carbon gasified (c_g"), as moles/mole inlet steam are:

$$w'' = \left[\frac{B''-B'}{B-B'}\right] w \tag{46}$$

$$m'' = \frac{\mu}{2\delta}\left[1 - \sqrt{1 - \frac{4\delta\eta}{\mu^2}}\right] \tag{47}$$

$$z'' = SD'' + 2b - 2m'' \tag{48}$$

$$y'' = 1-SD'' \tag{49}$$

$$x'' = K_3\, y''\, z''/m'' \tag{50}$$

$$N'' = x'' + y'' + z'' + m'' + w'' \tag{51}$$

$$c_g'' = z'' + m'' + w'' \tag{52}$$

Incremental steam decomposition occurring in hydrogenation zone:

$$\Delta SD'' = \left[\frac{B''-B'}{B-B'}\right] (SD - SD') \tag{53}$$

Total steam decomposition:

$$SD'' = SD' + \Delta SD'' \tag{54}$$

where $\mu = (2K_3-1)(1-SD'') + \delta(SD'' + 2b) + \alpha$

$\eta = K_3 (SD'' + 2b)(1-SD'')$

$$\alpha = a' - \left[\frac{c_g' - w''}{c_g - c_g'}\right](0.336\, c_g) - 2w'' + 1$$

$$\delta = \frac{0.336\, c_g}{c_g - c_g'}$$

B = theoretical total burnoff of fuel residue = 100%

B" = fractional burnoff in hydrogenation zone

SD" = total steam decomposition in hydrogenation zone

These relationships are solved for a given temperature, assumed reactor inlet and outlet conditions (which determine the values of K_3, a', w, c_g, B, SD), and known values of B', SD' and c_g' (from oxidation zone), by the assigning of arbitrary values to the hydrogenation zone burnoff B".

Solution of the material balance equations for the oxidation, steam decomposition, and hydrogenation zones under the condition of exit gas equilibrium resulted in the values given in Table 6. Here the exothermic heat of the oxidation zone is balanced approximately by the endothermic effect of the steam decomposition zone. Beyond the H_2 recycle point, the exothermic heat of coal hydrogenation is

balanced approximately by, 1) the heat requirement of steam decomposition which continues to occur to a small extent in the hydrogenation zone, and 2) the sensible heat required for preheating the coal feed and recycled hydrogen to the operating temperature.

4. Fuel Depth and Flow Rates. The assumption that 10% steam decomposition occurs in the hydrogenation zone (Table 6) can be checked for accuracy after completion of the rate calculations. The results in Table 6 are shown graphically in Fig. 6. The reaction rates of Equations 33 and 34 can now be evaluated at any fractional burnoff and assumed activity of carbon in the hydrogenation zone by reading partial pressure values from this plot and by obtaining the rates R_m and R_t from Figs. 5A and 5B. The results of these calculations, which are required for graphical integration of Equation 37, and later for Equation 31, are summarized in Table 7. The assumption of 1.1 activity of carbon with respect to the hydrogenation reactions is justified on the basis that, given sufficient residence time, the equilibrium CH_4 content based on carbon as β-graphite may be exceeded with carbon as coal.

Table 6.-COMPUTED GAS COMPOSITIONS AT VARIOUS POINTS IN FIXED BED REACTOR

Basis: O_2/H_2O inlet molar ratio = 0.15;
H_2/H_2O inlet molar ratio for pure carbon = 2.41, for coal = 2.01;
coal contains 75 wt. % C, 5 wt. % H.

Position	Assumed Inlet Steam Decomp., %	Theoretical Carbon Burnoff, %	Gas Comp., Mole %					
			O_2	H_2	H_2O	CO	CO_2	CH_4
O_2-H_2O Inlet to Reactor	0	100	13	--	87	--	--	--
End of Oxidation Zone	0	87.3	--	--	87	--	13	--
End of Steam Decomposition Zone	30	58.3	--	21.3	49.8	15.1	13.8	--
Point of H_2 Recycle	30	56.8	--	65.7	19.8	12.0	2.5	--
50% through Hydrogenation Zone	35	28.2	--	56.6	18.8	12.8	3.0	8.8
Outlet of Reactor	40	0	--	47.2	17.9	13.5	3.5	17.9

Position	Molar Quantities, mole/mole inlet steam							
	O_2	H_2	H_2O	CO	CO_2	CH_4	Total	Carbon Gasified
O_2-H_2O Inlet to Reactor	0.15	--	1.0	--	--	--	1.15	--
End of Oxidation Zone	--	--	1.0	--	0.15	--	1.15	0.150
End of Steam Decomposition Zone	--	0.30	0.70	0.21	0.19	--	1.40	0.493
Point of H_2 Recycle	--	2.32	0.70	0.42	0.09	--	3.53	0.511
50% through Hydrogenation Zone	--	1.96	0.65	0.44	0.10	0.303	3.45	0.850
Outlet Reactor	--	1.60	0.60	0.46	0.12	0.605	3.39	1.182

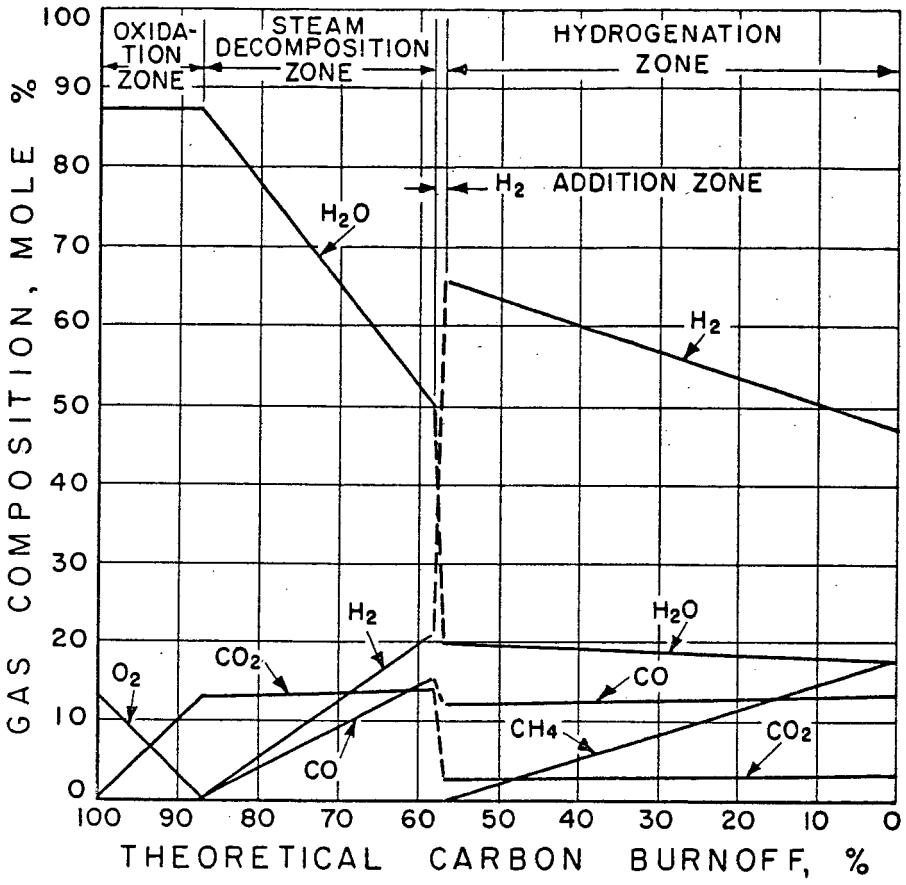

Fig. 6.-COMPUTED VARIATION OF GAS COMPOSITION WITH CARBON BURNOFF IN FIXED-BED REACTOR AT 1700°F. AND 50 ATMOSPHERES

Table 7.-REACTION RATES FOR VARIOUS PERCENT BURNOFF IN FIXED-BED REACTOR HYDROGENATION ZONE OPERATING AT 1700°F. AND 50 ATM.

(Activity of Carbon, $\gamma_c = 1.1$, $\gamma_c' = 1.0$)

Burnoff %	Ratio H_2/H_2O	Inhibiting Terms $\frac{p_{CH_4}}{K_1 p_{H_2}^2 \gamma_c}$	Inhibiting Terms $\frac{p_{CO} p_{H_2}}{K_2 p_{H_2O} \gamma_c'}$	Rates, moles/mole C-min. $R_m' \times 10^4$	Rates, moles/mole C-min. $R_t' \times 10^4$	Ratio $q = R_m'/R_t'$
56.8	3.32	0	0.499	87.0	94.5	0.921
50	3.25	0.06	0.498	85.5	95.1	0.900
40	3.15	0.16	0.492	84.0	93.1	0.902
30	3.04	0.28	0.489	74.1	86.1	0.861
20	2.90	0.45	0.478	60.0	72.0	0.834
10	2.78	0.66	0.462	40.4	52.2	0.774
5	2.71	0.77	0.462	28.1	38.3	0.734
0	2.65	0.91	0.450	11.6	21.0	0.555

From the data in Table 7, graphical integration of Equation 37 yielded a value of 86.25 min.-mole C/mole (inverse space velocity). The probable height of the hydrogenation zone is therefore:

$$H = 86.25\ F_o/5 \rho_c\ y_c \qquad (55)$$

Practical values of the inlet feed rate F_o, moles C/hr. sq. ft., can be selected on the basis of a conservative Lurgi rate, 140 lb. coal/hr. sq. ft., and the fact that the incremental burnoff prior to the hydrogenation zone was estimated as 100-56.8, or 43.2% (Table 6):

$$F_o = (140)(0.75)/(12)(0.432) = 20.2 \text{ moles C/hr.-sq. ft. for a coal containing 75 wt. \% carbon.}$$

Assuming a 40 lb./cu. ft. fuel bed bulk density, the estimated height of the hydrogenation zone is:

$$H = (86.25)(20.2)/(5)(40)(0.75) = 11.6 \text{ ft.}$$

which is applicable only for 65/100 mesh fuel particles. A fixed bed would operate with perhaps 1/4-inch average size fuel. Some correction is therefore required, but necessary data are lacking, for the effect of fuel size, since reaction rates per unit mass of fuel vary with effective surface area and method of contacting.

A verification of the amount of steam decomposition occurring simultaneously with the hydrogenation reactions can now be made, based on the fluid-bed rate data (Figs. 5A, 5B and Table 7), through integration of Equation 31:

$$n_m = -F_o \int_{B_o}^{0} q\ dB \qquad (56)$$

and the additional relationship,

$$n_t = -F_o \int_{B_o}^{0} dB = F_o B_o \qquad (57)$$

where n_m = methane produced in hydrogenation zone, lb. mole/hr.-sq. ft.

n_t = total carbon gasified by hydrogenation and by steam decomposition, lb. mole/hr.-sq. ft.

The incremental steam decomposition occurring in the hydrogenation zone, $\Delta SD''$, is then given by:

$$\Delta SD'' = w\ (n_t/n_m - 1) \qquad (58)$$

where w = methane produced (equilibrium value at outlet of reactor), mole/mole inlet steam. For this case w = 0.605 (Table 7), and the ratio n_t/n_m = 1.19 (graphical integration), so:

$$\Delta SD'' = 0.605\ (1.19\text{-}1) \text{ or } 11.5\%$$

which is in close agreement with the 10% steam decomposition previously assumed.

Based on these results, the estimated flow rates, space velocities and residence times for the proposed gasification process are:

a) Steam feed rate, lb./hr. sq. ft., = $18\ F_o/c_g$ = (18)(20.2)/1.182 = 308

b) Oxygen feed rate, SCF/hr. sq. ft., = $379\ bF_o/c_g$ = (379)(0.15)(20.2)/1.182 = 970

c) Hydrogen recycle space velocity, SCF/hr. cu. ft. hydrogenation zone = $379\ a'F_o/Hc_g$ = (379)(2.014)(20.2)/(11.6)(1.182) = 1125

d) Methane space velocity, SCF/hr. cu. ft. hydrogenation zone = $(379)\ wF_o/Hc_g$ = (379)(0.605)(20.2)/(11.6)(1.182) = 336

e) Approximate coal residence time in hydrogenation zone, hr., based on inlet volume of coal

$$= \frac{H \rho_c\ y_c}{12\ F_o} = \frac{(11.6)(40)(0.75)}{(12)(20.2)} = 1.44$$

f) Approximate gas residence time in hydrogenation zone, sec., based on average gas volume and 40% void space (ϵ) of the fuel bed

$$= \frac{4940PH\ c_g \epsilon}{N_{avg}\ F_o T} = \frac{(4940)(50)(11.6)(1.182)(0.40)}{(3.46)(20.2)(2160)} = 9$$

C. Fluid-Bed Reactor

1. Design Conditions. In the analysis of the fluid-bed reactor it is assumed:

a) The reactor is completely stirred with respect to coal, i.e., the percent carbon burnoff is uniform throughout the hydrogenation zone.

b) Gases move through the reactor in piston-type flow, i.e., backmixing is neglected.

c) The hydrogenation zone is at constant temperature (1700°F.) and constant pressure (50 atm.).

d) The same equilibrium outlet gas composition will be attained as was assumed for the fixed-bed case calculations.

e) 30% steam decomposition will be attained prior to the hydrogenation zone. In the hydrogenation zone, an additional 10% steam decomposition will occur.

f) The water-gas shift reaction is in continual equilibrium in the hydrogenation zone.

g) With the conditions of Items b, e and f above, the gas composition will vary with burnoff as in Fig. 6.

2. Fuel Depth and Flow Rates. By use of the procedure already described, graphical integration of Equation 37 gave 102.9 min.-mole C/mole for the reciprocal total carbon gasification rate (corrected for retarding effects) under the conditions listed above. Details are summarized in Table 8. The probable height of the hydrogenation zone is therefore $H = 102.9\ F_o/5\rho_c y_c$.

Table 8.-REACTION RATES FOR VARIOUS PERCENT BURNOFF IN FLUID-BED REACTOR HYDROGENATION ZONE OPERATING AT 1700°F. AND 50 ATM.

(Average Burnoff of Fluid Bed = 56.8%; Activity of Carbon $\gamma_c = 1.1$, $\gamma_c' = 1.0$)

Burnoff, %	Ratio H_2/H_2O	Inhibiting Terms $\frac{p_{CH_4}}{K_1 p_{H_2}^2 \gamma_c}$	Inhibiting Terms $\frac{p_{CO}\, p_{H_2}}{K_2 p_{H_2O} \gamma_c'}$	Reaction Rates, mole/mole C-min. $R_m' \times 10^4$	Reaction Rates, mole/mole C-min. $R_t' \times 10^4$	Ratio $q = R_m'/R_t'$
56.8	3.32	0	0.499	87.0	94.5	0.921
50	3.25	0.06	0.498	80.8	88.8	0.910
40	3.15	0.16	0.492	73.1	81.2	0.901
30	3.04	0.28	0.489	63.0	71.5	0.883
20	2.90	0.45	0.478	48.4	57.8	0.837
10	2.78	0.66	0.462	30.7	40.9	0.752
5	2.71	0.77	0.458	20.5	30.7	0.668
0	2.65	0.91	0.450	8.1	19.1	0.423

The carbon gasification capacity, F_o, is estimated by assigning a superficial velocity (v_f) of, say, 0.3 ft./sec. at the point of maximum gas flow. The total moles of gases permissible at a chosen pressure, temperature and fluidizing velocity is then $M_t = 4940\ Pv_f/T$ which with P = 50, T = 2160°R. becomes $M_t = 34.4$ moles gases/hr.-sq. ft. The total gases are at a maximum at the point of hydrogen recycle. From previous computations (Equations 38 to 45 and Table 6) the ratio of gases at this point is 3.531 moles/mole inlet steam. The total amount of carbon gasified was 1.182 moles/mole inlet steam. Therefore, the carbon input rate is:

$$F_o = \frac{(1.182)(34.4)}{3.531} = 11.5 \text{ moles C/hr.-sq. ft.}$$

For a fluid bed density of 35 lb. cu. ft. and fuel containing 75 wt. % carbon, the estimated height of the hydrogenation zone is:

$$H = (102.9)(11.5)/(5)(35)(0.75) = 9 \text{ ft.}$$

which again would be applicable only for 65/100 mesh fuel particles.

By use of the procedure of Equations 56-58, the estimated steam decomposition occurring simultaneously with the hydrogenation reactions in the fluid bed is found to be:

$$\Delta SD'' = 0.605\ (1.20 - 1) \text{ or } 12.1\%$$

which is in acceptable agreement with the 10% assumption on which the reaction rate calculations were based.

From these results the estimated flow rates, space velocities and residence times for the proposed gasification process are:

a) Steam feed rate, lb./hr.-sq. ft. = (18)(11.5)/1.182 = 175

b) Oxygen feed rate, SCF/hr.-sq. ft. = (379)(0.15)(11.5)/1.182 = 555

c) Hydrogen recycle space velocity, SCF/hr. cu. ft. hydrogenation zone = (379)(2.014)(11.5)/(9)(1.182) = 825

d) Methane space velocity, SCF/hr. cu. ft. hydrogenation zone = (379)(0.605)(11.5)/(9)(1.182) = 250

e) Approximate coal residence time in hydrogenation zone, hr., based on constant density of fluid bed = (9)(35)(0.75)/(12)(11.5) = 1.7

f) Approximate gas residence time in hydrogenation zone, sec., based on arithmetic average superficial velocity ($\bar{v}_f$) of the fluidizing gases and 60% void space (ϵ) of the fluid-bed = $H\epsilon/\bar{v}_f$ = (9)(0.60)/0.294 = 18.4

These approximate reactor calculations indicate that the hydrogenation zone fuel bed depths for either fixed-bed or a fluid-bed operation are within reasonable values for a practical system. It must be stressed, however, that no interpretation of these results should be made under conditions and assumptions other than those set forth. In particular, the results apply strictly to 65/100 mesh low-temperature coal char made by the Disco process. For lack of experimental reaction rate data at higher pressures, the reported rate data for 1700°F. were extrapolated to 50 atmospheres and were also extended beyond the range of H_2/H_2O inlet molar ratios investigated. The data also apply strictly to a fluid-bed operation, since they were obtained in this type of equipment.

The results derived by application of these rate data to the fixed-bed reactor, although indicative, must be viewed with reservation, since sufficient information is not presently available to correct for possible effects of particle size and of different flow characteristics and gas-contacting efficiencies between fluid-bed vs. fixed-bed operation. For simplicity in the calculations, a constant operating temperature, 1700°F., was assumed throughout the hydrogenation zone. It is possible to improve the results given here by taking into account the expected temperature distribution in the hydrogenation zone through a simultaneous heat balance with the reaction rate calculations.

Further information which is lacking for a more complete evaluation is:

a) Effect of moderate concentrations of CO and CO_2 in inhibiting the rates of the hydrogenation reactions.

b) Effect of gasification properties of various fuels, and

c) Exact costs of methane separation by liquefaction.

SUMMARY AND CONCLUSIONS

Thermodynamic analyses indicate that the proposed process for methane production via coal gasification with recycled hydrogen cannot be independent simultaneously of both external hydrogen and external heat. Operating conditions can be found where, theoretically, either 1) the process is thermally self-sufficient but lacks hydrogen, or 2) the process is self-sufficient with respect to hydrogen, but lacks heat. It is believed that it would be of greater advantage to operate the process according to Item 2 above, since the thermal requirements could be readily met by internal combustion of residual carbon with oxygen. The theoretical heat requirements based on carbon

as β-graphite were found to be in the range 25,000-100,000 Btu/lb. mole CH_4 produced. The heat requirements with coal as the gasification fuel would be still larger, since the exothermic heat of coal hydrogenation is not as large as that for hydrogenation of pure carbon. The use of oxygen for partial combustion would provide, simultaneously, a high-temperature zone for rapid steam decomposition. Decompositions of at least 30% are required for economical utilization of steam, since this is the primary hydrogen source.

Thermodynamic calculations of the revised process, with oxygen admission below the point of hydrogen recycle, show that both thermal and hydrogen self-sufficiency can theoretically be attained at 1700°F. and 50-200 atmospheres. The process is potentially more efficient in respect to the proportion of carbon in the fuel appearing as methane, and represents a method of achieving, theoretically, oxygen requirements less than those of the conventional Lurgi pressure gasifier.

Based on available data on reaction rates of 65/100 mesh low-temperature coal char (Disco) with hydrogen-steam mixtures, fuel bed heights for the hydrogenation zone were estimated at 9 feet for a fluidized-bed reactor, and approximately 11-12 feet for a fixed-bed reactor, at 1700°F., 50 atmospheres, with equilibrium exit gas compositions. These bed heights appear to be within achievable values for a practical gasifier design.

Since the use of oxygen is the preferred method of supplying the heat deficiency, then the proposed process, if operated as a fixed fuel bed, reduces to an adaptation of the Lurgi pressure gasifier modified for hydrogen recycle in the upper portions of the fuel bed. If operated as a fluidized bed, the proposed process with oxygen admission does not differ in principle from fluidized-hydrogenation-residual-fuel-gasification schemes already proposed or already under investigation.

As a single-vessel reactor, the method of methane production by hydrogen recycle would appear to be more effective in a fixed bed by virtue of the countercurrent movement of fuel with respect to the reacting gases. The use of a single-vessel fluid-bed reactor, where both oxygen and hydrogen are introduced, is seen to be of disadvantage by virtue of rapid mixing of fuel, resulting in some volatile matter being burned by oxygen. Since the volatile matter portion of the fuel is the most readily hydrogenated component, it appears that an effective fluid-bed system would require a separate reactor to conduct to completion the volatile-matter hydrogenating reactions, and a second vessel, immediately below the first, to gasify residual carbon with oxygen and steam. The hot gases from the second vessel would be passed directly into the hydrogenation reactor.

From the results of this feasibility study it can be concluded:

1) Hydrogen separation by methane liquefaction, coupled with hydrogen recycle, appears to be an attractive approach for pipeline gas production and therefore should be further explored for potential application to present coal hydrogenation methods under laboratory investigation.

2) The use of hydrogen recycle to the Lurgi pressure gasifier offers potential improvements in gasification efficiency and oxygen requirement per unit volume of pipeline gas produced.

ACKNOWLEDGMENT

This study was conducted under the sponsorship of the American Gas Association. Adaptation of the hydrogen recycle in coal hydrogenation investigations was suggested by E. L. Tornquist, Northern Illinois Gas Company.

LITERATURE CITED

(1) Blatchford, J. W., "The Production of Water Gas with Tonnage Oxygen," A.G.A. Proceedings-1950, 652-58.
(2) Channabasappa, K. C. and Linden, H. R., "Hydrogenolysis of Bituminous Coal," Ind. Eng. Chem. 48, 900-05 (1956).
(3) Cooperman, J. et al., "Lurgi Process," U. S. Bureau of Mines Bulletin No. 498. Washington, D. C.: Govt. Print. Office, 1951.
(4) Foch, P. and Loison, R., "The Gasification of Pulverized Coal by the Panindco Process - Recent Experiments," in "International Conference on Complete Gasification of Mined Coal," 224-34. Brussels: R. Louis, 1954.
(5) Goring, G. E. et al., "Kinetics of Carbon Gasification by Steam," Ind. Eng. Chem. 44, 1051-65 (1952).
(6) Goring, G. E. et al., "Kinetics of Carbon Gasification by Steam," Ind. Eng. Chem. 45, 2586-91 (1953).
(7) Hougen, O. A. and Watson, K. M., "Chemical Process Principles, Vol. III, Kinetics and Catalysis." New York: John Wiley and Sons, 1947.
(8) Parent, J. D. and Katz, S., "Equilibrium Compositions and Enthalpy Changes for the Reactions of Carbon, Oxygen and Steam." Institute of Gas Technology Research Bulletin No. 2 (1948) January.
(9) Strimbeck, G. R. et al., "Progress Report on Operation of Pressure-Gasification Pilot Plant Utilizing Pulverized Coal and Oxygen," U. S. Bureau of Mines RI 4971. Pittsburgh: The Bureau, 1953.
(10) Totzek, F., "Synthesis Gas from the Koppers-Totzek Gasifier," Chem. Eng. Prog. 50, 182-87 (1954).
(11) von Fredersdorff, C. G., Pyrcioch, E. J. and Pettyjohn, E. S., "Gasification of Pulverized Coal in Suspension." Institute of Gas Technology Research Bulletin No. 7 (1957) January.
(12) Wagman, D. D. et al., "Heats, Free Energies, and Equilibrium Constants of Some Reactions Involving O_2, H_2, H_2O, C, CO, CO_2 and CH_4," NBS Research Paper RP 1634; Journal of Research 34, 143-61 (1945).
(13) Wright, C. C. and Newman, L. L., "Oxygen Gasification of Anthracite in the Wellman-Galusha Producer," A.G.A. Proceedings-1947, 701-12.
(14) Zielke, C. W. and Gorin, E., "Kinetics of Carbon Gasification," Ind. Eng. Chem. 47, 820-25 (1955).
(15) Zielke, C. W. and Gorin, E., "Kinetics of Carbon Gasification," Ind. Eng. Chem. 49, 396-403 (1957).

Not for Publication
Presented Before the Division of Gas and Fuel Chemistry
American Chemical Society
Atlantic City, New Jersey, Meeting, September 13-18, 1959

Physicochemical Properties of Green River Oil Shale, Particle Size and Particle-Size Distribution of the Inorganic Constituents

P. R. Tisot and W. I. R. Murphy

Laramie Petroleum Research Center
Bureau of Mines, U. S. Department of the Interior
Laramie, Wyoming

This paper presents information obtained regarding particle size and particle-size distribution of the inorganic constituents of Green River oil shale. Oil shale, a stratigraphic rock composed of a complex mixture of organic and inorganic constituents in variable proportions, is one of our major potential sources of liquid fuels. Pyrolysis is the basic principle common to the many experimental methods devised for converting the organic matter to liquid products. Many retorting systems have been developed, some to commercial or semicommercial scale (4,10,11). The similarity in percentage of organic matter converted to oil in such widely differing processes as a batch analytical method (13) and various large pilot plants operated at retorting temperatures of 850° to 950° F., indicates that the maximum conversion obtainable of organic matter to liquid products is of the order of 66 percent, regardless of the method of applying thermal energy. The other products formed are approximately 9 percent gas and 25 percent coke which remains on the shale residue. The published data further indicate that the crude oils produced are of poor quality (1,8,12). A definite explanation of these phenomena are not known. Probably they are a function of the molecular structure of the organic matter, the nature of the organic-inorganic association, the preferred reaction mechanism in a thermal system, or a combination of these factors.

As only 66 percent of the organic matter is converted to liquid products and the resulting oils are of poor quality, it would be highly desirable to develop processes that would improve both yield and quality of oil, thereby enhancing the economy of oil shale. Comprehensive understanding of the fundamental properties and structure of oil shale may improve existing methods or may disclose leads for devising new and better processes for converting the organic matter to liquid products. In the light of this, part of the research in oil shale is directed to gain a better insight into its physicochemical structure.

This is the first of a series of papers. Fundamental properties of oil shale currently under investigation are: Particle size and particle-size distribution of the primary inorganic particles; pore structure of the inorganic constituents; surface area of the raw oil shale and the inorganic constituents; pore size, pore-size distribution, and permeability of the inorganic matrix devoid of organic matter; and type of bonding between the organic and inorganic constituents. Information of this nature regarding oil shale is virtually nonexistent.

Experimental

Oil shales that differed widely in oil yield (75 and 28.6 gallons per ton) were selected for this investigation. Samples were taken at random from 1-foot-sections of beds EF and B, respectively, of the Selective mine, Rifle, Colo. (14). The 2 samples, approximately 200 pounds each, were crushed to pass a 2-mesh-per-inch screen.

Representative samples were taken and prepared as needed from each of the crushed samples.

Preliminary Considerations and Tests

Particulate materials usually respond favorably to particle-size measurements, but this is not the case with the primary inorganic particles that form part of the highly consolidated organic-inorganic system that exists in oil shale. The term "primary inorganic particles" is designated to mean the individual inorganic crystals. These crystals are either partly or entirely encased by organic matter and in many instances are bound together, in varying degrees, with inorganic cementing agents. The extent of the inorganic cementation is a function of the organic content. No practical or effective method is known whereby particle-size analyses of the primary inorganic particles can be made as they naturally occur in oil shale. It therefore became necessary to isolate the inorganic constituents. Removal of the organic matter by solvent action would have been ideal, as then the inorganic constituents recovered would have retained essentially their initial characteristics. However, no single solvent or combination of solvents was found that effectively separated the organic matter. Since solvent action did not accomplish the desired separation, the organic matter was removed by thermal treatment.

It was essential for comparative purposes that the organic matter be removed from the inorganic phase under a consistent set of conditions for all of the studies utilizing organic-free mineral constituents. In some studies the organic-free mineral constituents were prepared from many pieces of oil shale to form a single sample, whereas other studies required that organic-free mineral constituents be prepared from individual pieces of oil shale in the form of cores 1-1/2 inches long and 1/2 inch in diameter. The conditions selected for removing the organic matter, based on a series of preliminary tests, were those found that removed the organic matter from oil-shale cores with minimum physical and chemical changes to the mineral constituents.

Preparation of Organic-Free Mineral Constituents

Figure 1 presents a schematic diagram of the steps taken to prepare the organic-free mineral constituents. Two composites consisting of 200 to 300 pieces of oil shale ranging in size from 0.25 to 0.375 inch were selected from (1-B) to represent the 75-gallon-per-ton oil shale. The individual fragments were large enough so that any size reduction sustained by the primary inorganic particles exposed at the surfaces of the individual fragments during crushing of the oil shale were considered negligible. The composite samples were placed in separate porcelain dishes, arranged in the form of a bed 1-1/2 inches thick, covered, and placed in an electric muffle at room temperature. A thermocouple was placed in the center of one of the samples to record the bed temperature. The samples were heated to 250° F. over a period of one hour. The temperature of the oil-shale sample was raised in increments of 100° F. per hour to 650° F. It was maintained at 650° F. for six hours, then raised to 675° F. for an additional six hours and then to 700° F., until degradation of the organic matter appeared to be complete. This procedure was followed to permit the organic matter to escape from the individual pieces of oil shale with minimum structural breakdown of the inorganic matrix. Degradation of essentially all the organic matter appeared to occur between 650° and 700° F. At this phase of the thermal treatment the individual pieces were encrusted with carbonaceous material. The porcelain dishes were uncovered, and the temperature was maintained at 700° F. for four hours. During this period the carbonaceous material began to disappear slowly. The temperature was raised to 725° F. and maintained at this point for four hours. Any carbonaceous material remaining was removed at 750° F. Chemical analyses indicated that the shale residue obtained from this treatment contained less than 0.1 weight-percent of the initial organic carbon.

Two composite samples of organic-free mineral constituents from 28.6-gallon-per-ton

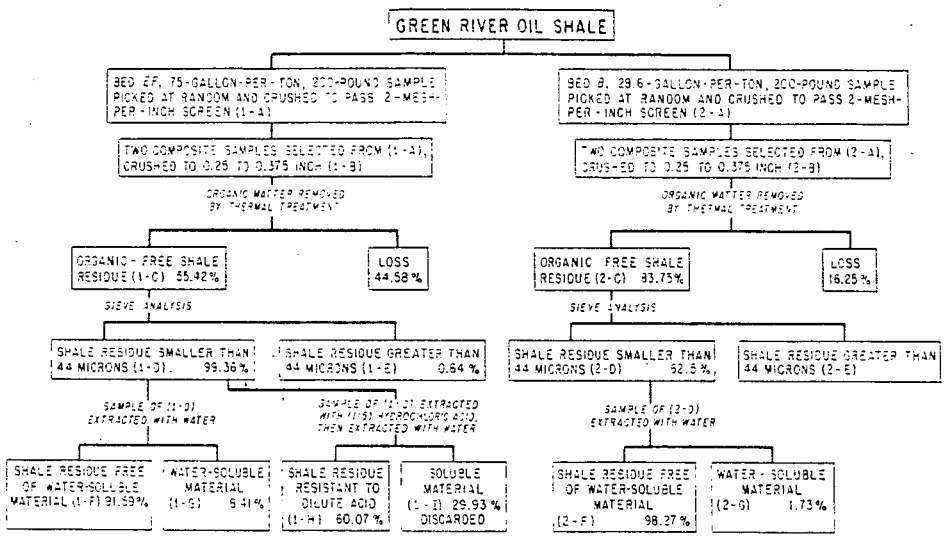

FIGURE 1.-SCHEMATIC DIAGRAM FOR PREPARING ORGANIC-FREE SHALE RESIDUE FOR PARTICLE-SIZE MEASUREMENTS

oil shale (2-C) were prepared in the same manner as described above. Oil shale of this degree of richness was selected, as it occurs at several different levels in the Selective mine. The inorganic mineral constituents recovered from the 75- and 28.6-gallon-per-ton oil shales represented 55.42 and 83.75 weight-percent of the initial oil shale, respectively.

Mineral Constituents

The major inorganic constituents in the oil shales studied were quartz, feldspars, dolomite, and calcite, which compose approximately 95 weight-percent of the total mineral matter. The minor constituents include illite clay minerals, pyrite, and analcite. The constituents most sensitive to thermal treatment are the illite clay minerals, pyrite, and the carbonates. Grim (2) has shown by differential thermal curves that illite does not undergo formation of new phases at 750° F., or below. According to Jukkola et al., (5) the dolomite and calcite in oil shale do not decompose below 1000° F. Samples of organic-free shale residue maintained at 750° F. for eight hours had an average loss in weight of 0.15 weight-percent indicating that the shale residue did not undergo any appreciable loss in weight on prolonged heating.

Chemical Changes During Thermal Treatment

As a result of chemical changes that occurred during removal of the organic matter, the shale residue (1-C) contained 5.07 weight-percent calcium sulfate and 4.51 weight-percent ferric oxide. Formation of these compounds introduced particles foreign to the original inorganic constituents, as calcium sulfate and ferric oxide have been identified in only trace amounts in the minable bed. The ferric oxide most likely resulted from oxidation of the iron pyrite, and the calcium sulfate probably was formed by interaction between calcite and either organic or inorganic sulfur or a combination of both. Apparently the calcite was attacked instead of the dolomite in the formation of calcium sulfate, as no magnesium sulfate or free magnesium carbonate was detected in the shale residue. The calcium sulfate could be removed by prolonged continuous extraction with water. Because of density difference between the ferric oxide and the remainder of the shale residue, the conglomerated ferric oxide could probably be removed by gravity separation, using an appropriate liquid medium. However, effective separation by this method was not accomplished. Failure to separate the ferric oxide was attributed to physical forces interacting between the fine particles and liquid medium. Therefore the ferric oxide was included as part of the shale residue.

Particle-Size Measurements, Sieve Analysis

Particle-size measurements of the larger particles in the rich shale residue were determined by passing each of the two composite samples (1-C) over 30-, 60-, 80-, 100-, 200-, 300-, and 325-mesh sieves and weighing the primary inorganic particles retained on each sieve. Any shale residue that did not readily pass successive sieves was moved over the screen surfaces by applying pressure with a small brush. This method reduced conglomerated masses but was not severe enough to fracture primary particles. Hence, any new particles formed in reducing the conglomerates by this method were essentially fragments of cementing agents or possibly of some of the illite clay minerals. The combined weight of the primary particles retained on the sieves, above 600 and down to 44 microns in diameter, amounted to 0.64 weight-percent of the shale residue (1-C).

Particle-Size Measurements in the Subsieve Range

Microscopic examinations of the shale residue in the subsieve range (1-D) revealed that it still contained conglomerated masses. Reduction of these masses, except for some of the ferric oxide, was best attained by subjecting the shale residue suspended in a liquid medium to ultrasonic vibrations. The apparatus used to produce the

ultrasonic vibrations was a Glennite Model U-621 ultrasonic unit rated at 44 kilocycles per second with a power output to the transducers of 100 watts. Primary particles of calcite and dolomite recovered on the 80- and 100-mesh sieves were exposed to ultrasonic vibrations without significant deleterious effects. From these observations it was concluded that the ultrasonic vibrations induced no appreciable shatter of the primary particles.

Each composite sample of shale residue in the subsieve range (1-D) was divided into three portions, as it was desired to obtain particle-size information of the initial shale residue (1-D), the shale residue free of water-soluble material (1-F), and that portion of the shale residue resistant to dilute hydrochloric acid (1-H). The water-soluble-free and acid-resistant residues represented 91.59 and 60.07 weight-percent of the initial shale residue (1-C). The respective specific gravities of the three residues were 2.7443, 2.7354, and 2.6892. The continuous water extraction removed 3.34 weight-percent of material other than calcium sulfate from the initial shale residue (1-D).

Many different methods and apparatus, each with its merits and limitations, are used for making particle-size measurements of materials in the subsieve range (6,15). The method selected for this work was the increment method of sedimentation, considered to be one of the most accurate methods; the apparatus was an Andreasen sedimentation vessel. One limitation of this method is that particles with diameters smaller than 0.5 micron cannot be measured owing to Brownian movement, which prevents free fall. Two important requirements for accurate particle-size measurements are a high degree of dispersion of individual particles and subsequent prevention of flocculation during the prolonged test period. These requirements were best attained when a suspension medium was used that consisted of distilled water containing 2 grams per liter of Daxad No. 23 as the dispersing agent (7). Periodic examination of the suspension and the formation on standing of a rigid sediment of minimum volume indicated that the two requirements were attained to a high degree.

Duplicate determinations were made on each of samples (1-D), (1-F), and (1-H). A weighed sample, sufficient to give an approximate volume concentration of 1 percent of the volume of the sedimentation vessel, was mixed with 200 ml. of suspension medium; and the suspension was subjected, with constant stirring, to ultrasonic vibrations for 30 minutes. The mixture was transferred to the sedimentation vessel, diluted to the reference mark with suspension medium, and thoroughly mixed before it was placed in a constant-temperature bath (70° F.) to minimize the effects of convection currents. The suspension medium used to analyze (1-D) was saturated at 70° F. with calcium sulfate to prevent any calcium sulfate in the shale residue from going into solution. After temperature equilibrium was attained, the vessel was removed, thoroughly shaken for several minutes, employing a tumbling motion, returned to the bath, and the first 10-ml. fraction immediately withdrawn and transferred to a tared beaker. Subsequent fractions were withdrawn and transferred to tared beakers at increasing time intervals, arbitrarily selected over a cumulative period of about 100 hours per analysis. Each fraction except the first was withdrawn at uniform rate, approximately 20 seconds per fraction, to minimize disturbance of the suspension. The number of fractions collected totaled 20 to 22. After evaporation of the liquid and drying at 220° F., each fraction was weighed and the correction applied for the dispersing agent. The corrected weight of the first fraction represented the initial concentration of shale residue in the suspension. The weight-percent of each subsequent fraction was calculated from the initial concentration, and its corresponding particle size was determined by Stokes' law, expressed as follows: (9)

$$r = \sqrt{\frac{9\,h\,n}{2(d_1-d_2)\,g\,t}},$$

where r is the radius of spherical particle (cm.); n, the viscosity of suspending medium (poises); h, distance (cm.) between liquid surface and pipette tip when sample is withdrawn; d_1, specific gravity of the particle; d_2, specific gravity of suspending medium; g, gravitational constant; and t, time in seconds. Stokes' law is based on the premise that particles are spherical and smooth and that the concentration of the suspension is dilute enough to permit free fall. Photomicrographs (Figures 2, 3, 4, and 5) revealed that the primary particles were essentially nonspherical. However, Lamar (7) states that irregular particles within the subsieve range have been shown to behave much like spheres. Hence, the results obtained by the sedimentation method should be valid.

The shale residue (2-C) from the 28.6-gallon-per-ton oil shale was subjected to a sieve analysis in the same manner described for the shale residue from the rich oil shale. The degree of cementation between individual primary particles was fairly extensive. As a result of this, only 62.5 weight-percent of the shale residue was reduced to within the subsieve range. Ultrasonic treatment did not effectively reduce the conglomerated masses retained on the sieves. To further reduce them would have required some form of crushing. Because of the high degree of cementation and low percentage (1.73) of water-soluble material (2-C), only the initial material in the subsieve range (2-D) was analyzed for particle size.

Interpretation of Results

Mathematical analysis of the direct analytical data from the sedimentation runs indicated that these data could best be expressed by converting them to a form that permitted graphic presentation, that is, cumulative weight-percent oversize as a function of the logarithm of equivalent spherical diameters. Figure 6 presents the cumulative size-distribution curve for the initial oil-shale residue (1-C). The linear plot represents the sieve analysis. If the primary particles had been spheres, the S-shaped curve would not show particles with diameters greater than 44 microns, as they would have been retained on the 325-mesh sieve. Overlapping of the two curves is attributed partly or entirely to the principle that sieves classify particles according to the least cross-sectional area. The material that remained in suspension after completion of the sedimentation run (7.20 weight-percent, with equivalent spherical diameters of less than 0.5 micron) was essentially calcium sulfate and illite clay minerals, as determined by X-ray diffraction. The total quantity of shale residue accounted for was 99.5 weight-percent of the shale residue analyzed.

Figure 7 presents the cumulative particle-size distribution curve of shale residue free of water-soluble material (1-F). The S-shaped curve represents the average particle size based on the analytical data from two composite samples. The degree of conformity between the two samples, as exhibited by the plotted points, was such that only one curve could be conveniently presented. The linear plot represents the sieve analysis. The total quantity of shale residue accounted for represented 98.8 weight-percent of the shale residue analyzed, of which 3.2 weight-percent remained in suspension. The material that remained in suspension was essentially illite clay minerals.

The cumulative particle-size distribution curve for the shale residue treated with dilute hydrochloric acid (1-H) is shown in Figure 8. The major constituents in the acid-resistant residue were quartz and feldspars. The S-shaped curve represents the average of two sets of experimental data taken from two composite samples of shale residue. The plotted points show the actual values calculated from the analytical data. The quantity of shale residue with equivalent spherical diameters less than 0.5 micron that remained in the suspension medium at the end of the run was 2.6 weight-percent. The total quantity of shale residue accounted for was 98.5 weight-percent of the shale residue charged to the sedimentation vessel.

Figure 9 presents the cumulative particle-size-distribution curve for the primary

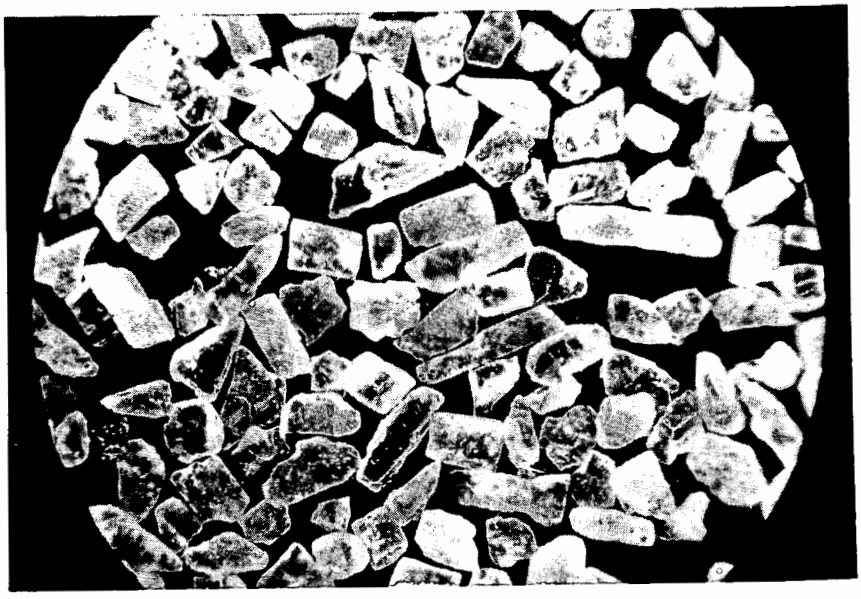

Figure 2. Photomicrograph of primary inorganic particles illustrating shape and roundness. Equivalent spherical diameter range, 175 to 250 microns. Magnification 30X.

Figure 3. Photomicrograph of primary inorganic particles shown above. Magnification 100X.

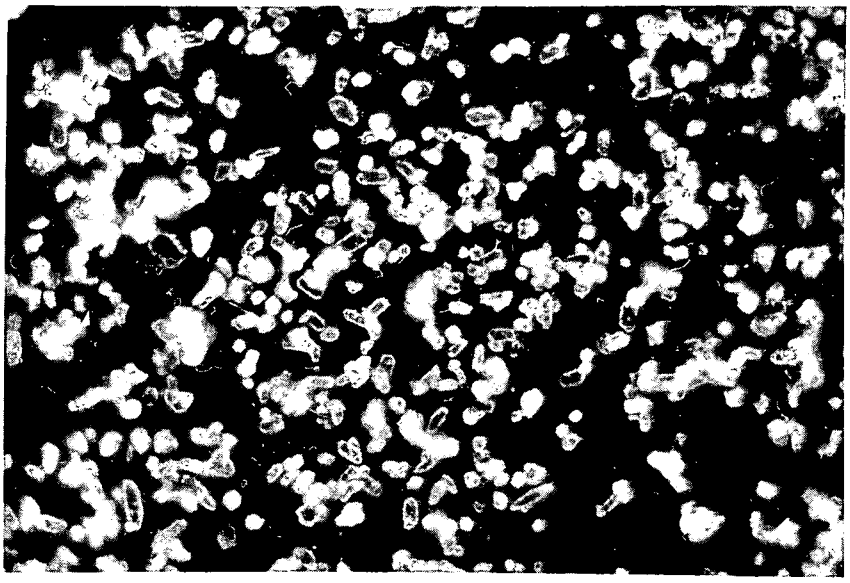

Figure 4. Photomicrograph of primary inorganic particles. Equivalent spherical diameter range, 5 to 15 microns. Magnification 210X.

Figure 5. Photomicrograph of primary inorganic particles, essentially quartz and feldspars. Equivalent spherical diameter range, 15 to 30 microns. Magnification 210X.

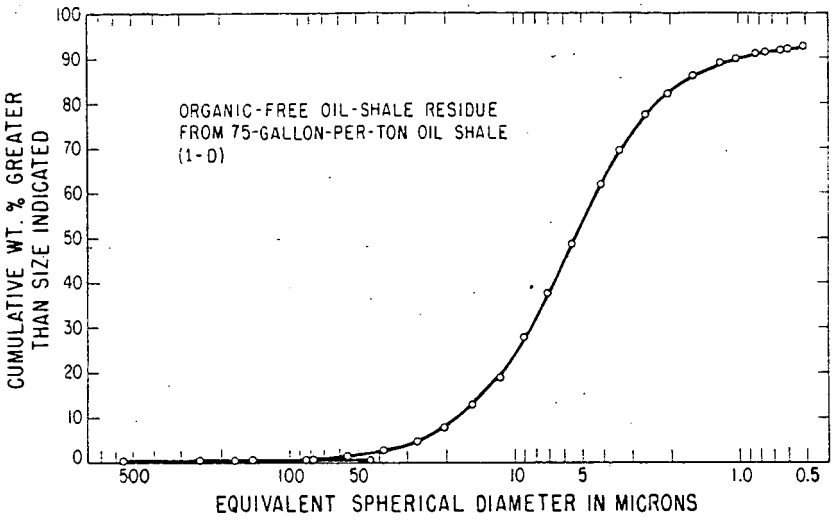

FIGURE 6.-CUMULATIVE PARTICLE-SIZE DISTRIBUTION CURVE OF THE PRIMARY INORGANIC PARTICLES IN RICH OIL SHALE

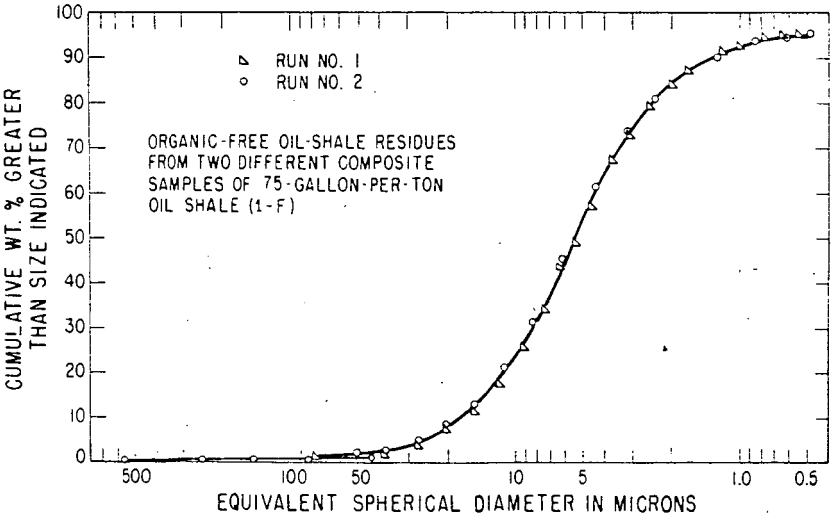

FIGURE 7.-CUMULATIVE PARTICLE-SIZE DISTRIBUTION CURVE OF PRIMARY INORGANIC PARTICLES FREE OF WATER-SOLUBLE MATERIAL

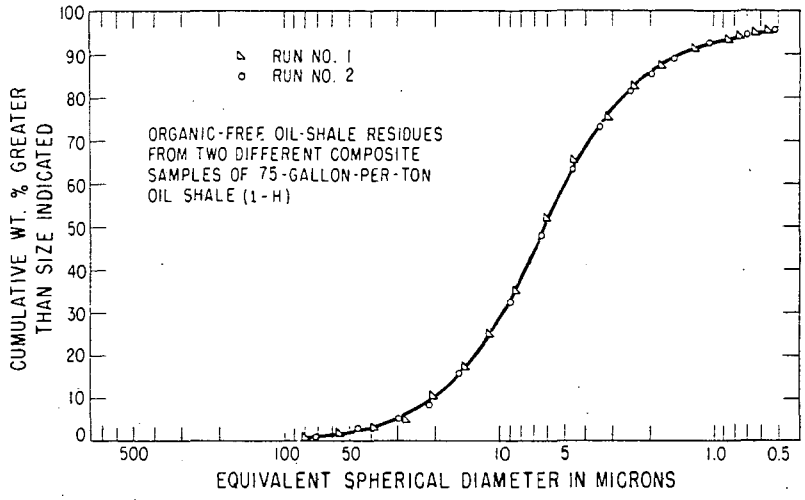

FIGURE 8.-CUMULATIVE PARTICLE-SIZE DISTRIBUTION CURVE OF PRIMARY INORGANIC PARTICLES FREE OF WATER-SOLUBLE AND DILUTE MINERAL ACID-SOLUBLE MATERIALS

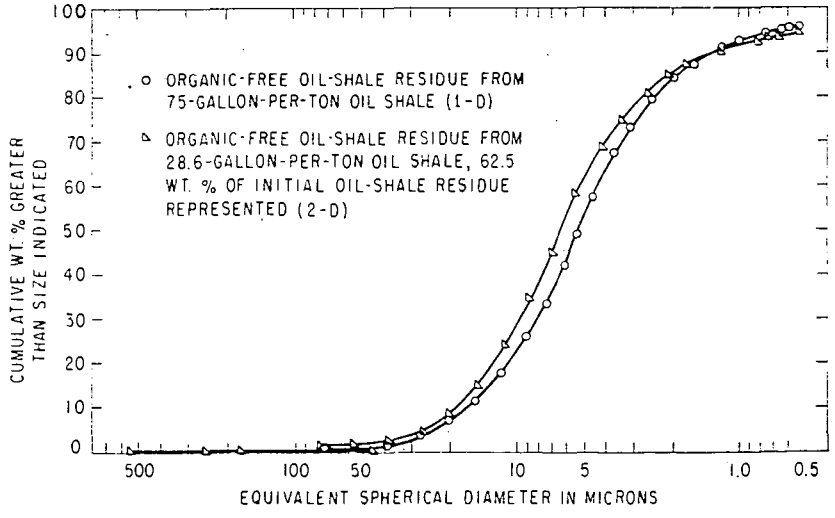

FIGURE 9.-CUMULATIVE PARTICLE-SIZE DISTRIBUTION CURVES OF PRIMARY INORGANIC PARTICLES IN 75-AND 28.6-GALLON-PER-TON OIL SHALE

inorganic particles (2-D), 28.6-gallon-per-ton oil shale, that passed through the 325-mesh sieve. The plot of Figure 6 is included in Figure 9 for the purpose of comparing particle size and particle-size distribution of primary inorganic particles in oil shale taken at two different levels within the oil-shale formation. The oil shales from these two levels differed widely in organic content. It is noted that both size and distribution of the primary particles within the two levels exhibit a high degree of similarity. Microscopic examination of the portion of the shale residue that did not reduce to primary particles (2-E) during the screen analysis indicated that the sizes of the primary particles constituting the conglomerated masses were of the order of those that passed the 325-mesh sieve.

The direct results of all the sedimentation analyses in the form of cumulative weight-percent oversize as a function of equivalent spherical diameters in microns plotted as S-shaped curves. The plots indicate that distribution of sizes of the primary inorganic particles in Green River oil shale tends to follow a log-normal distribution. Good agreement to log-normal distribution was noted between equivalent spherical diameters ranging from approximately 1.7 to 35 microns when these data were plotted on logarithmic probability paper. Departure from log-normal distribution was noted above and below these diameters. Cumulative frequency curves that are log-normal plot as linear lines on logarithmic probability paper. Information available from the cumulative frequency curves are, particle-size range of the primary inorganic particles, weight-percent of shale residue above or below a given diameter, or weight-percent of shale residue within any two size ranges except for the shale residue smaller than 0.5 micron. Two parameters that normally define distribution curves of this type (geometric mean size and standard geometric deviation) may be calculated from the S-shaped curves by reading appropriate intercepts. The geometric mean size is the value in microns corresponding to 50-weight-percent oversize, and the standard geometric deviation is the ratio of sizes corresponding either to 84.13 and 50.00 or 50.00 and 15.87 weight-percent oversize (3). The geometric mean sizes of the primary inorganic particles determined from the distribution curves of shale residues represented by (1-D), (1-F), (1-H), and (2-D) were 5.3, 5.4, 6.2 and 6.4 microns, respectively. The values of the standard geometric deviations for the above curves, as calculated from the ratio of sizes corresponding to 84.13 and 50.00 percent oversize, were 0.3, 0.4, 0.4, and 0.3, respectively. Calculated from the ratio of sizes corresponding to 50.00 and 15.87, the values obtained for the standard geometric deviation were 0.4.

Geometric Form of Primary Inorganic Particles

Information concerning two fundamental properties of the primary inorganic particles -- shape and roundness -- is best conveyed with photomicrographs. Figure 2 illustrates primary inorganic particles retained on a minus 60-plus 80-mesh sieve. The particles are predominantly rhombic. Increased magnification of a number of these particles brings out the third dimension and some of their surface characteristics, as noted in Figure 3. Figure 4 illustrates primary particles with equivalent spherical diameters ranging from 5 to 15 microns. The geometric configuration of the primary particles, with equivalent spherical diameters smaller than 5 microns, could not be brought out clearly with photomicrographs. However, microscopic examination of these particles revealed that their geometric form resembled that shown in Figure 4. Figure 5 illustrates the primary particles that were resistant to dilute hydrochloric acid. The equivalent spherical diameter of these particles, essentially quartz and feldspars, ranged from 15 to 30 microns. X-ray analyses indicated that the sharp-pointed particles were quartz.

Summary

The results of this investigation provide better understanding of the particle

size, particle-size distribution, and geometric form of the primary inorganic particles present in Green River oil shale. Because particle-size studies could not be made in the presence of the organic matter, it was removed by thermal treatment in a manner that minimized chemical and physical changes to the mineral constituents. By virtue of its high organic content, oil shale that assayed 75 gallons per ton yielded a friable residue amenable to this type of work. The portion of shale residue from the 28.6-gallon-per-ton oil shale that reduced to primary inorganic particles without crushing -- 62.5 weight-percent -- was used for particle-size studies.

The primary inorganic particles were essentially nonspherical, and their predominate geometric form appeared to be rhombic. More than 99 weight-percent of the primary inorganic particles analyzed had equivalent spherical diameters less than 44 microns. The distribution of sizes tend to follow a log-normal distribution between equivalent spherical diameters ranging from 1.7 to 35 microns. Departure from log-normal occurred below and above these values. The geometric mean size and standard geometric deviation of the primary inorganic particles free of water-soluble material in the 75-gallon-per-ton oil shale were 5.4 microns and 0.4, respectively. The corresponding values for that portion of the 28.6-gallon-per-ton oil shale residue analyzed were 6.4 microns and 0.3. The range of sizes and type of distribution of the primary inorganic particles of oil shales that differed widely in organic content and represented two different levels within the Green River formation appeared to be quite similar.

Acknowledgment

This project was conducted at the Laramie Petroleum Research Center, Laramie, Wyo. under the general direction of H. M. Thorne. The authors gratefully acknowledge the help of H. N. Smith, W. A. Robb, and J. A. Lanun for x-ray analyses and some of the analytical work. This work was done under a cooperative agreement between the University of Wyoming and the U. S. Bureau of Mines, Department of the Interior.

Literature Cited

(1) Cameron, J. B., Guthrie, B., Chem. Eng. Prog. 50 No. 7, 336 (1954).
(2) Grim, R. E., "Clay Mineralogy," McGraw Hill, New York, 238 (1953).
(3) Hatch, T., Choate, S. P., Jour, Fran. Inst. 207, 373 (1929).
(4) Hull, Q. W., Guthrie, B., Sipprelle, E. M., Liquid Fuels from Oil Shale, A Staff-Industry Collaborative Report, Ind. Eng. Chem. Vol. 43, 2 (1951).
(5) Jukkola, E. E., Denilauler, A. J., Jensen, H. B., Barnet, W. I., Murphy, W. I. R., Ind. Eng. Chem., 45, 2714 (1953).
(6) Lamarr, R. S., Amer. Ceram. Soc. Bull. 31, 283 (1952).
(7) Ibid, 285.
(8) Langford, J. D., Ellis, C. F., Ind. Eng. Chem. 43, 28 (1957).
(9) Loomis, G. A., Jour. Amer. Ceram. Soc. 21, No. 9, 398 (1938).
(10) McKee, R. H., "Shale Oil", The Chemical Catalog Co. Inc., New York, 150 (1925).
(11) "Oil Shale and Cannel Coal", The Institute of Petroleum, Manson House, 26 Portland Place, London, W. 1, 345 (1951).
(12) Ibid, 502.
(13) Stanfield, K. E., Frost, I. C., McAuley, W. S., Smith, H. N., Bur. of Mines Rept. Invest. 4825, 18 (November 1951).
(14) Ibid, 4.
(15) Symposium on New Methods of Particle-Size Determination in the Subsieve Range, A. S. T. M. Spec. Tech. Bull. No. 51 (Mar. 4, 1951).

Not for Publication
Presented Before the Division of Gas and Fuel Chemistry
American Chemical Society
Atlantic City, New Jersey, Meeting, September 13-18,1959

The Geometric Area Shape Factors of Coals Ground in a Standard Hardgrove Mill

L.G. Austin, R.P. Gardner, and P.L. Walker, Jr.
Fuel Technology Department, The Pennsylvania State University
University Park, Pennsylvania

INTRODUCTION

The relation of energy input on grinding to the production of fresh broken surface has received much study (1); and, consequently, comparative increases in surface areas of ground particles have been measured by a variety of methods. However, the absolute external or geometric surface area of coal particles, and the corresponding shape factor, have significance in other processes than grinding. For instance, in processes where coal is chemically reacted at high rates, the rate of reaction is partially controlled by the geometric area (2). The area of any sample of coal of which the density and sieve size distribution are known can be readily calculated from a knowledge of a shape factor k defined by

$$(\text{geometric surface area})\ \mu = k\ (\text{volume}) \qquad (1)$$

where μ is a sieve size. Aris (3) has shown that the ratio of volume to geometric area, that is μ/k, is a characteristic dimension for use in studies of the reaction of solids in beds. Hawksley (4) considers that the drag diameter, which is approximately equal to the diameter of the sphere having the same surface area as the particle, is the most fundamental dimension for use in hydrodynamic problems involving particles. The drag diameter is related to the sieve size by

$$d = \frac{6\mu}{k} \qquad (2)$$

The above remarks indicate that a knowledge of the values of k for coals is likely to be of interest in many industrial processes. Examples of such processes where the shape factor is of actual or potential importance are:

(a) the combustion of pulverized coal in central power stations,
(b) the gasification of pulverized coal,
(c) the production of low temperature coke and coal chemicals in fluidized bed processes,
(d) the firing of open cycle turbines with pulverized coal,
(e) the hydrogenation and chemical processing of coal suspensions, and
(f) the transport of coal in fluid suspensions.

REVIEW OF PREVIOUS WORK

As is well known, coal has a large internal surface area due to a very fine micropore system within the particle (5). Many methods of measurement of surface area determine this internal area in addition to the exterior

surface and, therefore, are not suitable for the measurement of shape factors. The fluid permeability technique, utilizing a modified Kozeny equation, does not in general measure internal surface area (6). This is so because the internal pore system of coal has a negligible permeability compared to the flow between coal particles in a packed bed. Romer (7) used an air permeability method to measure the geometric surface area of ground coal fractions. He did not, however, make available enough information to enable shape factors to be calculated. Skinner (8) pointed out that the hydrodynamic area as measured by permeability methods is of primary importance in the combustion of pulverized fuels and recommended that it should be used to measure shape factors instead of assuming a constant shape factor with size.

APPARATUS AND EXPERIMENTAL TECHNIQUE

Grinding of Coal--The coal under test was ground in a standard Hardgrove test machine according to the A.S.T.M. standard method (9). The ground product was carefully sieved into fractions and the fractions weighed. These fractions were then used for the density and surface area measurements described below.

Density of Coal Fractions--To measure the surface area by the permeability method, it was necessary to know the apparent density of the coal particles tested. Apparent densities were determined, at first, by water displacement in a specific gravity bottle. The coal powder was weighed, vigorously stirred with water to thoroughly wet and release entrapped air, and the density determined. The operation could be carried out in a few minutes and it was thought that in this time the water would not penetrate the internal porosity of the coal to any marked extent. This method gave reproducible results for the larger mesh fractions, but it was found difficult to wet and de-aerate the fine mesh fractions (-200 mesh). Consequently, mercury densities were determined using a mercury porosimeter (10). The pressure of mercury was increased until the rate of entry of mercury dropped suddenly and further pressure caused only a small further penetration. The sudden change-point was taken as equivalent to the geometric density, and the slow additional penetration as the filling of the internal pore system of the particles.

Measurement of Surface Area of Coal Fractions--The surface areas of the coal fractions were determined using the liquid permeability apparatus described by Lakhanpal, Anand and Puri (11) and shown in Figure 1. A coal sample was weighed and packed into tube A, being supported by a thin pad of glass wool over the constriction in the tube. The time taken for a given volume of water to flow through the bed under the mercury head was noted, as were the initial and final mercury heads, suitably corrected for the water pressure head on the right hand column of mercury, Δl. From the weight and density of the coal sample, the diameters of tubes A and C (determined by mercury calibration), the length of the bed, and the viscosity of water at the temperature of the experiment, the surface area of the coal in $cm.^2$ per g. of coal was calculated from equation (3a).

The method was found to be simple and quick and to give good reproducibility. The major difficulty was found in obtaining a bed free from air bubbles. When air was present, the bed had a characteristic mottled appearance at the surface of the tube and surface areas were both too high and poorly reproducible. This difficulty was overcome by allowing the coal

sample to soak in boiled-out water for an hour before use, with frequent stirring, and by packing the bed wet. If the coal was well wetted and packed under suction (from a water pump) with a continuous flow of boiled-out water, air bubbles were not found in the bed. The bed was kept completely full of air-free water at all times during the testing.

The instrument was tested by measuring the surface area of a sample of glass spheres of size 100-200 microns, the glass having a density of 2.50 g./cc. A microscope size count was made on the spheres and the surface area calculated as described later. Comparing the two areas gave a mean factor of k_0q^2 in equation (3) of 4.75, with the values from six tests lying always within ±6% of the mean. Carman (12) reviews values of k_0q^2 found for spheres and quotes values from 4.5 to 5.1, with a best value of 4.8. The value found was in good agreement with this, and it was concluded that the apparatus was working satisfactorily.

THEORY

Specific Surface Area of Tested Material--The specific surface area of a coal fraction was calculated from the following formulae, which can be easily derived.

$$d = 5\left(\frac{k_0q^2}{4}\right)^{\frac{1}{2}}\left(\frac{R_1}{R}\right)\left(\frac{1-\epsilon}{\epsilon}\right)\sqrt{\frac{\eta L \log(\ell_2/\ell_1)}{\epsilon t}\,10^5} \qquad (3)$$

$$S_0 = \left(\frac{6}{d}\right)10^4 \qquad (4)$$

where d is the surface area mean spherical diameter of the material in microns, S_0 is the specific surface area in sq. cm. per $cm.^3$ of material, k_0q^2 is a factor which varies with the shape of the pores in the bed, R is the radius of tube A, R_1 is the radius of tube C, ϵ is the porosity of the packed bed, η is the viscosity of water, L is the length of the packed bed, ℓ_1 and ℓ_2 are the pressure differentials across the bed initially and finally in cm. of mercury, and t is the time of flow in seconds. The factor k_0q^2 is 4 for circular pores, 4.8 for a bed composed of spheres and 5 for a bed composed of irregular particles (13). It should be noted that d is only an intermediate step in the calculation of the surface area S_0, and it is not necessary to attach any particular physical significance to it. However, values of d were calculated because these values could be compared with the nominal sieve sizes of the material tested. These values, consequently, gave a ready indication of an unsatisfactory test. S_0 is in no sense a mean of determined dimensions but is a direct measure of surface area. For the irregular particles of ground coal, equation (3) becomes

$$d = 5\sqrt{\frac{5}{4}}\left(\frac{R_1}{R}\right)\left(\frac{1-\epsilon}{\epsilon}\right)\sqrt{\frac{\eta L \log(\ell_2/\ell_1)}{\epsilon t}\,10^5} \qquad (3a)$$

In order to test the accuracy of the apparatus, the specific surface area of a sample of glass spheres was determined by microscope measurement and by the permeability method. The specific surface area by microscope measurement was calculated by using the following equation

$$S_o = 6 \int_0^N \mu_i^2 \, dN_i \Big/ \int_0^N \mu_i^3 \, dN_i \qquad (5)$$

where dN_i is the number fraction of spheres in the microscope diameter range $\mu_i + d\mu$. The integrations were performed graphically by plotting the cumulative number of particles below diameter μ_i against μ_i^2 and against μ_i^3 and finding the appropriate areas under the curves.

b) Calculation of area-to-volume shape factors.

The specific surface areas per $cm.^3$, S_o, of 10 sieve fractions of a coal ground according to the standard Hardgrove test (60 grinding revolutions) were determined. As the percentage weight of coal in any fraction, Δp say, and the density ρ were known, the surface area ΔS of the fraction was calculated from

$$\Delta S = \frac{S_o}{\rho} \cdot \Delta p$$

The cumulative total surface area, S, and cumulative weight p were then calculated from

$$S = \sum \frac{S_o \Delta p}{\rho}$$

$$p = \sum \Delta p$$

When S was plotted against p on semi-log paper, it was found that a smooth, shallow curve was obtained. Then

$$\frac{dS}{dp} = \frac{dS}{d(\log p)} \left(\frac{1}{2.3p} \right) \qquad (6)$$

and values of $dS/d(\log p)$ were obtained from the slope of the curve at any given value of p. The specific surface area per gram at a sieve size μ corresponding to weight p is clearly given by

$$S_\mu = \left(\frac{dS}{dp} \right)_\mu \quad cm.^2 \, g.^{-1} \qquad (7)$$

If ρ_μ is the density of coal of size μ and the shape factor for this size is k_μ from equations (7) and (2)

$$k_\mu = \left(\frac{dS}{dp} \right)_\mu \mu \rho_\mu \qquad (8)$$

It should be noted that k_μ is the shape factor at size μ and is not a mean over a range of sieve sizes. k_μ is independent of the size distribution of the ground coal, whereas any mean value of k would depend on the size distribution between the sieve sizes averaged.

RESULTS

Table 1 gives the analyses of the coals used in the tests. The four coals cover a range from low rank high volatile sub-bituminous coal to high rank low volatile anthracite.

Figure 2 gives the variation in apparent density of the ground coals with size. In general, the value of density determined at a given size varied about the mean line within a range of ±3%. Fortunately, the value of dS/dp in equation (6) is insensitive to small changes in density. The effect of density is mainly the direct proportionality shown in equation (8). The water densities,where determined, were equal to the mercury densities within the limits of accuracy of both methods.

Table 2 gives the size/weight distribution of the four coals ground for the standard 60 revolutions and the specific surface areas of the ground fractions. At least three area measurements were made on each fraction; the values obtained were always within ±3% of the mean and were usually within ±1%.

Figure 3 shows the cumulative surface area of material less than 30 mesh (U.S. standard sieve) plotted against the percentage weight undersize for coal B19426. Similar curves were obtained for the other coals tested. The numerical values of the slope were used to obtain shape factors using equation (6) and (8). Table 3 gives the shape factors at various micron sizes. Over the size range investigated (approximately 40 to 600 microns), the shape factor was found to be constant for a given coal, the determined values varying randomly about the mean within about ±4%. There were marked differences in the shape factors for the four coals investigated, the differences being considerably greater than can be explained on the basis of experimental errors of the various determinations made.

DISCUSSION OF RESULTS

The variation of apparent density of coal with size after grinding is to be expected, since stronger material will tend to collect in the coarser fractions. The stronger material will usually be denser since it will contain more mineral matter and denser, more coalified coal particles. This effect is more marked for the weaker coals for two reasons: a) there is a greater difference between the hardness of the mineral matter and the remainder of the coal and b) the grinding has proceeded to a more advanced stage for the weaker coals (although ground for the same number of revolutions). The concentration of denser material in the coarse fractions is partially counteracted by the larger size material having a greater probability of breakage (14).

It appears unlikely that shape factor is a function of the degree of grinding (at least, over the size range investigated). If it were, the factor

would be expected to vary for different sized fractions because the finer fractions contain material which has been broken several times. It is possible, however, that the shape factor varies from one type of grinding process to another.

An examination of Seyler's coal chart (15) indicates that over most of the coal range, an increase of 1% in the hydrogen content of a coal has an equivalent effect on the volatile matter (dry ash free) of about an 8.5% decrease in carbon content, the percentage being expressed on Parr's basis (16). Therefore, it is proposed that the rank of a coal be expressed by

$$\text{Rank Index} = \%\,C \text{ (Parr's basis)} - 8.5\%\,H \text{ (Parr's basis)} \qquad (9)$$

When the volatile matter contents of coals are plotted against this rank index, the points have a considerably reduced scatter about the mean line over that when percentage carbon content alone is used (17). This is also true when grindability indices are plotted against the proposed index as shown in Figure 4 (16). Figure 4 also shows the shape factors of the four coals tested as a function of the rank index. Although definite conclusions cannot be drawn from four results, it seems probable that the variation in shape factor has a similar relation to the rank of the coals as that found for grindability indices.

The geometric or hydrodynamic area obtained with the liquid permeability apparatus should not be a function of the chemical nature or roughness of the particle surface since the resistance to flow is due to the internal friction of the liquid. Also the mean free path of the liquid molecules is not great enough compared to the flow paths for the phenomena of slip to occur. Consequently, the variation of shape factor implies that coals fracture to different mean shapes depending on their rank. A high shape factor means that the particle is flaky, while shape factors approaching the value of six imply that the particles tend towards spherical or cubical shapes. Thus, on the basis of our limited results, anthracites and low rank sub-bituminous coals have more flaky particles, while the more easily broken bituminous coals tend to have more rectangular shaped breakage products.

It is possible that shape factors also depend to a considerable extent on the petrographic constituents of the coals, since it is known that different macerals have conchoidal, splintery, or irregular breakage (18).

CONCLUSIONS

The geometric-surface-area-to-volume shape factor was found to be constant for a given coal over the size range investigated, approximately 40 to 600 microns. It seems likely that the shape factors of coals are related to their rank in a similar manner to that of their grindability indices. Shape factors were found to vary from 7.2 for a medium rank bituminous coal (17.9% volatile matter, d.a.f.) to 9.4 for a high rank anthracite (4.5%) and 9.6 for a low rank sub-bituminous coal (42.4%).

ACKNOWLEDGEMENTS

We wish to express appreciation to G.C. Williams and R.R. Luckie who assisted in the experimental program. We appreciate the financial support of the Coal Research Board of the Commonwealth of Pennsylvania which made this work possible.

REFERENCES

1. "Crushing and Grinding Bibliography", Department of Scientific and Industrial Research (London), H.M.S.O., 1958, p. 99.

2. Walker, P.L. Jr., Rusinko, F. and Austin, L.G., "Advances in Catalysis", Vol. XI, Chapter on Gas Reactions of Carbon, Academic Press Inc., New York, 1959, in press.

3. Aris, R., Chem. Eng. Sci., 6, 262 (1957).

4. Hawksley, P.G.W., Brit. J. Appl. Phys., Supplement No. 3, 51 (1954).

5. Anderson, Robert B., Hall, W. Keith, Lecky, James A., and Stein, Karl C., J. Phys. Chem., 60, 1548 (1956).

6. Carman, P.C. and Arnell, J.C., Can. J. Res., 26A, 128 (1948).

7. Romer, J.B., Proc. Am. Soc. Test. Mat., 41, 1152 (1941).

8. Skinner, D.G. "Pulverised Fuel Conference", Inst. of Fuel (London), 1947, p. 519.

9. Am. Soc. Testing Materials Standard D409-51, Grindability of Coal by the Hardgrove Method.

10. Washburn, E.W., Proc. Nat. Acad. Sci., 7, 115 (1921).

11. Lakhanpal, M.L., Anand, V.D., and Puri, B.R., Nature, 176, 692 (1955).

12. Carman, P.C., "Flow of Gases through Porous Media", Academic Press Inc., New York, 1956, p. 14.

13. Ibid, p. 36.

14. Austin, L.G., "Breakage Functions of Coal Ground in a Standard Hardgrove Mill", to be published.

15. "Technical Data on Fuel", 5th Ed., British National Committee World Power Conference, 1950, p. 393.

16. Fitton, A., Hughes, T.H., and Hurley, T.F., Inst. Fuel (London), 30, 54 (1957).

17. Austin, L.G. Unpublished Results.

18. Stopes, M.C., Proc. Roy. Soc. (London), 90, 470 (1919).

TABLE 1

ANALYSES OF COALS USED

Coal	B-19447	B-17790	B-19426	St. Nicholas Anthracite
Constituent	As used,%	As used,%	As used,%	As used,%
Moisture	1.5	0.8	0.5	1.6
Ash	16.5	7.8	14.5	9.3
Carbon	65.5(83.5)*	78.8(87.6)*	75.2(90.6)*	84.2(95.5)*
Hydrogen	4.7(5.9)*	4.8(5.1)*	3.9(4.5)*	2.4(2.2)*
Nitrogen	1.1	1.5	1.5	0.85
Sulfur	4.5	1.6	1.8	0.5
Oxygen (by difference)	6.2	4.7	2.6	1.1
Volatile Matter (D.A.F.)	42.4	29.2	17.9	4.5

*Parr's basis

TABLE 2

SIZE-WEIGHT DISTRIBUTIONS AND HYDRODYNAMIC SURFACE AREAS OF SIEVE FRACTIONS FOR COALS GROUND ACCORDING TO THE STANDARD HARDGROVE TEST

Sieve Range U. S. Standard Mesh	B-19447		B-17990		B-19426		S.N.A.	
	p*	S_o**	p	S_o	p	S_o	p	S_o
16 x 30	100		100		100		100	
30 x 35	64.25	178	79.97	138	80.37	132	75.26	166
35 x 50	54.05	235	71.78	217	73.13	192	61.10	211
50 x 70	35.55	403	54.06	307	56.00	296	26.98	378
70 x 100	27.02	565	44.78	439	47.45	408	17.67	552
100 x 120	18.48	710	35.62	598	38.03	502	10.78	670
120 x 140	16.89	865	32.78	714	34.81	684	8.99	786
140 x 170	14.63	1001	28.78	948	31.22	744	7.23	1000
170 x 200	12.95	1171	25.95	1036	28.29	944	6.20	1156
200 x 230	11.17	1403	22.26	1235	24.69	1065	5.03	1398
230 x 325	9.82	1730	20.26	1635	22.48	1355	4.30	1717
Minus 325	7.94		11.14		16.29		3.20	
% Weight lost on grinding	0.66		0.72		0.83		(-0.1)	
Mean Hardgrove Index	52		93		99		30	

*p = % by weight below upper sieve size
**S_o = Surface area per unit volume of coal in size range given, $cm.^2/cm.^3$

TABLE 3

SURFACE AREA TO VOLUME SHAPE FACTORS FOR COALS
GROUND ACCORDING TO STANDARD HARDGROVE TEST

B-19447			B-17990			B-19426			St. Nicholas Anthracite		
μ *	$\frac{dS}{dp}$ **	k ***	μ	$\frac{dS}{dp}$	k	μ	$\frac{dS}{dp}$	k	μ	$\frac{dS}{dp}$	k
47.5	1421	9.6	44	1420	7.9	44	1240	7.1	47.5	1340	9.6
62	1124	9.6	62	1040	8.1	62	900	7.3	62	995	9.4
74	935	9.5	74	850	8.0	74	809	7.3	74	850	9.6
88	782	9.5	88	726	8.0	88	632	7.3	88	690	9.3
105	678	9.8	105	610	8.2	105	535	7.4	105	591	9.5
125	565	9.7	125	480	7.8	125	486	7.2	125	475	9.2
138	497	9.6	149	396	7.9	149	357	7.1	149	406	9.4
220	338	9.8	220	268	8.0	210	250	7.2	210	286	9.4
297	230	9.4	297	197	8.0	297	173	7.1	297	201	9.3
500	140	9.6	500	128	8.3	500	100	7.1	500	113	8.9
590	118	9.6	590	104	7.9	590	87.7	7.35	590	101	9.3
Mean k		9.6			8.0			7.2			9.3

* μ is sieve size in microns

** $\frac{dS}{dp}$ is the specific surface area in $cm.^2$ per g. at size μ

*** k is volume-to-surface area shape factor

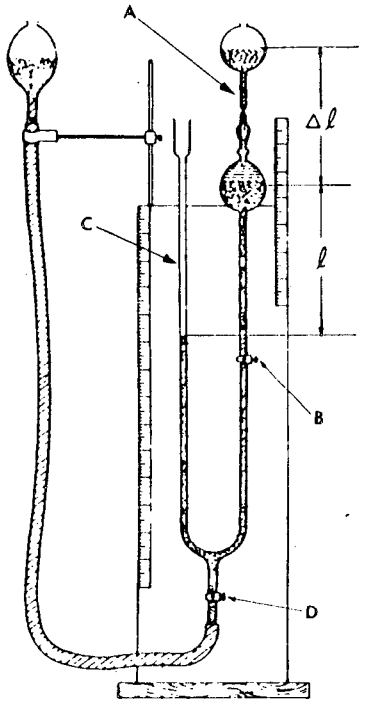

Fig. 1. DIAGRAM OF PERMEABILITY APPARATUS.

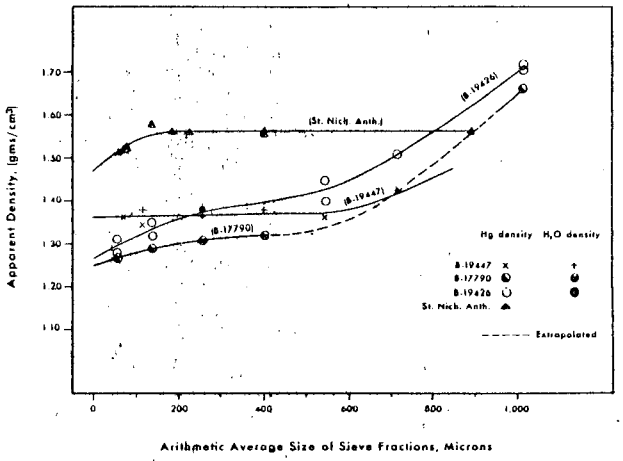

Fig. 2. APPARENT DENSITIES OF SIEVE FRACTIONS OF COALS GROUND ACCORDING TO STANDARD HARDGROVE TEST.

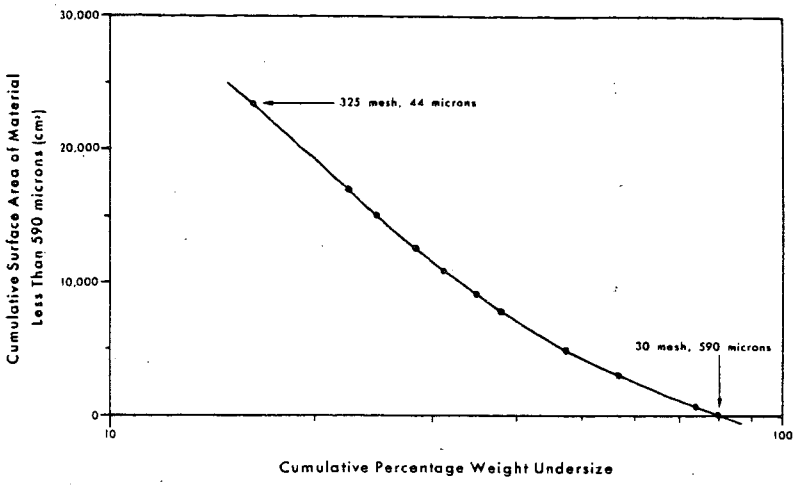

Fig. 3. CUMULATIVE SURFACE AREA AGAINST PERCENTAGE UNDERSIZE FOR COAL B-19426 GROUND ACCORDING TO STANDARD HARDGROVE TEST.

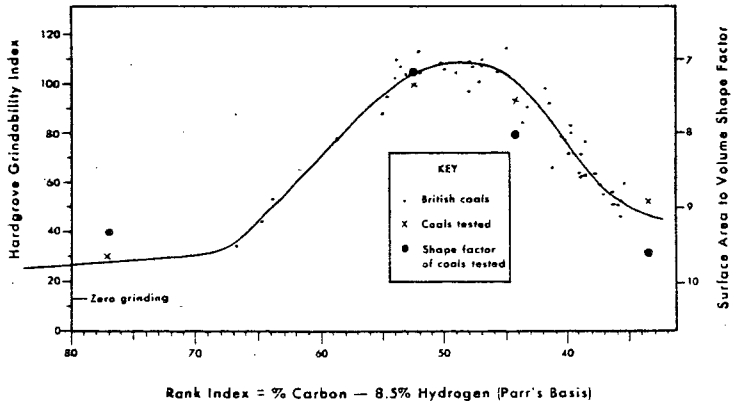

Fig. 4. GRINDABILITY INDEX AND SHAPE FACTOR AS A FUNCTION OF COAL RANK.

Not for Publication
Presented Before the Division of Gas and Fuel Chemistry
American Chemical Society
Atlantic City, New Jersey, Meeting, September 13-18, 1959

The Relation of Microscope Size to Sieve Size for Ground Coals

L.G. Austin, R.P. Gardner, and P.L. Walker, Jr.
Fuel Technology Department, The Pennsylvania State University
University Park, Pennsylvania

INTRODUCTION

The weight versus size distribution of a ground coal is an important parameter in many industrial processes, and there has been much study of such distributions (1). The simplest and most commonly used method of size analysis is sieve analysis, but the finest sieve which can be used with any degree of accuracy has a nominal aperture of 44 microns (U.S. standard sieve No. 325). For material below this size it is necessary to use less direct methods such as air elutriation, sedimentation velocities, and microscopic measurement (2). In the sub-sieve range down to 1 micron, measurement with an optical microscope is simple, avoids problems of agglomeration found with other methods, and gives results which are fairly reproducible. Although microscope counting and measurement is tedious, if two experienced personnel work together, results can be obtained at least as quickly as with most other methods.

To extend a sieve size distribution to sub-sieve sizes, it is necessary to know the relation between sieve size and the particular size property measured in the sub-sieve range. In the case of microscopic measurement, the size property is some characteristic visual dimension. The most commonly used dimension is the "projected area diameter", that is, the diameter of the circle which has the same area as the projected outline of the particle in the plane of the microscope slide. In the work described in this paper, the relation between microscope diameter (defined as above) and sieve size is investigated.

REVIEW OF PREVIOUS WORK

Skinner, Boas-Traube, Brown, and Hawksley (3) measured the ratio of microscopic diameter to sieve size for coal which just passed a 7-mesh sieve. They obtained a mean ratio of 1.42. They state that it is not known whether this ratio varies with size. Heywood (4) investigated this ratio for a number of different materials and found values between 1 and 1.8, depending on the geometric shape of the particles. He has also proposed (5) an empirical formula which gives this ratio as a function of m and n, where m is the microscopic breadth of the particle divided by its thickness and n is the breadth divided by the length. Heywood states (6) that the relation between microscope diameter and sieve size is dependent only on the geometry of the particles and not on their size. Guruswamy and co-workers (7) measured the ratio of microscope diameter to sieve size for a series of sieve fractions of a coal which had been broken upon being dropped on to a metal plate. The ratio appeared to increase slightly with decrease in size over a range of approximately 3000 to 100 microns sieve size, the ratio having a mean value of about 1.5.

APPARATUS AND EXPERIMENTAL TECHNIQUE

Microscopic size counts were performed on a number of sieve fractions of coal in the range of 30 to 325 U.S. standard sieve sizes. The measurements were made by projecting the field on to a ground glass screen on which circles of varying radii were drawn; the field was then moved to bring each particle under the appropriate diameter circle. By calibration with a microscopic scale, the representative size of the circles for a given magnification was known. Each particle was assigned on an area basis to a group lying between two circles. From such a count, the cumulative percentage number of particles below any given microscope size was obtained.

For sieve fractions below 170 mesh, slides were prepared in the following manner. A sample of the coal was stirred vigorously in several ml. of toluene until well dispersed, and a drop of the suspension was transferred to 1 ml. of a 10% ethyl cellulose in toluene solution. After stirring, a drop of this suspension was spread on a slide and allowed to thicken. Using this technique, extremely uniform and well dispersed fields were obtained. For larger sizes, it was found that the particles tended to project from the dried cellulose layer; and it was not possible to get clear images of such particles. Consequently, dry slides were prepared by tipping a small amount of the sieve fraction on to the slide and spreading the particles with a fine brush. For these sizes, agglomeration did not occur to any significant extent.

The coals tested were ground according to the standard Hardgrove test (8), as described in a previous paper (9).

THEORY

Let the external geometric surface area and the volume of the particle of sieve size μ be given by

$$S = k_1 \mu^2$$

and

$$V = k_2 \mu^3.$$

Then

$$dS = k_1 \mu^2 dN$$

and

$$dV = k_2 \mu^3 dN$$

where dN represents the number of particles of size $\mu + d\mu$. Over a short size range, k_1 and k_2 may be assumed to be constant and

$$\frac{S}{V} = \frac{k_1}{k_2} \frac{\int \mu^2 dN}{\int \mu^3 dN}.$$

Now $S/V = S_o$, the specific surface area of the material; and if a shape factor k is defined by $k = S_o\mu$, then $k = k_1/k_2$. Therefore,

$$S_o = k \frac{\int \mu^2 dN}{\int \mu^3 dN}.$$

Defining R by $R = d_p/\mu$, where d_p is the projected area diameter,

$$R = \frac{S_o}{k} \frac{\int_0^N d_p^3 dN}{\int_0^N d_p^2 dN} . \qquad (1)$$

For the size fractions and coals investigated, S_o and k were known from previous determinations (9). The integrals were evaluated graphically.

Although Equation (1) is derived without recourse to the concept of mean values, k/S_o is a specific-area (geometric area per unit volume) mean-sieve size, while $\int d_p^3 dN / \int d_p^2 dN$ is a specific-area-mean-microscope size. Thus, Equation (1) can be given as

$$R = \frac{\tilde{d}_p}{\tilde{\mu}} \qquad (1a)$$

where $\tilde{\mu}$ is a specific-area-mean-sieve size and $\tilde{d}_p$ is specific-area-mean-microscope size. In general, it was found that, within two or three per cent,

$$\tilde{d}_p \simeq \left(\frac{\int_0^{100} d_p^2 dN}{100} \right)^{\frac{1}{2}} \simeq \left(\frac{\int_0^{100} d_p^3 dN}{100} \right)^{\frac{1}{3}} . \qquad (2)$$

Thus, the specific-area mean, area mean, and volume mean microscope size were not significantly different.

RESULTS

Table 1 gives the analyses of the coals used. They range from a high rank anthracite to a low rank bituminous coal.

Figure 1 shows the relation between $\tilde{d}_p$ and $\tilde{\mu}$ determined for sieve ranges of 35 x 50, 50 x 70, 70 x 100, 100 x 120, 120 x 140, 140 x 170, 170 x 200, 200 x 230, and 230 x 325 U.S. sieve numbers. For sieve sizes smaller than 80 microns (approximately 170 mesh), the ratio R appears to be constant at 1.68, with no significant difference between the coals tested. For sieve sizes larger than 80 microns, however, the curve bends over sharply, giving a second straight line section which does not pass through the origin. The variability of the results tends to obscure any differences between the coals. The best-fit curve above a sieve size of 80 microns has the equation

$$d_p = 40 + 1.18\mu \qquad (3)$$

or

$$\mu = \frac{d_p - 40}{1.18} . \qquad (3a)$$

The disadvantage of using $\tilde{\mu}$ to correlate with $\tilde{d}_p$ is that any error in measurement of the specific surface, S_o, of the sieve fraction considered will reflect as an error in $\tilde{\mu}$. This is in addition to the error involved in microscopic measurements, which gives rise to inaccuracies in the $\tilde{d}_p$ values. If the arithmetic mean sieve size of the fraction is used, the surface area error is avoided, but no allowance is made for the size distribution within the fraction. Figure 2 shows the relation between the volumetric-mean microscope diameter (which is close in value to $\tilde{d}_p$, see Equation (2)) and the arithmetic mean sieve size. The general form is the same as Figure 1, but there appears to be significant differences between coals for the portion of the curve above 80 microns.

Figure 3 gives values of R as a function of microscope size for the best fit curves of Figures 1 or 2. Values of sieve size calculated using these values of R and measured microscope diameters lie within ±10% of the arithmetic mean sieve sizes for all the results obtained.

DISCUSSION OF RESULTS

Previous results (9) indicated no change in the shape factor k with size for a given coal in the range 40 to 600 microns, yet R decreased significantly above sieve sizes of 80 microns. This result appears to be in conflict with Heywood's prediction (6). Further, the values of R obtained for the larger sizes were lower than those reported by other workers (3,7).

The material below 170 mesh size was viewed in ethyl cellulose suspension; but it would be expected that this would tend to reduce R rather than increase it, since the thinner sides of the particles might lie in the line of sight. It is clear that the curve of d_p against μ must pass through the origin. Therefore, even if the minus 170 mesh results were not available, it would be predicted that the curve must bend towards the origin. The shape of the curve is not caused by errors in area measurements, since Figure 2 is substantially the same even though surface area measurements play no part in its compilation.

It would appear that the method of size reduction of the particles has a considerable influence on the values of R, since the values obtained by Guruswamy and co-workers (7) were significantly higher than the results presented here. It would also appear that, for the narrow size ranges used, the use of a volume-mean microscope diameter and an arithmetic-mean sieve size is at least as satisfactory as using specific area mean diameters.

Although the coals used had specific-surface-area-shape factors, k, differing by as much as 30% (9), a significant correlation between the values of R and k was not clear. A possible explanation for this is as follows. If the ground coals have about the same length and breadth ratio, n, but varying thickness to breadth ratios, m, then it is easily shown that the values of k may vary widely with a comparatively small change in R. For instance, assuming a rectangular prism shape with n = 2 and m varying from 1/0.3 to 1/0.5 (10), k will vary by almost 30% while R will vary by less than 10%.

It is fortunate that the extrapolation of the curves of Figures 1 and 2 to the origin gives a constant value of R for the sub-sieve fraction, since this is the size range of most significance. The use of a value of R of 1.68 enables sub-sieve microscope distributions to be joined on to the sieve size distribution, in the present work, where the coals were ground in a Hardgrove machine.

CONCLUSIONS

For coals ground in the standard Hardgrove test mill, the ratio of microscope "projected area" diameter to sieve size, for material finer than 170 U.S. sieve size was found to be 1.68 for all the coals tested. Above this size, the ratio appears to decrease with increasing size to a limiting value of about 1.2. Although there may be a significant variation of the values of R (at the larger sizes) with the type of coal ground, this variation appears to be less than ca. ±10% for the four coals tested.

ACKNOWLEDGEMENTS

We wish to express appreciation to G.C. Williams and R.R. Luckie who assisted in the experimental program. We appreciate the financial support of the Coal Research Board of the Commonwealth of Pennsylvania which made this work possible.

REFERENCES

1. "Crushing and Grinding Bibliography", Department of Scientific and Industrial Research (London), H.M.S.O., 1958, p.18.
2. Jarrett, B.A. and Heywood, H., Brit. J. Appl. Phys., Supplement No. 3, S 21 (1954).
3. Skinner, D.G., Boas-Traube, S., Brown, R.L., and Hawksley, P.G.W., "Determinations of Particle Size in Sub-Sieve Range", The British Colliery Owners Research Association and The British Coal Utilisation Research Association, 1954.
4. Heywood, H., "Chemical Engineering Practice", Vol. 3, Butterworths' Scientific Publications, 1957, p.40.
5. Heywood, H., Trans. Instn. Chem. Engrs. (Supplement) 25, 14 (1947).
6. Reference 4, p.42.
7. Guruswamy, S., Roy, L.C., Das Varma, R.L., and Srinivasan, S.R., J. Sci. Industr. Res. (India) 12B, 91-105 (1953).
8. Am. Soc. Testing Materials Standard D409-51, Grindability of Coal by the Hardgrove Method.
9. Austin, L.G., Gardner, R.P., and Walker, P.L. Jr., The Geometric Area Shape Factors of Coals Ground in a Standard Hardgrove Mill, presented before the Gas and Fuel Division at the September, 1959 meeting of the American Chemical Society.
10. Guruswamy, S., Brit. J. Appl. Phys., Supplement No. 3, S 81 (1954).

TABLE 1

ANALYSES OF COAL USED

Coal	B-19447	B-17790	B-19426	St. Nicholas Anthracite
Constituent	As used,%	As used,%	As used,%	As used,%
Moisture	1.5	0.8	0.5	1.6
Ash	16.5	7.8	14.5	9.3
Carbon	65.3(83.5)*	78.8(87.6)*	75.2(90.6)*	84.2(95.5)*
Hydrogen	4.7(5.9)*	4.8(5.1)*	3.9(4.5)*	2.4(2.2)*
Nitrogen	1.1	1.5	1.5	0.85
Sulfur	4.5	1.6	1.8	0.5
Oxygen (by difference)	6.2	4.7	2.6	1.1
Volatile Matter (D.A.F.)	42.4	29.2	17.9	4.5
Shape Factor (k)	9.6	8.0	7.2	9.3
Hardgrove Grindability Index	52	93	99	30

* Parr's basis

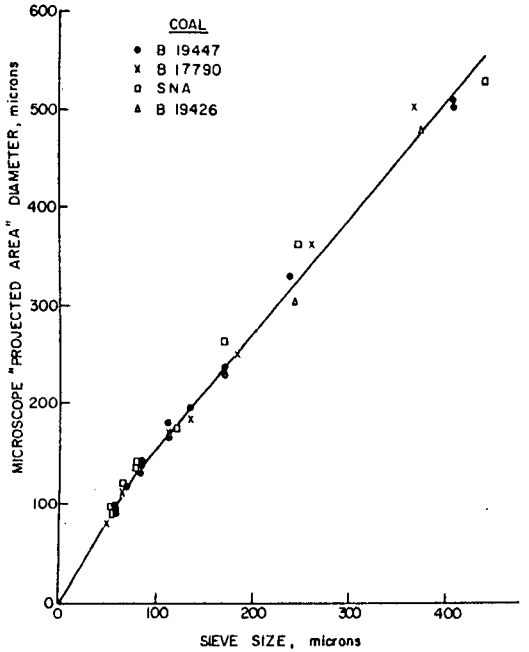

FIG. 1 – Relation between microscope diameter and sieve size for coals ground according to Standard Hardgrove Test.

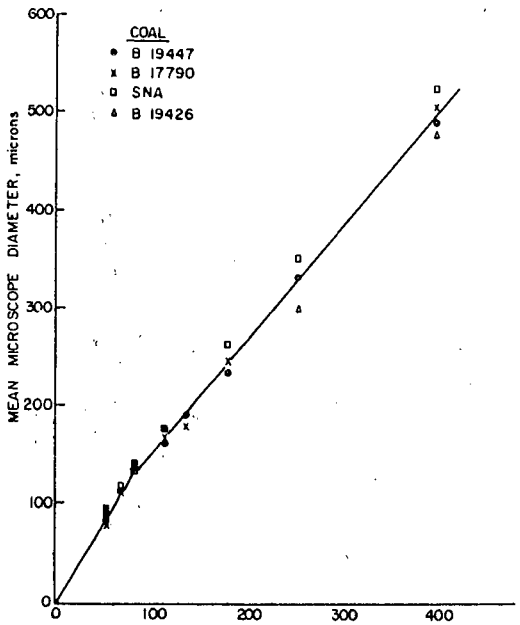

FIG. 2 – Relation of mean microscope size to arithmetic mean size.

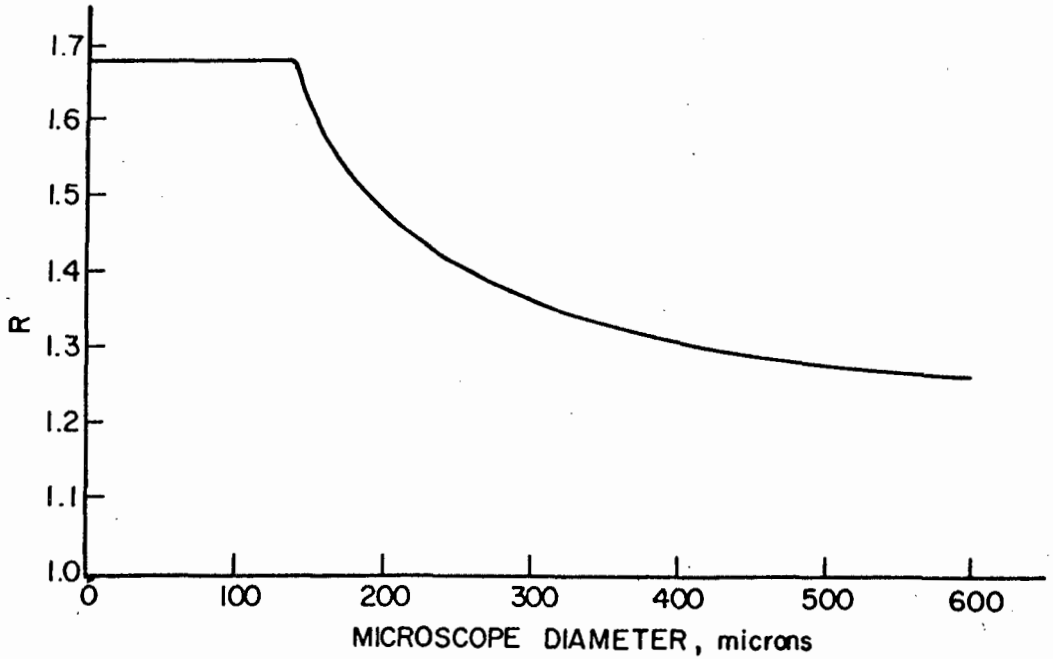

FIG. 3 — Change of microscope-size-to-sieve-size ratio (R) with microscope size for coals ground according to the Standard Hardgrove Test.

Not for Publication

Presented Before the Division of Gas and Fuel Chemistry
American Chemical Society
Atlantic City, New Jersey, Meeting, September 13-18, 1959

The Production of Fresh Surface during the Grinding of Coal in a Standard Hardgrove Mill

L.G. Austin, R.P. Gardner, and P.L. Walker, Jr.
Fuel Technology Department, The Pennsylvania State University
University Park, Pennsylvania

INTRODUCTION

For many years there has been considerable discussion as to whether the energy per unit volume required for size reduction of brittle materials is (a) proportional to the fresh area produced (Rittinger's Law) or (b) proportional to the reduction in volume of the particles (Kick's Law). Bickle (1) has given an excellent review of the available literature. For fine grinding, Rittinger's Law appears to be the law of most general application. Recent workers (2,3) consider such laws to be of limited utility in problems of mill design and operation. However, the relation of grinding energy to fresh surface area produced is of interest chemically as it offers a method of investigating surface energies of materials (4).

REVIEW OF PREVIOUS WORK

Although Rittinger's Law has been widely investigated for quartz, magnetite, and a variety of ores, there have not been many investigations of the law for coal. The primary reason for this is that coal contains an internal surface area (within micropores) that is large compared to the external area even for finely ground particles (5). Since most methods of area measurement measure, either completely or partially, this internal area, the increase in area upon grinding is obtained as the small difference between two large quantities. Consequently, the results are insufficiently accurate to be of much use.

Hardgrove (6) calculated proportional areas of ground coal from the sieve analysis. He assumed that shape factors and coal density remained constant throughout the size range and that shape factors were the same for different coals. The integration of the size distribution to a proportional area was carried out assuming that the minus 325 mesh size had a mean sieve size of 25 microns. Using these areas, he found the fresh surface produced to be proportional to the number of revolutions of the mill over a restricted range of revolutions. When large amounts of breakage had occurred, the increase in surface area on further grinding was less than that predicted by the increased number of revolutions; and Rittinger's Law did not hold. Hardgrove attributed this behavior to blanketing of the grinding by the fines produced. He defined the grindability of a coal in terms of the increase in surface area produced compared to that of the increase produced on grinding a standard coal the same number of revolutions, 60 revolutions being chosen as a standard condition. Hardgrove later found that there was an empirical relation between the grindability defined in this manner, and the per cent by weight of coal, p, passing a 200 mesh sieve, the relation being

$$\text{Hardgrove Index} = 13 + 3.465\ p. \qquad (1)$$

Romer (7) attempted to overcome some of the obvious objections to Hardgrove's work by measuring the surface areas of ground coals using an air permeability method. This method gave the hydrodynamic or geometric area of the particles. Romer found that the grindability indices calculated using the direct area measurements were considerably different from the Hardgrove indices, the surface areas being much higher than predicted for the products of coals of high Hardgrove indices. He then showed that Rittinger's Law applied when the load on the mill or the number of revolutions of the mill were varied. Thus, any non-applicability of Rittinger's Law in Hardgrove's original work was ascribed to inaccurate surface area measurements. Objections still remain to the surface areas obtained by Romer. The permeability method of area measurement is known to be inaccurate for a sample of mixed sizes in which the largest to finest size ratio is greater than 3 (8). Romer actually measured samples which consisted of coal of size range from one to 44 microns. Also, a certain amount of very fine material is lost during the grinding and sieving operations, and this surface area is not included in the measured area.

Bennet and Brown (2) argue that proofs of Rittinger's Law for coal are of little significance because the fresh surface area produced cannot be measured unequivocally.

EXPERIMENTAL PROCEDURES

Characteristics of Coals used in Tests - Four coals were used, ranging from an anthracite of 4.5% volatile matter to a low rank bituminous coal of 42.5% volatile matter and 6.2% oxygen content. The analyses were performed on the 16 x 30 mesh coal* which was the starting material for all tests. The proximate and ultimate analyses were carried out according to A.S.T.M. standard procedures.

Preparation of Coal Samples - Since the interest was in the properties of the coal actually used and not in those of the bulk sample supplied, no studies were made on differences in character between the bulk sample and the final sample. The sample for use was prepared from minus 1/2-in. material by passing it through a jaw-crusher followed by a disc mill and sieving out the 16 x 30 mesh fraction on a Rotap sieving machine. The 16 x 30 mesh fraction was removed after each pass through the jaw crusher or disc mill. Microscopic examination showed the sample to be almost free from adhering fines or agglomerates. Before use, the coals were spread on trays in a thermostatically controlled (to ± 0.5°C.) laboratory and allowed to reach equilibrium with the atmosphere. Grinding and weighing were performed in this laboratory.

Grinding of Coal - The coals were ground in a standard Hardgrove test machine according to the A.S.T.M. standard method (9), both to measure the grindability and to provide sufficient fractions of material for surface area measurement. Two of the coals were also ground for varying revolutions of the machine, ranging from 3 revolutions, to 140 revolutions. In every test, 50 g. of coal were charged to the machine and the product sieved, as described below.

Sieving of the Ground Coal - It was considered essential that good performance of sieving be obtained; therefore, a standard procedure was carefully followed in each case. The material from the mill was carefully brushed out into the top sieve of a series of 6 sieves (16 mesh to 120 mesh). The sieves were shaken in

---

* All sieve numbers refer to U.S. standard mesh.

a Rotap sieving machine for 10 minutes, the material through 120 mesh removed, the sieve cleaned if necessary, and the sieves reshaken for five minutes. This was repeated for five minute intervals until the amount of minus 120 mesh material coming through was small. (A total sieving time of 25 minutes was always sufficient). The same procedure was then followed using the minus 120 mesh material in another series of 6 sieves (120 to 325 mesh). The sieves required cleaning more frequently and a maximum sieving time of 35 minutes was sometimes required. Cleaning was carried out by separating the sieves a small amount, inserting a brush and brushing the underside of the top screen. The collected sieve fractions were weighed to the nearest 0.01 g.

It was found that this series of multiple sievings gave weight losses outside of the tolerance given in the A.S.T.M. standard. Therefore, for standard Hardgrove Index determinations, the ground coal was sieved through a 200 mesh sieve only and the multiple sieving performed after the initial weighings. When this was done, the weight loss in the single sieving operation was within tolerance; and if the weight loss in the multiple sieving was assumed to be of material below 200 mesh, the Hardgrove Index was the same as that for the single sieving, within the tolerance allowable (± 2%).

When the coal was ground for a few revolutions only and the amount of fine material formed was small, the minus 120 mesh material was sieved through tared 3 inch diameter sieves. The coal sample plus sieve was then weighed directly to the nearest 5 milligrams

Surface-Area Shape Factors and Apparent Density of Coal Fractions - The shape factors and densities of ground coal fractions were determined as described in an earlier paper (10).

Size Distributions of Sub-Sieve Fractions of Ground Coal - To extend the cumulative weight versus sieve size to sub-sieve size particles, 0.5 g. of the minus 325 mesh fraction was sedimented into a fine and a coarse fraction and microscope sizing carried out on each fraction. The "sinks" obtained after repeated sedimentation with a 1/2 hour settling period were found to be free from any appreciable quantity of fine material. The "floats" were filtered, dried and weighed. Slides of each fraction were prepared and microscopic counts were performed on each fraction, as described in an earlier paper (11). The magnifications used were x 100 on the "sinks" and x 600 on the "floats". The sink material had microscope diameters mainly from 10 to 80 microns in size, and the float material ranged in size from less than 0.8 microns to about 20 microns. A cumulative weight against size distribution was calculated (see theory) for each fraction; and since the respective weight of each fraction was known, a combined distribution could be calculated. Microscope diameters were converted to sieve sizes using the correlation found previously (11).

THEORY

Calculation of Weight Versus Sieve Size Distributions for Sub-Sieve Coal Fraction from Microscopic Measurements - From microscopic count measurements, the cumulative per cent number of particles, N, below a given microscope size was determined as a smooth function of microscope size, d_p. By plotting N against d_p^3, the percentage weight p below a given size d_p was obtained graphically

since

$$\left(p\right)_{d_p} = 100 \frac{\int_0^{d_p} d_p^3 \, dN}{\int_0^{100} d_p^3 \, dN} \qquad (2)$$

This assumes, of course, that the weight of a particle is proportional to the cube of its microscope diameter, but this assumption appears to be justified (12). The microscope size was then converted to sieve size by dividing by 1.68 (11).

Compilation of Accurate Sieve Size Versus Percentage Weight Undersize Curves - When experimental results of weight versus size for varying revolutions were plotted, the results were not very consistent. This was due to the inherent variability of the grinding and sieving operations and inaccuracies in sieve sizes. The results were made more consistent by cross plotting the percentage weight below a given size against revolutions of grinding, drawing the best fit curve to the points, and taking values from the curve for a replot of weight versus size. This technique was found to give a very consistent family of curves, which could be extrapolated accurately to sub-sieve sizes.

Surface Area Change on Grinding - The surface area of ground coal was determined from the percentage weight versus size distribution, the values of shape factor k, and the density of the coal. If p is the percentage by weight below size μ, then the experimental data on size distribution may be expressed graphically in the form, $p = F(\mu)$. As shown (10), $dS = d_p \, k/\mu\rho$. Therefore, the hydrodynamic area of coal between μ_1 and μ_2 is given by

$$S_{\mu_2-\mu_1} = \int_{\mu_1}^{\mu_2} \frac{k}{\mu\rho} \, dp \qquad (3)$$

or

$$S_{\mu_2-\mu_1} = 2.3 \int_{\mu_1}^{\mu_2} \frac{kp}{\mu\rho} \, d(\log p) \qquad (4)$$

From the experimental values, log p can be plotted against log μ; and p, μ, and log p may then be obtained for any value of μ. Since k and ρ are also known for this size, $kp/\rho\mu$ may be plotted against log p and S determined from the area under the curve.

Alternatively, if

$$\frac{d(\log p)}{d(\log \mu)} = n \qquad (5)$$

then

$$S_{\mu_2-\mu_1} = 2.3 \int_{\mu_1}^{\mu_2} \frac{kpn}{\mu\rho}\, d(\log\mu) \qquad (6)$$

This is somewhat more convenient as it allows a direct integration between any required sieve sizes. The values of n for any value of log μ are determined by taking the slope of the log p/log μ distribution plot at that point. Below sieve sizes of 200 microns, n was found to be constant.

Over the part of the distribution for which n is a constant

$$p = B\mu^n \qquad (7)$$

where n and B may be determined from the slopes and intercepts of the curve.

Now

$$S_{\mu_2-\mu_1} = \int_{\mu_1}^{\mu_2} \frac{k}{\mu\rho}\left(\frac{dp}{d\mu}\right) d\mu$$

(sq. meters when μ is in microns)

But from (7), $dp/d\mu = Bn\mu^{n-1}$.

Therefore,

$$S_{\mu_2-\mu_1} = \int_{\mu_1}^{\mu_2} \frac{kBn}{\rho}\mu^{n-2}\, d\mu$$

When k and ρ are constant,

$$S_{\mu_2-\mu_1} = \frac{kBn}{\rho(1-n)}\left[\frac{1}{\mu_1^{1-n}} - \frac{1}{\mu_2^{1-n}}\right] \qquad (8)$$

Kick's Law Calculations - Kick's Law may be expressed in the form (13)

$$E = C \ln\left(\frac{\mu_1}{\mu_2}\right) \qquad (9)$$

where E is the energy per unit weight required to reduce material of size μ_1 to size μ_2, and C is a constant for a given material and process. If material of size μ_1 is broken to a distribution of sizes, the energy required to produce a weight dp of material of size $\mu + d\mu$ is given by

$$dE = C \ln\left(\frac{\mu_1}{\mu}\right) dp \qquad (10)$$

Therefore, the total energy is given by

$$E = C \int_{p=0}^{p=100} \ln\left(\frac{\mu_1}{\mu}\right) dp \qquad (11)$$

It can readily be shown that when the energies required for various size reductions from the same starting material are to be compared, the precise value of μ_1 is not too important. Therefore, it was assumed that the 16 x 30 mesh starting material had a mean size μ_1 of 900 microns. Comparative values of E were obtained for various revolutions of grinding by plotting log $900/\mu$ against p (using the appropriate size distribution of the product) and integrating graphically. The areas were not significantly different when lower size limits of 1 or 0.1 micron were assumed.

RESULTS

Table 1 gives the analyses of the coals tested. Figure 1 shows the size weight distributions of coal B-19447, after correcting the results as described previously. The points in Figure 1 are very consistent and the distribution curves can be drawn with considerable precision. If the straight line portions of the curves are extrapolated and the values of n and B (see Equation 7) determined, then the results are again very consistent, as can be seen from Figure 2.

Table 2 gives the cumulative weight versus microscope size (and corresponding sieve size) calculated using Equation (2), expressed both as a percentage of the minus 325 mesh sample tested and as actual weight of the minus 325 sample. The weight loss on grinding (60 revolutions) and sieving was 0.66 g. per 100 g., and it was assumed that this loss was in the very fine material. It was added, therefore, to the cumulative weight down to 1.5 microns.

Figure 3 shows a complete sieve size-weight distribution for the coal tested, using a factor of 1.68 to convert microscope size to sieve size (11). It can be seen that over the range 3 to 300 microns, the distribution is a straight line on the log-log plot. This type of distribution has been noted previously (14,15,16) and extended below sieve sizes by air elutriation. Rosin and Rammler (17) used air elutriation to extend results to sub-sieve sizes and concluded that the distribution obeyed the Rosin-Rammler law. However, for small sieve sizes, the Rosin-Rammler distribution becomes the simple power distribution found in Figure 3. (In fact, a size distribution of broken coal (18) over a range of 0.004 to 5 inches which fits a Rosin-Rammler plot, also fits a log p-log μ plot over most of the same range). The departure of the curve from the straight line below three microns is almost certainly due to the assumption that all of the weight loss on grinding is less than 1.5 microns. The break in the curve suggests that the weight loss is in sizes of about three microns (sieve size) and less.

Figure 4 shows the surface areas of the ground coal fractions for coal B-19447 calculated using Equations (4), (5), and (8). The surface areas were

calculated assuming that the straight line part of the log p versus log μ distribution (Figure 3) could be extrapolated to a lower limit of 1, 0.1, or 0.01 micron. It was also assumed that the shape factor (a constant in the range from 40 to 600 microns (10)) was constant down to the lower size limit. It is clear that the lower size limit which is chosen considerably affects the absolute value of the surface area. The curve is a straight line when a lower size limit of about 1 micron is used. For the lower size limits of 0.1 and 0.01 micron, the area increases more with revolutions of grinding than Rittinger's Law would predict. Another feature of interest is that the extrapolation of the curves to zero revolutions gives an initial surface area of unground material of 1.2 $m.^2$/100 g. whereas the actual unground surface area is 0.8 $m.^2$/100 g. It appears that an initial small amount of grinding produces 0.4 $m.^2$ of surface area per 100 g. in addition to the 0.117 $m.^2$/100 g./revolution produced for the remainder of the grinding process.

Figure 5 shows the surface area change with grinding for coal B-17790, where a lower limit of 1 micron has been used. After an increase to about 16 $m.^2$/100 g., it appears that the increase in surface area is no longer proportional to the revolutions of grinding. Extrapolation of the straight line portion of the curve to zero revolutions again indicates an initial area of 1.2 $m.^2$/100 g. instead of the expected value of 0.8 $m.^2$/100 g.

Table 3 gives the surface areas from 1 micron to 1190 microns for the four coals ground according to the standard Hardgrove test and also gives the increase in surface areas on grinding. For coal B-19426 and the St. Nicholas anthracite, the results are based on measurements at 60 revolutions only; the cross plotting technique was not used as the data were not available.

Figure 6 gives the increase in E (Equation 11) with revolutions of grinding for coal B-19447. It can be seen that E is not proportional to revolutions of grinding over wide ranges of grinding. Therefore, Kick's Law does not appear to hold for grinding in accordance with the standard Hardgrove test.

DISCUSSION OF RESULTS

Rittinger's Law cannot in general be true, which can be seen if an extreme case is considered as follows. Let a grinding machine be grinding particles which have such strength that the grinding forces imparted by the machine do not exceed this strength. Work will be done without the production of fresh surface, but the material does not have an infinite strength, since a heavier machine would produce breakage. If no change of state of the material occurs, then the energy input is dissipated in a variety of ways. There will be the loss of energy as frictional slip over the surface of the ground material. Also, particularly for ball mills, forces will be transmitted through the material to deliver blows on the mill structure; and energy will be lost as heat of impact and impact waves. In both of these cases, the energy finally appears mainly as heat. In addition, when the ground material fractures, energy will be used to break force bonds across the fresh surface produced and to form internal cracks and flaws. Energy will also be liberated as heat of fracture.

The process of fracture may be loosely described in the following manner. When a particle of coal is crushed it must be raised to a strained state before it fractures. (This, in effect, is an activation energy for crushing). Energy is imparted by the grinding forces which are applied over distances corresponding to the deformation of the particle. The coal then breaks at a flaw

or series of flaws in the material, deformation is removed, and fracture waves propagate through the coal producing fresh surface (19). The excess energy of the fracture waves and the energy released on the relaxation of deformation appear eventually as heat of fracture.

From the above discussion it would appear unlikely that there would be a simple relation between the fresh surface produced and the total energy input to the grinding process; there are so many different ways in which the energy can be distributed. It seems plausible, however, to assume that under certain conditions the energy lost as frictional slip and impact is a fixed fraction of the total input. Fresh internal area does not seem to be produced; except, perhaps, in direct proportion to the external area (20). A fracture wave will propagate until it reaches a free surface and it will not end within the material. (Gross and Zimmerly (21) found that for quartz, internal area was broken out on grinding and impact crushing, rather than increased). Thus, if the energy used to produce fresh surface is a fixed proportion of the strain energy, which in turn is a fixed fraction of the total energy input, Rittinger's Law would hold. To investigate the surface to strain energy relation further, a distinction can be made between the "strength" of a coal and its "hardness". The strength is here arbitrarily defined as the strain energy required before a particle fractures (which is a function of the type of forces imparting this energy to the particle). The hardness is arbitrarily defined as the strength of surface bonds in the material. Clearly two particles may have the same composition and hence the same hardness but may have widely different strengths, if one is highly flawed and the other not.

Consider two such particles of similar "hardness" but different strengths. The stronger one will require the addition of more energy to fracture it, but it seems possible that on fracture it will break into many smaller pieces. On the other hand, the weaker particle will break more readily with a lower energy content but will break into fewer pieces with correspondingly lower fresh surface. Similarly, a large impulsive force of low energy application might cause breakage with small area production; whereas a smaller force applied for a much longer time and deformation would produce a larger surface area on eventual shatter. Thus it is possible that particles of entirely different strengths, and hence probabilities of breakage, have breakage functions which automatically compensate, so that the fraction of the strain energy which is used to produce fresh surface is constant. Bickle (22) states that this has been considered theoretically, but gives no reference to such studies. Such a concept would go part way toward explaining the validity of Rittinger's Law with progressive grinding, although the strength of coal particles is known to vary with size (23,24) and degree of grinding. This concept implies that grindability indices based on surface-area increase measure a parameter proportional to hardness rather than a combined effect of hardness and strength. It is interesting to see that there is a pronounced correlation between grindability indices and the Vickers Microhardness test (25).

As particles become smaller and stronger (in comparison to their size) on grinding due to the breaking out of flaws, they may eventually reach a stage where the crushing forces of the machine are insufficient to cause much breakage. Grinding experience indicates that it is extremely difficult to reduce anthracite below 0.1 to 1 micron in size in conventional grinding apparatus. It may be postulated that somewhere near this size range the major flaw structure of the coal has been completely broken out and that grinding is more difficult by an order of magnitude or more. Van Krevelen (26) states that Boddy found coal particles to be initially crushed to 1 micron in size. As the surface area of this material is of the same order as the macropore area of unground coal, Van Krevelen suggests that breakage to 1 micron is favored by the macropore system. For smaller particles, the coal tends to plastically deform rather than fracture;

this implies much greater strength and a low grindability. An alternative hypothesis is that agglomerates of fine particles tend to trap air and on grinding behave somewhat like miniature balloons. The crushing force is applied to the "balloon" and the energy is expended in compressing the contained gas. For grinding in liquid media, the fluid is incompressible and the forces are imparted to the coal particles; it is well known that liquid grinding can be used to produce very fine sizes.

In spite of the theoretical objections to Rittinger's Law, there is considerable evidence that under a restricted range of conditions the Law is closely obeyed. The correlation of the increase in surface area with grinding obtained in this work is not conclusive, since the lower size limit chosen for the integration to obtain surface area is rather arbitrary. Microscopic studies of the fine fractions of ground coal indicated that material below 1 micron in size was not present in large quantities, although there still remains the question of the fineness of the material making up the weight loss on grinding and sieving. From electron micrographs of ground coal, Preston and Cuckow (27) conclude that coals ground in the normal manner had few particles of less than about 1 micron in size. By taking a lower limit of 1 micron, it is not assumed that material less than 1 micron is absent but rather that 1 micron represents an effective lower limit for the straight line log p/log μ distribution extrapolated from the sieving results. The strict linearity, over a fairly wide range of grinding, of the results plotted in Figure 4 for the 1 micron lower limit would hardly occur by coincidence; and it must be concluded that the evidence for the accuracy of Rittinger's Law is quite strong.

Figure 7 shows the Hardgrove Grindability Indices of a number of British coals (15) and the four coals tested in this work, as a function of a rank index (10). It is clear that the grindability characteristics of a coal are closely allied to its rank. Although the British coals (because they are of one geological era) might be expected to form a fairly consistent pattern, the coals used in our experiments fit the mean line with as good an accuracy as the British coals. Deviations from the mean line are quite considerable in some instances, more than would be expected by experimental error of determination of C, H, or Hardgrove Index. This may be due to several causes:

a) The mineral matter of a coal might considerably influence its grindability.

b) Grindability, as measured by the Hardgrove Index, might not be an accurate representation of the grinding strength of the coal.

c) Differences in the amounts of macerals present in the coal might cause considerable change in strength.

d) The grindability might be influenced by factors which do not depend closely on rank, for example flaw structure.

At the moment, it is only possible to discuss cause (b) with knowledge obtained from our own results. Figure 8 shows the per cent by weight less than 200 mesh plotted against surface area for varying revolutions for coals B-19447 and B-17790. Clearly the increase in surface area is not related to p_{200} in the form of Equation (1). The surface area is not linearly proportional to p for coal B-17790, although a straight line could be drawn with a fair degree of accuracy.

Figure 9 shows p_{200} plotted against increase in surface area for the four coals ground for 60 standard revolutions, and it also shows the Hardgrove Index as a function of surface area increase. It can be seen that the Hardgrove Index is not proportional to the increase in surface area. (Surface areas used are

those calculated on the assumptions that the shape factor is constant over the range 1 to 1190 microns and that 1 micron is an effective lower limit; it has only been shown that the shape factor is constant over the range of 40 to 600 microns (10)).

From Figure 9 it can be seen that the increase in surface area is proportional to p_{200} only to a degree of accuracy of about ± 10%. This is of the same order as the deviations of Hardgrove Index values from the best fit curve in Figure 7, and it is possible that part of the deviations are caused by the Hard-Grove Index (which depends on p_{200}) not being an accurate representation of the increase in surface area. This is particularly likely to be true where a coal fractures to give products with an abnormal shape factor, for in this case two coals might have very similar size distributions on grinding but would have considerably different surface areas.

Callcott (28) argues that the increase in surface on grinding is of little significance in practical grinding studies. He analyzes the problem of grinding in the following manner: Given different sized feeds into a grinding machine, what will be the size distributions of the products? Or if different machines operate with different size feeds, how much of the difference in products is due to the different feed sizes and how much is due to differences caused by the machines? Callcott suggests using p as an index of grindability in preference to the Hardgrove Index (this was also suggested by Frisch and Holder (29)). He does not believe that the work on surface area increase during grinding justified the use of any index except a simple index of breakage defined by p. The significance of the grindability index p may be stated in these terms: If a certain coal produces 10 per cent of material below 200 mesh in the standard Hardgrove test and another coal produces 20 per cent, then it is likely that on grinding in an industrial mill, the first coal will have approximately half the throughput of minus 200 mesh material obtained with the second.

Thus, it would appear that p_{200} is a better index of grindability than the Hardgrove Index, both for the reasons given by Callcott and because it is a better index of surface area increase. The Hardgrove Index may be used instead of p_{200}, if it is borne in mind that a Hardgrove Index of 13 represents zero production of fresh surface. For scientific work it is recommended that the index used should be the increase in surface area per revolution of grinding (over the range in which linearity is obtained).

CONCLUSIONS

The log p versus log μ straight line portions of the distributions found for coals ground according to the Hardgrove test can be extrapolated to at least 3 microns sieve size. The weight loss on grinding appears to be mainly material of less than 3 microns sieve size.

For the two coals tested at varying revolutions of grinding, a negligible amount of grinding produced about 0.4 $m.^2/100$ g. of fresh geometric surface; but after this initial abnormal increase, the increase in surface area was proportional to the revolutions of grinding up to the condition of at least 20% of the material through a 200 mesh sieve. This was true when a lower limit of size of about 1 micron was used to calculate the surface area. Kick's Law did not apply. The percentage of material passing a 200 mesh sieve is very approximately proportional to the increase in surface area on grinding. More precise values of surface area increase per revolution of grinding will be obtained in future work, and these values compared to the rank of the coals used.

ACKNOWLEDGEMENTS

We wish to express appreciation to G.C. Williams and R.R. Luckie who assisted in the experimental program. We appreciate the financial support of the Coal Research Board of the Commonwealth of Pennsylvania which made this work possible. We express our gratitude to Messrs. R.M. Hardgrove and J.B. McIlroy of the Babcock and Wilcox Company for supplying coal samples and relevant analyses for our use.

REFERENCES

1. "Crushing and Grinding Bibliography", Department of Scientific and Industrial Research (London), H.M.S.O., 1958, p.1. See also pp. 159-183.
2. Bennet, J.G., and Brown, R.L., J. Inst. Fuel, 14, 135 (1941).
3. Callcott, T.G., ibid, 29, 524 (1956).
4. Sales, H., and Huttig, G.F., Tonind. Ztg. 186 (1954).
5. Anderson, Robert B, Hal, W. Keith, Lecky, James A., and Stein, Karl C., J. Phys. Chem., 60, 1548 (1956).
6. Hardgrove, R.M., Trans. Am. Inst. Chem. Engrs., 34, 131 (1938).
7. Romer, J.B., Proc. Am. Soc. Test. Mat., 41, 1152 (1941).
8. Carman, P.C., "Flow of Gases through Porous Media", Academic Press Inc., New York, 1956, p.36.
9. Am. Soc. Testing Materials Standard D409-51, Grindability of Coal by the Hardgrove Method.
10. Austin, L.G., Gardner, R.P., and Walker, P.L. Jr., The Geometric Area Shape Factors of Coals Ground in a Standard Hardgrove Mill, presented before the Gas and Fuel Division at the September, 1959 meeting of the American Chemical Society.
11. Austin, L.G., Gardner, R.P., and Walker, P.L. Jr., The Relation of Microscope Size to Sieve Size for Ground Coals, presented before the Gas and Fuel Division at the September, 1959 meeting of the American Chemical Society.
12. Heywood, H., "Chemical Engineering Practice", Vol. 3, Butterworth's Scientific Publications, 1957, p.40.
13. Walker, W.H., Lewis, W.K., McAdams, W.H. and Gilliland, E.R., "Principles of Chemical Engineering", McGraw-Hill Pub. Co., 3rd Edition, 1937, p.252.
14. Fuel Research Technical Paper 49, Dept. Sci. Ind. Research (Brit.) (1947).
15. Fitton, A., Hughes, T.H., and Hurley, T.F., J. Inst. Fuel (London), 30, 54 (1957).
16. Callcott, T.G., ibid, 29, 207 (1956).
17. Rosin, P. and Rammler, E., ibid, 7, 29 (1933).
18. Brown, R.L., Reference (1), p. 19.
19. Poncelet, E.F., Trans. Am. Inst. Mining Met. Engrs., 169, 37 (1946).
20. Johnson, J.F., Axelson, J.W., and Piret, E.L., Chem. Eng. Progr., 45, 708 (1949).
21. Gross, J. and Zimmerly, S.R., Trans. Am. Inst. Mining Met. Engrs., 87, 35 (1930).
22. Bickle, W.H., Reference (1), p.5.
23. Millard, D.J., Newman, P.C., and Phillips, J.W., Proc. Phys. Soc., 68B, 723 (1955).

REFERENCES
(contd.)

24. Gaddy, F.L., Bull. Va. Polyt. Inst., 49, Engng. Exp. Sta. Ser. 112 (1956).

25. Van Krevelen, D.W. and Schuyer, J., "Coal Science", Elsevier Publishing Co. 1957, p.274.

26. Ibid, p. 275.

27. Preston, G.D., and Cuckow, F.W., "Ultrafine Structure of Coals and Cokes", Brit. Coal Utilisation Research Assoc., 334 (1944).

28. Callcott, T.G., J. Inst. Fuel (London) 30, 466 (1957).

29. Frisch, M., and Holder, G.C., Combustion, June-July, 29 (1933).

TABLE I

ANALYSES OF COAL USED

Coal	B-19447	B-17790	B-19426	St. Nicholas Anthracite
Constituent	As used,%	As used,%	As used,%	As used,%
Moisture	1.5	0.8	0.5	1.6
Ash	16.5	7.8	14.5	9.3
Carbon	65.3(83.5)*	78.8(87.6)*	75.2(90.6)*	84.2(95.5)*
Hydrogen	4.7(5.9)*	4.8(5.1)*	3.9(4.5)*	2.4(2.2)*
Nitrogen	1.1	1.5	1.5	0.85
Sulfur	4.5	1.6	1.8	0.5
Oxygen (by difference)	6.2	4.7	2.6	1.1
Volatile Matter (D.A.F.)	42.4	29.2	17.9	4.5
Shape Factor (k)	9.6	8.0	7.2	9.3
Hardgrove Grindability Index	52	93	99	30

* Parr's basis

TABLE 3

HYDRODYNAMIC SURFACE AREAS OF COALS GROUND ACCORDING TO THE STANDARD HARDGROVE TEST

Coal	Hardgrove Grindability Index	Surface Area ground coal $m.^2/100$ g.	Increase in Surface Area $m.^2/100$ g.	Rank-Index of coal % C - 8.5 % H
B-19447	52	7.6	6.8	33.5
B-17790	93	15.9	15.1	44.2
B-19426	99	14.5	13.7	52.4
St. Nicholas anthracite	30	3.4	2.6	77.0

TABLE 2

SIZE DISTRIBUTION BELOW 325 MESH OF COAL B-19447 GROUND ACCORDING TO STANDARD HARDGROVE TEST

Microscope diameter, microns	Equivalent sieve size, microns	Cumulative % by weight of -325 fraction tested	Cumulative weight expressed as a % of total coal ground	Plus 0.66% weight loss of fine material on grinding
0	0	0	0	
0.7	0.4	0.0046	0.00035	
0.9	0.5	0.014	0.00104	
1.3	0.8	0.049	0.00356	
1.8	1.0	0.15	0.0108	
2.6	1.6	0.56	0.0408	(0.701)
3.5	2.1	1.24	0.090	(0.750)
4.4	2.6	2.18	0.16	(0.819)
5.8	3.5	3.67	0.27	0.927
7.3	4.3	6.00	0.44	1.10
8.8	5.2	8.51	0.62	1.28
10.2	6.1	9.90	0.72	1.38
13.1	7.8	14.7	1.07	1.73
21.0	12.5	29.2	2.12	2.78
26.2	15.6	36.1	2.62	3.28
35.0	20.8	44.9	3.26	3.92
43.6	26.0	56.0	4.07	4.73
52.5	31.0	70.6	5.14	5.80
61.0	36.4	83.8	6.10	6.76
70.0	41.6	93.7	6.82	7.48
78.6	47.0	100.0	7.28	7.94

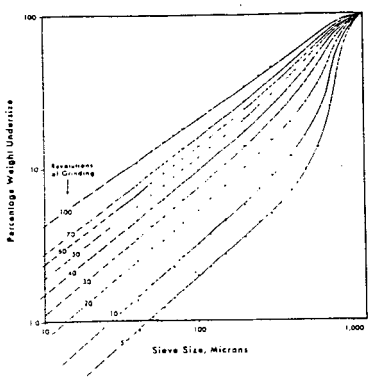

CORRECTED PERCENTAGE WEIGHT UNDERSIZE VERSUS SIEVE SIZE DISTRIBUTIONS FOR COAL B-19447

Figure 1

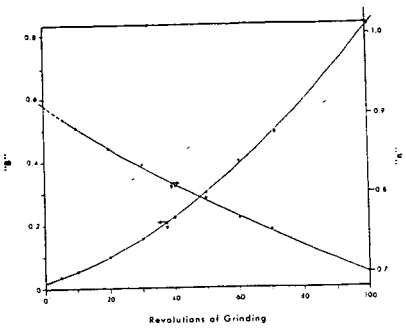

VALUES OF "n" AND "B" IN $p = B\mu^n$ FOR COAL B-19447 GROUND FOR VARYING REVOLUTIONS

Figure 2

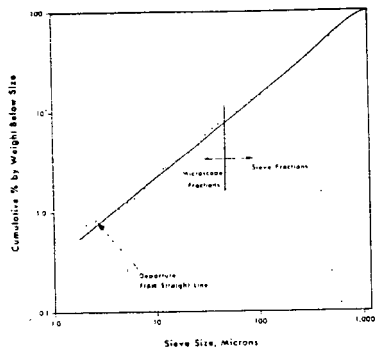

EXTENDED PERCENT WEIGHT UNDERSIZE VERSUS SIEVE SIZE DISTRIBUTION FOR COAL B-19447 GROUND FOR 60 REVOLUTIONS

Figure 3

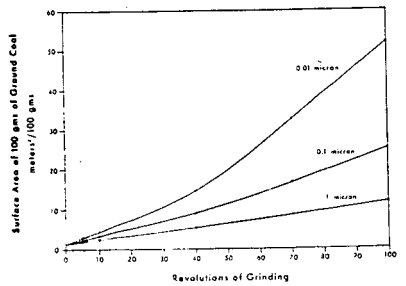

INCREASE OF HYDRODYNAMIC SURFACE AREA OF GROUND COAL WITH REVOLUTIONS OF GRINDING FOR COAL B-19447, ASSUMING 1, 0.1 AND 0.01 MICRONS AS THE SMALLEST SIZE PRESENT

Figure 4

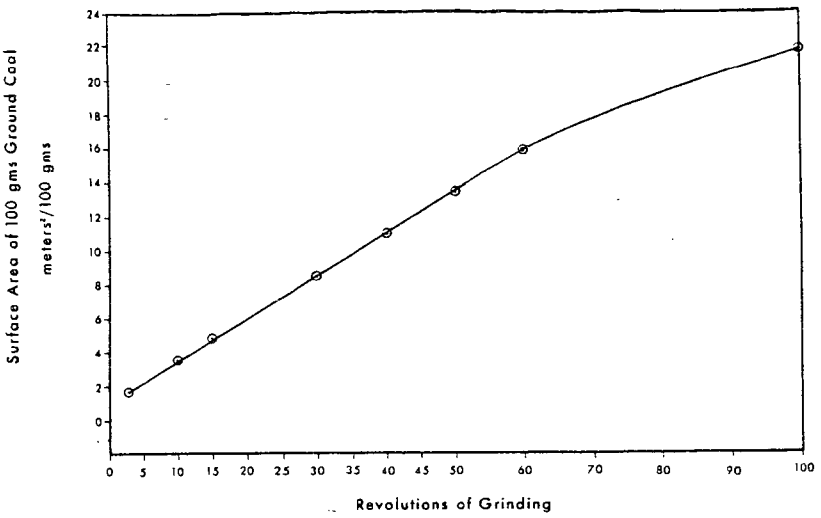

INCREASE OF HYDRODYNAMIC SURFACE AREA OF GROUND COAL WITH REVOLUTIONS OF GRINDING FOR COAL B-17790, ASSUMING 1 MICRON AS LOWER LIMIT

Figure 5

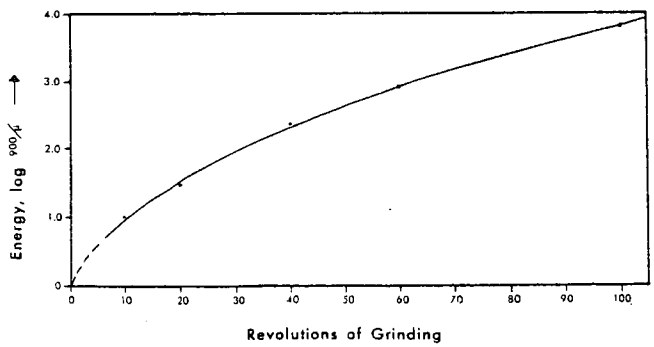

RELATION OF ENERGY FOR GRINDING PREDICTED BY KICK'S LAW TO REVOLUTIONS OF GRINDING (COAL B-19447)

Figure 6

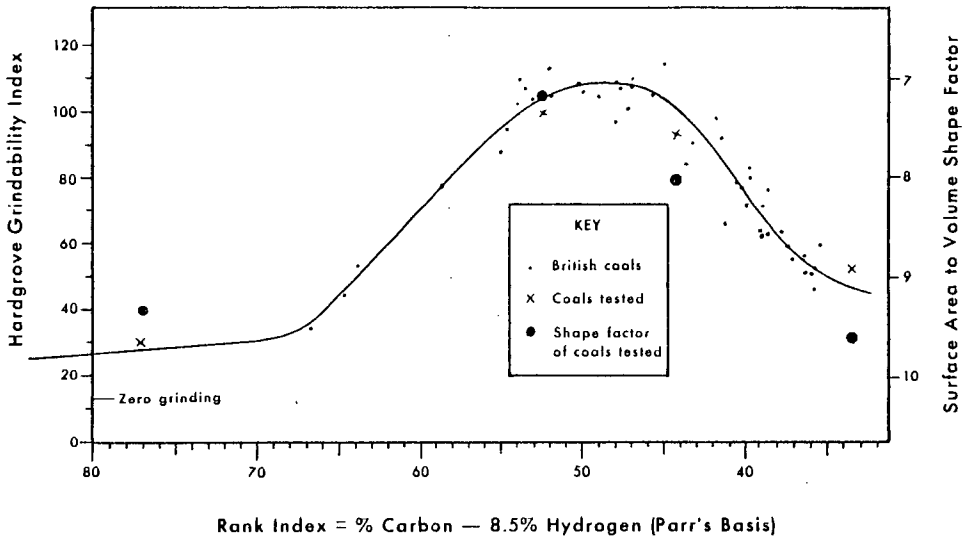

Fig. 7. GRINDABILITY INDEX AND SHAPE FACTOR AS A FUNCTION OF COAL RANK.

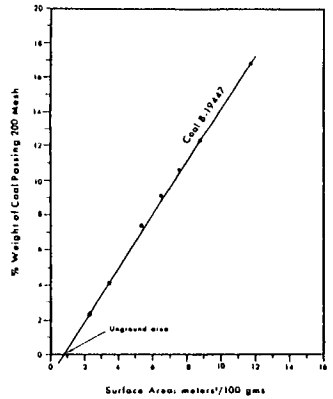

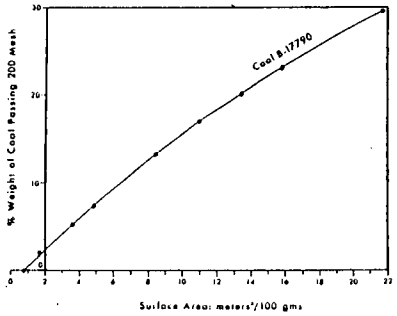

RELATION OF SURFACE AREA TO PERCENT WEIGHT THROUGH 200 MESH
FOR VARYING REVOLUTIONS OF GRINDING IN THE HARDGROVE MACHINE

Figure 8

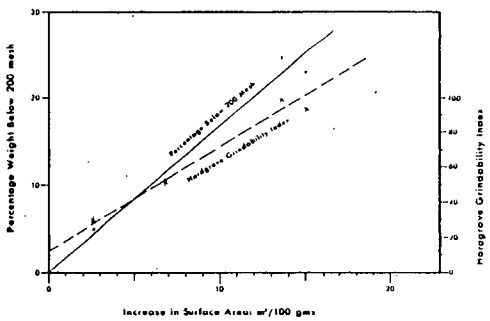

INCREASE IN SURFACE AREA ON GRINDING
ACCORDING TO STANDARD HARDGROVE TEST
AS A FUNCTION OF % WEIGHT THROUGH 200 MESH

Figure 9

Not for Publication
Presented Before the Division of Gas and Fuel Chemistry
American Chemical Society
Atlantic City, New Jersey, Meeting, September 13-18, 1959

Irradiation Studies on Coal and Its By-Products

I. Effect of Radiation and Oxygen at Ambient Temperatures on the Subsequent Plasticity of Bituminous Coals

Frank Rusinko, Jr., Allan Weinstein, and P.L. Walker, Jr.
Fuel Technology Department, The Pennsylvania State University
University Park, Pennsylvania

INTRODUCTION

The effect of radiation on materials is a subject which currently is receiving much attention. Such studies are important because of the changes induced in most materials when they are exposed to radiation. Changes may occur by many mechanisms, such as displacement of atoms caused by energy absorption from incident particles, ionization followed by bond breaking, and formation of free radicals. Studies of the radiation effects in solids indicate that the use of radiation can be a powerful tool for increasing the understanding of the nature of solids.

Organic-type materials, owing to a predominance of convalent bonds or weak van der Waals forces, are more severely changed or degraded than other solids. Changes that may take place in materials are hydrogenation, dehydrogenation, polymerization, cracking, decomposition, and cross-linking, with the degree of change depending upon the type of radiation, incident rate of radiation, extent of radiation time, chemical composition of material, initial state of material, and environment.

Since it is known that gamma radiation can either upgrade or degrade organic materials, a study of the possible effects of gamma radiation on changing the fluidity of bituminous coal is a logical step. For example, a decrease in fluidity for coals high in fluidity would be advantageous, probably resulting in an increase in coke yield and coke strength. On the other hand, an increase in fluidity for coals low in fluidity could result in their becoming satisfactory sources of coke.

EXPERIMENTAL

Coal Samples Used - Eight Pennsylvania bituminous coals were selected for study. Proximate and ultimate analyses of the coals are presented in Tables I and II.

Coal Preparation - The coals were ground to -40 mesh and stored under a nitrogen atmosphere until required for radiation studies. Approximately 50 grams of each coal were placed in quartz or Pyrex containers (4 in. long x 1-1/4 in. inside diameter) and sealed under each of the following conditions:

1. Vacuum - the samples were evacuated until the pressure was less than 10μ Hg and then sealed. The amount of oxygen available to the coal was ca. 2×10^{-6} cc./g.

2. Air - the samples were sealed immediately; these containers held air initially at atmospheric pressure. The amount of oxygen available to the coal was ca. 0.2 cc./g.

3. Oxygen - the samples were evacuated until the pressure was less than 10μ Hg. Oxygen was dosed into the container until the final oxygen pressure was approximately 700 mm. Hg, with the amount of oxygen adsorbed by the coal measured. The containers were then sealed. The amount of oxygen available to the coal was ca. 1.1 cc./g.

Radiation Studies - For radiation studies, the sealed samples were placed in a 40 mil thick cadmium container. Cadmium was used to decrease the slow neutron flux to a relatively low level, since it was desired to irradiate the coals primarily with gamma radiation. The cadmium container with 5 coal samples was lowered down a 3 in. diameter aluminum tube and positioned in the University nuclear reactor. The reactor, which can be classified as a light water cooled, light water moderated heterogeneous type, had its fuel elements located approximately 20 feet under water. Irradiation to a total dosage of 3.8×10^8 rads (requiring about 17 hours) was then carried out at ambient temperatures*. Approximately 90 per cent of the energy absorbed by the coal came from gamma rays and 10 per cent came from fast neutrons.

Gas Analysis - Analysis of the gas in the container following irradiation of the coals was made using gas chromatography. After releasing the gas from the container to the gas analysis system of the chromatographic unit, the gas was dried and its volume measured. The gas analysis was performed using either a 15-ft. #5A molecular sieve column with argon as a carrier gas or a 6-ft. silica gel column using helium as a carrier gas.

Plasticity Measurements - The conventional Gieseler apparatus, modified with auxiliary equipment for better temperature control and more accurate measurement of high fluidity values, was used to determine plastic properties of the coals. The tests essentially were made using the A.S.T.M. Proposed Method of Test (1). However, contrary to recommended procedures, the brake was not applied when the dial divisions exceeded 5 divisions per minute. Instead, the stirrer was allowed to move continuously until it travelled at least 600 dial divisions. For those coals where the stirrer moved more than 600 dial divisions, the brake was then used according to the Proposed Method of Test (1). This procedure was adopted in an attempt to break up the frothy coal mass which formed (and which would go up into the barrel of the Gieseler apparatus and cause sticking) when testing a highly fluid and highly swelling coal.

RESULTS AND DISCUSSION

Analyses of Gases Evolved From the Coals During Irradiation - Table III presents data on the total amount and analysis of the gas evolved from the coals following irradiation in vacuum and oxygen; values for the individual gases are accurate to ±5%. With the present chromatography apparatus, it was not possible to determine water vapor; the gas analyses, therefore, are reported on a dry basis. Other gases, such as ammonia and the oxides of nitrogen

* During the irradiations, it is estimated that the temperature in the coal containers did not exceed 40°C.

which may be formed during the irradiation, were not analyzed for in the present work. Gas analyses have not been reported for the coals irradiated in an air atmosphere because the nitrogen formed following irradiation was a composite of that released from the coal and that added initially in the air. That is, it was not possible to put the results on a basis of gas released from the coal since there was some uncertainty as to the volume of the sample container upon sealing, and hence, uncertainty as to the amount of nitrogen added initially. On the other hand, on the basis of vacuum-irradiation results, no free oxygen was released from the coals. Hence, in the oxygen-irradiation runs (there was oxygen found in the gas following irradiation for three of the coals), the amount of gas released from the coal could be calculated by placing the analyses on an oxygen-free basis.

It is seen from Table III that the amount of gas released from the coals on irradiation at ambient temperatures was quite small in comparison to the total volatile matter content of the coals. More gas was released consistently from the coal upon oxygen irradiation than upon vacuum irradiation, with the ratio of the gas-release volumes ranging from 1.8 to 5.0.

The presence of an oxygen atmosphere during irradiation is seen to have a marked (but not consistent) effect on the analysis of the released gas. As expected, the amount of carbon dioxide and carbon monoxide produced was greatly increased upon oxygen irradiation. The following reactions can be responsible for the increase in the amount of these two gases:

$$O_2 \rightsquigarrow O + O$$
$$C_f + O \rightarrow C(O)$$
$$C(O) \rightarrow CO$$
$$CO + O + M \rightarrow CO_2 + M$$
$$O_2 + O + M \rightarrow O_3 + M$$
$$C_f + O_3 \rightarrow CO + O_2$$

It is noted that a significant amount of carbon dioxide was also released from the coal during vacuum irradiation. It is suggested that this carbon dioxide was a result of decarboxylation of peripheral carboxyl groups on the coal (2,3), release of occluded carbon dioxide from the fine pore system, and/or oxidation of methane (for oxygen irradiation). The second possibility will be considered in more detail shortly.

The effect of radiation and atmosphere on the release of hydrogen from the coals is complex. For coals 167 and 169, release of hydrogen upon vacuum irradiation was negligible. On the other hand, oxygen irradiation of these two coals resulted in a substantial release of hydrogen. For the remainder of the coals, except 166, there was still a somewhat greater amount of hydrogen released upon irradiation in oxygen than in vacuum. For the low volatile coal, 166, the amount of hydrogen released upon either irradiation in vacuum or oxygen was essentially identical.

The effect of radiation and atmosphere on the release of nitrogen from the coals is also complex. For coal 169, the amount of nitrogen released upon oxygen irradiation was appreciably less than that released upon vacuum irradiation. On the other hand, for the other seven coals, oxygen irradiation resulted in the release of considerably more nitrogen than did vacuum irradiation.

From Table III, it is seen that the quantities of methane and ethane produced upon irradiation are very small. Again the results are complex. For methane, oxygen irradiation resulted in increased yields for coals 167, 169, A, and B and decreased yields for the other four coals. For ethane, oxygen irradiation resulted in an increased yield for coal B and a decreased yield for coals 166, 168, 169, C, and D.

Only in the case of coals 166, 167, and 168 was there any residual oxygen present after oxygen irradiation. For these three coals, 37, 11, and 22%, respectively, of the oxygen initially present (approximately 1.2 cc./g. of coal at S.T.P.) was recovered as oxygen following irradiation. This suggests that these coals were especially resistant to oxygen attack (also suggested from plasticity data to be presented later). Considering the large decrease in oxygen pressure during irradiation, the oxygen appearing as carbon dioxide and carbon monoxide in the product gas was small.

At this stage, the effect of the combination of radiation and oxygen atmosphere on the amount of the different gases released from the various coals is not well understood. However, the nitrogen results perhaps permit some understanding. Essentially, the nitrogen could come from three sources - peripheral amino groups, cyclic structures, and occluded nitrogen (4). Radiation, perhaps, would detach peripheral amino groups from the coal structure (the abundance of these groups in coal is small), these groups then reacting with hydrogen atoms to produce ammonia (2). However, in other irradiation studies, as yet unpublished, the authors have found pure ammonia to be quite stable to the radiation used in this research. For example, for a dosage of 10^8 rads, only ca. 0.4 per cent of ammonia (at pressures between 0.1 and 1 atm.) decomposed to hydrogen and nitrogen. Numerous workers (5) have shown that nitrogen present in cyclic groups in coal is largely resistant to removal by oxidation. Therefore, it would appear that the large increase in nitrogen-release from seven of the coals upon oxygen irradiation, in comparison to vacuum irradiation, cannot be explained on the basis of nitrogen-release from cyclic structures.

It seems more reasonable to attribute the majority of the nitrogen coming from the coals to occluded nitrogen. That is, coal is known to be permeated with molecular sized pores (6) which can trap gases. Vacuum irradiation could result in the release of nitrogen from these pores by two mechanisms. First, radiation could produce a small steady-state concentration of nitrogen atoms, which because of their smaller size, could migrate through the molecular openings more rapidly. Second, radiation could increase the magnitude of oscillations of some of the atoms in the coal around the molecular openings, because of their collison with fast neutrons. This increase in magnitude of oscillation would permit a more rapid transport of gas through the molecular openings (7). Oxygen irradiation of coal could result in the release of more nitrogen than that released during vacuum irradiation, since slight oxidation of coal is known to significantly increase the size of the molecular openings (8).

It is of interest to report some results lending support to the suggestion that radiation did enhance the removal of occluded gas from the pores of the coal. Prior to the filling of the quartz containers with oxygen for irradiation studies, the free space of the containers (with coal present) was determined using helium at room temperature for seven of the coals. Following the determination of free space and before filling the containers with oxygen, the coals were outgassed at room temperature to a pressure of

less than 10u Hg for 4 to 6 hours. Despite this outgassing, helium was found in the product gas following irradiation for three of the coals - the amount ranging from a trace for coal 168 to 0.05 cc./g. for coal B. In the case of coal B, the helium constituted ca. 16 per cent of the dry, product gas.

In the light of the conclusions for the source of most of the nitrogen, it is also probable that some of the carbon dioxide (in the vacuum irradiation) and hydrogen released from the coals was originally present as occluded gas.

Whether irradiation in oxygen, rather than in vacuum, is expected to decrease or increase the amount of methane and ethane released is difficult to predict. While enlargement of molecular sized openings during irradiation in oxygen could enhance the release of these hydrocarbons, their radiation-induced oxidation to carbon dioxide and water would decrease their concentration in the released gas. Both effects appear to be operative to varying extents depending upon the coal, as judged from the data in Table III.

Plasticity of Heated Coals Following Irradiation - Gieseler plasticity data were determined on the unirradiated and irradiated coals. At least three plasticity runs were performed on each sample of coal, with the over-all precision being ca. ±15 per cent. The plasticity data are presented in Table IV and Figure 1. Where more than one result is presented for a coal, duplicate irradiations have been performed.

The results clearly show that irradiation in vacuum or in a substantial partial pressure of oxygen can have a marked effect on the subsequent maximum fluidity of heated bituminous coals. Irradiation in the presence of a substantial partial pressure of oxygen generally had more effect on plasticity than did irradiation in vacuum. For six of the coals, vacuum irradiation had a relatively small effect on fluidity. The exceptions were coals A and B, where irradiation reduced maximum fluidities by ca. 50 per cent.

For six of the coals, air irradiation resulted in a significant (and in some cases very large) increase in maximum fluidity. For two of the coals (a low volatile coal and one of the high volatile A coals which showed a significant decrease in fluidity after vacuum irradiation), air irradiation had a negligible effect on fluidity.

The effect of oxygen irradiation on the fluidity of the coals was more varied. For five of the six high volatile A coals, oxygen irradiation substantially lowered the fluidity below that of the corresponding unirradiated coals. For high volatile A coal 168 and the medium volatile coal, oxygen irradiation increased the maximum fluidity over that of the unirradiated coals. Oxygen irradiation had a negligible effect on the fluidity of the low volatile coal.

It is of interest that major changes in fluidity upon irradiation were not accompanied by large changes in the temperatures at which the maximum fluidity occurred. As a typical example, consider coal A. The unirradiated coal had a maximum fluidity of 397 d.d.p.m. at 422°C. The maximum fluidity of the sample irradiated in air was increased markedly to 3566 d.d.p.m., but the temperature of maximum fluidity remained at 422°C.

The effect of pre-oxidation of coal at elevated temperatures and in the absence of radiation on the subsequent coking qualities of coal has

been widely discussed. Many workers (9-14) report that the fluidity of coal, as measured by the Gieseler plastometer, decreases following pre-oxidation. To the authors' knowledge, no published results are available which report that pre-oxidation in the absence of radiation increases the fluidity of coal. However, on the basis of the present results, mild oxidation (that is, with a limited amount of oxygen available to react with coal) promoted by radiation can increase markedly the maximum fluidity of some coals. Whether the same effects can be achieved (and as precisely) by mild oxidation in the absence of radiation will be investigated on the same coals as used in this work.

Work is also being continued in this area directed toward studying the effect of prior irradiation of coal on the nature of the coke and by-products produced upon carbonization. In addition, it is desired to understand the relationships between the chemical and physical properties of coals and the effect of radiation and atmosphere on their subsequent carbonization behavior. As expected, it is not possible on the basis of simple proximate or ultimate analyses to predict these effects.

CONCLUSIONS

The effect of radiation on evolved gas composition and plastic properties of coal is found to vary with the coal being investigated and irradiation atmosphere. Lower rank coals appear to be more affected by the combination of radiation and oxygen atmosphere than do higher rank coals.

By proper selection of atmosphere, together with radiation, the fluidity of coals can be altered to marked extents.

ACKNOWLEDGEMENTS

We would like to express appreciation to G.C. Williams for performing most of the Gieseler determinations. We appreciate the financial support of the Coal Research Board of the Commonwealth of Pennsylvania which made this work possible.

REFERENCES

1. A.S.T.M. Standards on Coal and Coke, Appendix III, p.129, 1954.

2. Breger, C.A., J. Phys. and Colloid Chem., 52, 551 (1948).

3. Tolbert, B.M. and Lemmon, R.M., U.S. Atomic Energy Commission Report UCRL-2704 (1954).

4. Stutzer, Otto and Noe, Adolph C., "Geology of Coal", The Univ. of Chicago Press, Chicago, 1940, p.25.

5. Lowry, H.H., "Chemistry of Coal Utilization", John Wiley & Sons, Inc., New York, 1945, p.478.

6. Anderson, Robert B., Hall, W. Keith, Lecky, James A., and Stein, Karl C., J. Phys. Chem., 60, 1548 (1956).

7. Breck, D.W. and Smith, J.V., Sci. Amer., 200, No. 1, 85 (1959).

8. Walker, P.L. Jr., unpublished results.

9. Rees, O.W., Pierron, E.D. and Bursack, K.F., Illinois State Acad. Sci., 47, 97 (1955).

10. Davis, J.D., Reynolds, D.A., Brewer, R.E. Naugle, B.W. and Wolfson, D.E., U.S. Bur. Mines, Technical Paper No. 702, (1947).

11. Wildenstein, R., Chaleur and ind., 34, 233 (1953). C.A. 47, 12788d, (1953).

12. Lambris, G. and Gerdes, J., Brennstoff-Chem., 22, 125 (1941).

13. Gillings, D.W. and Lawson, W., J. Inst. Fuel, 30, 446 (1957).

14. Inouye, K., Bull. Chem. Soc. Japan, 26, 157 (1953).

TABLE I

PROXIMATE ANALYSES (AIR-DRY BASIS) OF COALS USED

Coal	% Moisture	% V.M.	% C.	% Ash	A.S.T.M. Rank
166	0.9	16.2	73.6	9.3	Low Volatile
167	1.0	26.9	62.1	10.0	Medium Volatile
168	0.6	28.9	61.2	9.3	High Volatile A
169	1.9	38.4	51.9	7.8	High Volatile A
A	2.3	38.1	53.1	6.5	High Volatile A
B	1.8	36.7	55.6	5.9	High Volatile A
C	1.8	36.8	55.2	6.2	High Volatile A
D	1.3	38.2	53.4	5.7	High Volatile A

TABLE II

ULTIMATE ANALYSES OF COALS USED*

Coal	% N	% S	% H	% C	% O	% Ash
166	1.06	1.33	3.80	80.59	5.20	8.02
167	0.92	2.30	4.73	77.86	4.81	9.38
168	0.90	1.73	4.83	78.72	4.50	9.32
169	1.45	1.64	5.07	75.98	7.69	8.17

* Ultimate analyses of Coals A, B, C, and D are not available, as yet.

TABLE III

ANALYSES OF GAS EVOLVED FROM COAL (DRY BASIS) UPON IRRADIATION TO 3.8×10^8 RADS IN VACUUM AND OXYGEN

Coal	Volume of Gas Released cc./g. of coal, S.T.P.	Gas Composition - Per Cent					
		H_2	N_2	CO_2	CO	CH_4	C_2H_6
166-Vacuum	0.048	36.2	7.2	54.8	T	1.5	0.3
166-Oxygen	0.192	8.9	53.2	31.3	6.3	0.3	T
167-V	0.034	0.2	68.9	30.2	T	0.7	0.0
167-O	0.168	26.9	43.5	24.9	4.3	0.5	T
168-V	0.036	50.4	25.7	19.0	T	3.6	1.4
168-O	0.132	26.1	47.0	20.9	5.5	0.6	T
169-V	0.050	0.1	47.0	45.4	1.4	1.0	5.1
169-O	0.148	66.0	3.9	22.3	6.4	1.4	0.2
A-V	0.144	71.4	9.1	16.4	1.8	1.4	T
A-O	0.264	56.5	13.2	24.2	5.0	1.1	T
B-V	0.112	71.4	10.7	14.5	1.3	1.6	0.5
B-O	0.236	53.8	17.2	21.7	5.7	1.2	0.5
C-V	0.064	67.3	11.8	9.0	0.6	10.5	0.8
C-O	0.164	39.3	29.9	22.5	7.6	0.7	0.0
D-V	0.114	76.8	1.9	11.5	1.0	5.6	3.2
D-O	0.314	48.1	29.6	16.3	4.8	0.9	0.3

TABLE IV

EFFECT OF A RADIATION DOSAGE OF 3.8×10^8 RADS AND OXYGEN AT AMBIENT TEMPERATURES ON THE SUBSEQUENT MAXIMUM FLUIDITY OF BITUMINOUS COALS AS DETERMINED BY THE GIESELER APPARATUS

Coal	Initial Softening[1] Temp. °C.	Maximum Fluidity D.D.P.M.[2]	Maximum Fluidity °C.[3]	Solidification Temp.[4] °C.
166	433	1.4	472	494
166-Vacuum	423	1.2	454	488
166-Air	425	1.3	450	472
166-Oxygen	435	0.6	464	499
167	365	451	425	457
167-V	353	610	432	472
167-A	350	822	426	450
167-A	364	935	429	463
167-O	367	1117	440	490
168	347	2767	432	479
168-V	338	2530	427	452
168-V	354	1911	428	481
168-A	339	3936	428	458
168-A	345	3860	428	472
168-O	356	3651	439	489
169	342	1139	424	458
169-V	357	1016	431	468
169-V	337	900	426	460
169-A	337	3193	429	462
169-A	344	3029	427	465
169-O	370	222	436	467
A	348	397	422	457
A-V	347	177	424	458
A-V	350	190	428	458
A-A	344	3566	422	454
A-O	373	124	430	450
B	347	1583	430	462
B-V	351	853	429	461
B-A	349	1484	434	464
B-O	372	701	434	459
C	345	5098	434	470
C-V	347	5207	426	468
C-A	342	6878	423	465
C-O	356	2788	438	475

TABLE IV. (Contd)

Coal	Initial Softening Temp.[1] °C.	Maximum Fluidity D.D.P.M.[2]	Maximum Fluidity °C.[3]	Solidification Temp.[4] °C.
B	345	1778	421	460
D-V	340	1850	422	451
D-A	344	3461	423	456
D-O	356	1083	430	467

1 Temperature of first detectable continuous movement of pointer

2 Dial divisions per minute on the Gieseler scale

3 Temperature of maximum fluidity corresponding to maximum rate of pointer movement

4 Temperature at which pointer shows no further movement

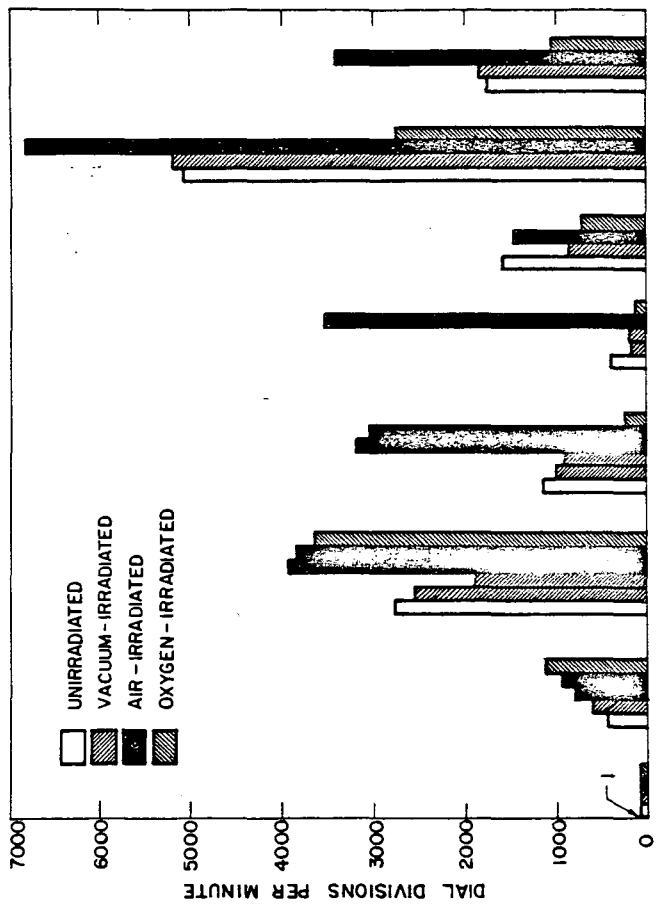

FIGURE 1 - EFFECT OF A RADIATION DOSAGE OF 3.8×10^8 RADS AND OXYGEN AT AMBIENT TEMPERATURES ON THE SUBSEQUENT MAXIMUM FLUIDITY OF BITUMINOUS COALS AS DETERMINED BY THE GIESELER APPARATUS.

Not For Publication

Presented before the Division of Gas and Fuel Chemistry
American Chemical Society
Atlantic City, New Jersey, Meeting, Sept. 13-18, 1959

Effect of Gamma Radiation Upon the Hydrocracking of a Heavy Paraffin

Work done at Columbia University, New York City 27, N.Y.

Present Address of Authors:

Ernest J. Henley, Stevens Institute, Hoboken, New Jersey
Ronald V. Repetti, Wright Patterson Air Force Base,
Dayton, Ohio

Introduction

Although a great deal of work dealing with the effect of ionizing radiation on hydrocarbons at low temperatures has been reported, very little has been published regarding the behavior of these systems at elevated temperatures and pressures. It has been well established that at room temperature pure hydrocarbons ultimately cross link and form insoluble gels (1,2). Recent work has shown that at elevated temperatures the reverse process seems to occur; i.e. degradation of the hydrocarbon molecules (3). If the latter findings are correct, radiation may then be regarded as a potential tool for those industries that customarily employ high temperatures, high pressures, and catalysts, to initiate reactions. An obvious application would be in the gasification processes where coal, waxes, and petroleum stocks are hydrocracked to natural gas substitutes. It was with this potential use in mind that the present investigation was undertaken.

Apparatus -

All runs were conducted in a static system. The reactor, was a type 303 stainless steel pressure vessel rated at 15,000 psia when cold and about 8,000 psia when at working temperatures. A lipless pyrex test tube served as a vessel liner and as a container for the wax samples. The capacity of the reactor with liner was 90 ml., and the entire system (reactor, liner, piping, etc.) had a capacity of 108 ml. Temperature in the autoclave was measured with a copper-constantan thermocouple whose junction was located about one third of the distance up the inside of the reactor. A gage was used whose

nominal pressure reading extended to 5,000 psi. Before using the gage it was calibrated with a dead-weight gage over the range of 200 to 3,000 psia, and was set to read true absolute pressure at 1,500 psia. The maximum deviation over the calibrated range was 20 psia. A blowout disc rated at 4,200 psia was incorporated in the system as a safety precaution. A 750 watt hollow cylindrical heater was employed that afforded a 1/4 in. air bath all around the reactor. Temperature within the reactor was maintained within ± 10°F of the desired level.

The Co^{60} radioisotope used has a half-life of 5.26 years and emits gamma rays of 1.17 and 1.33 m.e.v. per disintegration. The radiation facility is in the form of a pit, 20 in. x 20 in. square and 40 in. deep below ground level, into which a bundle of four 12 in. x 2 in. x 1/8 in. Co^{60} bars can be lowered. In situ dosimetry was accomplished with the Fricke dosimeter. The dose rate was 46,000 R/hr.

Two analytical systems were used, one for gaseous and one for solid products. The small amount of liquid residue produced in some runs was not analyzed. The gaseous products were analyzed with a Perkin-Elmer Model 154 Vapor Fractometer. A combination of packed columns was used that made possible the quantitative analysis of mixtures of hydrogen, nitrogen, argon, and hydrocarbons from C_1 to C_5. A Leeds and Northrup Speedomax Recorder was used in combination with the fractometer. The Perkin-Elmer Company claims for its instrument an analytical reproducibility of ±0.25% and an accuracy of ± 1-2%, both figures being absolute percentages. The actual experimental reproducibility was found to be ± 0.5%.

For those runs where a solid wax residue remained, the wax was examined for evidence of physical change by taking the melting point of the sample. The equipment used was a scaled-down version of the ASTM D87-42 apparatus for the determination of paraffin wax melting points (4). An ASTM 14F paraffin melting point thermometer having a range of 100-180°F and a maximum scale error of 0.2°F was used in the apparatus. In order to check the results obtained by the melting point method, several wax samples were examined for evidence of change by running them, and corresponding control samples, in a standard Beckmann boiling point elevation apparatus. Toluene was chosen as the solvent for these analyses.

Procedure - Experimental

A large quantity of paraffin wax was melted in a 1000 ml. Erlenmeyer flask and while molten, about twenty ml. was poured into each of thirty clean, lipless, pyrex test tubes that had previously been numbered and tared. The samples were then carefully degassed under vacuum. The wax was purchased from the Fisher Scientific Company and had a melting point of 126°F. From a published correlation between melting point and molecular weight (5), it was possible to estimate the molecular weight of this straight chain paraffin to be about 345.

Before charging, the reactor was cleaned thoroughly with a wire brush and then it and all other parts of the system were flushed with acetone. The reactor was then pressure tested, the sample was inserted, and then the system was thoroughly sparged with nitrogen.

To make a run the system was inserted in its heating jacket and the power was turned on. The duration of the initial heating period varied between 30 and 50 minutes, the latter duration being necessary to reach 900°F. The automatic temperature controller then maintained the temperature level to within ± 10°F of the desired setting. At the conclusion of a run the final temperature and pressure were recorded and the reactor was withdrawn from the heater and allowed to cool. About three hours were required for the reactor to cool from 900°F to ambient tem perature.

The gas analysis was complicated by the fact that due to a small amount of liquid present after each run, there existed an equilibrium between the gaseous and the liquid products, hence the composition of the gas is a function of the number of samples taken. Figure 1 shows the variation of product composition with reactor sampling pressure. This difficulty was circumvented in most of the analyses by obtaining, with a syringe, a 50 ml gas sample at a reactor pressure of 500 ± 5 psia and another at 200 ± 5 psia. In this way several analyses of a gas sample could be made in order to determine the reproducibility of the analysis, and it would also be possible to compare the product composition of different runs, provided that they were compared for the same sampling pressure. Toward the end of this investigation a small gas cylinder of 857 ml. capacity became available, and by using it as a reservior into which all of the reactor gas was bled, it

was possible to isolate virtually all of the product gas from the liquid residue in the reactor, and thus arrive at a composition for the total amount of gas produced.

Discussion of Results

Figure 2 shows a plot of reactor temperature vs. pressure as suggested by Shultz and Linden (6). The graph clearly shows that until about 860°F is reached, nothing happens other than heating of the gas in the reactor. At 860°F cracking begins, and because of the additional gas formed, the pressure begins to rise rapidly. The maximum duration of a cracking run was only 5 hours which was not sufficient to attain equilibrium. Figure 2 shows a typical plot of pressure vs. time for a run in progress. Because of the nearly constant rate for run times exceeding 3 hours, no attempt was made to obtain data for very long durations. Instead, runs of 2, 3, 5, and 5 hour duration were made, with the greatest number of duplicate runs at 2 hours. Figure 3 shows typical product spectra for the cracking runs. It is readily seen that the products are almost identical for radiation and for non-radiation runs. This tends to indicate that the same type reaction prevails for both processes, and that if radiation has any influence, it serves merely as an accelerator.

From the experimental data a value of S, designated as the moles of gas formed per gram of wax initially present, was computed for each run. In computing S it was necessary to know n, the number of moles formed during the reaction. Accordingly, a correction factor z was introduced so that at 900°F, the expression $PV = z(nRT)$ would be valid. The factor was computed as the ratio of the actual system pressure at 900°F, (determined by heating a gas with no wax in the reactor) to the perfect gas pressure at 900°F for a comparable quantity of gas. The value of the factor was taken to be 0.78. Figure 4 shows a plot of S vs. run time wherein all the calculated S values for 2 hour radiation runs were averaged to give a point, and the same procedure was followed to obtain the other points shown. The points shown represent the averages of over thirty runs. The initial hydrogen pressure in each run was about 1000 psi.

It is of interest to determine the value of G, which is the number of gas molecules formed per 100 ev. of incident radiation. Figure 5, shows a plot of G vs. run duration. The G values are in the range of 60,000 to 80,000, and are seen to decrease with increasing run duration. The experimental G values are low when compared with the results obtained by Lucchesi, et al. (10) who report a value of about 560,000 for the same conditions. However, the latter value was determined for a short radiation exposure administered during the first minute of cracking. It has been shown in these experiments that the cracking rate is very rapid at first and therefore the G value would necessarily be quite high for shorter duration runs. Figure 5 shows that the G value curve is asymptotic with the ordinate axis and it can be seen that for a run duration of about one minute, the value of G would be appreciably higher than 80,000.

Since the points considered until now have indicated that radiation served to accelerate the cracking reaction, it is important to determine if this conclusion can also be reached by a statistical analysis of the data. The value chosen for comparison between runs was S, the moles of gas formed per gram of wax charged. Since the number of paired sets of radiation and non-radiation runs was small, it was necessary to employ a non-parametric test (7). A suitable one is the Wilcoxon Signed Rank Test (8). By means of it one is able to show that at the 0.025 level of significance radiation has served to increase cracking yields. Or, put in different words, there is a possible error of 2 1/2 percent when one concludes that radiation increases cracking yields.

Acknowledgement

A portion of this work was supported by a grant from the Consolidated Natural Gas Co.

References

(1) Charlesby, A., The Cross Linking and Degradation of Paraffin Chains by High Energy Radiation, Proceedings of the Royal Society (London), vol. 222A, 60 (March 23, 1954).

(2) Lawton, E. J., Balwit, J. S., and Bueche, A. M., The Effect of Initial Molecular Weight on Properties of Irradiated Polyethylene, Industrial and Engineering Chemistry, vol. 46, 1703 (August 1954).

(3) Lucchesi, P. J., Tarmy, B. L., Baeder, D. L., Long, R. B., and Longwell, J. P., High Temperature Radiation Chemistry of Hydrocarbons, Industrial and Engineering Chemistry, vol. 50, No. 6, 879 (1958).

(4) A.S.T.M. D87-42, Standard Method of Test for Melting Point of Paraffin Wax, A.S.T.M. Standards, vol. 5, 14 (1955).

(5) Bennett, H., Commercial Waxes, Chemical Publishing Co., New York, 70 (1956).

(6) Shultz, E. B., and Linden, H. R., Hydrogenolysis of Petroleum Oils, Industrial and Engineering Chemistry, vol. 48, No. 5, 894 (1956).

(7) Hoel, P. G., Introduction to Mathematical Statistics, John Wiley & Sons, Inc., New York, 2nd Ed., 281 (1954).

(8) Bowker, A. H., and Lieberman, G. J., An Introduction to Engineering Statistics, Stanford University, Stanford, California, chapter 7, 32 (September 1957).

FIGURE 1

VARIATION of PRODUCT COMPOSITION
With REACTOR SAMPLING PRESSURE

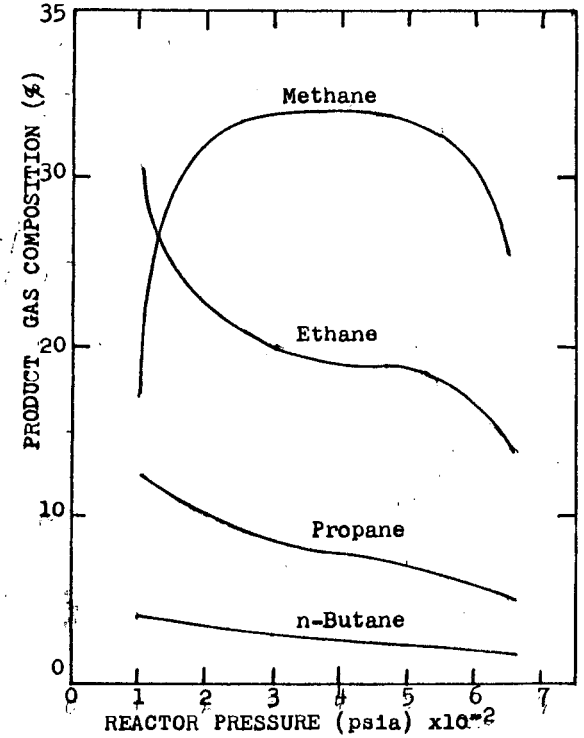

FIGURE II

HEAT-UP CURVE for RUN #56

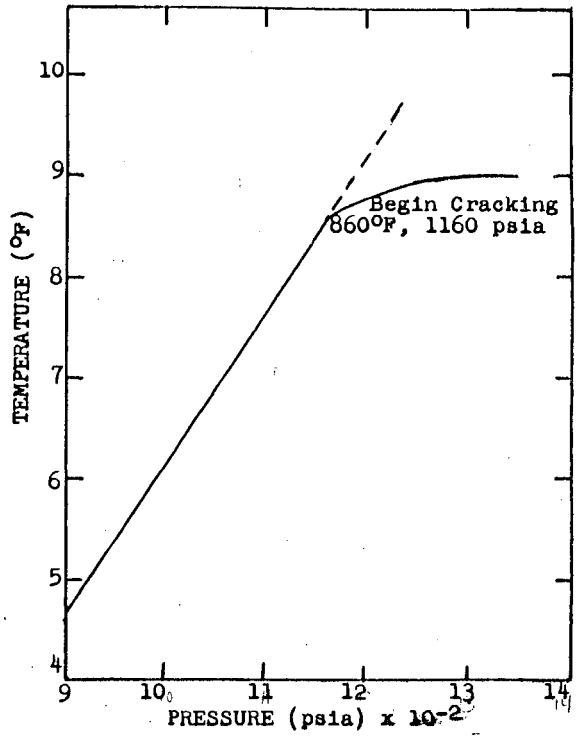

FIGURE III

TYPICAL SPECTRA of PRODUCTS FORMED by HYDROCRACKING

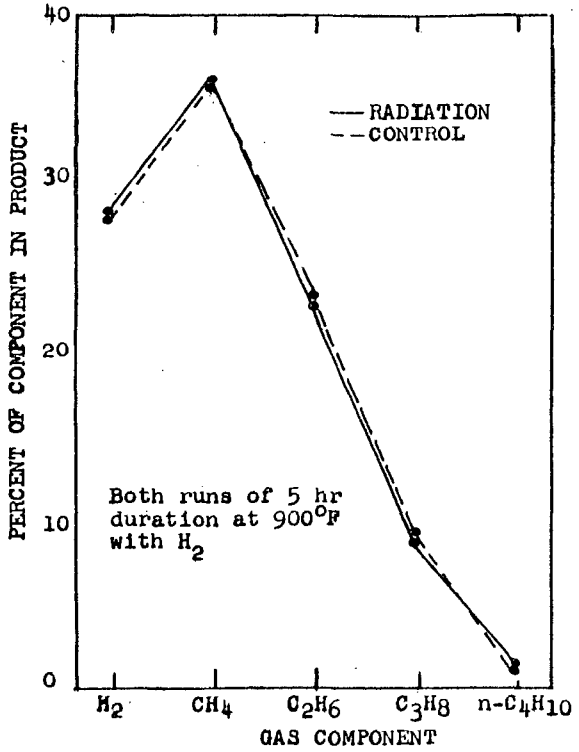

FIGURE IV

VARIATION of S with DURATION of 900°F HYDROCRACKING RUNS

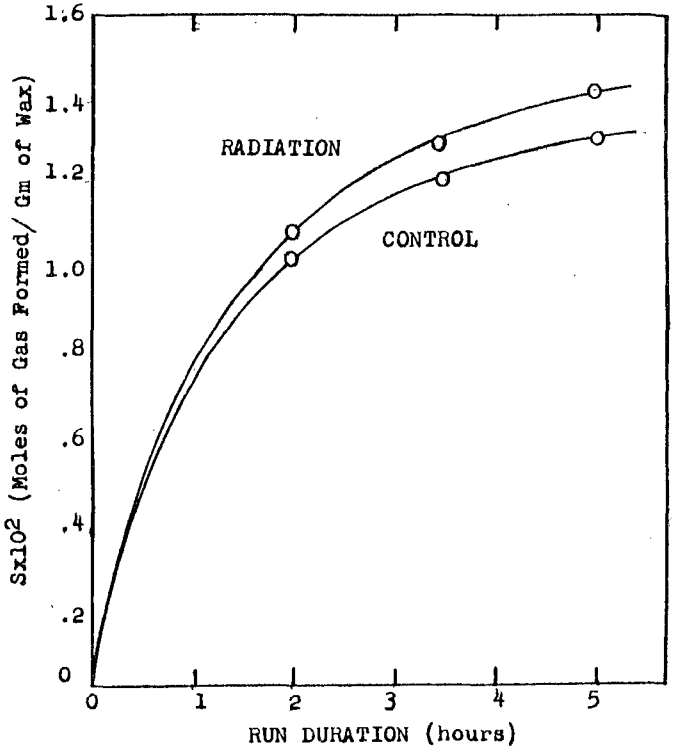

FIGURE V

VARIATION of G withDURATION
of 900°F HYDROCRACKING RUNS